Characterisation of Blast Loading from Ideal and Non-Ideal Explosives

Dain George Farrimond

The thesis presented is for consideration towards the degree of
Doctor of Philosophy in

THE DEPARTMENT OF CIVIL AND STRUCTURAL ENGINEERING,
UNIVERSITY OF SHEFFIELD

Monday 11$^{\text{th}}$ December, 2023

Declaration

I, Dain George Farrimond, certify that all the material contained within this document is my own work, except where it is clearly reference to others.

Date:

Signed:..........................

Abstract

Explosive detonation in its simplest form can be characterised by an instantaneous release of energy at an infinitely small point in space as a solid explosive material. This is a result of chemical decomposition of an explosive which reforms as high pressure and temperature gases which expand radially. This supersonic expansion of detonation products compresses the surrounding medium resulting in a shock wave discontinuity which propagates away from an explosive epicentre at high speeds. This has the potential of significant damage to anything the shock wave iteracts with.

Shock wave quantification work conducted in 1940‘s through to the 1980‘s was done so to understand the effects of large scale explosive detonation which was an immediate threat due to the discovery of the nuclear bomb. Highly skilled experimental and theoretical scientists were assigned the task of capturing the effects of large scale detonations through innovative solutions and development of pressure gauges. The in-depth fundamental understanding of physics, combustion and fluid dynamics the researchers utilised resulted in the well-favoured semi-empirical blast predictions for simplistic free-field spherical/hemispherical blasts.

A broad amount of literature has been published on free-air characterisation of spherical/hemispherical explosives, with the detonation process and subsequent shock wave formation mechanics being well understood. However, there is yet to be a definitive and robust understanding of how deterministic a shock waves spatial and temporal parameters are for simplistic scenarios. This goes as far as some studies suggesting that semi-empirical tools are not as effective as previously assumed. Often the use of numerical simulations provide reasonable insights to blast loading conditions imparted on structures and scenarios with higher complexities. However, when the validation data used is assumed to exhibit erroneousness, the schemes are no longer characteristically high in fidelity. The

lack of quantified variability and confidence in the data which is published, are significant issues for engineers when designing infrastructure that is both robust enough to withstand extreme loading, and not overly conservative that there are cost and material waste implications. This issue is investigated thoroughly within this thesis, highlighting the sensitivity of blast parameters across the scaled distance ranges, and determining their predictability with both numerical simulation and semi-empirical tools.

The vast majority of free-field characterisation has been conducted using military grade explosive which exhibit ideal detonation behaviours; meaning the detonation reaction is effectively instantaneous. Ideal explosives, by the theoretical definition, can be categorised by a simplistic instantaneous energy release. In far-field regimes, any explosive with ideal-like compositions and behaviours should be scalable with mass. This assumption is not valid for homemade explosives (HME), such as ANFO (Ammonium Nitrate + Fuel Oil), whose compositions are usually homogenous, resulting in a finite reaction zone length. These can be long enough to cause failures in detonations and exhibit a variety of different energy releases depending on the mass of the charge resulting in HME's having different TNT equivlence values depending on their scale.

Early works of ANFO characterisation was done so in the desire to replace TNT, to assess its capability of producing similar yields for a fraction of the manufacturing costs. This meant the hemispherical detonations of ANFO which have led to its overall classification, were done using charges of over 100kg and therefore non-ideal reaction zone effects become negligible in comparison to the overall charge size. Yields presented in this region were consistently measured at around 80% of a similar TNT detonation and has therefore been incorrectly assumed a rule for ANFO across all mass ranges within published literature.

There is a distinct lack of characterisation of non-ideal explosives throughout the mass scales, posing a significant implication for designing structures to withstand the threat of HMEs. With the knowledge that energy is released at a much slower rate when detonating these compositions, the assumption that large scale trials accurately capturing the behaviour of a small charge masses, when scaled down, is not verified. Most HMEs will be hand held devices or, at the very least, backpack size, meaning the threat currently is not predictive with confidence through validated data conducted under well-controlled conditions. Small scale ANFO trials have demonstrated this to be the case within this thesis, with theoretical mechanisms proposed which offering a prediction method of the behaviour of non-ideal detonation across all mass scales.

Findings in this PhD thesis will offer a conclusion on whether shock waves in free-field scenarios are deterministic for both ideal and no-ideal explosives, with a particular emphasis on the far-field range. The results presented are developments in the accurate quantification of shock wave loading conditions a structure is subjected to through explosive detonation and should be used by engineers to establish robust, probabilistic but accurate designs.

Acknowledgements

It is important to express my deepest thanks to those whom without their consistent support and guidance this thesis would not have been possible. To my PhD Supervisors; Professor Andy Tyas alongside Dr. Samuel Rigby and Professor Samuel Clarke, throughout this journey there have been struggles which were unforeseen and unprecedented but despite this the three of you have provided not only insightful knowledge of explosive characterisation invaluable to this research but a support network which has enabled to get the best out of both myself and the situation. I have learnt a great deal from the three of you during my, thus-far, short researching career, and am excited for what the future has in store for where my learning could continue.

I would also like to pay special thanks to the employees at Blastech, for both the high quality experimental work they conduct and for being incredibly welcoming during my time working alongside them, conducting both University and commercially funded experimental work. I feel privileged to have been able to work within an industry recognised research team concurrently to my studies which has provided me with an invaluable experience other PhD students do not get access to quite as readily.

To my friends and family, the people in my life who have provided consistent support throughout the duration of my PhD journey. There has been an overwhelming number of discussions had with all of you regarding both rewarding and challenging aspects of the PhD process. Thank you for being my think tank outside of academia and providing the best advice anyone could ask for when taking the time to listen about the intricacies of my research.

Finally, and most importantly, I would like to thank Laura. You have been my rock throughout this whole process, listening to my endless ramblings, notions and hypotheses I have had regarding aspects of my research. Without you this thesis would not have been possible.

Dain George Farrimond,
Monday 11th December, 2023

Contents

List of Figures

List of Tables

Nomenclature

A	Area
D_{CJ}	Chapman-Jouguet detonation velocity
D_{∞}	Infinite charge diameter
E	Detonation energy per unit mass
F	Original image
i	Specific impulse
i_r	Reflected positive phase specific impulse
$i_{r,min}$	Reflected negative phase specific impulse
i_{so}	Incident positive phase specific impulse
$i_{so,min}$	Incident negative phase specific impulse
K	Hopkinson-Cranz scaling factor
N	Resulting subtracted image
P	Pressure
P_{CJ}	Chapman-Jourguet pressure
P_{max}	Max Overpressure
P_o	Ambient air pressure
P_r	Reflected pressure
$P_{r,neg}$	Negative reflected pressure
P_{so}	Incident pressure
$P_{so,neg}$	Negative Incident pressure
P_{SS}	Secondary shock pressure
R	Distance from charge centre (stand-off)
R^2	Coefficient of determination
ρ	Charge density
t	Time
t_a	Time of arrival

t_d	Positive phase time duration
t_{d-}	Negative phase time duration
td_{ss}	Secondary Shock positive phase time duration
τ_{ss}	Secondary shock delay parameter
$\delta\tau_{ss}$	Time difference between arrival of primary and secondary shock
V_{od}	Velocity of detonation
W	Charge mass
Z	Scaled distance

Chapter 1

Introduction

The overall aim of this PhD thesis is to comprehensively characterise the effects various explosive compositions and sizes have when detonated across a full range of distances from a target. This will focus primarily on the far-field range of distances, the time at which the shock wave has propagated to a significant distance away from the explosive centre as to not be affected by late-time chemical reactions within the fireball. The context of this work looks at providing key analytical procedures which are validated for the most simple and ideal explosive compositions and assessing their application to non-ideal compositions.

This chapter will provide an outline of the structure of the thesis as well as detailing the motivation behind the current research.

1.1 Background and Motivation

The discovery and use of the nuclear bomb in 1945, initiated a critical need across the globe to better understand the effects of explosions with extremely large yields. This was essential to ensure procedures and strategies could be implemented for civilian safety against potential large scale threats. Between 1945-1963, a large number of nuclear tests were undertaken by the United States in the attempt to quantify the disastrous consequences these events would have on civilian infrastructure. The severe environmental damage caused by these tests induced the first instance of global cooperation to eliminate the testing of nuclear weapons. There was however still a need for quantifying the effects of said events to understand the fundamentals of explosions and how this knowledge could be used to improve design practices of structures to withstand them. Vast investment at this time into testing of high explosives, with yields within similar margins to nuclear detonation, produced some of the more widely regarded quantification data sets [87]. This was then utilised to develop a semi-empirical prediction tool for free-air blast scenarios [90]. Blast resilient design specifications to this day still make use of these tools for prescribing loading conditions a given target will be subjected to for a given mass of Trinitrotoluene (TNT) - the baseline to which all comparisons are made in blast engineering.

This tool has however had its accuracy questioned over more recent years with researchers debating whether it provides reasonable enough representations of an explosive event across a full-field of distances between charge and target [13]. Logic would suggest that with more modern and precise experimental procedures, the results should tend towards those predicted, with a reduction in the uncertainty. However, the problem has been that many modern researchers have reported a significant lack of repeatability in experimental measurements when comparing directly to the tool's predicted parameters, and the much older data sets used to produce them [56]. There is however a clear divide in the blast protection community regarding the fundamental understanding of explosive characterisation; those who exhibit large variability in experimental blast measurements and interpret this to be inherent of explosive detonation, and those which undertaking similar testing, recorded consistent and deterministic data.

Modern day architecture has moved towards more material and energy efficient designs whilst appealing aesthetically through atrium-like open spaces, glazed cladding for additional lighting and unique structural forms for visual effect. These three additions, among others, to civilian infrastructure have one key disadvantage: the catastrophic effects, both structurally and to civilians, they can have as a result of being subjected to explosive loading conditions. This in conjunction with the rapid expansion of the geographic extent of urban areas has resulted in a rise in spatially complex civilian environments. Blast resilient design of infrastructure has become essential as a results of an increasing number of explosions occuring in civilian areas. In 2021 alone there were a total of 5,226 recorded terrorist attacks on civilian structures, with the 18 worst events resulting in 1241 deaths alone [79]. The frequency and variety in modern day explosive events and their interaction with structures provides enough of a challenge for engineers to combat without the predicted methods used for design being questioned. Whilst ever there is uncertainty in the predictive tools used to design civilian infrastructure, there is also an uncertainty in safety assurances of structures when subjected to explosive loading. There is, therefore, a need to establish whether the prediction tools developed by Kingery and Bulmash[87] are accurate for a full range of distances between charge and target across various explosive types.

This thesis presents research which will contribute to the existing knowledge of quantifying reflected blast loading on targets by characterising the effects across a range of charge-to-target distances for a variety of explosives. The research aims to provide evidence which supports the notion of explosive variability through re-examination of both historic and newly recorded data, whilst developing new and robust experimental data processing techniques. The investigation into different types of explosives will provide improvements to the fundamental understanding of the mechanisms and characteristics of their detonation, and the resulting yields.

1.2 Scope and Objectives of the Thesis

When designing infrastructure to withstand explosive loading conditions, the engineer is faced with the task of assigning a given charge composition, shape, mass and location from a target. These variables often will not be known, and therefore a probabilistic analysis is required. The ability to determine an accurate prediction for a prescribed event is essential to introduce confidence in probabilistic studies. Whilst all of these variables can significantly alter the pressures associated with the resulting blast wave, there still is the issue of whether current empirical and numerical predictive methods are reasonable estimations to a real event.

Whilst there have been significant developments in numerical analysis and their potential to output accurate predictions, it is important to revisit experimental trials to somewhat re-establish the benchmark fundamental explosive parameters from simple scenarios. Only when the discussion over inherent explosive variability is finalised, can reliable and accurate numerical models be developed. This thesis, has several objectives which are directly related to issues outlines above:

1. To identify a clear benchmark of free-field explosive characterisation of ideal explosives, and its associated variability with distance, which can be used in yield comparison studies of various composition types.

2. To develop validated experimental methodologies and tools for analysis to establish reliable data to inform the understanding of fundamental explosive physics.

3. To establish scalability of explosives which exhibit non-ideal detonation behaviours, and evaluate whether TNT equivalence theories are valid.

1.3 Thesis Outline

The remainder of this thesis is organised into the following chapters:

- **Chapter 2** - Literature Review and Theoretical Background

  This chapter will provide a detailed overview of previously published literature regarding explosive blast loading gained through both experimental and numerical analysis across a number of charge compositions, sizes, shapes and location from a target. The aim of this chapter is to scrutinise existing hypotheses and conclusions authors have made regarding the fundamental principles of blast wave development and loading alongside the quantification of variability a given explosive type exhibits in line with Objective 1.

- **Chapter 3** - Standardising Experimental Methodologies and Analysis

  This chapter establishes both experimental methodologies and methods of analysis through extensive validation against recorded data and numerical modelling with Objectives 2 and 3 in mind. The effects of generally assumed insignificant experimental features are studied and highlight the need for strict control measures during explosive testing and modelling.

- **Chapter 4** - Ideal Explosive Blast Characterisation

  The validated techniques developed in Chapter 3 were used across a range of different ideal high explosive compositions in the far-field ranges to determine whether they are applicable across simplistic free-air scenarios to achieve Objective 4. These methods are exercised against current standards of readily available prediction tools to access their accuracy and consistency.

- **Chapter 5** - Non-Ideal Explosive Blast Characterisation

  This chapter aims to complete Objective 5 by providing a detailed characterisation of non-ideal explosives not yet fully discussed within the available literature. The content attempts to assess the scalability of non-ideal explosives and compares the resulting yields to that of ideal explosives and the respective prediction tools.

- **Chapter 6** - Summary, Conclusions and Future Work

  This chapter summarises the research presented within this thesis and makes suggestions for future developments towards improving the current understanding of explosive loading conditions within a full-scale range of standoff distances in line with Objective 6.

1.4 Published Articles

It is important to note that all experimental work alongside the analysis was undertaken by the author of this thesis with technical assistance from Blastech Ltd. All numerical simulations were undertaken by collaborators at DSTL whom had no further input into the narrative of this research. The work contained within this thesis has been used to publish peer-reviewed journal papers which can be quickly accessed using these QR codes:

(a) Farrimond et al.[49]

(b) Farrimond et al.[50]

(c) Hobbs et al.[72]

(d) Barr et al.[10]

Figure 1.1: QR code links to published articles

Chapter 2

Literature Review and Theoretical Background

2.1 Introduction

This chapter discusses the fundamental understanding of explosive detonation and the subsequent blast wave propagation and interaction with structures. Throughout this discussion, a review of published literature will be undertaken relevant to the subsequent subject areas investigated within the content of this thesis.

2.2 The Detonation of Explosives

During the detonation process of an explosive, enough energy is provided to the physical solid mass which propagates through the composition in the form of a reaction wave. This results in an exothermic decomposition over a very short duration of time producing hot dense gases [1]. The reaction process occurs over a given amount of time (varying dependant on charge composition) and is confined within the explosive mass itself until the wave reaches the extents of the explosive. This means that the gaseous detonation products occupy the same volume as the solid mass previously did and therefore exhibit extremely high temperatures and pressures [101] of around 10-30GPa and 3000-4000°C respectively [32]. The detonation wave is continually reinforced by the energy released from the material detonating immediately ahead of it until the explosives extents are reached.

Developing the knowledge of the detonation process is fundamental to investigating and characterising the behaviours of detonating explosive compositions. This will be considered regardless of reaction chemistry and detonation dynamics, across a range of masses and distances from a target. A clear review of the different detonation processes are presented with a discussion around the effect these can have on free air shock loading.

Taylor[167–169] proposed a very simplistic approach to explosive detonation which hypothesised an instantaneous release of energy from a infinity small point in space resulting in a radially expanding shock front. In actual fact, detonation occurs over incredibly small time scales, with the ongoing reactions exhibiting high complexity chemical decomposition and oxidation processes. Zukas and Walters[182] proposed assumptions for the detonation process which enabled a more robust approach to be adopted to understand an explosives detonation behaviour:

- The implementation of a one dimensional analysis which considers detonation products only propagating behind the shock front with no lateral loses i.e and infinite charge diameter.
    - In reality, all charges have a finite boundaries which means loses in energy development will incur due to product expansion prior to full potential detonation reactions occur
- A perfectly planar detonation wave propagates through the explosive to avoid shock front curvatures.
    - When the detonation front reaches the finite boundaries and energy is lost, the front slows at its peripheries and propagates at higher speeds towards the centre of the charge, therefore exhibiting a curvature.
- The reaction is perfectly stoichiometric and occurs instantaneously, with detonation products being in thermodynamic equilibrium.
    - Detonation by nature is not in thermodynamic equilibrium, the reaction process occurs over some finite amount of time.
- The whole process occurs at constantly velocity which in itself assumed a steady state reaction zone.

  - Detonation velocity is directly proportional to the reaction process and therefore is not a constantly velocity in line with the point above.

With these assumptions in mind, the accepted view of a high explosives detonation structure consists of four distinct reaction regions, quoted by Paterson[111] and displayed in Figure 2.1:

1. The pre-detonation region which is yet to be subjected to the propagating shock wave and therefore the composition is unaffected.

2. The leading shock front, travelling at supersonic velocities, compresses the explosive and initiates the detonation through exothermic decomposition of molecular bonds. In the simplest form, detonation theories presented by Chapman[26] and Jouguet[84] (C-J) assumed the reaction to occur instantaneously with the flow becoming sonic at the C-J point. At this point, the energy released behind the sonic front is able to support the detonation front at constant velocity and pressure[55]. von Neumann[177] however argued that detonation was to occur over a finite time and reaction zone length, resulting in a significant difference in pressure and temperature either side of this region. This was further developed to consider the existence of an induction period of time related to reaction initiation time lag once compressed by the leading detonation wave[166].

3. The reaction zone, in which an increasing amount of energy is released with a function of distance travelled along a given explosive composition, results in an acceleration of the products away from the shock front and therefore propelling the shock front forward[11]. The reaction zone is a function of characteristic time taken for the chemical decomposition of the explosive and therefore the rate at which energy is released.

4. Upon reaction completion, the detonation products begin to expand with the loss of inertial confinement of the solid state with a rarefaction wave travelling in the opposite direction the detonation wave[31].

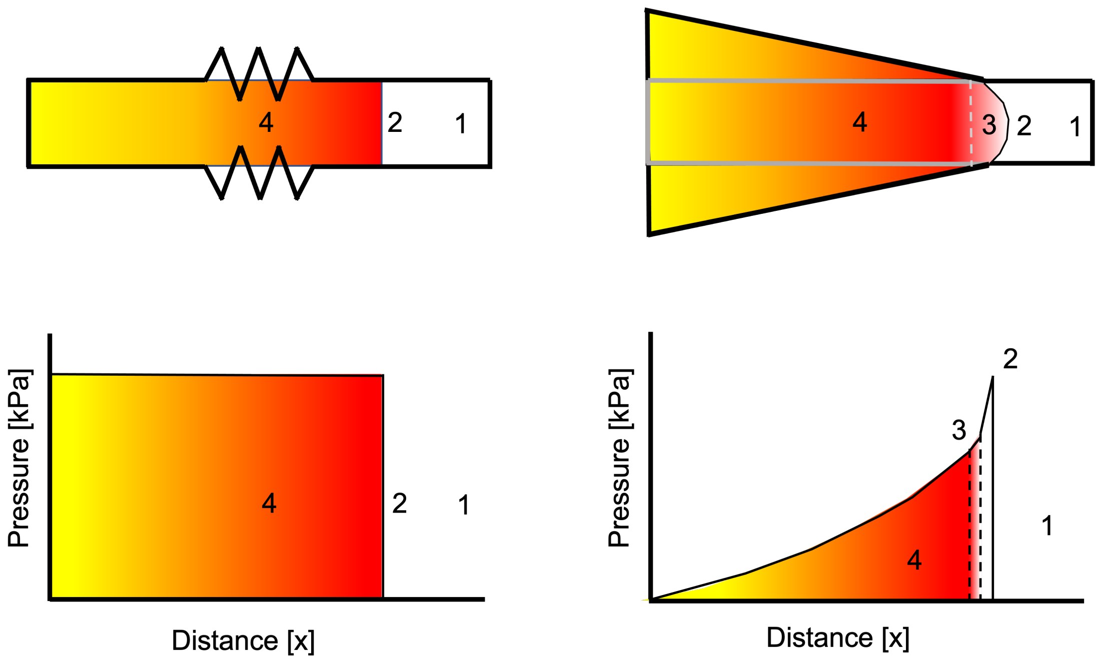

Figure 2.1: Schematic representations of detonation theories: C-J theory (left) displaying the planar like pressure wave with distance and no lateral losses, and the theory proposed by von Neumann[177] *(right) which details finite reaction zones and detonation product expansions. Note the numbering system aligns with detonation process discussed above.*

The detonation theories outlined categorise explosives in to two groups: Ideal and non-ideal explosives. Ideal explosives, when detonated, exhibit behaviours which are captured by C-J theory with high levels of agreement through the use of thermochemical computer codes[48], such as Cheetah[58] and EXPLO5[161]. These tools have integrated the C-J theory into their methodology, to predict the behaviour of an explosive based on its composition, heat of formation and density[179]. In reality, most commercial available explosives, and certainly all home-made explosives (HME), often result in detonation velocities and pressureswhich do not follow C-J theory, labelled non-ideal[159]. This group of explosives are generally heterogeneous fuel-oxidiser mixtures which when detonated result in non-monotonic relationships between detonation and density which is not captured by thermochemical calculations[114].

The C-J theory makes the assumption that for a planar detonation in an infinite diameter charge, D_∞, the reaction zone structure would not alter the maximum velocity of detonation to which is calculated[75]. The reality is that charges have a finite diameter and therefore are subjected to lateral energy loses through detonation product expansion, thus never exhibiting their maximum potential velocity. Fundamentally, as the diameter of an explosive composition reduces, the amount of energy lost through product expansion increases, resulting in detonation behaviours unclassifiable by standard C-J theory. This reduction in energy continues up to the diameter at which the reaction zone no longer releases enough energy to sustain the detonation process[142], called the critical diameter of an explosive composition, d_{cr}.

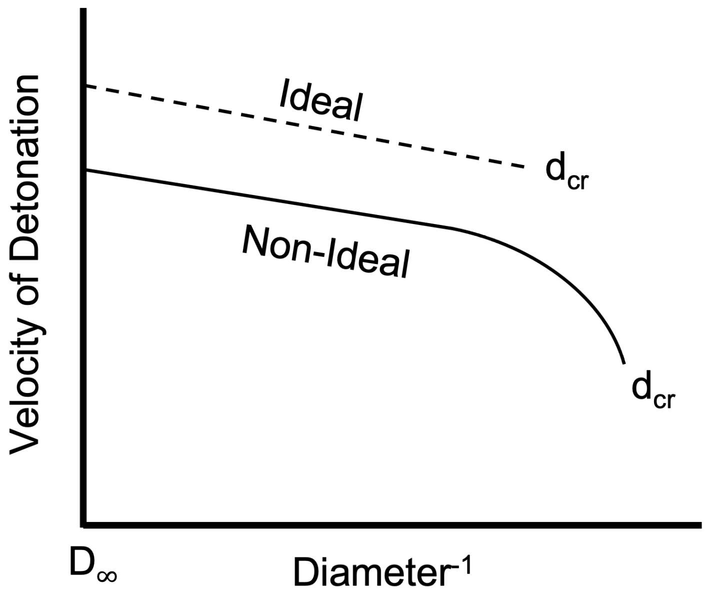

Figure 2.2: Schematic representations of detonation velocities and how they vary with charge diameter for ideal (dashed) and non ideal (solid) explosives adapted from work presented by Scott[142].

The reason C-J theory is unable to capture the behaviour of non-ideal explosives is due to the assumption that reactions occur instantaneously. An increase in non-ideality of an explosive is a direct result of a larger reaction zone and characteristic time for full decomposition of the explosive to occur. For military grade explosives, which exhibit ideal like behaviour, the reaction zone length are small (∼1mm) and therefore the d_{cr} can be within a few millimetres. For the non-ideal explosives, the reaction zone is significant larger (∼10mm) meaning the d_{cr} is orders of magnitude bigger[94]. This behaviour is represented by Figure 2.2.

2.3 Air Shock Formation

Once the detonation process reaches the extents of an explosive composition there is a discontinuity between it and the surrounding medium. This discontinuity results in both the rapid expansion of detonation products into the surrounding medium and a reflective wave propagating back towards the detonation epicentre. The expanding detonation products displace the surrounding medium at speeds dependent on the magnitude of energy contained within the wave itself. Air is the medium of choice within this thesis it is important to note that it is a compressible fluid. This means that rapid expansions and disturbances to the surrounding air results in higher pressure components of the expansion travelling quicker than the lower pressure components over small periods of time. This transitions the expansion into an effectively instantaneous increase in pressure and density, propagating away from the explosive in the form of a shock (or blast) wave[7], represented by Figure 2.3. It is important to note that Figure 2.3 represents the fireball and shock wave breakout of a hemispherical charge. Shapes which exhibit geometrical variations would result in different breakout procedures and thus loading conditions in near-field regimes which self-heals far-field.

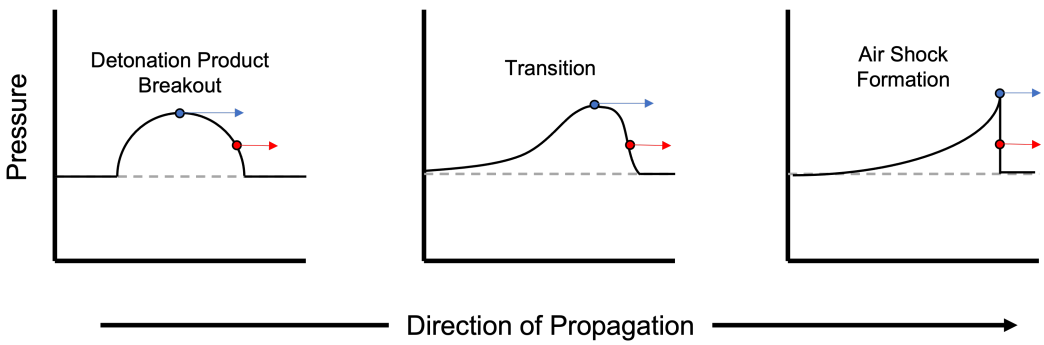

Figure 2.3: Schematic representation of the formation of air shock from hemispherical explosive detonation: Depicted by Initial pressure pulse related to the detonation product breakout (left), transitioning into a front loaded pulse due to a range of particle velocities (middle) to a point where a near-discontinuous shock wave forms (right), adapted from Kinney and Graham[90].

The detonation of an explosive and the subsequent expansion of the gaseous fireball products displace the surrounding air and compresses it into a high pressure discontinuity with undisturbed air ahead of it. As the expansion propagates, a temporal decay in pressure and velocity back to ambient air pressure is experienced. For spherical/hemispherical explosive charges, the detonation product cloud halts its expansions at distances some 20 charge diameters away from the epicentre, which up til this point would be described as the near-field regime[173]. The shock wave preceding the detonation products continues to propagate radially until it either interacts with a target (reflected) or decays away (incident), defined as the far-field regime. Figure 2.4 provides a visual representation of this behaviour.

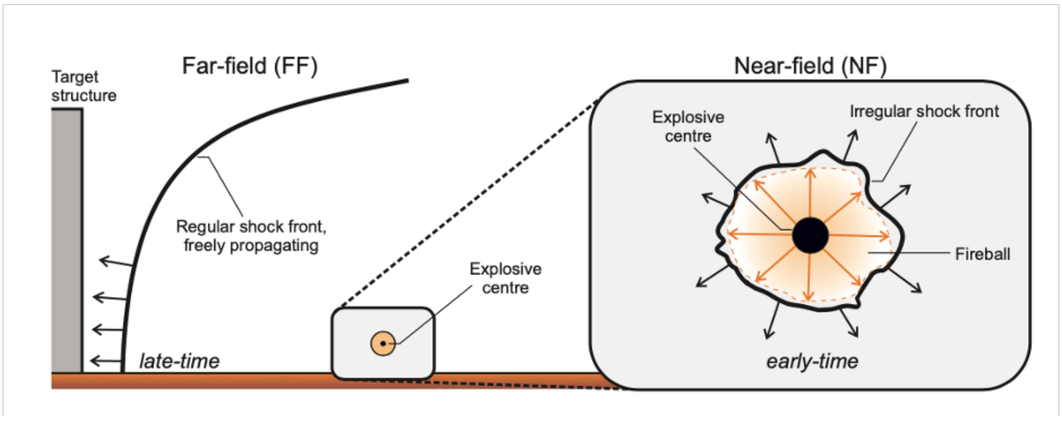

Figure 2.4: Schematic representation of the the different scaled distance regimes discussed by Tyas[173]

It is important to note that common blast engineering practices consider far-field regimes, in which an air shock is fully formed and has propagated far enough away from the detonation epicentre to not be affected by the fireball. In close proximity to the detonation, where the air shock has not detached from the fireball, the current knowledge of blast loading is significantly undefined. This is due to the difficulty in measuring such high pressures and impulses without damaging equipment. In conjunction to this, any interaction in this regime is a result of both fireball products and potentially a slower loading profile, as seen in Figure 2.3.

Naturally, there are a number of variables which dramatically affect the characteristics of these shock waves including: the distance the explosive is away from a target, known as the standoff distance; the shape, size and type of the explosive used; and both the detonation and interaction mechanisms occurring which alter the intrinsic characteristics of the waves. For the contents of this thesis, hemispherical charges are the only shape considered to make direct comparisons with the broad range of historical data available. Having an understanding of how each of these parameters effects the characteristics of a shock wave is important for probabilistic-based analysis of loading conditions on a structure.

Figure 2.5 presents an idealised shock wave pressure-time history defined as the modified Freidlander waveform which can be approximated by Equation (2.1)[57]. Considering a point far enough away from the detonation epicentre to be characterised by a fully formed air shock, the behaviour is characterised by a near-instantaneous rise in overpressure, P_{so} and P_r for incident and reflected results respectively. This has a characteristic arrival time, t_a, and a temporal decay back to ambient conditions, P_o, which occurs over a duration of time, t_d. The waveform parameter, b, controls the decay of the pressure-time curve. Through integrating the pressure-time history with respect to time, a impulse-time history can be plotted. This can be attributed to the change in momentum, or specific impulse i, a given area experiences from the different loading conditions, denoted by the coloured regions in Figure 2.5. This period of a shock waves behaviour is defined as the positive phase which is considered the most destructive part of blast loading[182].

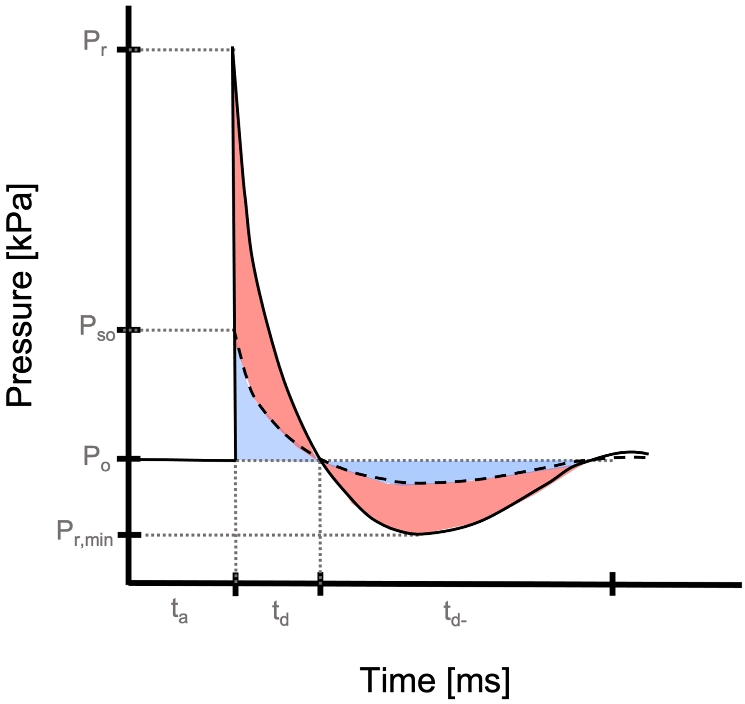

Figure 2.5: Indicative Freidlander shock wave pressure–time history with reference to both reflected (red) and incident (blue) forms with respect to each other.

$$P(t) = P_{max}(1 - \frac{t}{t_d})e^{-b\frac{t}{t_d}} \tag{2.1}$$

The rapid overexpansion of the medium results in a lower density partial vacuum behind the shock front which forces air back towards the detonation epicentre to maintain equilibrium conditions, defined as the negative phase of a shock wave[107]. Similarly to the positive phase, the time taken for conditions to return to ambient is defined as the negative phase duration, t_{d-}, with the maximum underpressure defined by $P_{so,min}$ and $P_{r,min}$. Figure 2.6 presents a schematic of the negative phase mechanism which details the aforementioned processes. It is important to note that for hemispherical charges, the negative phase measured at the ground surface is found to be greater due to the rising fireball. This creates a convectional lower pressure regions, thus resulting in a greater underpressure[133]. Further to this, at some time after the arrival of the positive phase, secondary and tertiary waves arrive at the same recording position. This phenomena is a result of rarefaction waves from detonation product expansion, coalescing at the point of detonation, and reflecting radial outwards. This is similar to a pulsing-like effect with subsequently lower yields associated with each iteration of shock.

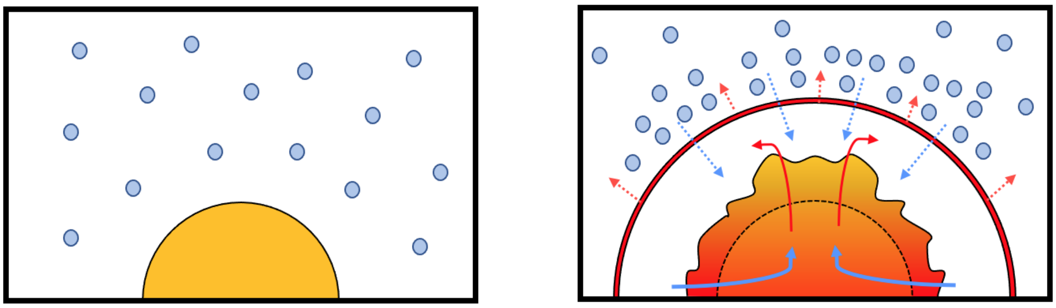

Figure 2.6: Indicative behaviour of negative phase process: Pre-detonation of charge with reference air particles (left), and Post-detonation with reference to shock wave condensed air particles, leaving a vacuum with an under pressure.

2.4 Secondary Shock

Needham et al.[106] discussed the phenomena of secondary shocks occurring sometime after the formation and propagation of a primary shock, resulting in an imploding moving shock which coalesces at the detonation epicentre and reflects back outwards. The results of this process is presented in Figure 2.7, where P_{SS} is the associate shock pressure and td_{ss} is the phase duration of the secondary shock. Whilst the feature is documented across a number of articles[7], historically there seems to have been little effort made to quantify or characterise its effects. This is mainly due to exhibiting low yields and therefore corresponding to low impact on structures or civilians.

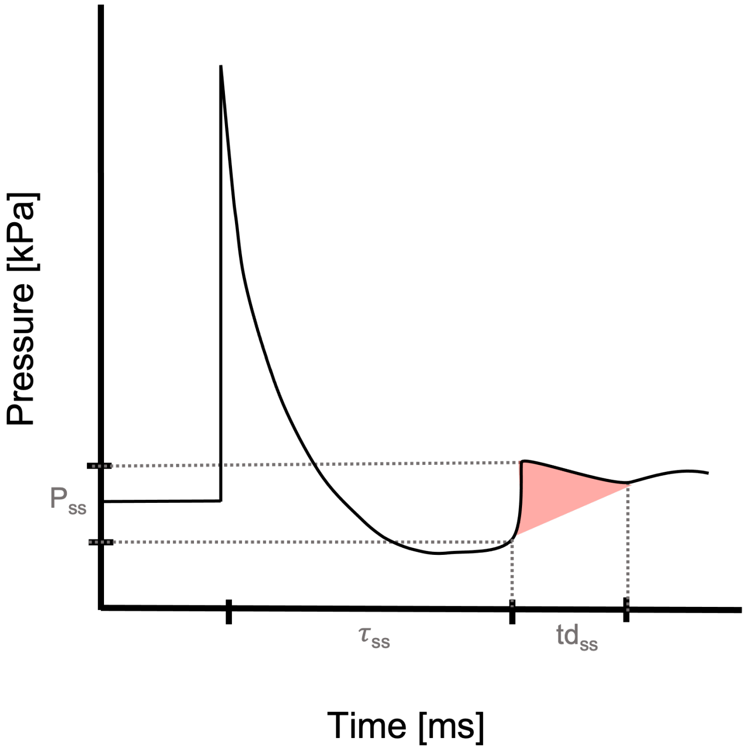

Figure 2.7: Indicative Freidlander shock wave pressure–time history with reference to the secondary shock phenomena and the blast parameters associated.

Work presented by Gitterman and Hofstetter[62] began to compile a considerably large data set of the secondary shock arrival time, and its subsequent delay after the arrival of the positive phase, across a range of explosive compositions, sizes and scaled distances. The reason for this analysis was to help improve the predictions of negative phase parameters as currently numerical models struggle to capture them with definitive accuracy. With near-field blast parameters within the fireball holding difficulty to prescribe with standard methods, it is believed that the behaviour of a secondary shock could be used as an indicator for post-detonation products within the fireball.

With the aforementioned in mind, the secondary shock delay parameter, τ_{ss}, was introduced by Rigby and Gitterman[129] who attempted to normalise each explosive by scaling the delay parameter by standard detonation velocities and the cube-root of the packing density, defined by Equation 2.2. The thinking behind this methodology was to correlate the parameter with the characteristic time for complete detonation of a finite hemispherical charge, where ρ is charge density, V_{od} is velocity of detonation, W is charge mass and δt_{ss} is the time difference in arrival times between primary and secondary shocks. The data presented in Figure 2.8 was obtained from the authors of the aforementioned articles and improved by including standard TNTe values for each explosive, which seemed to provide increased linearity of the data when compared to the least-squares fit defined by Equation 2.3.

$$\tau_{ss} = \delta t_{ss} V_{od}/(\rho W)^{1/3} \tag{2.2}$$

$$\tau_{ss} = 2.45 log_{10}(Z) + 1.36 \tag{2.3}$$

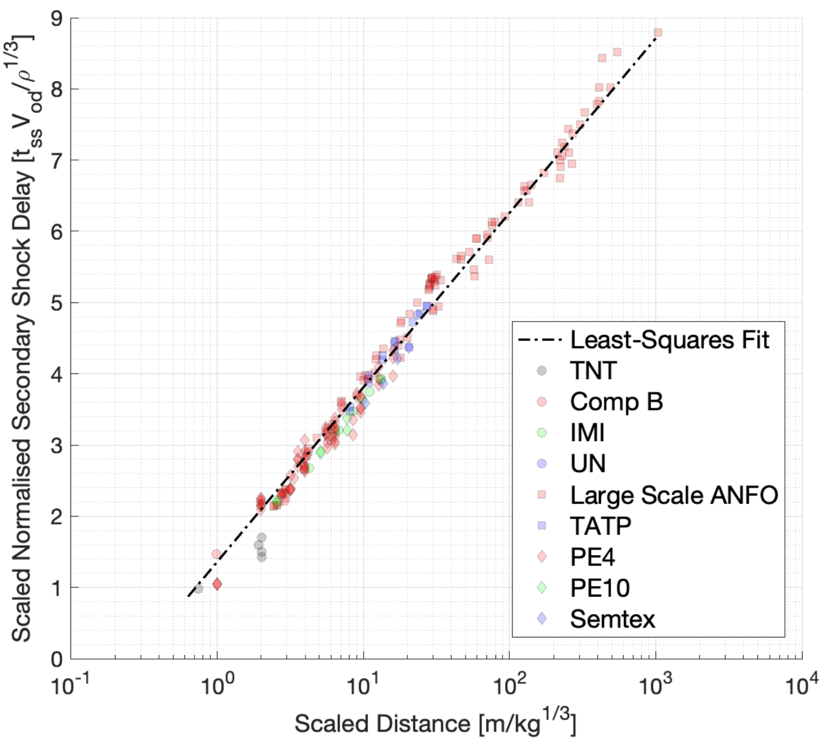

Figure 2.8: Secondary shock delay parameter evaluated for all explosives scaled accordingly compared with a least-squares fit to data, extracted from Rigby and Gitterman[129]

The least-square fit, detailed by Equation 2.3, was tested against experimental data and theoretical examples presented by Rigby and Gitterman[129] and was found to provide remarkably accurate results. The issue with this methodology is that the secondary shock parameter defined by this analysis has units of $m^2/kg^{2/3}$ which holds no physical meaning and therefore a different consideration is required to assign a real mechanism to the behaviour.

Despite analysis undertaken of the large data for the delay in arrival time [62,129,133], there is still a gap in characterising the other secondary shock blast parameters. There is a need for a theoretical mechanism which captures the behaviour of secondary shocks across a variety of explosives and scaled distances which can be implemented into predictive tools to provide more realistic and valid predictions.

2.5 Scaling Laws

2.5.1 Mass and Energy Proportionality

A fundamental finding proposed separately by Hopkinson [74] and Cranz [33], suggested that through cube-root scaling of the distance a charge is away from a target, results in consistencies in the yields from two different explosive charge. This can be achieved provided the same shape of charge and direct equivalent masses can be established. This means that the blast parameters at a given distance away from the centre of the explosive, R, with mass, W, will be comparable to that at a distance, KR from a mass of K^3R. As a blast wave spherically propagates, energy dissipates into the surrounding medium in all three dimensions, hence the cube-root scaling, which led the aforementioned authors to develop Equation 2.4, where E, is the energy released per unit mass of the explosive material.

$$\frac{R}{E^{1/3}} = \frac{KR}{(K^3E)^{1/3}} \tag{2.4}$$

The amount of resulting energy produced upon detonation of an explosive, is inherently dependent on the equivalent mass of the explosive, W. This leads to Equation 2.5, which introduced the notion of scaled distance, Z, measured in units of $m/kg^{1/3}$.

$$Z = \frac{R}{W^{1/3}} = \frac{KR}{(K^3W)^{1/3}} \tag{2.5}$$

The Hopkinson[74] and Cranz[33] cube-root scaling, assumes the pressure associated with a blast is directly proportional to the energy released so does not require scaling. It is only time-related parameters which require scaling by the cube-root of the explosive mass Kinney and Graham[90].

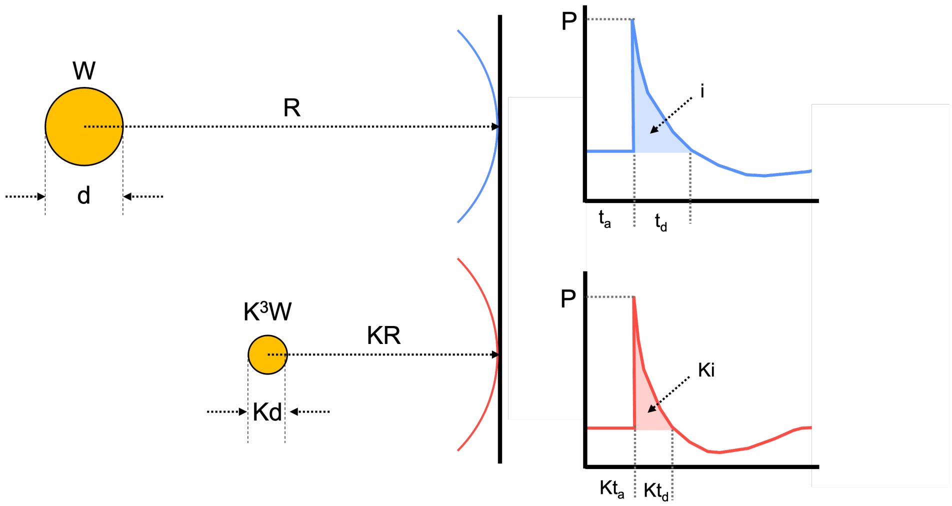

Figure 2.9: Representative schematic of Hopkinson[74]-Cranz[33] scaling, adapted from Baker[7]

2.5.2 Charge Shape

The effect of charge shape has been investigated throughout literature to assess and characterise the differences in the blast parameters induced. Both Wu et al.[180] and Sherkar et al.[146] undertook the numerical simulation of explosive detonation for spherical and cylindrical across a range of scaled distances, charge orientations and detonation positions on the charge. Presented were the distributions in blast parameters which concluded that charge shape has a significant effect. When standoff distance from the detonation point is greater than 35 charge diameters $Z>3m/kg^{1/3}$, the effect of charge shape can be ignored. Similar ranges were presented by Xiao et al.[181], but all came to the agreement that the information presented was not sufficient enough to identify the precise scaled distance at which charge shape effects could be ignored definitely. Shi et al.[147] countered this finding when a variety of 1kg TNT explosive trials consisting of four different charge shapes in near-field scenarios were conducted and agreed that the blast parameters recorded are far more sensitive in the near-field when non-spatial symmetry of an explosive creates non-uniform detonation processes. This was displayed by high speed video frames which showed how variability in breakout shape decreased with scaled distance but only becoming negligible at $Z>5m/kg^{1/3}$.

Spherical and hemispherical charges exhibit far more similarities through radial detonation mechanics and subsequent shock wave breakout. Early works presented by Brode[19] undertook numerical simulations of spherical blast waves which have been used in conjunction with experimental trials using large scale TNT hemispheres[87] to develop fast-running engineering computer codes, such as ConWep[76]. These methods were all based on the assumption of spherical charges detonation in free air, or a hemispherical charge detonation on a flat surface.

Assuming a perfect reflecting plane, a hemispherical charge of mass, W, in theory a spherical charge of mass, $2W$, would produce the equivalent blast parameters. The issue with this theory is that in reality, hemispherical charges detonated on a ground surface would result some energy be lost through cratering. A shape factor of 2 in this instance would be conservative, however the aforementioned work presented a realistic factor of 1.8. This has been integrated within design code and are validated for spherical and hemispherical charge[135]. These simplistic scenarios are fundamental to continue the understanding into both detonation and shock wave mechanics. Although uncommon within real-world blast application, without a robust knowledge on the behaviour of blast loading in simplistic scenarios, confidence in the understanding of non-spherical explosive detonation will never be established.

2.6 Semi-Empirical Prediction Methods

2.6.1 Positive Phase Parameters

As mentioned previously, Taylor[167], Brode[19] and Granstrom[66] were the pioneers of explosive shock wave prediction. Their developing theories which assumed instantaneous energy release at a infinitesimal small point source captured the behaviour of simple explosive scenarios. These however were not perfectly applicable for use when considering the effects loading as on infrastructure[126].

There has been significant research since, expanding the fundamental understanding of explosive events alongside characterising resulting blast wave features through experimental analysis[85]. Baker[7], Remennikov[123] and Esparza[45] all provide summaries of contemporary and historical experimental quantification of blast parameters.

Discussed in more detail within Section 2.9.2, is this history around the quantification of blast loading and the effects imposed on structures. The broad range of works investigating high explosive detonations was collated by Kingery and Bulmash[87], whom presented high-order polynomial relationships which capture the explosive behaviour of spherical and hemispherical TNT detonations across scaled distances spanning from the edge of a explosive charge, out to around Z$\simeq$ 40m/kg$^{1/3}$. It is notable that the data collected was a combination of both direct measurements, in the far-field region, and inferred measurements from tracking smoke trials[37]. This was supported with rudimentary numerical analysis, in the near-field[19], therefore holding this region in doubt of its fidelity.

The high-order polynomial relationships only exhibit the behaviour of TNT detonations across a scaled distance range and therefore should not be mistaken for a representation of a physical mechanism directly. With this being said, the relationships are usually summarised and used as a set of well defined curves, as presented in Figures 2.10a-b.

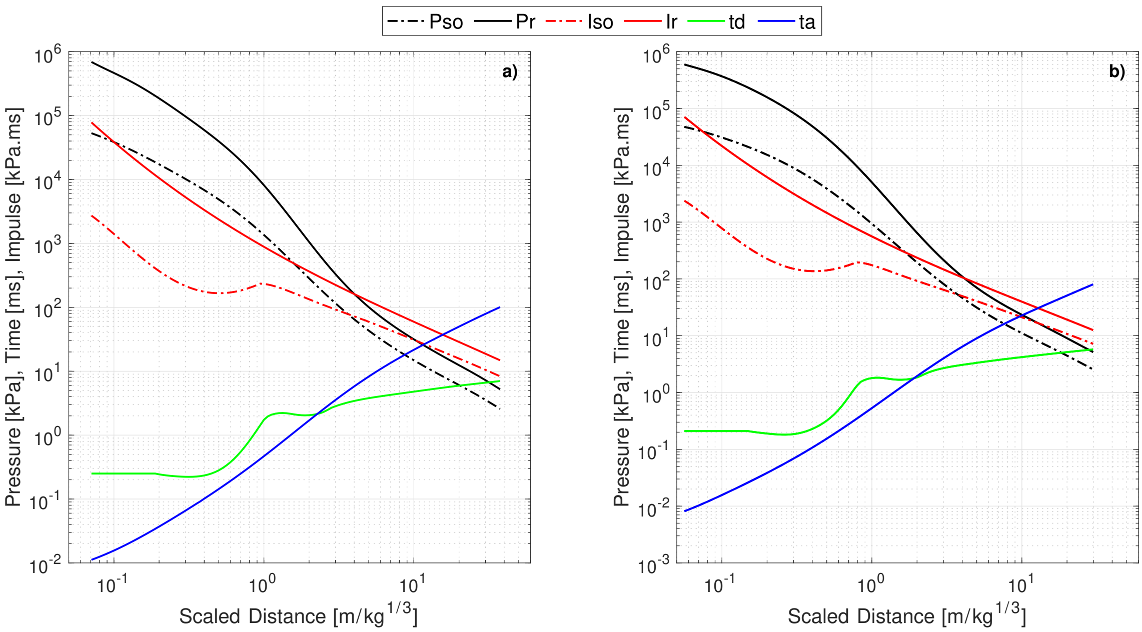

Figure 2.10: The semi-empirical curves for incident and reflected positive phase blast wave parameters for a 1kg TNT explosive detonation with respect to scaled distance, established by Kingery and Bulmash[87]: a) Hemispherical charge of TNT detonated of a ground surface, b) Spherical charge of TNT in free air.

2.6.2 Negative Phase Parameters

The positive phase of a blast event is reasonably understood in terms of the underlying fundamental physics. Vast quantities of experimental and numerical work have been conducted to characterise and quantify the associated blast parameters and to validate empirical predictions, as discussed in Section 2.9. Whilst negative phase parameters are available in literature and blast related design manuals[176], Bogosian et al.[13] presented scepticism of the associated empirical curves due to the original data source being unclear. Rigby[126] undertook a thorough review of available historical literature and highlighted the work by Granstrom[66] to be the likely source of data used to develop the empirical curves, seen in Figure 2.11. This is defined as the 'Cubic Negative' curve fit approximation (detailed in the second case of Equation 2.6).

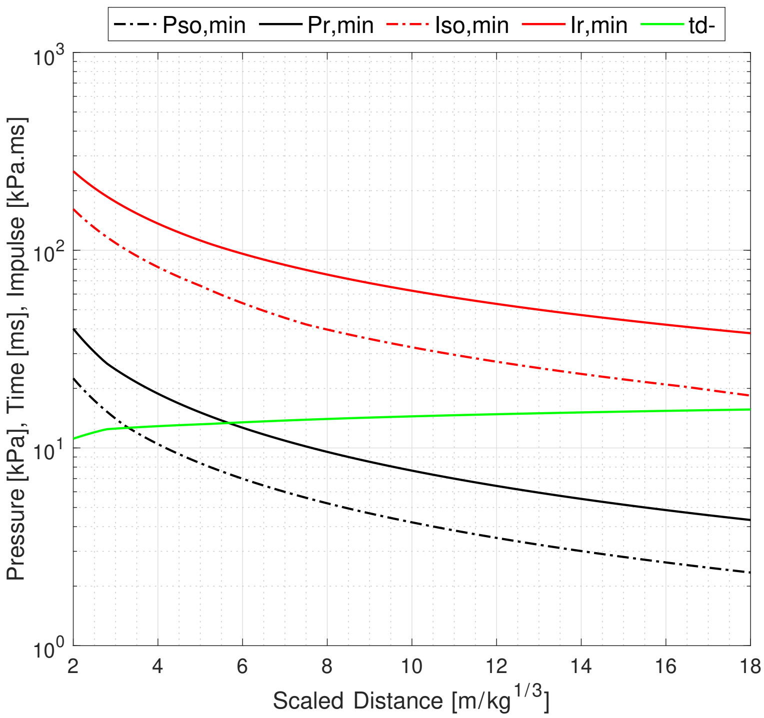

Figure 2.11: The semi-empirical curves for incident and reflected negative phase blast wave parameters for a 1kg TNT explosive detonation with respect to scaled distance, established by Granstrom[66]: a) Hemispherical charge of TNT detonated of a ground surface, b) Spherical charge of TNT in free air.

There is however, limited validation of the negative phase on the whole with many researchers historically omitting their effects due to the associated parameters being orders of magnitude lower than the positive phase. The physical mechanisms ongoing during this time of lower pressure in reality can still pose some serious threats to infrastructure and civilians.

$$P_r(t) = \begin{cases} P_{r,max}(1 - \frac{t}{t_d})e^{-b\frac{t}{t_d}}, & t{\leq}t_d. \\ -P_{r,min}(\frac{6.75(t-t_d)}{t_d^-})(1 - \frac{(t-t_d)}{t_d^-})^2, & t_d < t \leq t_d + t_{d-}. \end{cases} \tag{2.6}$$

2.7 TNT Equivalence

The mass term, W, referred to throughout this section is actually the equivalent charge mass in kilograms of trinitrotoluene (TNT), which is widely accepted as the benchmark in explosive characterisation. Discussed in more detail with Section 2.9.2, the quantity of TNT free-air testing which has been conducted over a multiple decades. These were collated by Kingery and Bulmash[87] and used to develop semi-empirical predictive curves for 1kg TNT explosives, shown in Figures 2.10 and 2.11. Using these, the results of detonating explosives of differing compositions have been collated, with their masses scaled until predictions of 1kg of TNT are able to accurately capture the behaviour of an equivalent mass of the given explosive. This scaling factor is defined as the TNT equivalence, TNT_e.

The problem with TNT equivalence is mainly the lack of significant rigour associated with the testing methodologies adopted for establishing the parameter. Cooper[30] outlined in the overview on TNT equivalence that historically there have been various and widely different testing methodologies to estimate the factor, all of which exhibit their own uncertainties. This is a direct cause of the published spreads in TNT_e for nominally identical charge masses and compositions tested, and therefore the same energy release. It is noted, that in the extreme near-field, where the recorded blast parameters are highly proportional to the fireball chemistry, different explosive compositions will exhibit a varying TNTe as a result different chemical de-combustion[81,151]; a finding which was verified by Shin et al.[149].

Further justifying the sensitivity of detonation characteristics in the near-field was works presented by Simoens and Lefebvre[152]. A variety of experimental trials highlighted how the detonator position, and thus the associated detonation process, caused variations in pressure recordings but impulse effectively stays constant. This is due to impulse being directly related to the overall energy released during detonation. If using impulse as the only measuring parameter for TNT equivalence, the theory proposed by Taylor[167,168,169] on explosives being theorised as infinitesimally small points of energy release would hold credibility.

Far-field scenarios, the region is which the shock wave detaches from the fireball and therefore no longer influenced by the ongoing thermochemical combustion reactions, there is presently no physical explanation for TNT equivalence to vary. Dewey[38] used high speed video techniques to track a propagating shock wave resulting from a hemispherical propane-oxygen explosion and converting its velocity into the shock waves pressure through Rankine-Hugoniot relationships[7]. A constant TNT equivalence value within the far-field range, $Z>3\text{m/kg}^{1/3}$, was evaluated. Similar findings have been presented when conducting both well-controlled PE4 explosive trials in far-field regimes and comparing them to high fidelity numerical simulations, both converge on a $\text{TNT}_e \simeq 1.2$[132,135]. However despite a broad range of published literatures attempting characterise this factor for different explosives, there is no widely accepted methodology of establishing TNT_e[32]. Some authors exhibiting large variation in TNT equivalence across an entire scaled distance rather than variability being confined to the near-field domain[56].

The TNT equivalency factor of an explosive composition is highly related the variability associated in experimental data captured. It therefore requires further investigation to establish whether all explosives can be defined by an equivalent mass of TNT, or whether variations are inherent of explosions.

2.8 Blast Variability - Real or Systematic?

Explosive testing within the available literature provides a wide variety of methodologies for undertaking experimental blast work and the analysis of the resulting data. However, varying conclusions regarding the output yield a given explosive has when detonated a certain distance from a target, alongside the associated variability it exhibits between nominally identical tests, have been made. There is therefore a necessity to further improve current practices and develop new techniques for experimental testing and data processing to ensure the fundamental understanding of shock wave propagation is fully understood. Clearly, if blast experiments are viewed as naturally varying, approximate, and even first-order in nature, then our ability to rigorously validate numerical modelling approaches is hampered. This clearly has negative connotations for the use of modelling tools for design. It is important to fully understand the nature of blast parameter variability, and its dependence on extrinsic features such as experimental set up, control, and interpretation of data. The contention around this subject matter however poses a clear need for defined experimental procedure which adopt precision. These require validation to encouraging a movement towards an acceptable experimental and analytical standard which provides a consistency in resulting blast parameters from explosive testing.

Whilst any published article will defend and justify its findings, multiple contrasting conclusions regarding explosive variability from similar testing regimes, cannot all be scientifically correct. The philosophy around research in modern times, for blast engineering in particular, has seemingly moved away from critically analysing why certain data appears to exhibit particular trends, making links through tangible justification of fundamental physical mechanisms and principles. Instead, a more literal acceptance of recorded data is commonly taken. Inductively creating theories justifying the accuracy of the data regardless of the underlying physics required for the data to be valid.

The Falsification Principle, proposed by Popper[113], suggested that scientific theory should make predictions which can be tested, and the theory rejected if these predictions are shown to be incorrect. Adopting critical rationalism is something which enables science to hone in on realistic physical theories which is void of highly-controlled experimental data to falsify them. Take the paradoxical opinions in the blast community regarding consistency in blast parameters; what are the underlying reasons for why different research groups are experiences varying levels of consistency?

It is of great importance to establish the route causes for these conflicting conclusions and to develop best practices based on the findings. This chapter will access the features of a blast waves development as it propagates away from the source of the detonation. Through careful analytics, experimental procedures and improved methods of analysis are proposed for use across a range of idealised high explosive types.

2.9 Historical Review of 'Best' Practices

The measurement of shock wave data from explosive events has been of interest since the first explosion occurred, most probably around similar times as the invention and subsequent detonation of gun powder. The ability to release significantly large quantities of energy over small periods of time through detonation, created an interest in developing weapons to release shock waves of catastrophic capabilities[63].

With increasing interest into powerful energetics came extensive testing regimes which looked at detonating large quantities of various types of explosives. This required instrumentation to record characteristics of these events to provide a fundamental understanding of shock wave phenomena. Due to the threat severity of nuclear war at the time, instrumentation engineers and scientists were faced with an incredibly difficult task of recording the effects of equivalent blasts with limited resources and time constraints.

The development of best practice for blast damage and shock data capture is not something which came easy, and has taken many decades to establish reliable instrumentation in which these events can be recorded with the highest levels of precision. Shelton[145] documented that during the first nuclear tests conducted by the US, 'blast damage and shock data were obtained by two methods: those that were improvised by inquisitive scientists; and those that were measured by sophisticated instruments'. The creativity and innovation from the scientists working on these large scale trials are to be commended for having a well-rounded understanding of fundamental explosion physics enabling their efforts in effective instrumentation development. The iterative procedure of testing and modifying instrumentation over many years resulted in the technology available for us today. It is however important to establish the historical context of how these instruments came to be developed. This will help understand why the current methodologies adopted for testing results in sporadic data sets between nominally identical trials.

Reisler et al.[118] meticulously reviewed all available literature, both within the public domain and that which is classified. The article detailing the testing and development of systems which were capable of not only withstanding, but recording disastrous effects from nuclear explosions. The vast majority of devices deployed during these early tests were passive, inexpensive to produce and required minimal effort to deploy. These however, reported spreads in accuracy of shock wave parameters between 10-20% of the values numerically predicted. As the development of electronic transducers began, data could be recorded with respect to a time base, thus establishing a detailed understanding of the development of explosive shock wave phenomena from the instance of detonation. These transducer measurements were found to obtain accuracies of between 3-5% which showed vast improvements in the quality of data recorded despite their need to be coupled with electronic recording systems such as oscilloscopes.

This brings the thinking back to that discussed by Shelton [145], in that there was a skill, and in some scenarios improvisation, required to use these systems to record highly accurate data. The capabilities of these scientists to understand and predict what the effects of a given explosive should be, and testing their predictions against constantly evolving instrumentation provides definitive confidence in their research. It is safe to conclude that the instrumentation developed during the nuclear period was successful at capturing shock parameters with accuracy for long duration blast waves. Despite the era these instruments were developed, the quoted accuracy of between 3-5% when comparing recorded data to numerical models are within the similar regions to modern research programmes looking into high explosive detonations [135].

The use of high explosives for large scale blast phenomena analysis closely followed the initial ban on atmospheric testing of nuclear explosives in 1958. The reason for this was to provide effective simulations of a nuclear weapon's blast characteristics without the major environmental concerns of nuclear detonation. The majority of the instrumentation adopted for testing at the start of this era was that which were established during the nuclear testing era. This movement meant that measuring devices no longer required the need to be radiation-resistant but did require the response and recording rates of gauges to be considerably faster relating to much shorter shock wave durations associated with high explosives [8]. Reisler et al. [119] again provided a comprehensive overview of the development of instrumentation during this period. Detailed was how the state of the art recording systems for electronic gauges progressed from the 20-40 kHz frequency of recordings range to 500 kHz through the use of digital recording systems which are still used today. This still achieved the high accuracy recorded data when compared to numerical models.

Blast related research placed greater demands on data capture systems to provide increased frequency response whilst upholding precision in the data. However, greater temporal accuracy of recordings does not necessarily result in consistency and reliability of recorded data from repeat trials. The knowledge of what an experimental trial is aiming to accomplish and an understanding of the physical processes any given instrumentation uses to capture the data is paramount for achieving reliable and accurate data. When reviewing the quality of published works between the start of shock wave quantification in the 1940‘s all the way through to modern times, there is a clear discrepancy in the results published which requires investigating.

2.9.1 Data Capture between 1950 - 1980

Corresponding to the era in which instrumentation was being constantly tested and improved, the research undertaken into blast phenomena produced some of the more widely-regarded data sets which helped develop semi-empirical prediction tools for free-air blast scenarios[87]. This well-known method utilises poly-logarithmic curves fitted to the compilation of both rudimentary numerical analysis results and experimental measurements ranging from small to large scale events (< 1kg to >400,000 kg). These semi-empirical curves are generally accepted standard practice for predicting blast loads from a given explosive mass at a given distance from the target. As a result, the KB method has been implemented into the UFC-3-340-02 design manual[176], the predictive computer code Conwep[76,77], and commercial finite element code LS-DYNA[116].

Figures 2.12a-d present experimental recordings from TNT charges with masses between $0.45 - 450,000kg$, which were spherical and hemispherical in shape, recovered from 22 individual references dated between 1940 and 1980 (of which were discovered in Reisler et al.[119] and documented in Table 2.1, The data points have been scaled to an equivalent hemispherical shape, if required, using a shape factor of 1.8[76,77], and 1kg in mass to compare accordingly with KB predictions. Despite a low amount of anomalous results, the four positive phase parameters compare well with the KB curves and are fairly consistent across the entire tested scaled distance range. It is worth noting that Kingery and Bulmash[87] made use of some of the presented data in order to produce the high order polynomial predictive curves, so whilst this comparison is self-referential, it does highlight the general consistency of the measured blast parameters during this era across a full range of charge masses and distances.

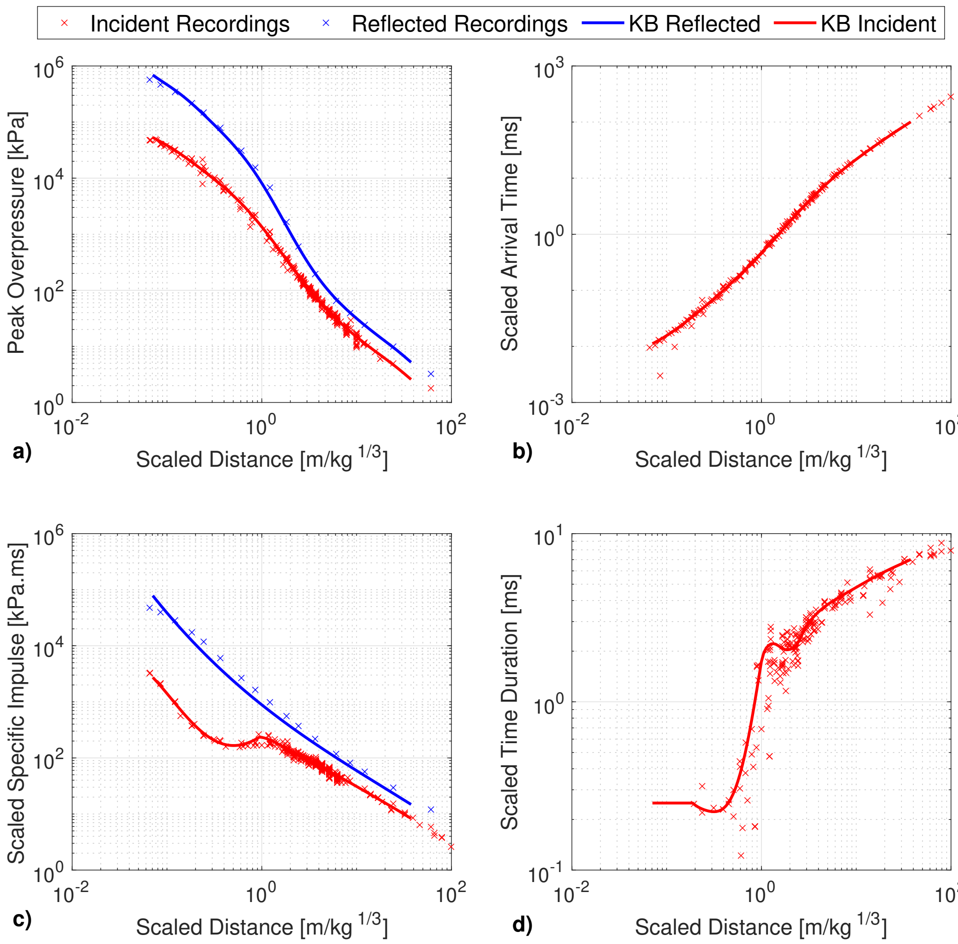

Figure 2.12: Compiled blast parameters from TNT explosive trials with varying mass as a function of scaled distance, which has been scaled to a 1kg equivalent hemispherical charge, using a shape scaling factor of 1.8 and compared with KB predictions: a) Peak overpressure, b) Scaled peak specific impulse, c) Scaled arrival time, d) Scaled positive phase duration

Figures 2.13a-d again present experimentally recorded blast parameters when detonating Pentolite - another commonly-used high explosive at the time. A variety of smaller scale masses of between 0.1-3.8kg, of which a collection of spherical and hemispherical charges were used. The raw data was scaled accordingly to be equivalent in shape and size to a surface burst 1kg hemisphere of TNT. The data presented was extracted from 6 individual references, detailed in Tables 2.1 scaled to an equivalent TNT explosive using a TNTe =

1.2. This value is in line with averages for both pressure and specific impulse in far-field scenarios evaluated by Shin et al.[149].

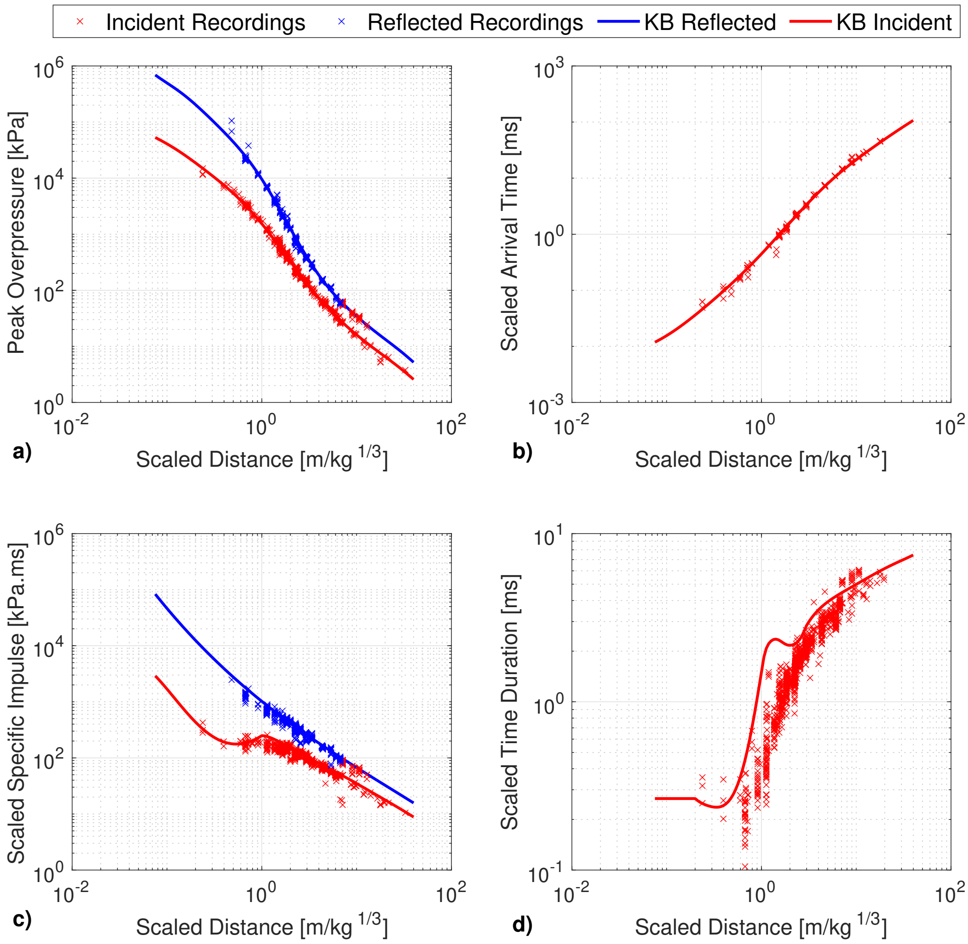

Figure 2.13: Compiled blast parameters from Pentolite explosive trials with varying mass as a function of scaled distance, which has been scaled to a 1kg equivalent TNT hemispherical charge using a shape scaling factor of 1.8, and a TNTe = 1.2 (Shin et al.[149]), comparing to KB predictions: a) Peak overpressure, b) Scaled peak specific impulse, c) Scaled arrival time, d) Scaled positive phase duration

The consistency in this data is much the same as that presented in Figures 2.12a-d and holds good agreement with the KB predictions. These two extensive data sets provide reasonable evidence to support the hypothesis that explosive positive phase parameters are predictable for ideal high explosives across a range of charge sizes and scaled distances. It is also important to note that, although not perfect for every single data point, a single TNTe value can be used to establish a generalised equivalent behaviour of ideal explosives. This does however begin to exhibit higher variations at small scaled distances, $Z<1m/kg^{1/3}$.

It is a reasonable conclusion to make that for far-field scenarios, Z>3m/kg$^{1/3}$, where the propagating shock wave has detached and is no longer effected by expanding fireball features, the positive phase blast parameters are consistent and can be defined by a single TNTe value.

Reference	**Explosive Type**
Granstrom [66]	TNT
Ammann and Whitney [2]	TNT
Dobbs et al. [40]	TNT
Fisher and Pittman [54]	TNT
Shear and Wright [144]	TNT
Kingery and Pannill [89]	TNT
Groves [69]	TNT
Smale and Sigs [155]	TNT
Chabia et al. [25]	TNT
Shear and Day [143]	TNT
Kingery [86]	TNT
Reisler et al. [121]	TNT
Reisler et al. [122]	TNT
Davis et al. [35]	TNT
Swisdak [163]	TNT
Esparza [44]	TNT
Kingery and Coulter [88]	TNT
Rudlin [137]	TNT
Fisher [53]	TNT
Weibull [178]	TNT
Lutzky [95]	TNT
Reisler et al. [120]	TNT
Esparza and Moroney [46]	Pentolite
Johnson et al. [83]	Pentolite
Kingery and Coulter [88]	Pentolite
Sultanoff and McVey [162]	Pentolite
Goodman [64]	Pentolite
Goodman and Giglio-Tos [65]	Pentolite
Hoffman and Mills [73]	Pentolite

Table 2.1: Reference list for historic data extracted from within this era for both spherical and hemispherical TNT and Pentolite detonations.

2.9.2 Data Capture between 1980 - Today

The accuracy of the KB method has been questioned over more recent years. Paradoxically, it would seem that with more modern and precise experimental procedures, the results should exhibit a reduction in uncertainty and an improvement on the precision. Many contemporary researchers have however reported a significant lack of repeatability in experimental measurements when comparing directly to KB parameters, and the much older data sets used to produce them.

Bogosian et al.[13] utilised an extensive experimental database of recorded explosive parameters and compared it with KB predictions of similar explosives. Typical uncertainties of between 70–150% and 50–130% for peak pressure and specific impulse respectively from nominally identical far-field ($1<Z<40\text{m/kg}^{1/3}$) tests were presented. Similar levels of uncertainty have been found in related studies, with the general observation being a reduction in uncertainty as distance from the charge increases[16]. Formby and Wharton[56] explored the TNT equivalence of a variety of hemispherical explosive compositions with the results demonstrating relatively high levels of variability: ±30% and ±15% for pressure and specific impulse respectively. These recordings were at large scaled distances, leading to a general impression that there will always be some degree of randomness in blast pressure measurements[156].

In Figure 1 of the article presented by Formby and Wharton[56], a site layout including pressure gauge position and height, in relation to explosive centre, was presented to highlight terrain features and large changes in surface height. The authors note that the presence of these features could influence the recorded data through inducing both wave reflection and/or shielding yet continue to suggest the yield of an explosive varies with scaled distance in a free-air scenario. Borenstein[18] performed a sensitivity study of blast parameters taken from the 303 individual measurements discussed in Bogosian et al.[13] and highlighted that these comprised of different explosive shapes, sizes and composition and were scaled directly to TNT as a collective. This resulted in quantification of a more extrinsic representation of blast parameter variability, which the authors seemingly incorrectly attributed to the inherent randomness of explosives.

Stoner and Bleakney[160] reported data recorded from free-air tests, using a variety of charge shapes, sizes and compositions. When separated into nominally identical test groups and analysed, the results presented much lower levels of variability in pressure, between ±0.6–6.5%, again with the observation that variability reduced with an increase in scaled distance. Esparza[44,45] presented blast parameter results from a variety of high explosive compositions. Despite not quantifying variability in the recordings, visually the data holds agreement with itself for nominally identical tests.

Tang et al.[164] also undertook a variety of incident and reflected measurements from a range of PE4 masses, formed into spherical and hemispherical charges, resulting in similar magnitudes of variability quoted by Stoner and Bleakney[160]. This experimental data was compared against both KB predictions and hydrocode numerical simulator, Air3D, which presented reasonable levels of agreement for medium to large scale charges[165]. Reflected data agreed signifcantly better to KB predictions than incident pressures justified to be a result of the difficulty in recording purely incident shock waves. Rickman and Murrell[125] and Tyas et al.[175] conducted well controlled small-scale experimental high explosive testing using pressure transducers which provided comparable results to KB predictions for normally reflected conditions at far-field scaled distances.

Ohashi et al.[108] made use of optical methods to record shock wave propagation of small-scale explosive tests with varying masses. The article presented a method of converting radius-time data into incident pressure of a given shock wave using Rankine-Hugoniot jump conditions. The results of this analysis, when scaled, provided remarkably low variability between tests and also compare well with KB predictions.

The articles mentioned show the other contrasting opinion of the blast industry in that KB predictions are incredibly accurate, and that variability between nominally identical tests should be minimal. Rigby et al.[135] gave an in-depth literature review of articles which discuss experimental variability of far-field blast parameters and how they compare with the KB predictions. Systematic experimental and analytical errors are suggested to be the reason as to why such high levels of variability have been documented, rather than inherent randomness of explosive events. In an attempt to tackle systematic analytical variability, the authors used an exponential 'Friedlander' curve fitting method to determine blast parameters from each experimental trial in an unbiased manner.

The results showed very good test-to-test consistency across the measured blast parameters (arrival time, reflected peak overpressure, and reflected specific impulse) typically within a range of ± 2.5% (arrival time) and ± 6–8% (pressure and impulse) of the mean values for each set of repeat tests. The recorded positive duration was the only parameter to exhibit higher levels of variability with all but one value achieving a ± 9% range of the mean value. Positive phase duration typically exhibits higher levels of experimental spread due to the difficulty in determining when overpressure returns to zero when signal noise is present[96]. No signal will ever be perfectly noiseless, and therefore the positive phase duration will always carry an enhanced level of uncertainty. Errors or uncertainties in this parameter contribute very little to the overall loading, since a curve fit can always be tailored with a different decay parameter in order to match a prescribed specific impulse value. Hence, studying sources of uncertainty in positive phase duration are of lesser importance and will not be considered further.

Chiquito et al.[27] and Bogosian et al.[14] both used similar methods of functional fitting curves to experimental data, and both presented results exhibiting enhanced consistency and reduced subjectivity of analysed blast data. The analytical techniques proposed account for errors during the post processing section of the testing but not account for any systematic errors which may have been introduced into the experiments during test setup.

The aforementioned articles and resulting data presents a clear divide in the blast community in whether it is reasonable or not to accept free air far-field blast parameters as inherently variable. As stated by Borenstein[18], there are clear reasons as to why extrinsic and intrinsic sources of variability should be considered:

1. The generalised real-world application of predicting explosive parameters which include safety factors and variability margins accounting for the unpredictability of explosive size, shape, composition and separation distance from a target (extrinsic).
2. The specific, scientific approach of assigning precise loading characteristics for a particular charge shape, size and composition and looking at how removing those as independent variables results in increased consistency (intrinsic).

This provides an important, but seemingly overlooked steer to the blast research community: in order to produce robust and reliable models that account for *extrinsic* variations in blast properties, it is imperative to understand and be able to quantify *intrinsic* sources of variability. This is where well-controlled scientific testing and processing can make significant contributions to our understanding of, and ability to predict, blast load parameters from *known* explosive sources.

2.10 Non-Ideal Explosive Characterisation

When reviewing the last 50 years of both accidental and intentional terror related large scale explosive events, presented in Table 2.2, there has been an large number of lives lost, people exhibiting significant injury and money spent to remediate the destructive effects. Whilst the information presented in Table 2.2 does not cover every instance of explosive event across the world, it provides a range of masses and types of explosives causing catastrophic effects.

Non-ideal explosives are common across the vast majority of events listed. Home-made compositions, such as ANFO, are the weapon of choice for most terror related threats due to the relative ease and low costs associated with acquiring their constituents. The accidental explosions noted in Table 2.2 were a direct result of stockpiling large quantities of material which does foster the ability to detonate under extreme circumstances of pressure and temperature. Take the most recent example which discusses the explosion of approximately 2750 tonnes of AN following a fire in the warehouse where it was being stored[131].

In 1963, the Nuclear Test Ban Treaty was enacted, which prohibited the detonation of nuclear weapons for any form of research. This caused problems for departments of defence and security across the globe due to an essential requirement to better understand the effects of devastating explosions on both military and civilian infrastructure. Large scale trials were conducted using TNT-stacked charges and provided data which is held in high regard for its accuracy (see Chapter 4), and was used to develop fast-running empirical models still used today[87]. This data was the pinnacle of blast data capture for its time and has provided insights into the fundamental mechanisms and characteristics of explosive shock waves. Through vast quantities of research making efforts towards quantifying and characterising other ideal high explosives (such as Pentolite, PE4, PE8, PE10 etc) across an entire range of scaled distances, numerical simulations have been extensively validated.

The problem with testing regimes using ideal explosives is the cost associated with the large-scale trials and so an inexpensive and readily-available alternative in ANFO, was investigated to compare directly with tests conducted using TNT, and nuclear weapons prior[112]. Large scale trials were conducted from the 1970s onwards, making use of hemispherical charges with masses ranging between 18,000-572,000kg, boosted with various compositions of explosives at such small percentages of the overall mass they were considered negligible[61,62,112,138,139]. The findings from these tests began to characterise the general behaviour of ANFO as an explosive used alternatively and led to an empirical TNTe=0.82[112].

As previously mentioned, an ideal detonation is one in which its temporal characteristics of velocity, time and pressure match those of which can be predicted through theoretical evaluation. Assuming a planar detonation in an infinite diameter charge, the detonation process would be independent of reaction zone size, in which case the detonation wave would propagate at a maximum theoretical value within the charge Horie[75]. In reality, charges with a finite diameter are dependent on reaction zone, of which large ones result in larger losses of energy and thus detonation performance. For every explosive composition there is a thermodynamic break point at which the diameter is so small detonation cannot be sustained, denoted by the critical diameter C_d. Ideal explosives are described to exhibit small reaction zones and thus compare well to theoretical predictions of temporal characteristics. Non-ideal explosives, such as ANFO, are known to have much larger reaction zones - in the order of 100mm[29]. Scott[142] suggested that explosive compositions with large critical diameters as a result of large reaction zones, require much greater masses to achieve steady detonation which compare to theoretical values. Despite this knowledge, the findings from the large scale testing of ANFO when collated by Petes et al.[112] influenced the idea that the non-ideality of ANFO was irrelevant as a seemingly constant TNTe was assigned to the composition.

Figure 2.14 contains a compilation of data from 7 different testing regimes (see Table 2.3), 6 of which are large scale hemispherical and spherical ANFO trials in free field scenarios and the2 containing smaller mass regimes. It is important to note that whilst the

Year	Event	Explosive	Estimated Mass [kg]	Effects
1970	Sterling Hall Bombing (Madison, USA)	ANFO	~100	57 I, $13.6million
1983	Beirut Barracks Bombing (Beirut, Lebanon)	PETN	~9000	307 D, 150 I
1983	US Embassy Bombings (Beirut, Lebanon)	ANFO	~900	63 D, 120 I
1992	St. Mary Axe Bombing (London, United Kingdom)	Semtex	~45	3 D, 91 I
1993	World Trade Center Bombing (New York, USA)	Urea Nitrate	~600	6 D, 1042 I, $65 million
1993	Bishopsgate Bombing (London, United Kingdom)	AN/Sugar	1000-2000	1 D, 44 I
1995	Oklahoma City Bombing (Oklahoma City, USA)	AN/NM	~2500	168 D, 680 I, $652 million
1996	Manchester Shopping Mall (Manchester, United Kingdom)	AN/Sugar	~1500	212 I
1996	South Quay bombing (London, United Kingdom)	AN/Sugar	~1500	1 D, 44 I
1996	Khobar Towers Bombing (Khobar, Saudi Arabia)	C4	~2300	19 D, 498 I
1998	US Embassy Bombings (Tanzania, Kenya)	Equivalent TNT	~900	224 D, Over 4000 I
2000	USS Cole Bombing (Aden, Yemen)	Equivalent TNT	~450	17 D, 40 I
2000	**Enschede fireworks disaster (Enschede, Netherlands)**	**Equivalent TNT**	**~4000**	**23 D, 1000 I**
2002	Bali Nightclub Bombing (Bali, Indonesia)	KCIO3/S/AI	~1000	204 D, 209 I
2003	Marriott Hotel Jakarta Bombing (Jakarta, Indonesia)	KCIO3/S/AI	~50	12 D, 150 I
2003	British Consulate Bombing (Istanbul, Turkey)	AN/Al	500-1000	59 D, 750 I
2003	Casablanca Bombings (Casablanca, Morocco)	TATP/AN	5-10	45 D, 100 I
2004	Australian Embassy Attack (Jakarta, Indonesia)	KCIO3/S/AI	500-1000	9 D, 150 I
2004	US Embassy Attack (Tashkent, Uzbekistan)	AN/Al	5-10	2 D, 9 I
2004	Madrid Train Bombings (Madrid, Spain)	Dynamite	5-10	193 D, 2050 I
2005	7/7 Underground Bombing (London, United Kingdom)	HP/BP	5-10	52 D, 770 I
2008	US Embassy Attack (Sana'a, Yemen)	Equivalent TNT	~50	18 D, 16 I
2011	Oslo Bombing (Oslo, Norway)	ANFO/Al	~1000	77 D, 319 I
2013	Boston Marathon Bombings (Boston, USA)	Equivalent TNT	5-10	3 D, 280 I
2013	**West Fertilizer Company explosion (Texas, USA)**	**AN**	**7500-10,000**	**15 D, 160 I**
2015	Paris Attacks (Paris, France)	TATP	5-10	137 deaths, 416 injured
2015	**Tianjin explosions (Tianjin, China)**	**AN**	**~800,000**	**181 D**
2016	Brussels Attacks (Brussels, Belgium)	TATP	15-20	35 D, 340 I
2017	Concert Bombing (Manchester, United Kingdom)	TATP	Unspecified	23 D, 107 D, £13 million
2020	**Beirut explosion (Beirut, Lebanon)**	**AN**	**~2,750,00**	**Over 200 D, Over 6500 I, $10-15 billion**

Table 2.2: Historical explosive events across the world noting the explosives which detonated and the overall effects associated adapted from National Academies of Sciences and Medicine[105]. The events noted in bold are accidental whilst the rest are terror events with D and I corresponding the Deaths and Injuries respectively.

data extracted from Carton[22] is presented, the charge shape used was flat and square, detonated in one corner rather than centrally which introduces complexity. The lower values of TNTe extracted have been directly related to irregularities in the detonation mechanics. This occurred due to the variety of geometrical differences this methodology included when comparing to results from a centrally detonated spherical or hemispherical charge. Sherkar et al.[146] explained that charge shape needs to be taken into consideration when regarding resulting blast parameters, provided standoff distance from the detonation point is less than 35 charge diameters. Past this standoff the effect of charge shape can be ignored. The lower two values of TNTe extracted from Carton[22] were measured at much closer standoff distances than the quoted 35 charge diameter. They were therefore omitted from any further analysis to avoid any reasonable doubt relating to charge shape and detonator position.

Reference	**Explosive Type**
Sadwin and Swisdak[139]	ANFO
Carton[22]	ANFO
Gitterman and Hofstetter[62]	ANFO
Giglio-Tos and Reisler[61]	ANFO
Petes et al.[112]	ANFO
Figuli et al.[52]	ANFO
Edwards[42]	ANFO

Table 2.3: Reference list for historic data extracted for both spherical and hemispherical ANFO detonations.

Clearly shown from the Petes et al.[112] data alone is that once above a mass of around 120kg, ANFO behaves with a seemingly constant TNTe=0.82. This finding was related to a stable detonation and having an average detonation velocity of around 4200m/s (∼80% of that of TNT). For charges smaller than 120kg, the results suggested that the charge diameter was not large enough to permit steady state detonation conditions, thus resulting in lower equivalence values. This information seems to have been lost in time, with more modern approaches towards quantifying the effects of smaller-scale ANFO both experimentally[22,27,52] and numerically[67,68,157] making reference to equivalency features relating to larger scaled charges. Instead an approach which determines a non-steady detonation state of ANFO and the resulting blast parameters for smaller charges is necessary.

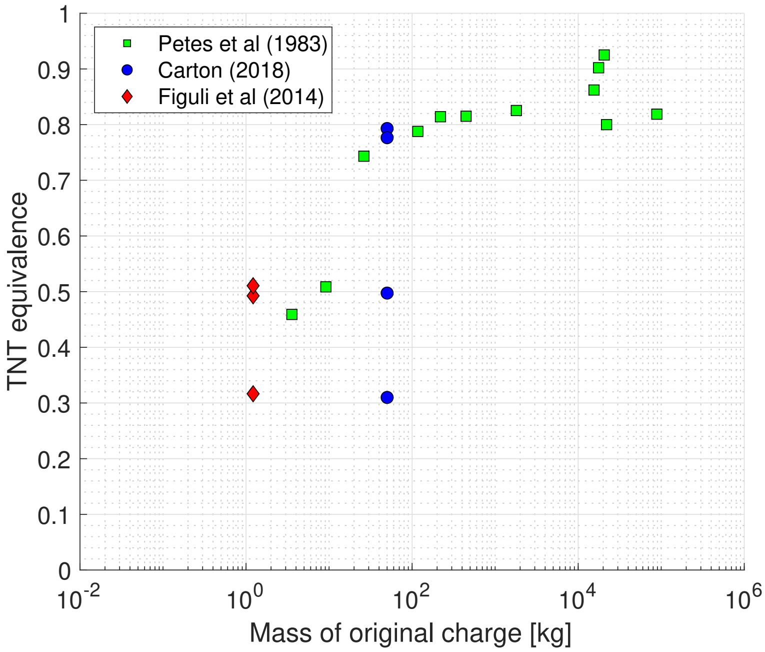

Figure 2.14: Pressure evaluated TNT equivalence ratio for unconfined ANFO with respect to the mass of the charge extracted from Petes et al.[112]*, Figuli et al.*[52] *and Carton*[22]

The data from the aforementioned reports of large scale trials has been compiled for the purpose of validating the assumption that constant TNTe across all scaled distances and masses of charge was made shown in Figures 2.15a-d. The raw data points have been scaled to an equivalent hemispherical shape, if required, using a shape factor of 1.8[76,77], and 1kg in mass of TNT using a TNTe=0.82, as defined by Petes et al.[112], to compare accordingly with KB predictions. It is clear to see the data presented across all positive phase parameters agree remarkably well with the aforementioned KB predictions when scaled appropriately. This finding suggests that whilst non-ideal explosives are considered to have different time scales associated with their detonation chemistry, that once a certain scale is reached they behave like an ideal explosive with consistent comparisons to TNT. This provides validation to[167] who suggest the theory that all explosive detonations can be considered as point source energy releases, with localised variations, reaching an equilibrium at a given distance away from the explosive centre.

There is a reasonable increase in the variability of data at smaller scaled distances, similarly to the ideal explosives in Figures 2.12a-d and Figures 2.13a-d. One safe assumption for this would be relating this directly to the variations in booster composition and size creating highly variable chemistry within the regions in which the fireball still has an effect on the resulting shock wave properties.

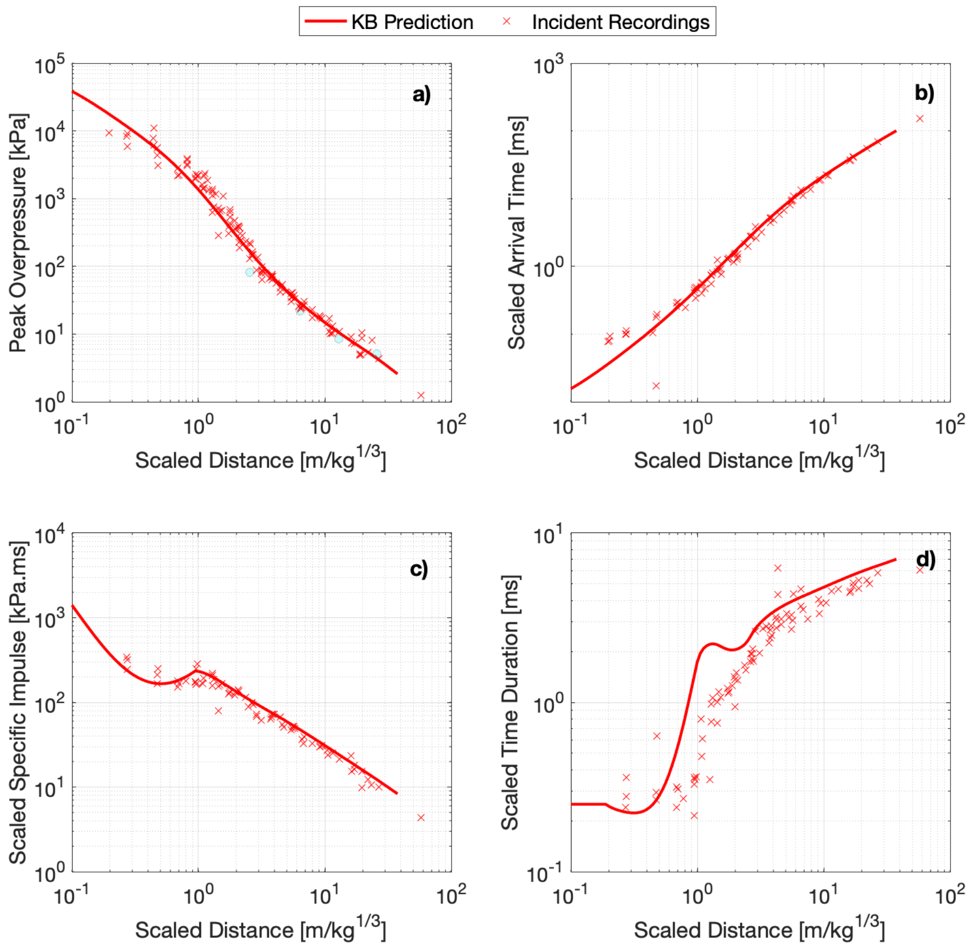

Figure 2.15: Compiled blast parameters from ANFO explosive trials with varying mass as a function of scaled distance, which has been scaled to a 1kg equivalent hemispherical charge, using a shape scaling factor of 1.8, a TNTe=0.82[112], and compared with KB predictions: a) Peak overpressure, b) Scaled arrival time, c) Scaled peak specific impulse, d) Scaled positive phase duration

Another justification could be related to the inconsistencies in ANFO used for the trials, again referring back to the discussion of introducing systematic errors into a testing regime in Chapter 3. ANFO comes in prill form, with a variety of sizes and fuel oil absorption variations. Without careful consideration of these parameters, explosive yields are speculated to vary. Considering the scale of the historically tested charges, the prill volume is assumed to be generally homogeneous exhibiting consistent characteristics, however when taking small samples, the composition would be heterogeneous.

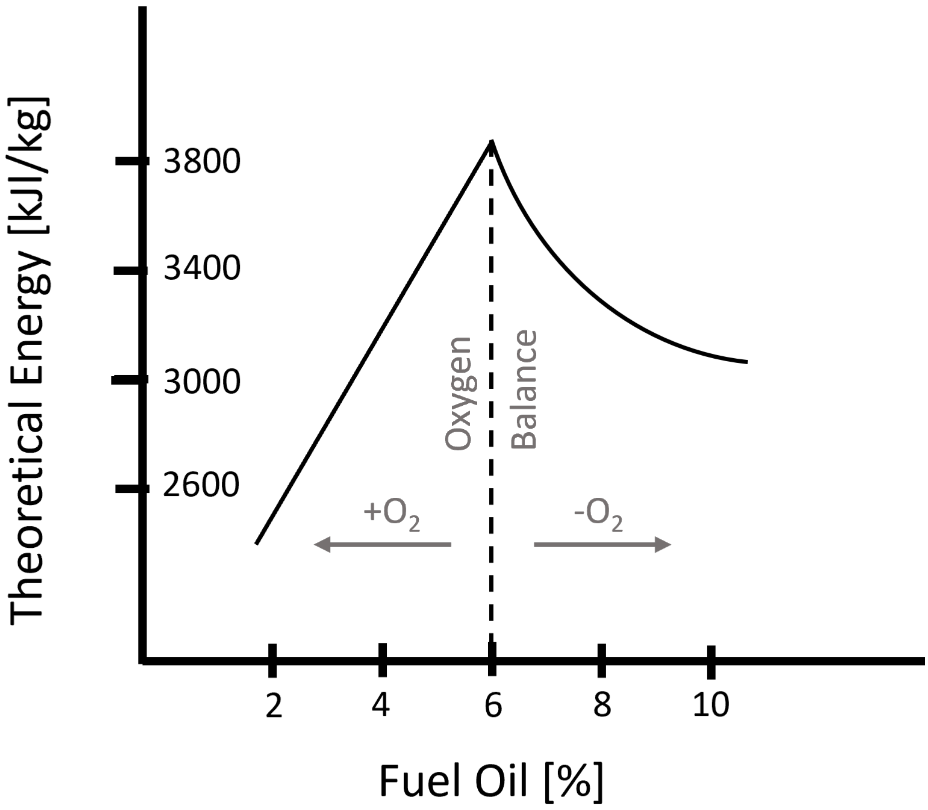

Figure 2.16: The theoretical energy of ANFO as a function of fuel oil content, adapted from Petes et al.[112]

Figure 2.16 represents the theoretical energy output and sensitivity of ANFO as a function of the fuel oil content. As detailed by Petes et al.[112], at 6% FO the composition is stoichiometric, meaning full potential energy release from both the AN and the FO is attained during the detonation process. From a thermodynamic standpoint, both oxygen rich and deficient compositions result in a reduction in the total detonation energy available, and therefore the percentage of FO has a major influence on the overall energy released. Whilst strict regimes of quality control may have been implemented, ensuring an accurate percentage of FO throughout the entire composition of the charges across each test would be difficult. With large scale charges, self-compaction and void collapse could result in displacement of FO within regions of the charge and therefore variations could be experienced.

Similar can be said for the prill size distribution. Dobrilovic et al.[41], McKay et al.[99], Petes et al.[112], Salyer et al.[140] all investigated varying the densities of ANFO charges to quantify how it affected velocity of detonation and other blast parameters. The findings suggested that generally larger prills are harder to detonate than smaller prills, and that a steady state detonation is only consistently achieved at bulk density of between 0.80-0.85g/cm^3). This means densities either side of this region would result in variations in detonation affectivity and thus the resulting blast parameters. In the larger scale charges, ensuring a constant bulk density throughout a charge would be incredibly difficult due to hydrostatic compaction of the lower layers of ANFO.

A further difference between ANFO and ideal explosives is the lack of binder, and therefore the overall density, and consequential air voids in a ANFO charge, are thought to be an influence on yields through meso-structural detonation mechanics. With large scale charges, self compaction of the charge would result in a more homogenous material and therefore a more efficient detonation process, comparing closely to ideal explosives. Smaller scale charges could begin to provide evidence to help the fundamental understanding of increased variability in ANFO compared to ideal explosives.

Despite ANFO being used both commercially in mining/quarrying processes, and a common explosive for terror threats, there seems to be little available published data characterising the explosive across a range of scaled distances for small charge sizes. Figuli et al.[52] undertook free-field ANFO explosive testing using 1kg spherical charges, which showed yields equating to a TNTe 0.32-0.51, different to figures used within numerical modelling strategies suggested by Sochet et al.[157] and Grisaro and Edri[67]. The lack of data results in uncertainties on how best to model and predict the blast wave properties emerging from detonations of small ANFO charges. Specifically, it cannot be definitively concluded if the TNTe value for ANFO is consistent across scales, or whether the reaction mechanics are affected by the physical length scale over which the detonation wave transits.

2.11 Summary

Whilst explosive characterisation has been investigated heavily over the last few decades, there is still no definitive conclusion on whether or not the associated parameters are deterministic. There requires a fundamental and somewhat crude review of experimental data capture and analysis methods to understand why there are discrepancies between researchers and to conclude on inherent variability of a given explosive. Standardised techniques are required to investigate the effects of different compositions with confidence. Whilst ever there are differences in experimental control, there is an expectation of variable data. This thesis aims at developing validated methods of characterisation for simplistic blast scenarios as a result of any given composition detonation. A comparison will be made between ideal and non-ideal explosives, which exhibit detonation behaviours on significantly different time scales.

Chapter 3

Standardising Experimental Methodologies and Analysis

3.1 Development of Experimental and Analytical Procedures

This chapter will detail how the experimental methodology used by the University of Sheffield has been modified and improved through the careful consideration of the control measures in place for each test and the results gathered from them. The improvements to the testing regime have been compared to historic data and numerical simulations to both co-validate the precision of experimental testing and the value of established numerical models. The aim of this chapter is to confirm the underpinning consistency of shock wave parameters through developing experimental and analytical techniques of data capture and processing respectively.

3.1.1 Preliminary Test Methodology

The far-field arena-style tests undertaken at the University of Sheffield (UoS) Blast and Impact Laboratory in Buxton, UK, has been a long established capability resulting in a number of blast quantification research articles[49,128,129,132–134,175]. Figure 3.1 displays the general arrangement that has been adopted for the far-field blast trials undertaken at Buxton, which makes use of two rigid reflective surfaces in the form of a reinforced concrete bunker 4m in height and a blockwork wall 2.20m in height, 4.46m in width, separated exactly 10.0 m apart. For each of the trials, hemispherical explosive charges, were formed using a 3D-printed mould (see Figure 3.2), and detonated at varying stand-off distances between the two walls.

Figure 3.1: General arrangement of the test pad at the University of Sheffield Blast and Impact Laboratory: Site photograph taken approximately from the location of the high speed video camera

Kulite HKM-375 piezo-resistive pressure gauges were used to record the reflected pressure-time histories in each test at both locations. The gauges were threaded through, and made flush to the surface of a small steel plate (approximately 110 × 150 × 10 mm) which was fixed to these walls. The plates were fixed to the two reflective surfaces, achieving a 10mm height from the centre of gauge to the ground surface level to ensure pressures recorded were normal to the charge. The charges were placed on a small steel plate (150 × 150 × 25 mm) prior to detonation, in order to avoid repeated damage to the concrete testing pad. The pressure was recorded using a 16-bit digital oscilloscope and TiePie software, with a average sampling rate of 195 kHz at 16-bit resolution. The recording was triggered automatically using TiePie's 'out window' signal trigger on a bespoke break-wire signal, formed by a wire wrapped around the detonator. The 'out window' trigger initiated with a voltage drop outside the normal electrical noise experienced in the break-wire. This coincides with the detonation of the charge breaking the circuit.

Figure 3.2: Photographs of the moulding stages of a 250g PE10 hemispherical charge in which the 3D printed mould is used to provide consistency in charge shape and density, which can be seen when removed from the casing.

High speed video (HSV) recordings of the propagating shock front were taken in an attempt to quantify the variability of shock wave arrival time recordings. As seen in Figure 3.3, the explosive charges were situated between a Photron FASTCAM SA-Z high speed video camera, fitted with a Tamron SP AF70 70-200 mm zoom (F2.8) lens, and a zebra board ran perpendicular to the blockwork and bunker walls. The camera was positioned to record the shock wave as it propagated towards the blockwork wall and had the charge location out of the camera's field of view to avoid excessive light from the fireball corrupting the contrast of the images. The camera was placed inside an armoured protective housing to avoid any fragment damage during testing.

A long-span zebra board served to provide a high contrast background such that distortions in light, caused by changes in refractive index of the propagating shock front, would feature as sharp dark bands in the HSV recordings. This allows the position of the shock front to be identified in each frame, and therefore enables wider-field arrival time measurements from a given trial[78]. The frame rates of the recordings and exposure time varied between 10,000–36,000 /s and 9.4–26.2 μs due to varying weather/light conditions. Frame rates and exposure times were altered before to each test in order to maximise the contrast of the zebra board stripes, and the sharpness of the propagating shock front. Through trial and error it was found that a maximum of 20 μs exposure time was allowed to achieve reliable data which exhibited minimal motion blur. If the lighting conditions meant that the video was not visible at this shutter speed or faster, then the data would be unreliable and therefore discarded from analysis. The resolution of the camera, when set to these parameters, was 1024 x 512 which resulted in an average pixel size of around 50mm for the far-field set up adopted. This resulted in a best possible accuracy of $Z=\pm0.075m/kg^{1/3}$ per pixel.

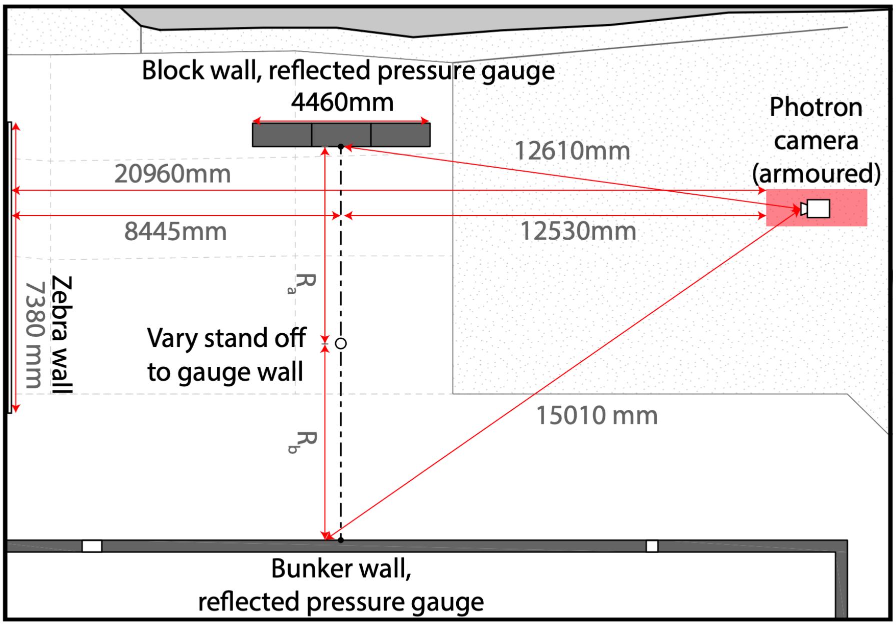

Figure 3.3: General arrangement of the test pad at the University of Sheffield Blast and Impact Laboratory: Schematic including HSV camera positioning

The experimental work undertaken aims at achieving the highest precision during trial setup which includes measurements of distance to a target, charge mass and shape consistency. Despite being well regarded, the adopted methods still incorporated both systematic experimental errors which had room for improvement alongside research dependant bias into the assignment of blast parameters for a given trial. It was important to establish methods for eliminating or minimising these errors as best as possible both analytically and experimentally. The implementation of new experimental capabilities and methods of analysis are discussed. Within the remainder of this chapter, analytical and experimental improvements will be denoted by **Ai** and **Ei** respectively.

3.2 Pressure Gauge Data

Detailed within this section is the discussion of experimental and analytical improvements made to testing regimes to ensure high fidelity data capture of free-air reflected blast parameters. The content outlines known systematic features within the adopted methodologies and aims to use fundamental knowledge of shock wave propagation, and its interaction with structures, to omit any errors and establish highly consistent data sets.

3.2.1 Analysis of Positive Phase (Ai)

The raw pressure-time histories from far-field shots, recorded at the University of Sheffield, have tended to exhibit large uncertainties in the opening few microseconds after the arrival of a shock. This has been associated with sensor ringing and smaller variations in natural electrical noise from the recording apparatus, as seen in Figure 3.4[135]. Precise determination of key blast wave parameters is therefore challenging and alludes to an emphasis on the importance of functional signal analytics for improved blast parameter characterisation[14].

The raw trend seen in Figure 3.4 shows reasonable levels of consistency to KB predictions, which initially provides justification to the quality of the semi-empirical tool for far-field shots. There are still some parameters which do not compare quite as accurately. Background electrical noise precludes accurate and automatic determination of the positive phase duration, t_d. This is the time it takes for the overpressure to return back to atmospheric conditions. This feature is due to a recorded signal oscillating around the origin for a non-zero period of time. For the data presented in Figure 3.4, the end of the positive phase would be prescribed as between $12.6 - 12.7ms$ and the positive phase time duration would be prescribed as $t_d = 2.7 - 2.9ms$ depending on where the analyst defines the parameter.

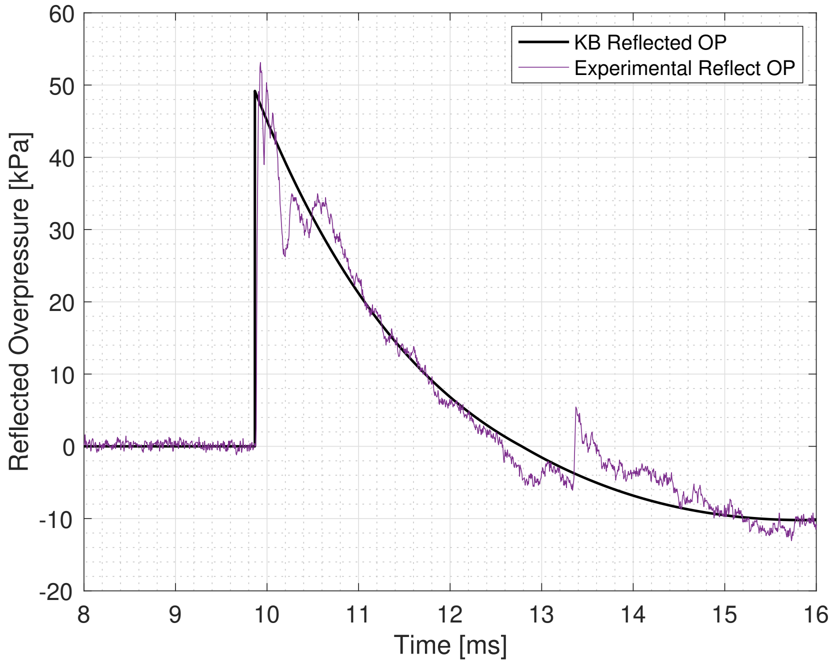

Figure 3.4: Example historic test results using a 250g PE4 hemispherical charge reflected pressure recording at 5 m stand-off compared to KB predictions for a 300g TNT hemisphere

Prior to any analysis or scaling being applied to the data, it is important to establish how nominally identical raw recordings compare. Figure 3.5 displays a compilation of as-recorded positive phase pressure-time history profiles for 250g hemispherical PE4 detonations at various stand-off distances. Since pressure was recorded at two stand-off distances for each tests (2m to the bunker wall and 8m to the blockwork wall in test 1, 3m and 7m respectively in test 2, etc.), the results from different tests but identical stand-off distances can be compared. Qualitatively, each pair of results are in excellent agreement, with minimal variations in the blast pressure histories. The raw peak pressures at 2m stand-off (Z$\sim$3 m/kg$^{1/3}$) exhibits a higher level of variability when compared to the other pairings. This is in agreement with the working hypothesis of enhanced variability in the regions described by Tyas[173], hypothesised to be due to Rayleigh-Taylor (1882, 1950d) and Richymyer-Meshkov (1969, 1960) surface instabilities.

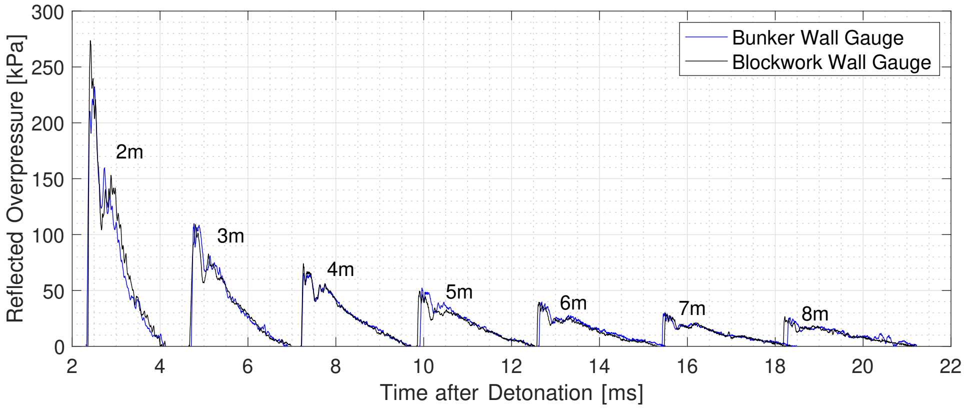

Figure 3.5: Compilation of the entire raw data set of 250 g PE4 hemispherical ground burst comprising of two recordings at each scaled distance. Positive phase only

It has previously been shown that the specific impulse of a pressure signal can vary significantly depending on which value of positive phase duration is taken [96]. This alongside the significant drop in the opening few milliseconds of the positive phase, can cause specific impulse values to be significantly lower than of a perfect reflection recording (as represented by the KB prediction in Figure 3.4). A solution to overcome these errors, discussed within literature [14,49,135] is to fit a modified Friedlander curve, defined by Equation (2.1), to the experimentally recorded data. No signal will ever be perfectly noiseless, and therefore the positive phase duration will always carry an enhanced level of uncertainty. Errors or uncertainties in this parameter can contribute to the overall loading. However, a curve fit can always be tailored with a different decay parameter in order to match a prescribed specific impulse value. Hence, studying sources of uncertainty in positive phase duration are of lesser importance that other positive phase parameters but it is still a reasonable indicator of explosive yield.

The aforementioned technique was examined through automatically fitting a modified Friedlander curve to individual pressure signals. This is done to determine how best to quantify variability of the pressure signal without introducing user error or losing physical meaning of the signal. The aim of adopting an automated approach was to provide a more reliable benchmark of explosive characterisation in far-field regions. The aim of this was to achieve variabilities associated with the positive phase blast parameters that were statistically unbiased. The automated method was initially validated using 65 of the 144 historic PE4 pressure-time histories recorded at the University of Sheffield [128], and was then used to process the remaining PE4 shots to assess its flexibility.

3.2.1.1 Determination of Best-Fitting Procedures

Considering equation (2.1), the parametersrequired for thr curve fitting approach are arrival time t_a, and time duration of the positive phase t_d. Through the use of MatLab's in-built curve fitting toolbox the max overpressure, P_{max}, and decay parameter, b, can be established using these known parameters. The process was coded to run through multiple variations of curves fitted to a given percentage of the recorded data after the arrival time was ignored. A curve was fitted to remaining data and extrapolated back to the defined arrival time. This provided a range of different blast parameters for a single given trial which could then be statistically investigated whilst trying to omit the effects of the 'sensor' ringing within recorded data. The general algorithm of the curve-fitting routine is defined as follows:

1. **Determination of t_a:** This parameter typically appears and is recorded as a sharp, unambiguous rise to peak pressure, with a maximum rise time of only a few (< 10) recorded samples ($\approx$50 μs) depending on recording frequency of the chosen oscilloscope. This can be seen in Figure 3.7a and is easily discernible in the raw data, i.e. the main peak in the gradient of the pressure signal[129].

2. **Assignment of t_d:** The electrical noise in each trial was recorded with a 10% pre-trigger to the detonation so an estimation of the effect of the noise could be made for more accurate t_d determination. As seen in Figure 3.6, the electrical noise is shown to be normally distributed around the true mean value meaning that when integrating pressure, with respect to time, the effect of electrical noise cancels out and has negligible effect on peak specific impulse. Therefore the difference between the assigned t_a and the time at which the maximum specific impulse occurred would be assigned as the positive phase duration, t_d, as seen in Figure 3.7b. This finding of normally distributed noise was consistent across all historical recordings.

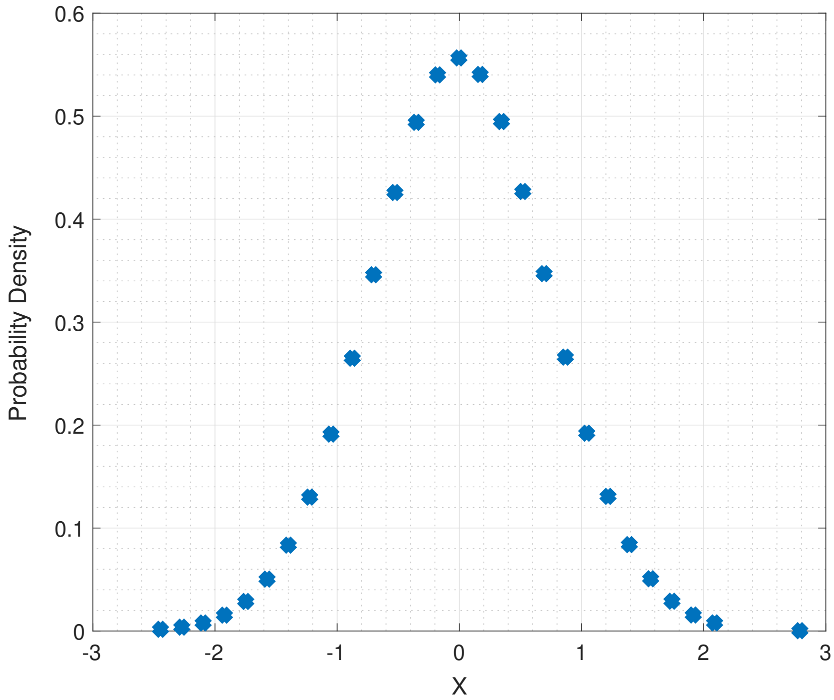

Figure 3.6: Example historic test recording of electrical noise prior to arrival of the shock wave with its distribution presented, where X is associated to the voltage recorded in the system

3. **Incremental removal of start of positive phase**: Inputting the time-based parameters and the raw pressure-time data into equation (2.1) provides a generalised curve with corresponding values for peak pressure and the decay coefficient, P_{max} and b respectively. Using Matlab's curve fitting toolbox, these parameters were fit to successively more curtailed pressure signals (in increments of a single percent, starting with the full signal) and extrapolating back to the arrival time of the shock, obtaining a spectrum of different peak pressures, specific impulses and decay coefficients from the results of a single test.

4. **Determination of optimal removal ratio**: Peak pressure and peak specific impulse values were seen to form a 'fan' around a central representative value (see Figure 3.8a). This was caused by fitting curves to the real physical features in the data and the additional variation induced by sensor ringing and inherent electrical noise. The mean values of the collated results for both peak pressure and specific impulse were calculated and the curve fits which satisfied both mean values within a $\pm 5\%$ region were defined as the 'optimal model fits' to the raw data. The mean

of these parameters were then evaluated, giving the automatically-generated peak pressure and peak specific impulse from that test. The decay coefficient was determined from iterations of the integral Equation 2.1, which enables the full pressure signal to be reconstructed.

3.2.1.2 Example of Curve Fitting Procedure

Initially, a simple verification of the automated procedure of blast parameter assignment was undertaken. Figures 3.7a and 3.7b show the pressure and specific impulse signals (through cumulative trapezoidal integration with respect to time) from a historic test with a 250g PE4 at 4m stand-off ($Z = 6.3496$ m/kg$^{1/3}$). Overlaid on both figures are the automatically assigned time based blast parameters, t_a and t_d, by implementing steps 1 and 2 of the curve fitting algorithm. These automated values are in good agreement with those determined from visual inspection of the raw data, and provide some initial confidence in the accuracy of the self-defining parameter routines.

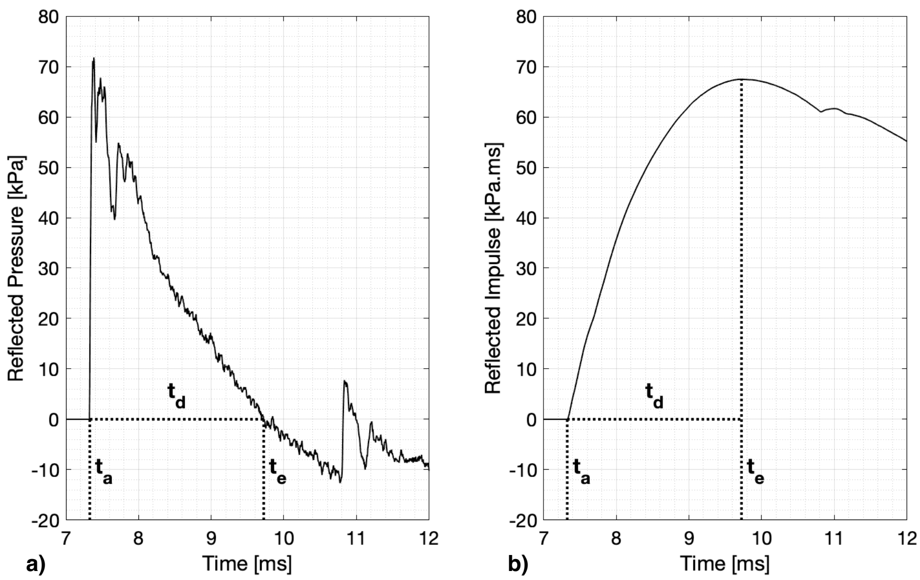

Figure 3.7: Example historic test results using a 250g PE4 hemispherical charge at 4 m stand-off: a) Raw pressure, and; b) Raw specific impulse with respect to time for a single test, highlighting the assignment of shock wave arrival time, t_a, and positive phase duration, t_d

The results from step 3 of the algorithm are shown for the same test in Figures 3.8a and 3.8b. With successive removal of between 0–50% of the positive phase data and back extrapolating to the defined arrival time parameter, a variety of different fitted Friedlander curves are seen, represented by the coloured 'fanning' envelope at $t = 0ms$ in Figure 3.8a. Peak pressures between 50–72 kPa are determined at this stage of the algorithm which is ±12kPa, or ±10%, of the KB prediction for the same given scenario. For a non-statistical based analysis, these variations are an improvement on those seen in articles expressing the hypothesis of inherent randomness between nominally identical explosive trials. This provides a potential explanation for sources of error introduced by the analyst.

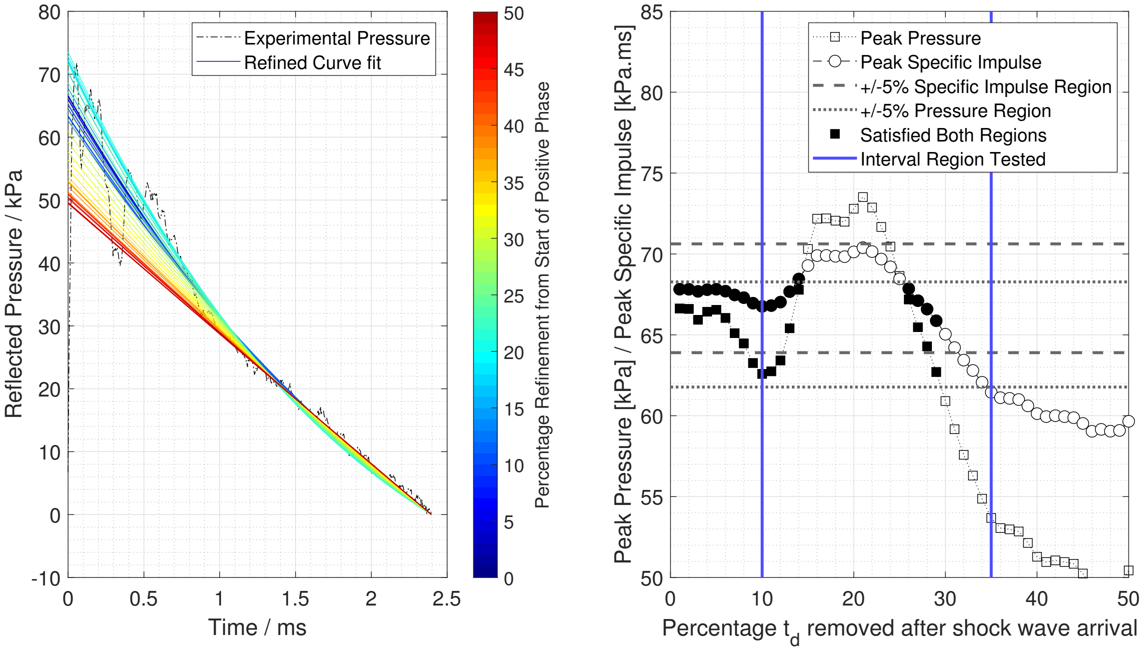

Figure 3.8: Example curve-fitting for historic test results using a 250g PE4 hemispherical charge at 4 m stand-off: a) all fitted curves to raw data with iterations based on percentage t_d removed immediately after t_a, and; b) Variations in fitted peak pressure and specific impulse as a result of the percentage of t_d removed, and definition of final range (solid markers) for which mean parameters are evaluated

Figure 3.8b visually represents the peak pressures and specific impulse envelopes with respect to the percentage of t_d removed (from the start of the positive phase). The cyclic pattern in the opening 0–35%, and the fanning envelope introduced previously, is a result of fitting to different proportions of peaks and troughs in the electrical signal. The reductions in both parameters after 35% represents the progressive loss of credible data and thus would result in the inaccuracy of representing features of the given blast wave. The dip in peak pressure and specific impulse around 10% is as a result of fitting to the first major sensor ringing loss, seen for this test at $t =\sim 0.3ms$ after arrival in Figure 3.8a. A region of cyclic parameters was seen consistently at approximately 10–35% positive phase removal for all validation tests. Accordingly, this interval was set as the representative region over which the mean values were evaluated in step 4 of the algorithm, visually displayed by the vertical lines in Figure 3.8b.

Step 4 assigns the most statistically representative parameters within this reduced region. First, the mean peak pressure and mean peak specific impulse between the entire region of 10–35% positive phase removal is calculated. Then, any percentage positive phase removal that results in a peak pressure or peak specific impulse deviating from this initial mean by more than 5% is discounted, and the mean values from each new, reduced dataset are calculated. This is shown visually in Figure 3.8b, where the vertical lines denote the initial region where the first mean is taken (10–35%), the hollow markers indicate those that are excluded from the final mean calculation, and the solid markers indicate those data points that are included in the final mean calculation that satisfy the requirements stated above but only the ones falling inside the 10–35% region were considered.

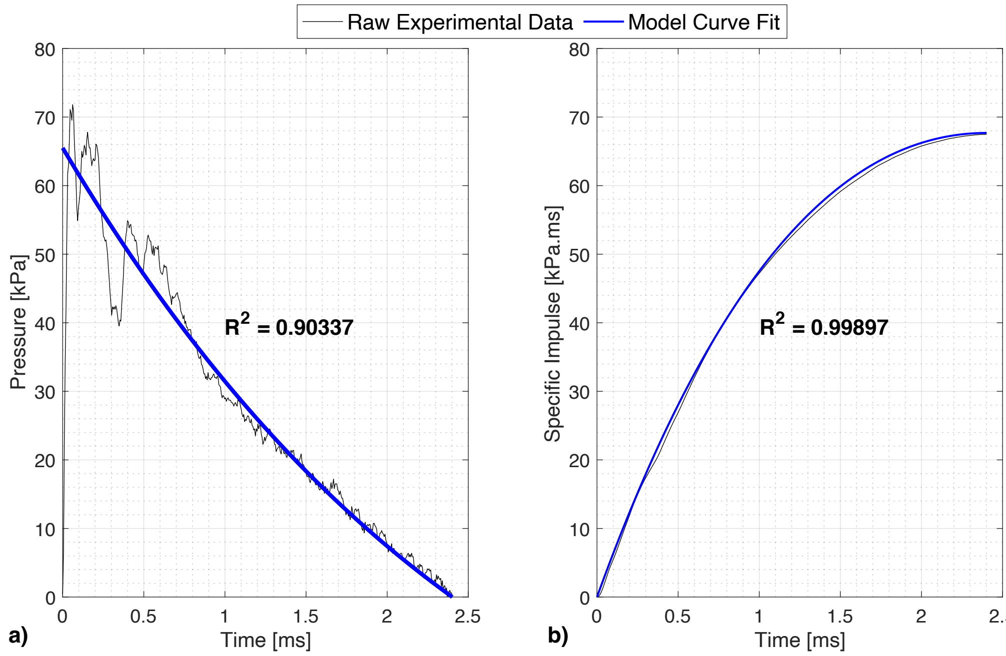

Figure 3.9: Example historic test results using a 250g PE4 hemispherical charge at 4 m stand-off with optimal fits overlaid: a) Overpressure, and; b) Specific impulse

Finally, Figures 3.9a and 3.9b display the raw data from the example historic test (250 g PE4 hemisphere at 4 m stand-off), and the resulting modified Friedlander curve fits determined from the automated process. The high R^2 values noted on each figure show that the generalised model fits compare well to the raw data. Due to the nature of pressure signals being easily influenced by ringing and other electrical noise, the R^2 of the model pressure fit will always be lower than that of a specific impulse fit. This justifies the findings presented by Bogosian et al.[16] which discuss the impulse measurements were inherently more reliable than those for peak pressure. It is worth reiterating that although Figures 3.9a and 3.9b present optimal fits from a given test, they are evaluated from a large number of different potential fits.

A secondary aim of this analysis was to confirm whether a consistent value of 0.25 t_d removed after the arrival time was suitable as a general rule in line with conclusions made by Rigby et al.[135]. Only 10 of the 65 validation pressure-time histories resulted in optimum curves whose parameters were determined from trial fits outside of 0.25 ± 0.03 t_d, and this was mainly due to the level of sensor ringing and electrical noise that was present. With low levels of sensor ringing, the optimal amount of data removal was found to range between 0–$0.2t_d$, meaning that a Friedlander curve could effectively be fit to the entire data set without any loss of accuracy. For tests with intermediate to excessive sensor ringing, or for poor signal-to-noise ratios, a value of $0.25t_d$ was deemed suitable and can be used as a general rule in the absence of more sophisticated techniques such as the one presented in this article.

3.2.1.3 Compiled Results

The optimal blast parameters determined from the automated process for the 65 PE4 pressure-time histories used to validate the method[135], the remaining 79 historical PE4 recordings[133,175] and the additional 10 PE4 trials conducted as part of this research are presented in Figures 3.10a–d as a function of scaled distance. Positive phase duration (Figure 3.10b) was not determined in the historic tests and so are omitted here.

The data presented in Figures 3.10a–d have been expressed using the Hopkinson-Cranz scaling[33,74] assuming a constant TNT equivalence of PE4 of 1.20[132]. For comparison, KB predictions have also been included in these figures. The recorded blast parameters demonstrate excellent agreement with the KB predictions, particularly in the region of $Z > 3$ m/kg$^{1/3}$. The agreement between experiment and prediction reduces when approaching smaller scaled distances, $Z < 3$ m/kg$^{1/3}$, although the results are still typically within 10-20%. The fundamental cause in this deviation has not been fully determined, yet the working hypothesis it that it is likely due to irregular features of the fireball/air interface giving rise to non-consistent shock wave properties between tests in the mid-to-near field.

An additional consideration is a singular value of TNT equivalence may not be appropriate for scaled distance regions in which the fireball and shock wave propagate in unison as the chemical processes ongoing from a TNT detonation may not be directly scalable to those from another given explosive. Upon the shock wave detaching from the fireball, the recorded parameters are scalable as the comparison is made between shock waves travelling through the same medium, unaffected by any external factor. This is the subject of ongoing work considering the mechanisms of explosives.

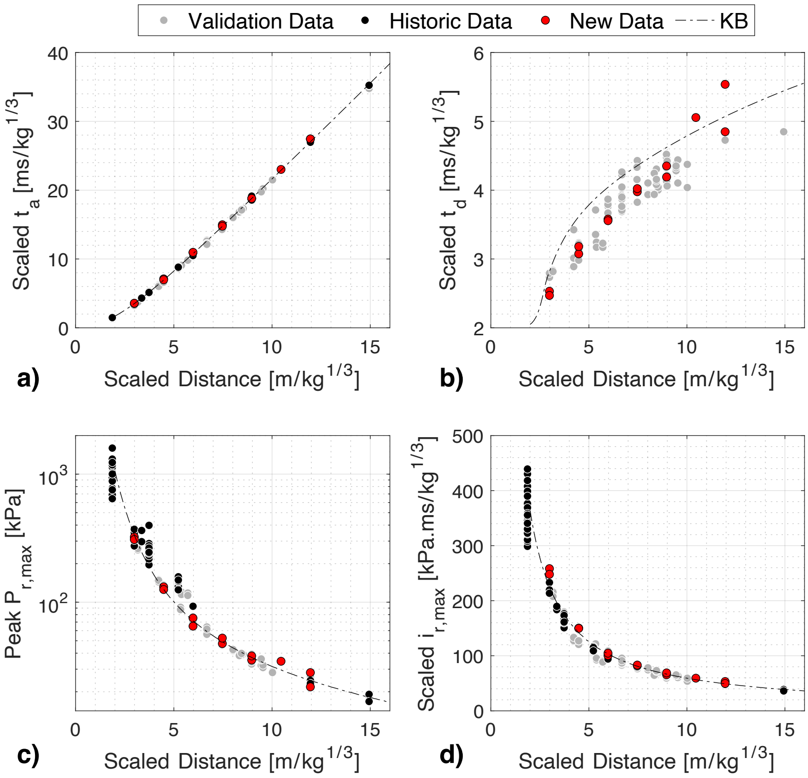

Figure 3.10: Compiled blast parameters from hemispherical PE4 trials as a function scaled distance, compared with KB predictions: a) Scaled arrival time, b) Scaled positive phase duration, c) Peak reflected pressure, d) Scaled reflected peak specific impulse

When considering test-to-test repeatability, there are two main conclusions to be drawn, both in agreement with findings published in the literature. Firstly, uncertainty in experimentally record blast parameters generally reduces with an increase in scaled distance[16,115] seen predominantly in Figures 3.10c and 3.10d. Secondly, despite best efforts to remove unconscious researcher-dependent bias, peak pressure, specific impulse and positive phase duration, in nominally identical scenarios, demonstrate much higher levels of test-to-test variability than shock front arrival time. This can be seen when comparing Figures 3.10b–d with 3.10a respectively. It is suggested that test-to-test variations are non-negligible for $Z < 3$ m/kg$^{1/3}$ and the source of these variations are to be investigated in future works.

3.2.2 Modifications for Positive Phase Improvement (Ei)

The results from the far-field trials presented in this thesis begin to build a coherent fundamental understanding of the nature of experimentally recorded far-field loading from a given charge composition, shape and mass. The importance of these findings provides a starting point to establish characteristics of more challenging blast loading conditions both in the near-field and those in complex environments. Knowledge of which can be supplemented with high-fidelity, validated numerical modelling.

Considering Figure 3.5, the standard 'sensor ringing' feature can be seen across each of the positive phases recorded at each increment of standoff. The results of which have historically been assigned to being technical incapabilities of the pressure gauges used in the trials. Although the aforementioned analytical techniques have shown to effectively omit the effects of this feature, it was important to establish its root cause and attempt to rectify it for future testing regimes.

Reisler et al.[119] reviewed extensively the development of pressure gauges throughout the high explosive era. Examples of recorded pressure-time histories for different gauges across numerous researchers and trials were provided within. One interesting finding in this article was that represented by Figure 3.11, which showed similar oscillations in the opening 25% of the positive phase duration recorded as the tests undertaken at the University of Sheffield. The fact that a similar finding was recorded using a pressure probe directed the thinking towards a real physical shock feature rather than a individual technical failure of the gauge causing early time oscillations.

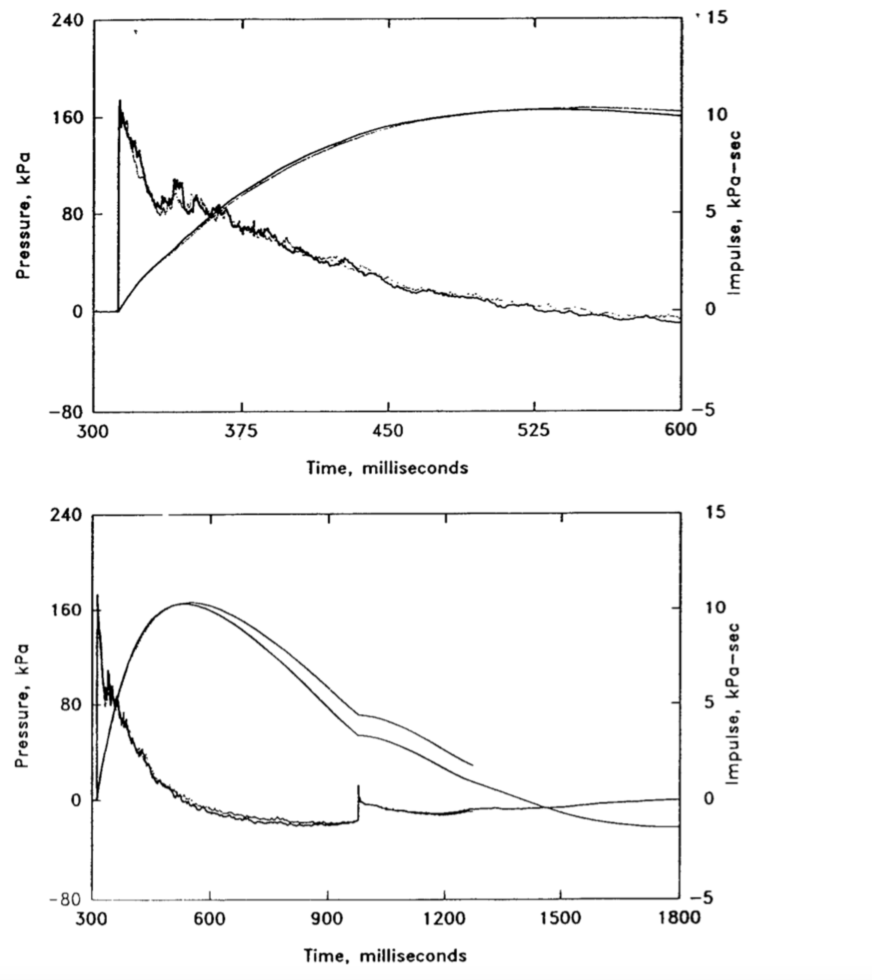

Figure 3.11: Example historic test results from a 1000lb high explosive height of burst shot recovered from Reisler et al.[119], displaying a comparison between a pressure probe (dotted) and a Kulite pressure gauge within a baffle plate (solid) across two different time bases, similar to the methods adopted in this thesis.

Understanding the mechanisms and magnitudes of blast loading on targets is of key importance for the analysis and design of the response of protective structures. Vast amounts of numerical work has been undertaken throughout literature with experimental work to validate its accuracy[179]. However, there has yet to be a synergistic approach to anomaly or systematic feature finding in experimental trials using validated models. The experimental results and analysis discussed within this thesis have been used to validate far-field numerical models for various high explosives. These can be implemented into much more complex numerical simulations to produce validated and accurate prediction for near-field and complex conditions. It was important to use these models to try and reverse engineer a physical justification to any systematic errors which could contribute to the variabilities seen in experimental data.

3.2.2.1 Synergy of Modelling and Experimental Studies

Whittaker et al.[179] validated APOLLO blastsimulator, developed by EMI, using an in-house explicit afterburn method (leveraging Cheetah and EXPLO5), against experimental data for PE4 and PE10 explosives and then for PE8 in works presented by Farrimond et al.[50]. The agreement attained gives confidence in the standard equation of states (EOSs) and subsequent parameters developed for these particular explosives, which can be utilised in numerical modelling for more complex scenarios. Numerical modelling generally is taken at its most simplified form to try to establish key explosive characteristics from basic scenarios which can then be mapped into more complex settings. These elementary numerical models usually do not account for minor environmental variations, such as terrain levels, reflective surface blemishes and energy loses, therefore omitting any shock wave mechanisms which could occur because of the aforementioned.

The oscillations identified in the raw pressure-time history traces from Figure 3.12a, and others within this thesis, have been previously attributed to a consistent feature of 'sensor ringing'[49,135], which was an assumed systematic technical limitation of the gauges used. The numerical models developed in the aforementioned articles with validated EOS's for a given explosive previously utilise simplistic, and fairly unrealistic baseline conditions. This is denoted by the idealistic shock wave behaviour simulated against experimentally recorded reflected pressure and specific impulse for 250g PE10 hemisphere at 2m stand-off as seen in Figures 3.12a and 3.12b.

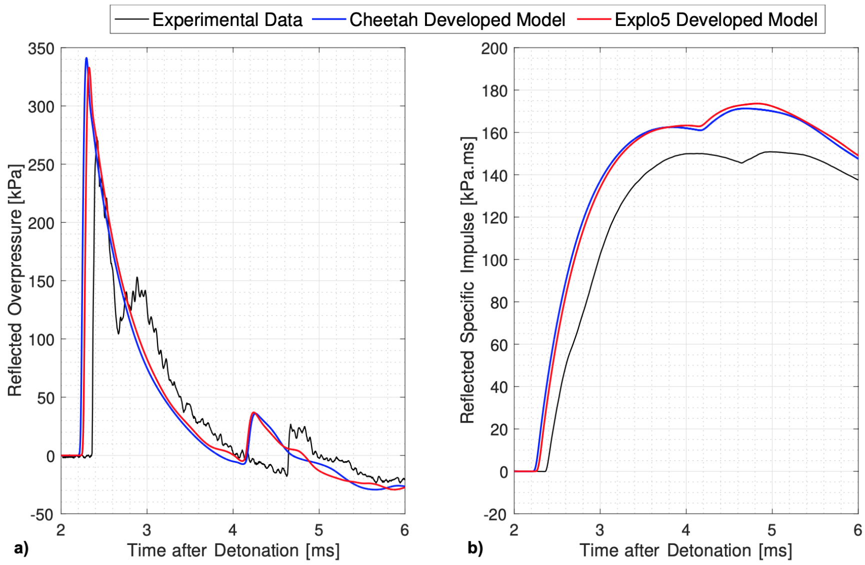

Figure 3.12: Comparison between experimentally recorded data for a 250 g hemispherical PE10 charge detonated 2 m away from a reflected gauge and Apollo numerical modelling (with EOS parameters developed using Cheetah and Explo5): a) Reflected overpressure, b) Reflected specific impulse, both with respect to time after detonation occurs

The numerical models utilised quarter-symmetry, with both the ground, vertical symmetry plane, and a boundary wall at the required stand-off distance defined as perfectly reflecting surfaces with afterburn features included using an explicit method. The Explosive EOS parameters used in this study were generated using the thermochemical code Cheetah v7, which, due to export control reasons, are not available for publication. Therefore, an alternative thermochemical code, EXPLO5, was also used to determine the EOS for the explosives. The surrounding medium of the numerical simulation was assumed to be air defined by the parameters in Table 3.1.

	Parameter	**Units**	**Value**
Perfect Gas EOS	R	$Pa/(K.kg/m^3)$	288
Caloric EOS	$E0$	J/kg	-2.375e5
	c_{v1}	$J/kg.K$	723.3
	c_{v2}	$J/kg.K^2$	0.0749

Table 3.1: Table of EXPLO5 Equation of State Parameters for Air.

These parameters have only been used for a complementary comparison to the Cheetah study and have not been fully assessed or validated, but are provided as representative values in Table 3.2. It is important to note the developed parameters were produced purely based on the explosive composition, correct density and a best guess of plasticiser material (finding the exact composition may improve the results), all done using the same default methodology. No calibrating to experimental data or tweaking of technique or parameters to improve results was performed.

	Parameter	**Units**	Explosive Type		
			PE4	PE8	PE10
JWL	Density	g/cm^3	1.59	1.57	1.55
	A	kPa	3.62E+08	3.35E+08	3.21E+08
	B	kPa	7.89E+06	7.24E+-6	9.40E+06
	R1	N/A	3.99	3.94	4.40
	R2	N/A	1.15	1.13	1.23
	w	N/A	0.27	0.27	0.271
	Detonation Velocity	m/s	7700	7608	7735
Detonation Products	E_0	kJ/kg	-5.36E+06	-5.32E+06	-5.18E+06
	Gas Constant	J/kg.K	282	282	269
	CV1	J/kg.K^2	738.8	672.9	738.2
	CV2	J/kg.K^3	0.4321	0.4502	0.3847
Combustion Products	E_0	kJ/kg	-3.99E+06	-3.57E+06	-4.51E+06
	Gas Constant	J/kg.K	286	287	283
	CV1	J/kg.K^2	488	309	453
	CV2	J/kg.K^3	0.295	0.409	0.320
Other	Stoichiometric Ratio (Air/Exp)	N/A	0.716:0.284	0.726:0.274	0.709:0.291

Table 3.2: Table of EXPLO5 Equation of State Parameters for Explosives.

Figure 3.12 shows both numerical models to be almost identical in this scenario, but with both somewhat over–predicting the peak reflected pressure and impulse of the event whilst not capturing the ringing seen in the opening $\sim 0.5ms$ of the positive phase. Hereafter, APOLLO blastsimulator using the Cheetah–determined equation of state parameters was the chosen method of numerical prediction due to the similarity in modelling results. The arrival time of the primary shock at this scaled distance is predicted sooner than the experimentally recorded which in conjunction with larger pressure predictions too begins the narrative that the models are experiencing a bigger energy release than what was recorded.

The arrival of the secondary shock in the numerical models is much earlier than that seen in the experimental data, which can lead to artificially high specific impulse predictions as the secondary shock arrives during the positive phase of the event. Other published literature describes the numerical secondary shock as arriving much *later* than the experimentally-recorded value when using numerical codes which do not explicitly account for afterburn[129], and it has been shown that including a calibrated secondary energy release can bring the secondary shock in line with the experimental recordings[141]. Whilst this method holds empirically based variable prescription, it is clear that the arrival of the secondary shock is intimately linked to the post-detonation pressure–volume–energy relations of the fireball, and is a known limitation of current modelling capabilities. This feature is believed to be due to the over prediction of the sound speed within the fireball.

The results from the simplest form of the numerical simulation led developments to consider energy losses to the ground surface. In the experimental methodology, the explosive charge was detailed as being placed on top of a steel anvil to reduce progressive damage to the ground; this alone is enough evidence to suggest some energy is being lost to the ground surface and therefore the first modification to the simplistic model was to take these into account. A 10% energy loss was applied to the simulation, in line with TM5-8858[77], by using 225 g rather than 250 g of PE10, the results of which are shown in Figure 3.13. This is conceptually similar to the 1.8 spherical equivalence factor adopted in the KB predictions, and brings the modelling results much more in-line with the experimental data.

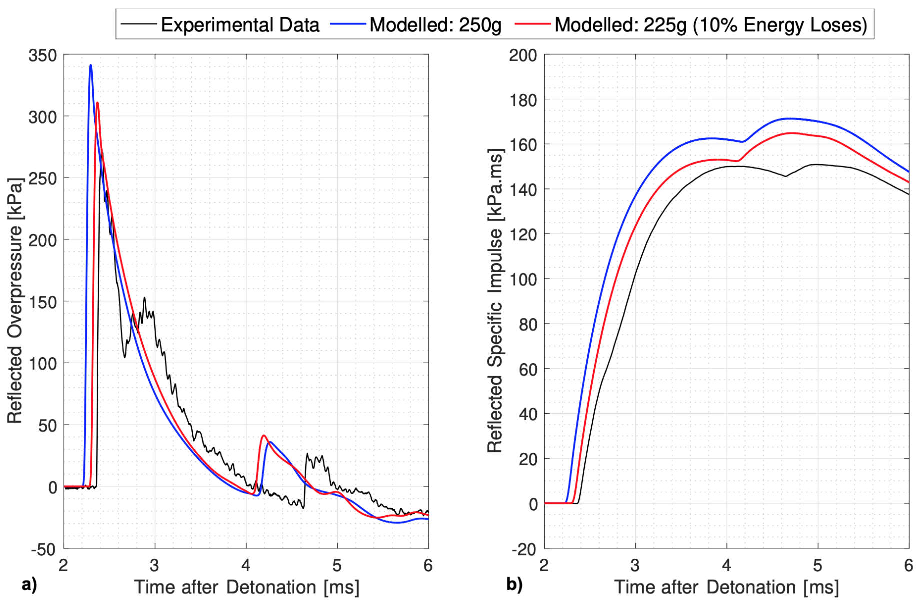

Figure 3.13: Comparison between experimentally recorded data for a 250g hemispherical PE10 charge detonated 2m away from a reflected gauge and numerical model evaluating using APOLLO when accounting for energy losses into the ground a) Reflected overpressure, b) Reflected specific impulse, both with respect to time after detonation occurs

The ‘sensor ringing’ seen in the experimental data was still not captured in the model detailed in Figures 3.13a and 3.13b. In higher fidelity numerical analysis, the pressure gauges were detailed as being made flush to a steel plate which protruded 25 mm from the reflecting surface. The significant drop in the pressure seen in Figure 3.14a over the opening 25% of the positive phase is enough evidence to support the necessity of accurate models to verify experimental procedures. By capturing some of the more complex early-time behaviour initially attributed to ‘sensor ringing’, numerical analysis and experimental procedures can work collaboratively to achieve higher levels of accuracy overall. This is a key insight for future experimental trials as it means if a truly flush surface can be achieved without any opportunity for clearing and reflected wave interactions, the statistical accuracy of the recorded data quoted in this article may be improved on further and the ’sensor ringing’ maybe omitted. Shin et al.[148] ran numerical analysis which however suggests once in the extreme near-field region, $Z < 1.6$ m/kg$^{1/3}$, the effects of clearing is negligible and should be ignored for design purposes.

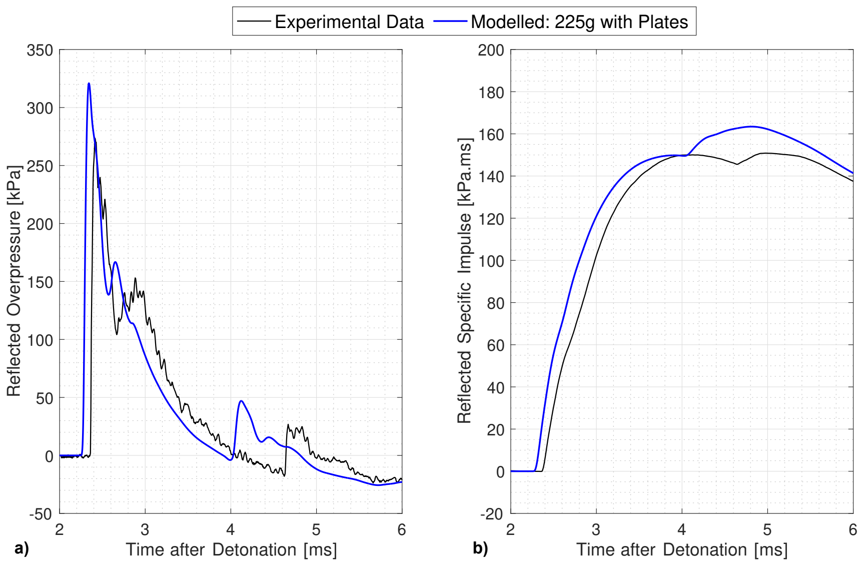

Figure 3.14: Comparison between experimentally recorded data for a 250g hemispherical PE10 charge detonated 2 m away from a reflected gauge and numerical model evaluating using APOLLO when accounting for energy losses into the ground and substantial terrain features a) Reflected overpressure, b) Reflected specific impulse, both with respect to time after detonation occurs

3.2.2.2 Blast Arena Modification

The fact that the numerical modelling has allowed the identification of systematic features within the experimental arrangement is testament to the synergistic nature of modelling and experimentation, especially when high levels of control are attained as they are in this study. A larger steel plate, with a minimum distance of 1.5m from the gauge to the edges of the plate, was affixed to the bunker wall to ensure that the aforementioned localised clearing effects would not interfere with the positive phase of the shock.

A repeat trial was conducted using a 250g PE10 hemisphere detonated 5m away from this surface and compared to the original trials, the data of which is presented in Figures 3.15a and 3.15b. The new results indicate that whilst these 'sensor ringing' oscillations alter the qualitative form of the pressure trace, their influence on the quantitative blast parameters, determined through curve fitting, or integration of the pressure signal to find specific impulse, are negligible when comparing the raw data to the curve fit itself as seen in Figures 3.9a and 3.9b.

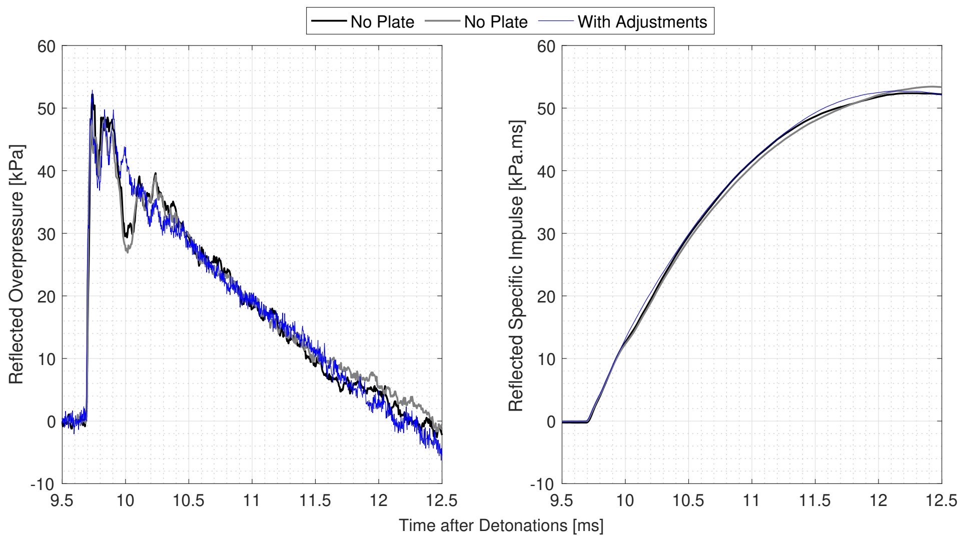

Figure 3.15: Comparison between experimentally recorded data, time-shifted so the arrival of the positive phases align exactly, for a 250 g hemispherical PE10 charge detonated 5 m away from a reflected gauge with adjustments to the blast arena and without: a) Reflected overpressure, b) Reflected specific impulse, both with respect to time after detonation occurs

3.2.2.3 Top vs Bottom Detonation in Ideal Explosives

Another important notion to take from the trial results presented in Figures 3.10 is the agreement of findings presented by Bogosian et al.[16]. Both suggest that specific impulse values developed from curve fitting techniques are much more reliable than peak overpressure. However, the physical reasoning for the clear spread in the data seen at $Z < 3$ m/kg$^{1/3}$ for the two parameters is still yet to be fully determined. The hypothesis detailed by Tyas[173] made definitive justification to the experienced spread through links to fluid dynamic instabilities which is a physical and logical explanation. What was not considered in full detail however was how the experimental procedure of top detonating the hemispherical charge could effect the close-in shock wave/fireball blast parameters.

Sherkar et al.[146] undertook an analysis on the influence of a charge shape and detonation point on explosive parameters and found that for scaled distances of $Z > 3.15$ m/kg$^{1/3}$ the independent variable made no difference to shock wave parameters. This finding is in line with the working hypothesis defined by Tyas[173]. The predictions at smaller scaled distances are however significantly variable as charge shape and detonation point is altered. As the majority of the data presented within this thesis, unless specifically specified, was the result of a top detonated hemisphere it was important to investigate, using both new experimental data and validated numerical modelling, whether or not detonator position could be be an influencer of parameter variability in the $Z < 3$ m/kg$^{1/3}$ region.

Using a validated EOS for PE4, both top and bottom detonated scenarios were considered for the standoff range of 1.25-2m assuming a TNTe=1.2, corresponding to $Z = 1.87 - 2.99$ m/kg$^{1/3}$. Experimental data used for a direct comparison to both the CFD simulations and KB predictions presented. According to numerical simulations presented in Shin et al.[148], the near-field modelling can ignore the effect of clearing as it is negligible. The gauge plate features discussed in Section 3.2.2 was therefore removed from the simulation, resulting in minor changes to the overall pressure-time history. It is however important to note that the aforementioned article makes use of AUTODYN for modelling capabilities where as the study presented in Figure 3.16 uses APOLLO.

The nearest standoff of 1.25m, a scaled distance of $Z = 1.87$ m/kg$^{1/3}$, considered was chosen as it shows to exhibit the most variability in the resulting output blast parameters from historic trials. The results from experimental tests, numerical simulations and KB predictions are presented in Figures 3.16a-d for this region to both consider the effects of detonator position but also test the validity of KB predictions at these scaled distances. What is evident from these plots is the distinct differences between top and bottom detonated results when considering the general form of the experimental pressure-time histories.

The bottom detonated trials, represented by Figures 3.16b and 3.16d, show that both KB predictions and numerical simulation over-predict the peak reflected pressure, but the specific impulse values agree reasonably well. This begins to reiterate shock wave development and formation theory discussed by Kinney and Graham[90] in Chapter 2. The theory shows a clear transition of the pressure-time history from a rounded pressure pulse, which then begins to expand radially at its own speed for each portion of the pulse, therefore the higher pressure and temperature regions expanding faster, resulting in a progressively sharper rise to peak pressure, and thus the shock discontinuity.

Figures 3.16b and 3.16d are believed to display a shock in this transition period. The overall energy released from the detonation is representative of KB and numerical model predictions for a 250g PE4 charge but the peak pressure is lower and time duration is longer in the experimental trial. It is clear that neither numerical modelling or KB predictions are able to accurately capture the transition period of the shock front as both over-predict the peak pressure considerably. At these scaled distances KB predictions were developed using numerical simulation which explains why the two compare reasonably well. It is clear that these methods assume a fully formed shock discontinuity occurs sooner than in reality and therefore the real physical behaviour of the early development of the shock is not captured correctly.

Figures 3.16a and 3.16c represent the top detonation of 250g PE4 hemisphere. These result in a much lower peak pressure when compared to KB predictions but peak specific impulse values presents much lower too. This is a direct result of the varying detonation dynamics, resulting in differences in rates of energy release. This induces a more inconsistent behaviour when compared to a standard free-air assumption. Reassuring is the strength of numerical modelling at this scaled distance which although has not captured either the pressure-time or specific impulse-time histories perfectly, the same general trend can be qualitatively seen. Quantitatively, the numerical simulation is different to the experimental data which is speculated to be related to the exact position and orientation of the detonator. In the numerical simulation, a perfect, infinitesimally small detonation point is prescribed at the very top of the charge. In reality despite best efforts, the detonators used in testing are approximately 5mm into the top of a charge, do not expand radially and may not be perfectly orientated. This therefore will resuls in different detonation dynamics. The fact, that qualitatively, the trends show similarities gives rise to the testing methodology but validates the sensitivity of the results at this scale.

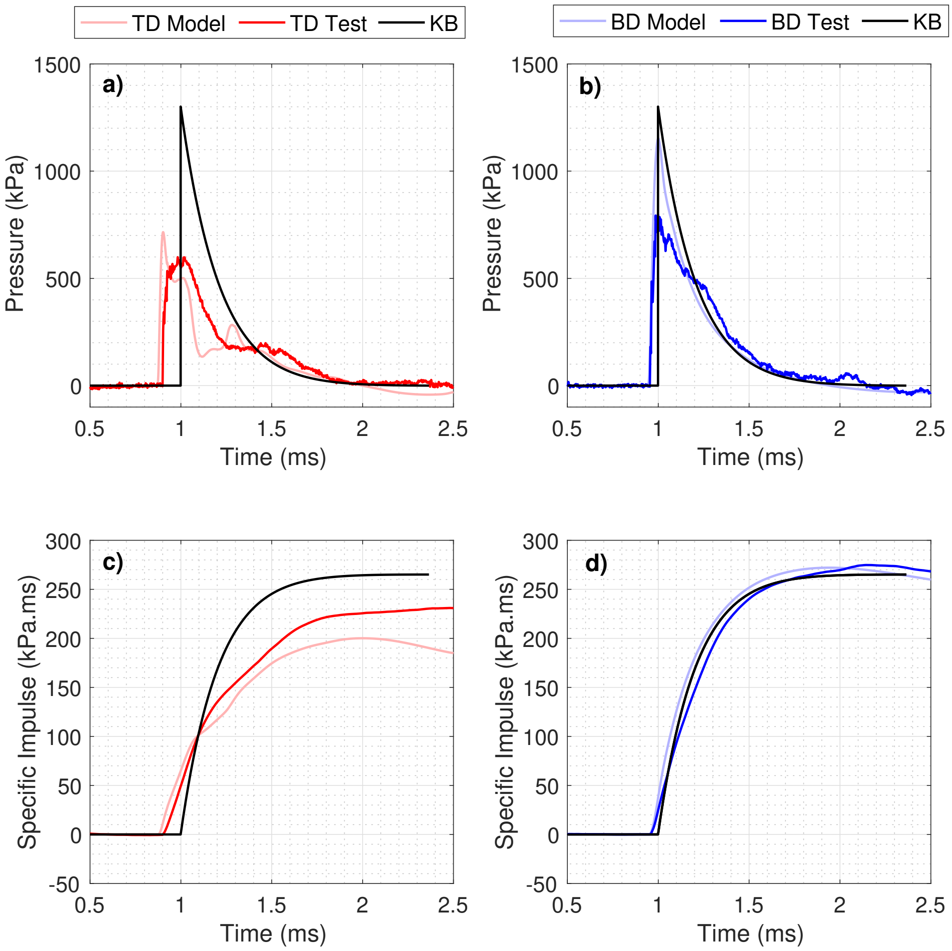

Figure 3.16: A comparison of top and bottom detonated 250g hemispherical PE4 charges recordings of reflected pressure and specific impulse against time at 1.25m standoff (corresponding to plots a and c, and b and d respectively) which make reference to KB predictions and numerical simulations.

For the top detonated trials, there is believed to be a slower expanding detonation cloud and resulting shock wave associated with the top portion of the charge. This expands prior to the detonation wave reaching the bottom of the charge. When the detonation wave reaches the bottom of the charge, and the reflective surface, the resulting detonation products would begin to expand laterally along the reflected surface in the form of jets, and radially back outwards. The jetting-like behaviour has been attributed to the first rise in the pressure-time histories seen in Figure 3.16a, with the secondary radial expansion being attributed to the rise approximately 0.3ms later experienced in both the numerical simulation and experimental data.

The additional near-field experimental results, considering the standoff range of between 1.25-2m, are presented in Figures 3.17a-h. These trials aimed at deducing the distance the effect of detonator position becomes irrelevant to the overall blast parameter data. The raw data presented in the aforementioned plots is considered in a qualitative sense against KB predictions. The results suggest that for standoff distances greater than 1.5m, $Z > 2.24$ m/kg$^{1/3}$, both top and bottom detonated trials behave consistently in terms of the overall energy released, and thus the resulting peak specific impulse trends which are captured well by KB predictions as shown in Figures 3.17f and 3.17h. As the standoff distance is reduced, the KB predictions generally capture the energy released in bottom detonated trials, but top detonated results show a lower energy release overall. This is directly related to the non-spherical expansion of the detonation wave and its products, resulting in inconsistent energy releases, seen in Figures 3.17b and 3.17d. KB predictions generally over-predict the peak overpressure at these scaled distances too, which is related to the lack of comprehension in the physical shock formation in the empirical tool at these scaled distances.

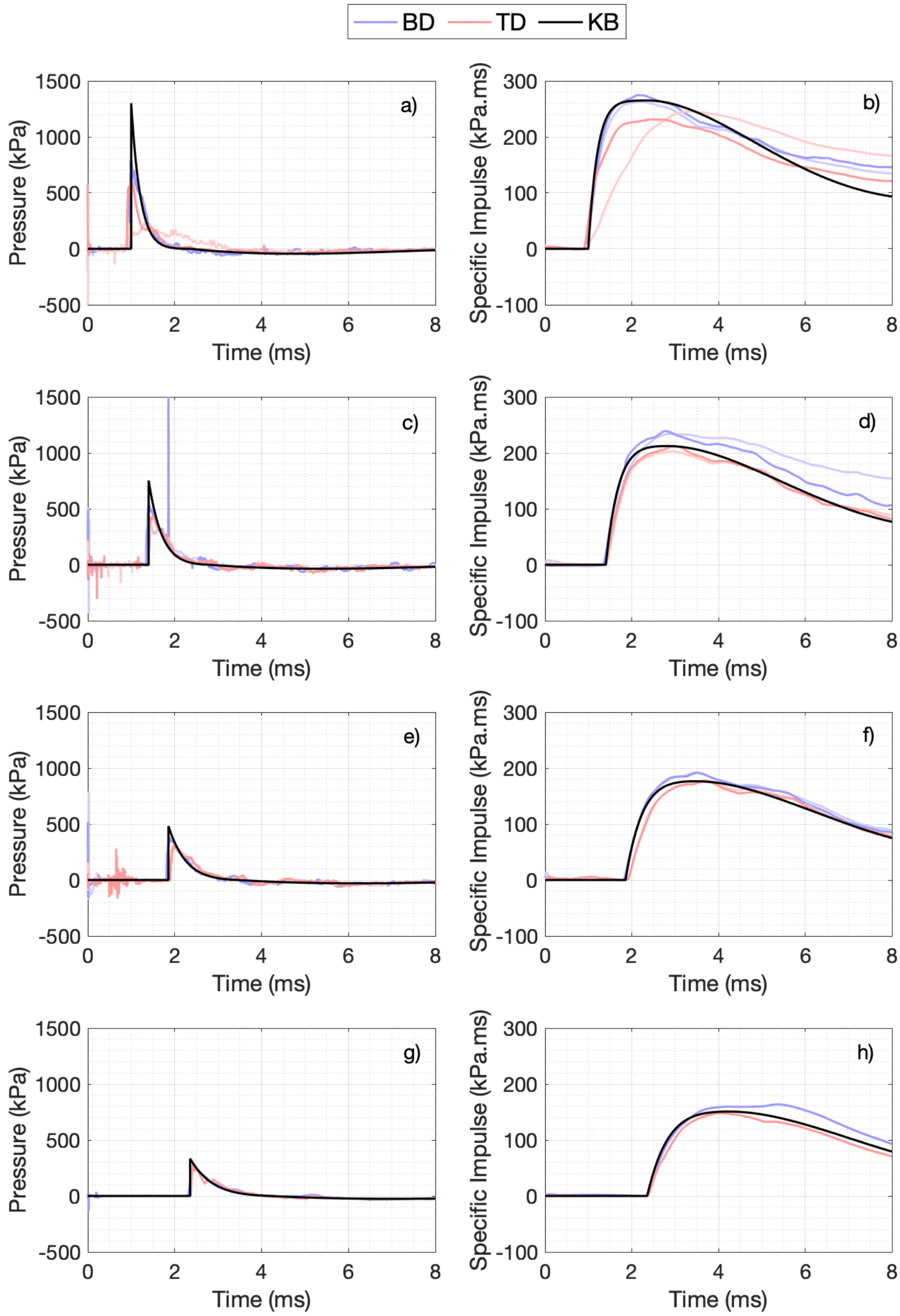

Figure 3.17: A comparison of two top and bottom detonated 250g hemispherical PE4 charges recordings of reflected pressure and specific impulse against time at 1.25m, 1.5m, 1.75m and 2m standoffs (corresponding to plots a, c, e and g, and b, d, f and h respectively) which make reference to KB predictions.

Interestingly, the blast parameters from the new top detonated data at 1.25m standoff, shows to be in line with the lower bound of those presented in Figures 3.10c and 3.10d. The historic data presented in both Figures 2.12a-d and Figures 2.13a-d was conducted by different research teams, which reinforces the narrative of ensuring the systematic differences between testing regimes are considered when comparing results. The historic data at $Z > 3$ m/kg$^{1/3}$ shows agreement with the newly conducted trials, which validates the hypothesis that at this scaled distance blast parameters are less sensitive to the imperfections, but are for near-field scenarios, $Z < 3$ m/kg$^{1/3}$. The team conducting the historic trials may not have been as strict in their control measures, with variations in the detonator placement resulting in greater variability. The fact the repeat shots in this study show low levels of variability suggests that these are a more appropriate characterisation of the detonated explosives. Future tests will look at studying the near-field region with much more rigour to establish the consistency in the blast parameters similarly to that discussed within this thesis for far-field scenarios.

These trials show that the top detonated experimental methodology utilised for the majority of the data referred to in this thesis, will give rise to spreads of data in near-field regions, $Z < 3$ m/kg$^{1/3}$. Data recorded in this region will be influenced by detonator position, orientation, charge geometry and placement imperfections alongside any other systematic experimental and analytical errors induced during the trials. This finding provides evidence towards the overlooked systematic errors incorporated into blast related experimental work which result in the justifications of 'inherent' high levels of explosive yield variability.

3.2.3 Analysis of Negative Phase (Ai)

Rigby et al.[133] undertook an intensive assessment of the negative phase of the ideal explosive, PE4, and compared various methods of approximating the associated trends. The secondary, and subsequent, shock phenomenon are not accounted for in any empirical predictions presented within the aforementioned article. This is justified by the low magnitudes they exhibit compared to the negative phase presented in ideal explosives. Further noted is the affect clearing has on a pressure trace, a given time after the arrival of the primary wave. This is associated with the speed of a clearing wave being 340m/s and then taking the distance from the nearest edge of a reflective surface. Clearing and reflections from other surfaces are wave phenomena which will be picked up on experimental recordings. Without a fundamental understanding of the systematic errors associated with a testing methodology, data could be misinterpreted, with these features considered to be real physical parameters of a free-air shock interacting with a single surface.

Whilst this thesis neglects both these experimental features, the 'Cubic Negative' curve fit approximation (detailed in the second case of Equation 2.6), developed by Granstrom [66], presents as the most effective method of approximating the negative phase both qualitatively and quantitatively for the ideal explosive in question. This provides further justification as to the source of negative phase semi-empirical curves. Shown in Figures 3.18a-d is the considerable effects experimental features can have on the overall loading from the same explosive detonation. It is important to note that the data presented in the aforementioned figure was recorded during the same trial using two different recording locations. Interestingly, the general form of the raw data exhibits rather obvious differences when t=17.5-22ms which is approximately 7-12ms after the arrival of the primary shock.

Using a 340m/s clearing wave speed and the distances to the nearest sides of the walls, the time at which the clearing waves would arrive at the respective pressure gauges would be approximately 12ms and 7ms after the arrival of the primary shock. With the bunker wall being effectively infinitely long but 4m tall, only one clearing wave would interact with the negative phase data. The blockwork wall on the other hand has three finite edges, two of which were 2.25m resulting in two clearing waves interacting with negative phase simultaneously around 17ms after detonation. This is clearly denoted by the lower pressures in Figure 3.18a associated with the time periods mentioned.

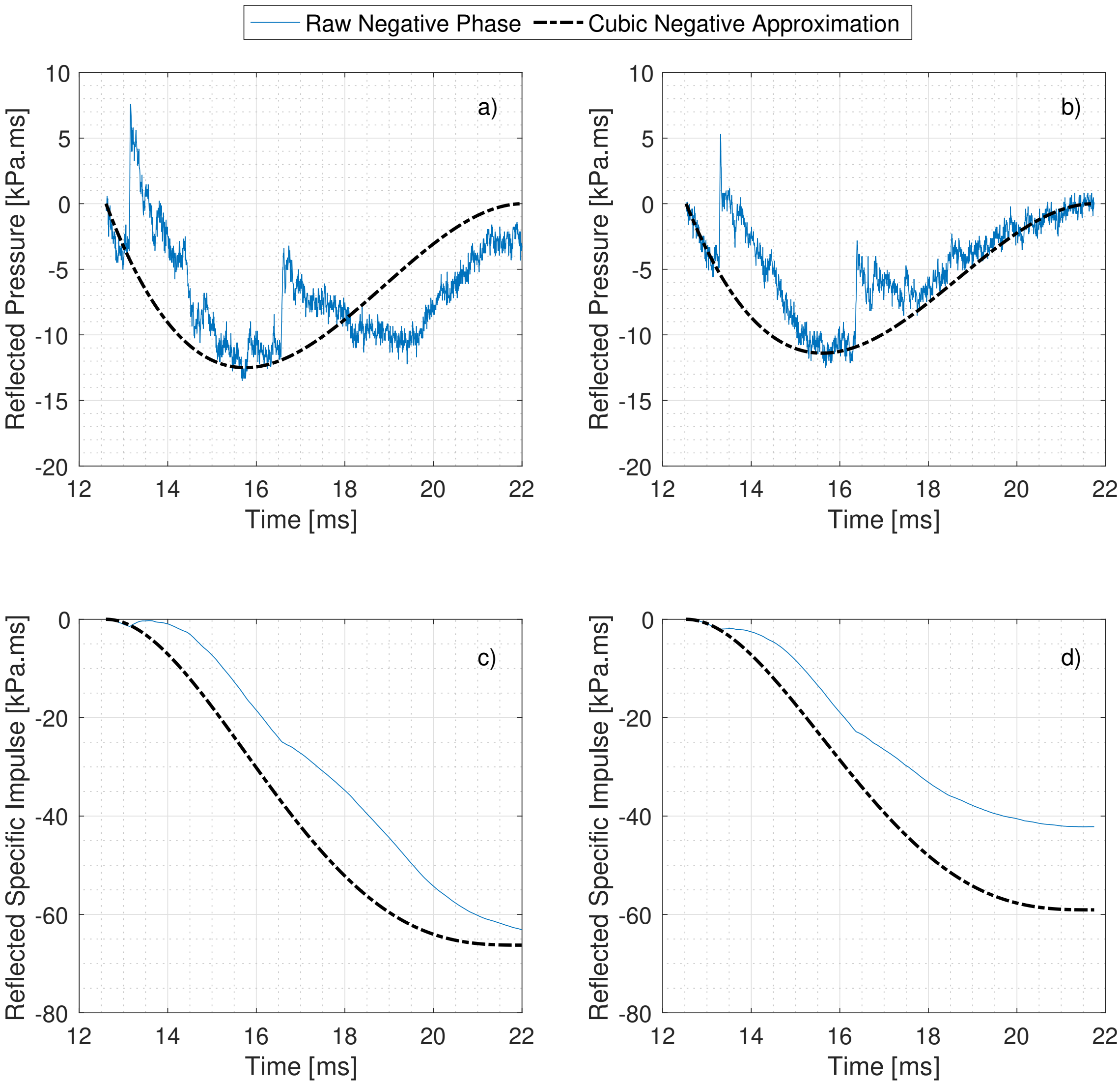

Figure 3.18: Comparison of negative phase results from a 250g PE4 trial with two reflective recording points 5m either side of the explosive, where plots a) and b) represent the raw negative pressure-time plots and plot c) and d) are the corresponding impulse-time plots for the blockwork and bunker walls respectively.

2112 #### 3.2.3.1 Compiled Negative Phase Parameters

2113 The 'Cubic Negative' approximation investigated by Rigby et al.[133] was implemented on this data set to validate the findings further as presented in Figure 3.18. It is clear to see a reasonable prediction for the negative phase loading is established across all three parameters regardless of secondary shocks and any other experimental features.

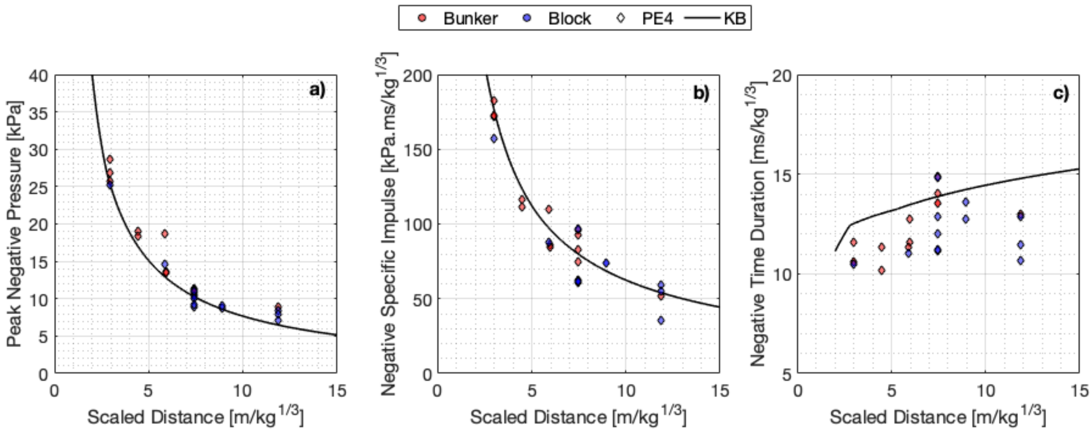

Figure 3.19: Compilation of scaled negative phase parameters resulting from visual analysis of 250g PE4 hemispherical charge using a TNTe=1.22: a) Negative Pressure, b) Scaled Negative Specific Impulse and c) Negative Phase Time Duration.

What is yet to be established is a rigorous validation of quoted negative phase parameters. The difficulty in characterising these parameters is associated with the lower magnitudes of the negative phase parameters and therefore it is much easier to misinterpret the actual values within the noise of the recorded data. Reducing the noise for the secondary shock is not possible as its magnitudes is inherent to the rating of the gauge. To avoid gauge failure, the rating needs to be high enough to withstand the primary blast wave prior to secondary waves arriving. That alongside experimental features, related mainly to clearing, means that developing automated analytical tools, similar to that presented in Section 3.2.1, hold more difficulty. Taking this into account, the negative phase parameters are established visually within the contents of this thesis to validate both the 'Cubic Negative' and semi-empirical approximations across a number of different explosives.

Figures 3.19a-c displays visually interpreted negative phase parameters from 250g hemispherical PE4 trials across the far-field testing range. This data was scaled using a TNTe=1.22, in line with findings from Farrimond et al.[50], and compared directly to the empirical curves established by Granstrom[66]. The agreement with predictions of peak negative pressure, $P_{r,min}$, suggest that whilst the experimental methodology induced variations during the negative phase, the general maximum pressure experienced is in line with approximations. It is important to note, if the reflecting surfaces were smaller, clearing waves would arrive at the recording positions sooner, resulting in variations to the established $P_{r,min}$ values. Figures 3.19b and 3.19c present as comparing well to the approximations due to including the behaviours of secondary shock and clearing features respectively discussed by Rigby et al.[133]. Section 3.2.3.2 discusses the strength in the 'Cubic Negative' approximations when empirically accounting for secondary shock loading.

3.2.3.2 Secondary Shock Phenomena

The secondary, and successive shocks, of an explosive are noticeable features in a pressure-time history. Despite some preliminary efforts of establishing yield prediction parameters through experimental work[62,129,133], there is yet to be a rigorous investigation of all shock wave parameters. Noted in Rigby and Gitterman[129] is the inability of numerical modelling to capture the negative phase and secondary shock behaviours accurately. The root cause is currently unknown but is speculated to be related to erroneous detonation mechanics integrated within simulations, proving it necessary to establish the behaviour of secondary shocks empirically. The secondary shock, unlike the initial shock, has to travel through the detonation product fireball and therefore, the properties of the surrounding medium (such as temperature, sound speed etc.) are believed to strongly influence the behaviour and timing of the secondary shock.

In Rigby et al.[133] there is no mention of the inclusion of afterburn within the numerical simulations and therefore an under prediction of the fireball properties results in additional reactions being omitted and the secondary shock arriving later. The APOLLO simulations documented in Farrimond et al.[50], use explicit afterburn which results in an early arrival of the secondary shock. This was related to inaccuracies in defined caloric EOS detonation and combustion products over predicting the speed of sound within the fireball[179]. Whilst the arrival time of secondary shock is a known flaw in numerical simulation, the loading form of the shock is captured accurately and parameters compared to experimental work for validation.

With the successive shock waves occurring in the wake of the primary shock, alongside any systematic experimental features within the recordings, producing a standardised and automated analytical tool for all parameters currently holds difficulty. Figures 3.20a-d present scaled secondary shock parameters, using a TNTe = 1.22, which have been established and compared to KB predictions for primary shock waves.

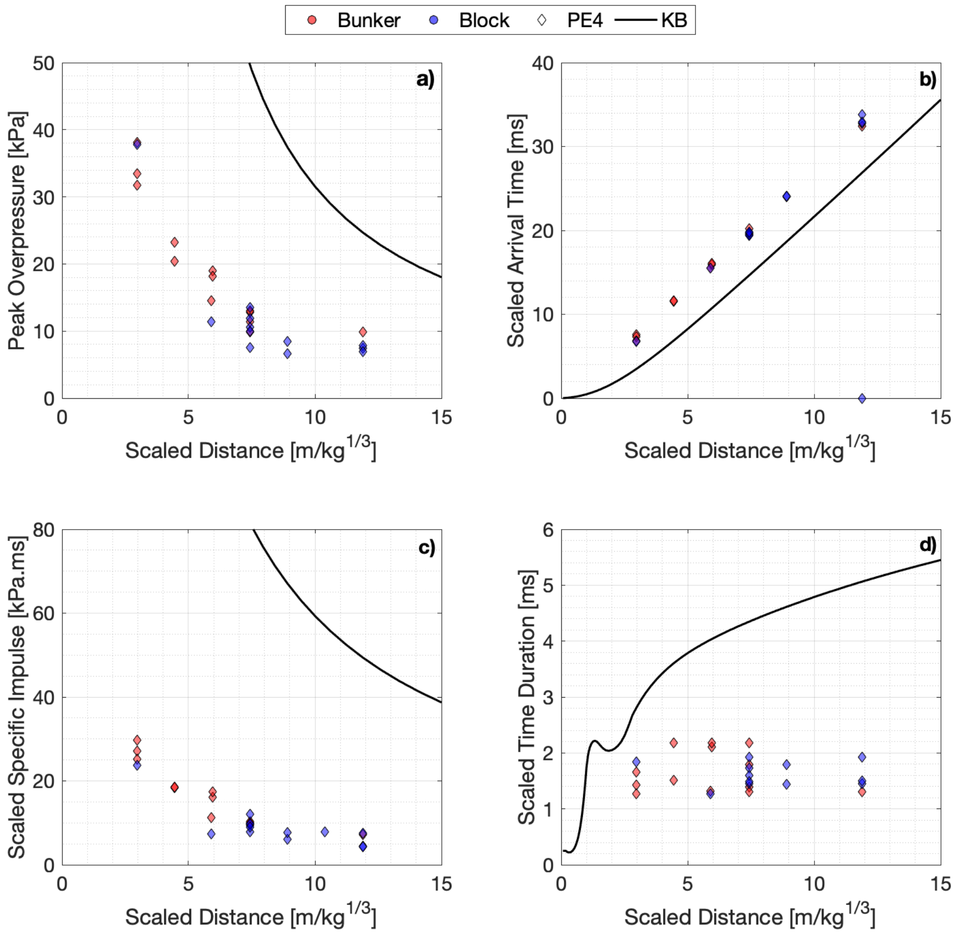

Figure 3.20: Compilation of scaled secondary shock parameters resulting from visual analysis of 250g PE4 hemispherical charge using a TNTe=1.22: a) Negative Pressure, b) Scaled Negative Specific Impulse and c) Negative Phase Time Duration.

KB predictions across the four blast parameters visually shows a lack of agreement when scaling the PE4 secondary shock data based on the corresponding TNTe=1.22. General consistency within the data itself is experienced at each increment of scaled distance. This finding was surprising based on both the difficulty in assigning these parameters within the negative and the unpredictability of the temporal characteristics of a secondary shock wave as it propagates through chaotic fireball and detonation products. When comparing the result directly with those presented in Figures 3.10a-d, similar behaviour are exhibited with respect to scaled distance suggesting that secondary shock waves present similarities to a free-air shock wave for far-field scenarios. Future work should consider methods of predicting secondary shock parameters through the development of similar semi-empircal prediction curves to that presented by [87].

The delayed offset of $\sim 5ms$ on average in scaled arrival time of the secondary shock, when compared to the KB predictions, is displayed in Figure 3.20b. The initial conclusions to this was that is was directly linked to the time delay between a detonation wave travelling to the charge extents, a rarefaction wave collapsing towards the centre of detonation, coalescing and then reflecting back out as the secondary shock. However, this mechanism in 250g hemispherical charges would be over in around 0.01-0.02ms, when considering a constant detonation velocity of 7800m/s in PE4. The question then posed was what makes up the remaining 99% of the offset time in secondary shock arrival time. This phenomena is discussed in more detail in Section 4.2.3.1 when more data is available across a number of different explosives.

3.2.4 Future Considerations for Pressure Gauge Work

The main concern with current practices of pressure gauge related blast trials is the lack of systematic feature consideration when designing a testing facility and analysing any resulting data. The shock wave mechanisms of clearing and reflection, discussed in Section 2, can have detrimental effects to a pressure-time history depending on the features the analyst wants to consider. Despite best efforts, the blast arena trials conducted at the University of Sheffield are not absent of systematic features but make best attempts at reducing them, as discussed in Section 3.2.

Future pressure gauge work and blast trials should make more use of numerical models and create synergetic solutions to how data is captured. Through a fundamental understanding of the parameter, variations to experimental methodologies can be made to improve the accuracy and consistency in the desired blast parameter. This will push the community in the direction of a clear and coherent understanding of blast wave mechanics and achieve general consistency across the full range of scaled distances.

3.2.5 Pressure Gauge Summary

This section focusses on the analytical and experimental techniques which can be adopted for pressure gauge type recordings across the far-field range. Within this thesis, the application of the aforementioned methods on PE4 hemispherical detonations, demonstrate high levels of accuracy of output blast parameters from both the positive and negative phase. These have been used to validate the KB predicting tools across the far-field range. These tools will be referenced throughout the duration of this thesis to assess the validity of their application across both ideal and non-ideal explosives in the far-field range.

3.3 High Speed Video (HSV) Recordings

Detailed within this section of the thesis is the discussion of how high speed video recordings can be used to develop a more robust understanding of free-air blast parameters. Ultra high speed recordings are shown to provide both qualitative and quantitative information on the detonation wave physics, alongside the early expansion of the fireball and subsequent shock wave.

3.3.1 Far-Field HSV Analysis (Ai)

As mentioned in Section 3.1.1, high speed video cameras were utilised for recording the shock wave propagation through the surrounding air medium as the result of an explosive detonation. Visual representation of an explosive trial offers a full spatial and temporal understanding of a detonation event, within the confines of camera resolution. If utilised correctly, HSV provides a much more robust understanding of shock wave development in far-field scenarios whilst reducing the number of trials required to get a similar representation using pressure gauges alone. The following sections discuss the various procedures which have been iteratively developed to track shock waves within the literature, and present newly automated tools to analyse high speed video recordings of far-field explosive detonations.

3.3.1.1 Shock Wave Edge Detection Process

Rigby et al.[130] presented an edge-detection process for explosive video recordings using high speed video cameras. The inbuilt MatLab function, *edge*[21], was suitable for optical tracking of the fireball/air interface in near-field explosive analysis due to the presence of a clear contrast between the luminous fireball and the ambient air. However, when testing the modified '*edge*' function for far-field scenarios the absence of a fireball in the images and low variations in light intensity across the shock front resulted in the most noticeable edges being those of the zebra board behind the shock front. This caused any analysis using this method to output alone the outlines of the background image rather than any shock wave propagation.

Hargather and Settles[71] presented an image subtraction method which identifies the regions of greatest variation in pixel brightness between two consecutive frames. This method is particularly suited for situations with imagery of low contrast but with a clear schlieren disturbance[59]. A simplified approach was developed based on this idea is presented in Equation 3.1.

$$N_{i,j,k} = F_{i,j,k+1} - F_{i,j,k} \tag{3.1}$$

where N is the resulting image subtracted video file, F the recorded video file, i and j are the pixel locations in terms of columns and rows respectively, and k is the frame number. A comparison exercise was undertaken between the Hargather and Settles[71] method and the simplified approach developed during this research in Equation 3.1. The results were nominally identical for the videos tested but the simplified approach completed much faster due to the equation being simplistic. Despite the image subtraction method being suited for low levels of lighting, weather conditions at the University of Sheffield testing site vary massively throughout the year and therefore had justification for some trial recordings yielding impractical footage for analytical purposes.

Whilst the method presented in Hargather and Settles[71] has been shown to work well against a structured, repeatable background, other work using similar methods[103] has been shown to yield accurate results with a highly variable "noisy" background. The accuracy of this method for images with low contrast backgrounds has yet to be proven, however it is envisaged that more sophisticated techniques (e.g. PIV) would be needed instead of the simple edge detection and image subtraction technique described herein.

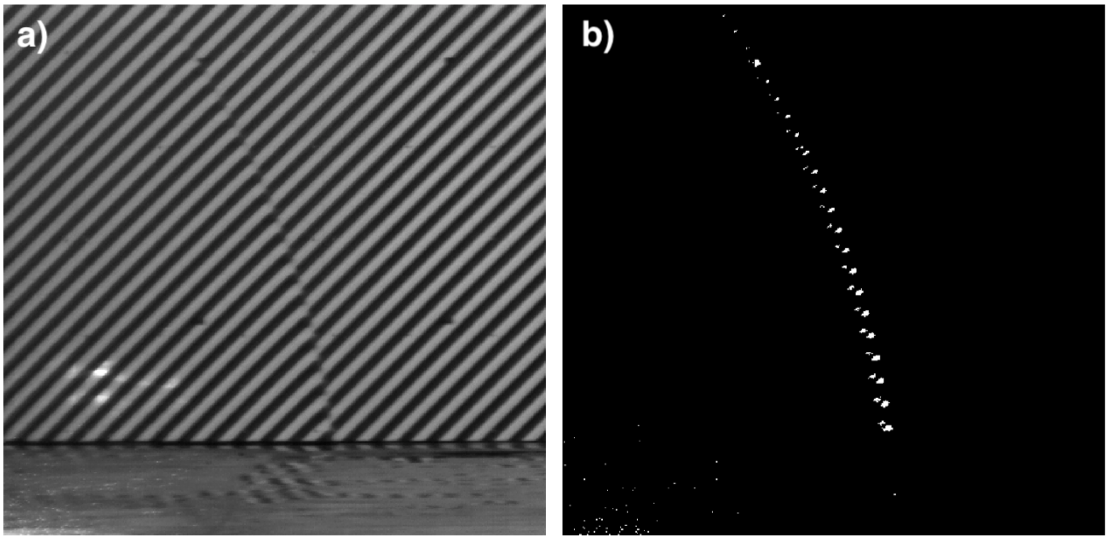

Figure 3.21: HSV stills from a test using 250 g PE4 hemisphere at 4 m stand-off: a) Raw video footage, and; b) Corresponding image subtraction

Utilising the simplistic image subtraction method results in frame-by-frame outlines of the disturbances caused by the propagating shock wave as seen in Figure 3.21b. Whilst it is clear from the presented images where the spherical expansion of the shock front is generally, prescribing an actual position of the front held some ambiguity. A bespoke algorithm was written to accurately locate the propagating shock wave amongst random light variations between frames from the subtracted images which aimed at identifying large disturbance regions and assigning a specific singular pixel within said region as the position of the shock front. The process consists of three stages: *Pixel cluster identification*, *Intensity changes along radial spokes* and *Radial distance confirmation*, the concept of which is shown Figure 3.22.

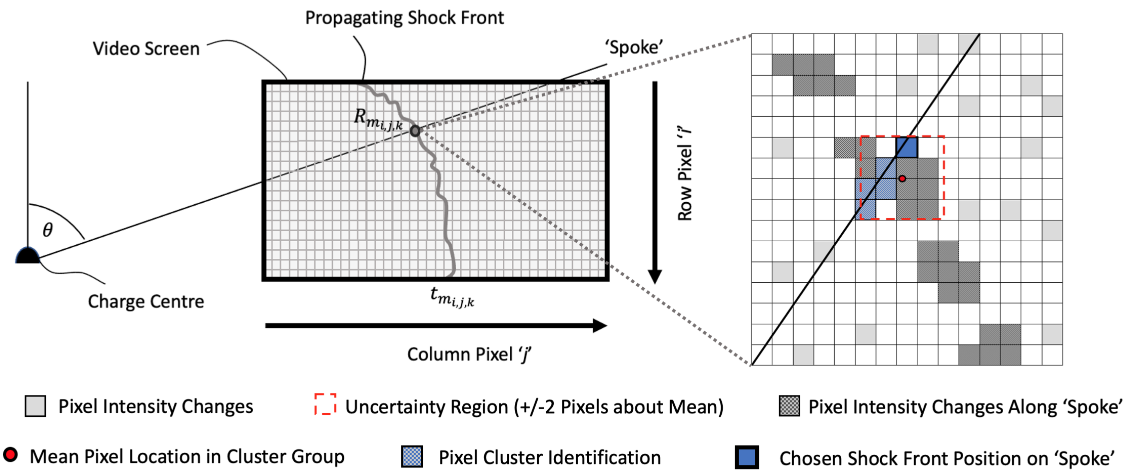

Figure 3.22: Method for detecting location of Shock Front through intensity changes on a virtual 'spoke' overlaid with pixel cluster identification

1. **Pixel cluster identification**: After eliminating any random light variation between subsequent frames through light intensity filtration, a clearly defined propagating shock wave can be identified by clusters of pixels, as seen in Figure 3.21b. The clustering size is directly related to the camera's shutter speed, i.e. the lower frame rates resulted in an increased blurring effect and large clusters. A MatLab script was written to locate the areas of each frame which had five or more connected pixels with large levels of light change in the image subtracted video, N. It is anticipated that with a higher frame rate, the number of connected pixels may reduce along with a more defined shock front, but 5 pixels was sufficient for all far-field videos discussed within this thesis.

2. **Intensity changes along radial spokes**: In a similar manner to previous studies[130], the second stage of the algorithm discretised the camera resolultions domain into 1° increments along virtual *'spokes'* which span from the charge centre to the extents of the recording boundary. The location of any pixels which have light intensity changes along each *'spoke'* are stored for each increment of angle and each frame. Due to the explosive charge being out of shot in each recording, the location was approximated through scaling-based calculations using the size of a pixel in the plane of the charge and known geometric relationships between the charge location, zebra board, camera and the pressure gauge in field of view, following proceedures outlined by Gerasimov and Trepalov[60] and Kucera et al.[93]. Fiducial markers on the zebra board, spaced 1.23 m horizontally and 1.33 m vertically, were used to cali-

brate the corresponding pixel size of ∼3 mm for video resolution of 1024x560, which was consistent across all far-field videos discussed.

3. **Radial Distance Confirmation**: The pixel locations saved as a result of stage one and two were then compared directly to automate the shock front locating algorithm along each *'spoke'* and remove any random light variation between frames. A MatLab script was written to compare stages one and two with an uncertainty region of ±2 pixels about the mean pixel location of the stage one results. This presented all the pixels which satisfied both stages of the analysis. The difficulty then came with assigning a distance to the regions of pixels which have been assigned in 3D space from a 2D image. Due to the spherical expansion of the shock wave and a fixed camera location, considerations had to be made to account for the camera recording the front of the shock wave in a different position to where the front would be along the gauge line used as the reference for calibration, as seen in Figure 3.23. To find the radial distance a given pixel is away from the charge, the locations of the camera, explosive and shock wave pixel location on the zebra board, denoted by subscript i, j and k respectively, were set up with coordinates in 3D space, x, y and z. The distances between each of the three locations were calculated using Equations 3.2, 3.3 and 3.4, where a is the distance between the explosive and the camera, b is the distance between the explosive and pixel's relative location on the zebra board, and finally c is the distance between the camera and the pixel's relative location on the zebra board (again see Figure 3.23 for reference).

$$a = \sqrt{(x_i - x_j)^2 + (y_i - y_j)^2 + (z_i - z_j)^2} \tag{3.2}$$

$$b = \sqrt{(x_j - x_k)^2 + (y_j - y_k)^2 + (z_j - z_k)^2} \tag{3.3}$$

$$c = \sqrt{(x_i - x_k)^2 + (y_i - y_k)^2 + (z_i - z_k)^2} \tag{3.4}$$

The distances evaluated from the above outline algorithm are then used to calculate the area of the triangle, A, enclosed between the three points in 3D space using Heron's formula (Equations 3.5 and 3.6). Assuming that the shock wave is expanding spherically, and the line between the camera and the shock wave pixel location is a tangent to the sphere, and therefore the radius, r, of the shock front would be equal to the height of the triangle, *abc*.

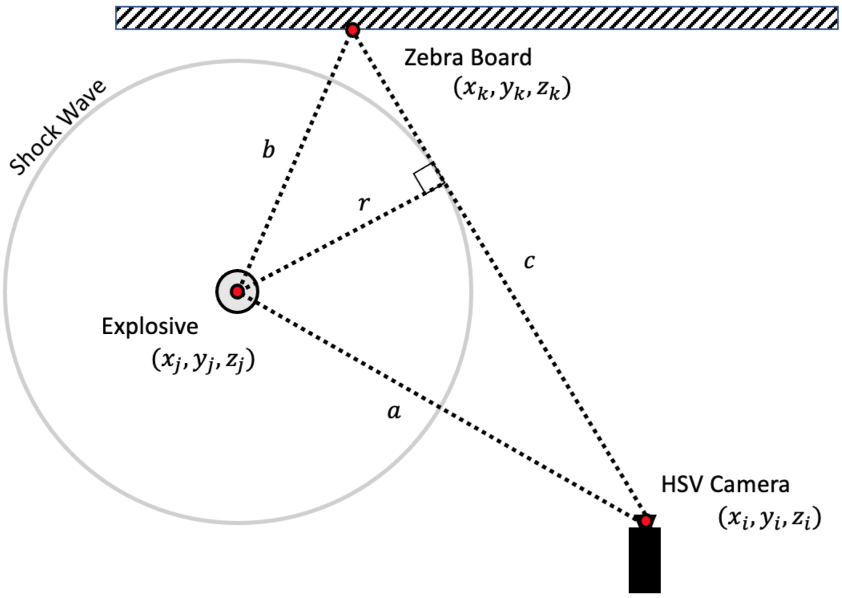

Figure 3.23: Schematic of shock wave radius calculation in 3D space to be used in conjunction with Equations 3.2–3.6

After calibrating, the pixel furthest away from the charge centre was identified as the position of the shock front along a particular *'spoke'*, at a given time. This was done to achieve test-to-test consistency regardless of the frame rate and associated blurring. It is important to note that although strict experimental procedures were in place, focal lengths were difficult to record as a manual zoom was used. Despite the levels of zoom being consistent, lens distortion effects subsequently were not accounted for during each test and thus would cause minor variations between videos recording different stand-off distances. Previous research has suggested that lens distortion results in minimal levels of uncertainty in pixel size calibration [136] but across a large testing pad could begin to induce some variation between different test setups. The presented within this thesis for far-field trial minimised the severity of lens distortion by comparing only like-for-like tests which would therefore remove the uncertainty associated with recordings made at the extents of a camera resolution for one standoff which corresponds to a more central region for a different standoff tested.

$$A = \sqrt{s(s-a)(s-b)(s-c)} \tag{3.5}$$

$$s = \frac{a+b+c}{2} \tag{3.6}$$

$$r = \frac{2A}{c} \tag{3.7}$$

3.3.1.2 Example of Edge Detection Algorithm

The results from the edge detection algorithm for a single test (250g PE4 hemisphere at 5m stand-off) are presented in Figure 3.24. KB predictions are also presented on the aforementioned figure, again using Hopkinson-Cranz scaling and a TNT equivalence of 1.22 to compare the raw data directly to an equivalent prediction. The high levels of agreement highlights the repeatability and accuracy in the results from the presented automated image tracking and arrival time interpolation algorithms discussed throughout the section and therefore validates them for use across all other far-field high speed video recordings of shock front propagation. When comparing Figures 3.10a and 3.24, the full-field data extracted from a single video gives a clear justification for the use of HSV over pressure gauges when studying shock wave arrival time.

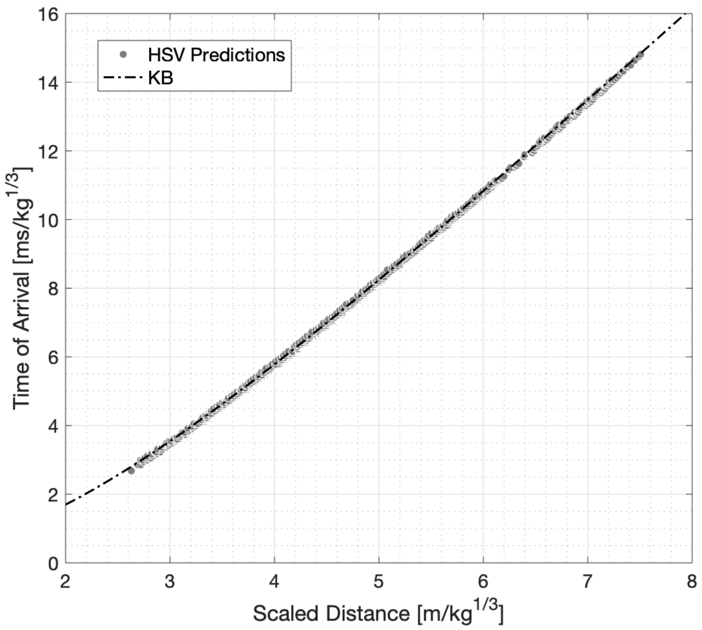

Figure 3.24: Shock front arrival time from a 250g PE4 hemispherical charge placed at a 5m stand-off, recorded using HSV and scaled using 1.22 TNT equivalence factor to compare to KB predictions

The results from the edge detection analysis of the primary shock, presented in Figure 3.24, provides confidence in the methodology introduced which could be utilised for all explosives tested in the far-field testing regime. Unfortunately for the PE4 trials tested, the technique was in development and therefore the critical parameters required to achieve accurate credible data were not yet known. Despite the method being suited for low levels of lighting, when weather conditions were unfavourable, videos yielded data which exhibit unclear shock discontinuities and therefore were omitted from detailed analysis. Provided the lighting conditions during testing are ideal, the analysis presents clearly defined edges of the shock with less noise from over-exposing the video. In certain instances when the conditions were preferable, the analysis was able to extract secondary shock wave data which was visible to the naked eye providing another benefit for this analytical method; this will be discussed in Chapter 4.3.3.

3.3.1.3 Shock Wave Arrival Time Interpolation

Blast parameters such as peak incident and reflected pressure can be linked to shock velocity (Mach number) through the well-known Rankine-Hugoniot jump conditions[90]. There is motivation, therefore, to understand how blast wave arrival time (and thus Mach number) varies with changing distance from the centre of the explosive, as this will provide insights into the variability of pressure and impulse parameters and the implications therefore on designs.

A method, presented visually in Figure 3.25, was proposed to interpolate arrival time data at increments of 0.1 m/kg$^{1/3}$ scaled distance along each virtual *'spoke'* for a given far-field shock wave tracking HSV recording. In doing this, a direct comparison could be made between pressure gauge recordings of arrival time, with discrete scaled distances, and high speed video recordings with discrete increments of time between each frame but a variety of processed scaled distances using the methods detailed in Section 3.3.1.1.

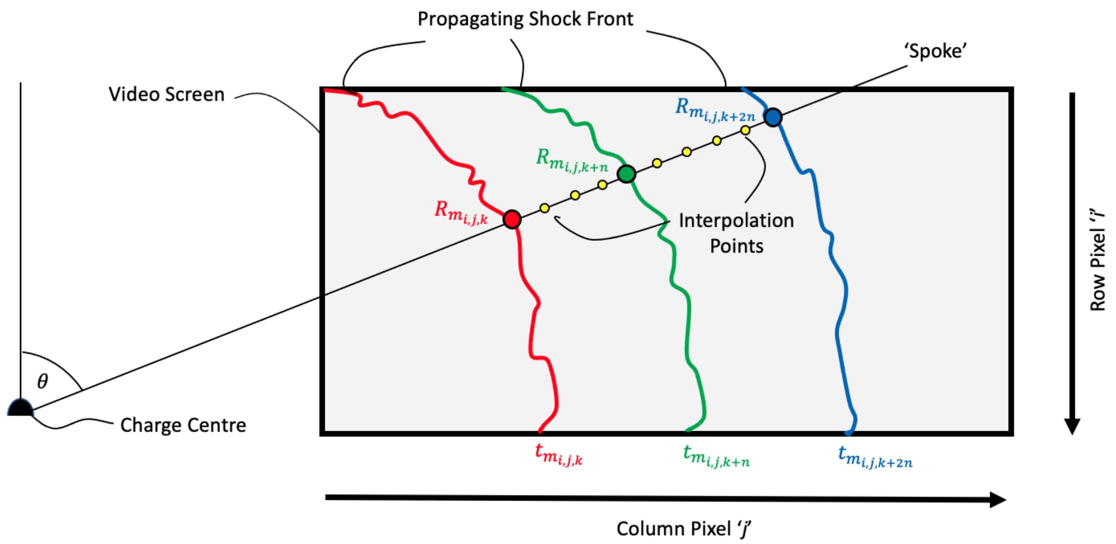

Figure 3.25: Method of interpolation of shock front arrival times along a virtual 'spoke' for prescribed scaled distances

Through collecting the interpolated arrival times with respect to scaled distance along each radial spoke, different types of analysis become available for comparing the results from HSV trials directly to those corresponding the pressure gauge trials. The synergy between two testing methodology provides validation of the each data acquisition and analytical method adopted alongside providing both precise measurements from discrete individual gauges and more generalised full-field representation using camera footage.

3.3.1.4 Extrapolating Blast Wave Features

An important thing to note, is that the techniques discussed in Section 3.3.1 can be used to evaluate a more robust understanding of other features of free-air blast waves, provided that the experimental conditions are favourable. The tools aforementioned could be implemented to track not just the primary wave propagation but all subsequent waves and reflections. The ability of tracking secondary shocks is purely down to the sharpness of the visible propagation on the video recording, improved providing the lighting is adequate. This data extraction can be used to develop the understanding of the secondary shock phenomena discussed in Section 3.2.3.2 when acquired through pressure gauge recordings.

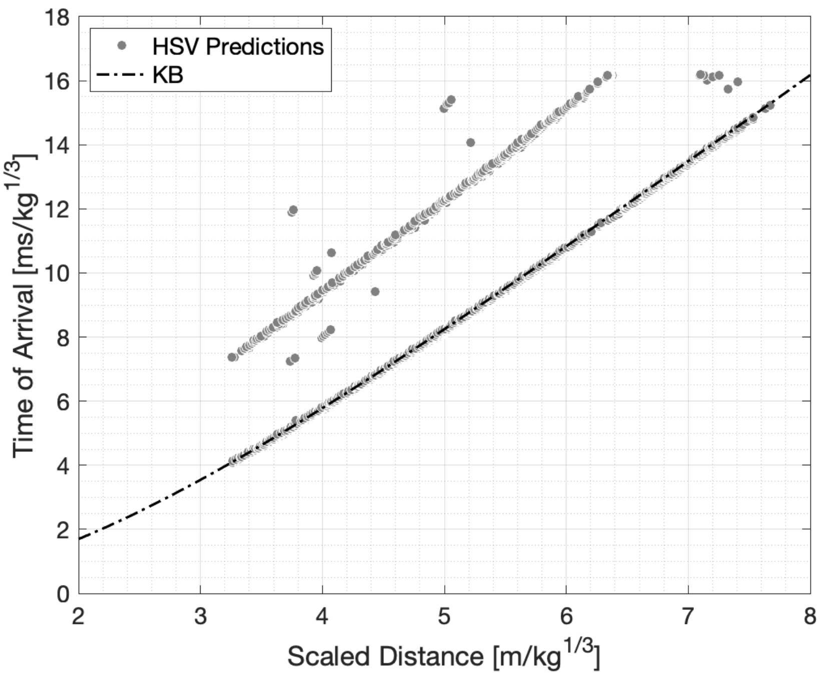

Figure 3.26: Shock front arrival time from a 250g PE4 hemispherical charge placed at a 5m stand-off, recorded using HSV and scaled using 1.22 TNT equivalence factor to compare to KB predictions, detailing the capture of the secondary shock propagation.

Figure 3.26 is an example of extracting subsequent shock data from a 250g hemispherical

PE4 charge placed at a 5m standoff distance. It is important to note that despite the clear trends of both primary and secondary shock propagation there are other data points which disagree with the data. The cluster of data points at the extents of the camera view, $Z >$7m/kg$^{1/3}$ in this test, is a result of the primary wave reflecting back towards the charge centre detailed by a reduction in distance travelled with time. The reflected wave propagation was not of interest for the contents of this thesis and so improvements to the tracking algorithm was not made to account for this change in direction of the wave. The other anomalous results which appear around the secondary shock data points are analytical errors associated with the light intensity of pixels during the image subtraction being more variable for weaker shocks. As mentioned above, with preferable lighting conditions, the HSV extracted data for both primary and subsequent shocks will exhibit less scatter.

3.4 Future Considerations for HSV Work

3.4.1 Far-Field Methodology Errors (Ei)

Despite the clear capability of the presented HSV data capture techniques and analysis, there are still concerns with the accuracy due to systematic errors which have yet to be fully considered and mitigated from the current experimental practice. Figure 3.27 displays the results of implementing the shock wave arrival time tracking algorithm, discussed in Section 3.3.1.1, for a nominally identical trial to that presented in Figure 3.24 - a 250g PE4 hemispherical detonation at 5m standoff from a reflected surface. It is important to note during this trial, an arbitrary intentional but non-obvious skew of the camera's field of view was made during the experimental setup away from the charge to assess the sensitivity of the analytical techniques to systematic errors in camera placement.

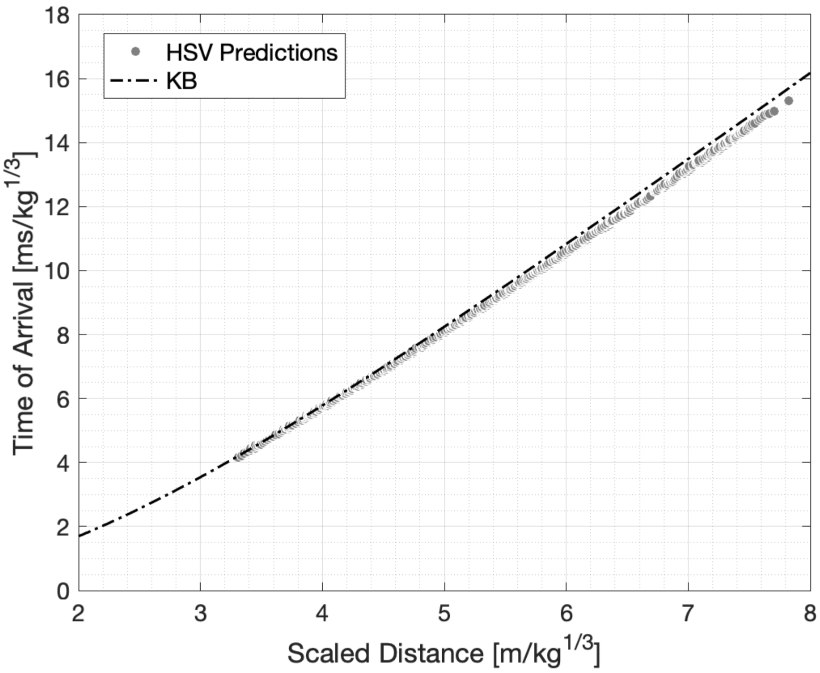

Figure 3.27: Shock front arrival time from a 250g PE4 hemispherical charge placed at a 5m stand-off, recorded using HSV and scaled using 1.22 TNT equivalence factor to compare to KB predictions, showing the effect off having testing procedure not perfectly square.

The systematic rotation in any direction would skew the number of pixels contained between the reference markers used to calibrate each frame of the video. This causes it to appear a smaller distance than what it would be if all equipment was perpendicular as per the analytical techniques assumptions. If a lower number of pixels is measured for the same known distance, each individual pixel size would increase in value. As the lengths calculated at each stage of the analytical process are directly proportional to these pixel sizes, a reduction in size would result in everything appearing to travel faster than a real shock wave. This is visible from the behaviour presented between the experimental data and KB predictions within Figure 3.27. With this knowledge, a reduction is required to the calibrated pixel size to account for the skew in the experimental setup.

In doing so, a skewed angle between the camera and the zebra board of approximately 2° was evaluated. This value of angular rotation was used to investigate the sensitivity of evaluated shock wave positions when only minor tweaks to assumed camera positions are made. The magnitude of this rotation is minor but across the distances covered during this experiential setup accounts for almost 750mm additional distance theoretically assigned hence the shock wave tending to arrive sooner than KB predictions in the experimental data.

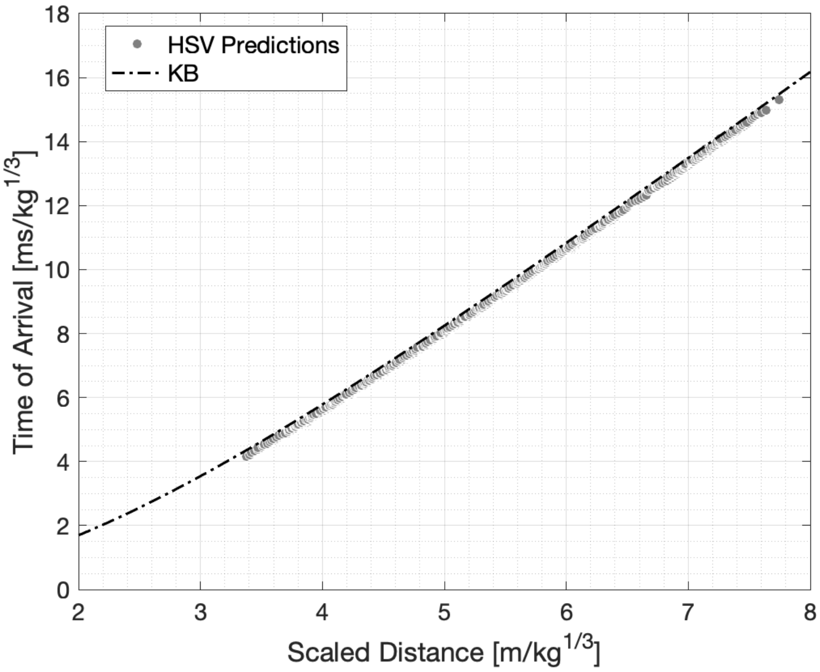

Figure 3.28: Re-analysed data from Figure 3.27 with an adjustment to the calibrated pixel sized to account for the skewing of the FOV during camera rotation.

The HSV data when adjusted for this skew presented a more reasonable comparison to KB predictions with an offset in the data. This generally suggests the shock wave has travelled further than predictions in the same amount of time, as seen in Figure 3.28. This has been deduced to be an effect of the prescribed initial boundary conditions set for the theoretical charge location, not visible within the video but is known through real-world measurement. The distance to which the camera's FOV extends is calculated using the visible pressure gauge position and the pixel size established during calibration. This distance was then subtracted from the known standoff to assign the location of the theoretical charge with respect to the pressure gauge in the respective video. Knowing the pixel size is larger during the skewed test means that the location of the explosive off screen has been re-defined as being closer to the gauge wall that what it is in reality. This is why generally a faster arriving shock wave is established.

It is essential to ensure the correct positioning of all initial reference markers and boundary conditions prior to conducting any future far-field HSV recordings. Despite the large quantity of data which can be extracted from HSV recordings, if the positions are not in-line with assumption made in the analytical procedures then the results will be inaccurate. The time committed to setting up cameras with high levels of precision is significant but the gain in data quantity in comparison to that collected during pressure gauge trials outweighs this.

This is just one of many errors which could result in strange behaviours of the analytically established arrival time data which should be consistent with KB predictions in far-field regimes. Ensuring the assumptions made in the analytical procedures align with the actual experimental setup clearly holds importance for data accuracy. This finding is linked with that discussed in Section 2.9 where the clear disregard for systematic errors in methodologies and analysis have resulted in published articles suggesting far-field blast parameters exhibit inherent variability. In actual fact, if these errors are accounted for, nominally identical data is consistent and is highly comparable to KB predictions.

3.4.2 Extracting More Parameters (Ai)

The strength in using high speed video techniques for experimental trial data extraction is the vast quantity obtained from a single trial. Despite work being undertaken relating arrival time data to pressure within the available published literature using Rankine-Hugoniot principles, there is still a gap in extracting the specific impulse of a shock wave using optical methods.

Murphy and Adrian[104] looked at developing a particle image velocimetry (PIV) system which measures velocity fields as a result of detonating explosives. The method was effective in far-field scaled distance ranges when comparing to assumed triangular blast wave profiles, but struggled in near-field instability and turbulence regions. Hargather and Settles[70] made efforts at using optical techniques to measure and attempt to scale explosive parameters in the gram-range. Whilst the authors made efforts at characterising arrival time and pressure through Rankine-Hugoniot conditions and time duration through theoretical assumptions proposed by Kinney and Graham[90], no link was made to specific impulse of the shock wave.

The current background orientated schlieren methodology used for far-field HSV data capture at the University of Sheffield could be developed to incorporate PIV analysis. To do so, it is essential for the far-field recordings to be calibrated to account for lens distortion and any further experimental errors associated with camera orientation which can be done so effectively using MATLAB's in-built camera calibration software. Once calibrated, an interesting development of this method would be to assess the velocity field measured using PIVlab, another in-built MATLAB GUI, in the attempt assign the time at which the positive phase ends for a propagating shock wave. Adopting a triangular blast wave profile approximation, the pressure at a given position, evaluated through arrival time, and the time at which positive phase ends, an estimation of specific impulse of the shock wave can be achieved at that given point.

3.5 Summary

The main body of established blast literature covers yield results of idealised high explosives when detonated in various scenarios. As mentioned throughout Chapter 3, the variety in conclusive findings does pose difficulty for truly understanding the fundamentals of blast wave phenomena alongside the associated inherent variability of recorded data.

The real-world implications of this lack of clarity is the uncertainty of both the effects an explosive threat yields alongside the confidence in protective measures to withstand the given threat. Engineers face a constant battle of providing improved efficiency and aesthetics in design, both of which may result in a reduction in the intrinsic robustness of a structure, thereby increasing the need for considered and holistic blast protection measures. Whilst ever there is a major disagreement between the consistency of yields resulting from a given explosive, there will always be a lack of confidence in protective structures implemented and therefore massive safety factors applied to ensure the upper bound of quoted variability is accounted for.

The need for a precise intrinsic quantification and characterisation of prescribed blast scenarios will enable better probabilistic assessments of threats which can be taken into consideration with more confidence at design stages of any protection regime. The idea that extrinsic sources of variability are included in experimental work used for numerical model validation is concerning when considering that some article quote spreads in pressure and impulse ±50%. This uncertainty should be prescribed at a later stage when considering the likely threats rather than including extrinsic error through poorly executed research.

This chapter has focussed on developing validated methods of experimental and analytical capabilities which result in consistent data from nominally identical trials. A detailed review of historical blast data has been presented which opens up the discussion, in line with Objective 1 of this thesis, of whether recorded blast parameters are in fact deterministic across a range of scaled distances. The historic data provides confidence in the consistency in explosive yields across two well documented compositions used during the high explosive era, but more recent research has highlighted variability regions as high as ±130%.

This chapter has scrutinised experimental methodologies adopted during free-air blast loading trials and the subsequent data analysis with the aim of providing validated techniques and procedures. This can provide data which facilitates development in blast wave theory as opposed to causing further confusion within the industry as to whether explosions are inherently variable or not. The presented techniques in this chapter have shown that for far-field scenarios, $Z > 3\text{m/kg}^{1/3}$, blast parameter variability can be minimised and is therefore considered deterministic regardless of early-stage detonation mechanics. The techniques have however highlighted the need for strict experimental procedures, especially when considering near-field loading conditions as these are highly sensitive to spatial variation of the energy release upon detonation. The remainder of this thesis will focus primarily on far-field studies to characterise the effects of a variety of different explosive compositions across a range of scaled distances.

Chapter 4

Ideal Explosive Blast Characterisation

4.1 Introduction

Considering the established hypothesis in Chapter 3, in that explosive yields are in fact deterministic when experimental methodologies adopt strict experimental control and automated analytical tools, a variety of different ideal high explosives have been examined to simultaneously further validate the tools presented in the aforementioned chapter. The aims of these analyses are to improve data consistency across a range of different ideal explosives and to quantify the levels of variability each blast parameter exhibits across a range of scaled distances.

Through conducting well-controlled trials across a number of ideal explosives and scaled distances a comprehensive understanding of definitive variability regions, in line with the hypothesis proposed by Tyas[173], can be established. When comparing the extracted data set independently and to semi-empirical predictions, developments to the fundamental understanding of explosive air shock and confidence in KB predictions and TNT equivalence can be established for different ranges of scaled distance.

4.2 Pressure Gauge Data

In similar fashion to Chapter 3, this section will consider the data captured using pressure gauges during experimental trials. This will be used in the attempt to both validate the on-going hypothesis of far-field blast parameters being deterministic and to assess the capability of the methods developed for analysis across a number of ideal explosives.

4.2.1 Positive Phase Blast Parameter Variability

This section will evaluate the explosive output of three ideal high explosives; PE4 (nominally 88% RDX with 12% Plasticiser/Taggant), PE8 (nominally 86.5% RDX with 13.5% Plasticiser/Taggant) and PE10 (nominally 86% PETN with 14% Plasticiser/Taggant), using tools established in Chapter 3. The choice of explosives used for the assessment techniques was based on their usage within a military setting, ease of acquisition through UK energetics vendors and predominantly due to the vast amount of historical testing undertaken at the University of Sheffield.

PE4 and PE8 are effectively the same explosive, with similar RDX and binder percentages, despite the variation in their binder compositions. The former explosive, PE4, was designed to match the American standard miltary grade explosive of C4 which is confirmed in the findings presented by Bogosian et al.[15], Rae and McAfee[115]. PE8 was a later developed RDX based explosive which was designed to supersede PE4, therefore providing no change for the end users of the explosive. PE10 again was designed to provide a similar explosive yield to PE4 but was PETN based rather than RDX offering a different explosive composition. The reasoning behind the development of this explosive was two fold: firstly to work better in colder environments; and secondly due to RDX being recognised as a problematic and bioavailable explosive which has tendencies to infiltrate watercourses[171].

With all the above mentioned, the results of any trials adopting the same methodology and data analysis for these three explosives is hypothesised to yield the same blast parameters. This was assumed true for far-field free-air scenarios, where any afterburn related to secondary chemical reactions ongoing in the fireball minimally affects the overall positive phase pressure-time history. The results of the far-field tests will be assessed and compared against both semi-empirical predictions and high-fidelity numerical modelling. This comparison had the overall aim of demonstrating that far-field blast parameters, $Z > 3\text{m/kg}^{1/3}$, can essentially be considered deterministic, whilst providing an example of the synergistic nature between the two.

4.2.1.1 Intrinsic Data Set Variability

To assess the intrinsic variability in a given data set, each positive phase blast parameter has been normalised against the mean value of that particular parameter for nominally identical recordings. By adopting this analysis approach, the consistency in the data set can be deduced and can help determine as to whether the working hypothesis of deterministic blast parameters holds credibility across a range of scaled distances and explosive types. The analysis considered the three explosives mentioned above to determine the inherent variability in the explosive yield of three ideal high explosives when adopting validated methods of conducting experimental trials and data analysis discussed in Chapter 3.

Figures 4.1a-d represent the findings from the initial intrinsic data set variability assessment of each positive phase blast parameter after adopting experimental procedures and analysis as detailed in Chapter 3. Notably what can be seen is a high level of repeatability in the processed positive phase blast parameters across all three explosives and scaled distances considered.

Reflected peak pressure, peak specific impulse and positive phase duration exhibit similar levels of spread across the entire range of scale distances tested; typically around ±6–8%, with a slight reduction in consistency as scaled distance reduces seen in Figures 4.1a, 4.1b and 4.1d.

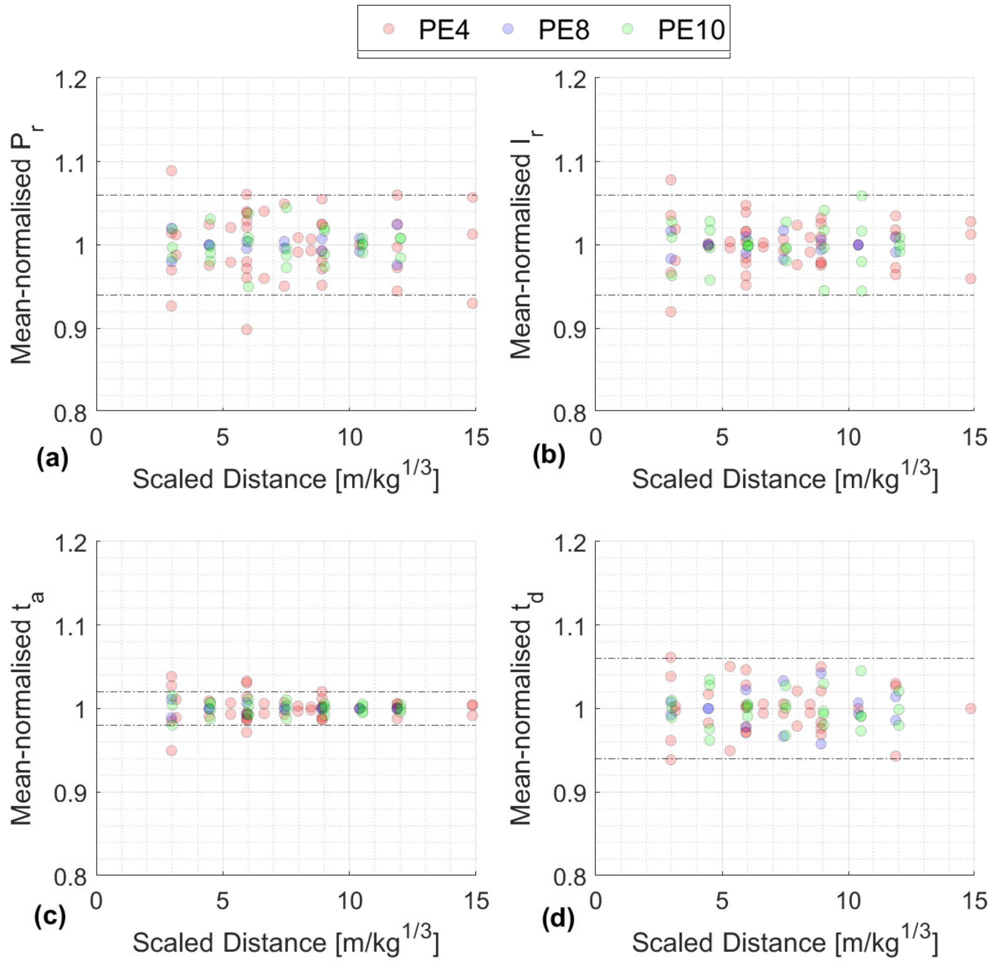

Figure 4.1: Compiled blast parameters from RDX and PETN based explosive trials as a function scaled distance, normalised against the mean of nominally identical trials: a) Peak reflected overpressure (Mean-Normalised P_r), b) Scaled reflected peak specific impulse (Mean-Normalised I_r), c) Scaled arrival time (Mean-Normalised t_a), d) Scaled positive phase duration (Mean-Normalised t_d)

The arrival time of the shock wave, in Figure 4.1c, exhibits a considerably smaller spread, within ±2% when $Z > 3\ m/kg^{1/3}$, which is to be expected for a parameter of generally much lower magnitudes. Again, a noticeable increase in variability as scaled distances reduces in line with findings presented in Rigby[127].

The consistency of the experimental results presents a clear indication that for small-scale, far-field, geometrically simple scenarios, the blast positive phase parameters are essentially deterministic with quantifiable but limited levels of variability. Despite only a few data points at each scaled distance, there is a clear reduction in arrival time variability as scaled distance increases which holds true for all three explosive types. Although not as evident across the other blast parameters, a reduction is present, which agrees with the idea proposed by Stoner and Bleakney[160] and Bogosian et al.[16] that variability levels differ with scaled distance.

The results of this analysis provides enough evidence to suggest that as the near-field is approached, $Z < 3\text{m/kg}^{1/3}$, a much greater spread in the arrival time data, and thus other blast parameters, is observed which agreed with findings presented by Simoens and Lefebvre[153]. This not only provides evidence to the hypothesis of scaled distance regions over which fireball surface instabilities are prominent, as discussed by Tyas et al.[174], Rae and McAfee[115] and Rigby et al.[130], but when compared with other published works on blast variability starts to build a more robust understanding of the development of explosive shock fronts.

4.2.1.2 Comparison Against Semi-Empirical Predictions

To assess the robustness of the KB prediction method and the accuracy of the data presented within this thesis, a Mean Absolute Error (MAE) analysis was undertaken between the results from each explosive and those predicted for varying quantities of TNT. This analysis was done to establish the best possible TNT equivalence value to represent each explosive. It is expected that due to the three explosives in question being designed to result in similar explosive yields on detonation, that the TNT equivalence values for far-field free air scenarios should be similar across all explosives tested.

The results presented in Figure 4.2d shows that generally speaking the positive phase duration tends to hold higher levels of variability due to the difficulty in assigning a specific value to the parameter. This is due to noise in the signal making the true point at which conditions return briefly back to atmospheric difficult to determine. It is further deduced that experimentally recorded results are around 90% of KB predictions which would cause any MAE analysis for a TNT equivalence value to be skewed. Thus, positive phase duration has been omitted from the considered MAE analysis.

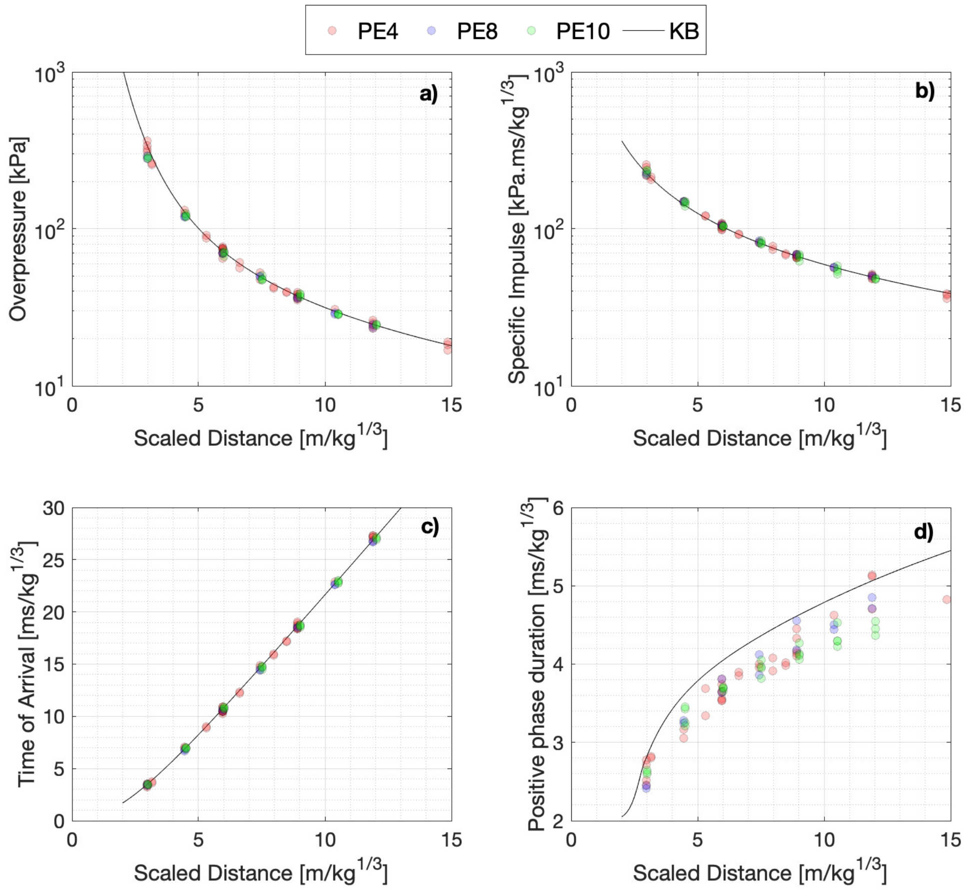

Figure 4.2: Compiled blast parameters from RDX and PETN based explosive trials as a function scaled distance, compared with KB predictions: a) Peak reflected overpressure, b) Scaled reflected peak specific impulse, c) Scaled arrival time, d) Scaled positive phase duration

The analysis was performed for definitive far-field scenarios, $Z > 3\text{m/kg}^{1/3}$, in light of the fact that for smaller scaled distances the variability levels rise. This believed to be a result of not only systematic experimental errors but also ongoing chemical reactions in the fireball resulting in fluid dynamic instabilities which differ from composition to composition. Therefore the decision was made that evaluating a TNT equivalence value for only the free-air shock propagation in the far-field was the philosophy of this analysis. This was undertaken through comparing the scaled mass equivalent shock produced from the explosives in question to KB predictions for 1kg of TNT.

It was found through averaging of the MAE values for pressure, specific impulse and arrival time at all far-field scaled distances, the three explosives all resulted in very similar TNT equivalency factors: PE4 and PE10 resulting in an equivalence of 1.22; and PE8 resulting in an equivalence of 1.24. This was a further reassurance and validation in both the experimental and data analysis techniques adopted for these trials as the three explosives were designed to have the same explosive yield. The TNT equivalence factors were applied to each of the corresponding compositions and subsequent recorded blast parameters presented in Figures 4.2a-d. The scaled results show a striking agreement between each blast parameter (expressed as a 1kg hemispherical TNT charge), and KB predictions.

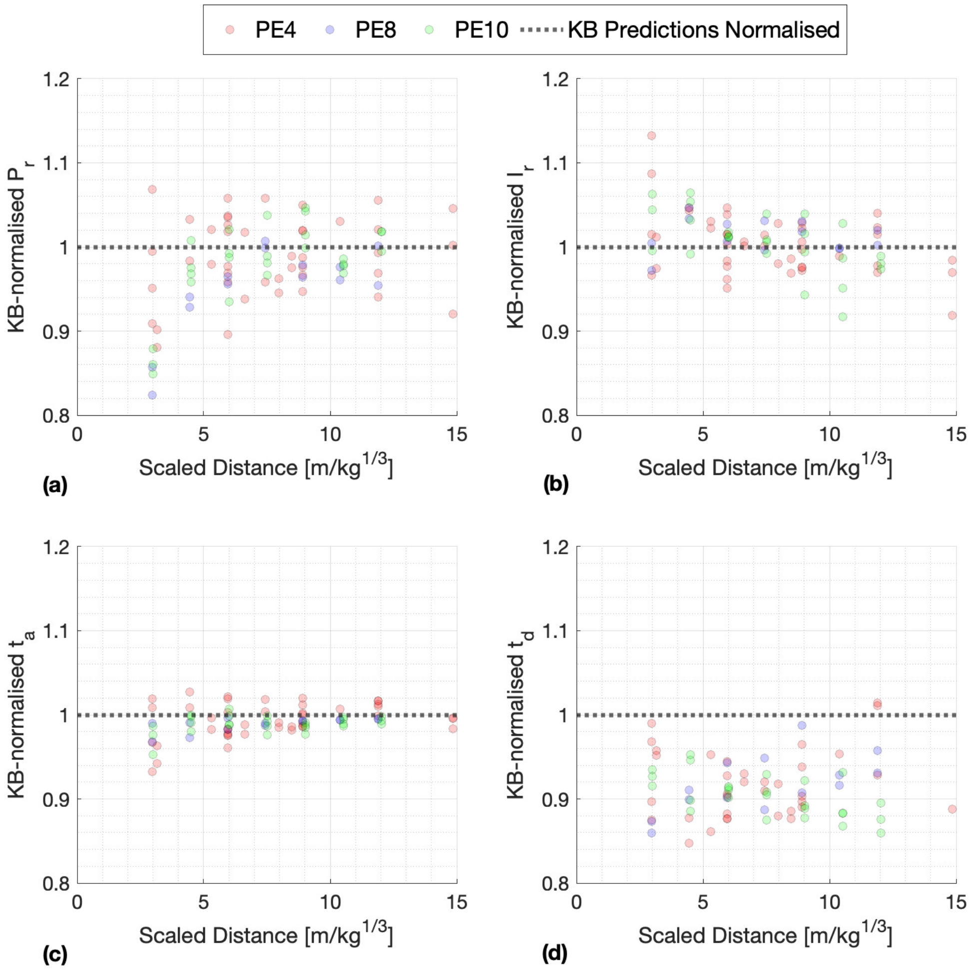

Figure 4.3: Compiled blast parameters from RDX and PETN based explosive trials as a function scaled distance, normalised against KB predictions for nominally identical trials: a) Peak reflected overpressure (KB-Normalised P_r), b) Scaled reflected peak specific impulse (KB-Normalised I_r), c) Scaled arrival time (KB-Normalised t_a), d) Scaled positive phase duration (KB-Normalised t_d)

Despite Figure 4.2d again showing experimentally recorded values generally lower than KB predictions, this finding follows the same trends presented in Figures, 2.12d, 2.13d and 3.10b. This, along with the agreement of each blast parameter with KB predictions in all of the remaining subplots in the aforementioned figures, validates the hypothesis that for far-field scenarios, ideal high explosive blast parameters are deterministic despite the variety in researcher, methodology, composition, analysis techniques and finally the year the trials were undertaken.

In order to establish specific levels of variability that the scaled experimental recordings had in comparison to KB predictions, a similar approach to that discussed in Section 4.2.1.1 was adopted in which the experimental recordings were normalised but by the KB prediction of the parameter at each scaled distance for which data was available.

Figures 4.3a-d present the results of the KB normalisation, which shows that for far-field loading in simple geometrical scenarios, existing semi-empirical predictions are in fact remarkably accurate and compare well to experimental data. This suggests that semi-empirical methods can be used with confidence as a first-order approach for quantifying the blast load conditions from a small-scale high explosive in simplified far-field situations. The slight increase in the variability as the scaled distance reduces to the extent of those presented in these trials. This gives rise to the ongoing hypothesis that as recordings approach the near-field there is less certainty in the data captured.

Interestingly to note from Figures 4.3a and 4.3b is the opposing correlation of recorded peak pressure and specific impulse to KB predictions. Taking into account the fact that the data presented was the result of a purely top detonated testing regime, the findings presented in Figure 3.16, found in Section 3.2.2.3, show comparable results to facilitate this discussion.

The peak pressure recorded in a top detonated blast is much lower than that of a bottom detonated simulation as result of inconsistent detonation product break out. The faster arrival time associated with top detonation is a direct result of the early expansion and the un-spherical propagation of products and shocks associated with the decomposition at the top of the charge. This then re-adjusts when the detonation wave reaches the bottom of the charge, effectively releasing all of the potential energy and the remaining detonation products begin to radially expand. This results in mach stems formation and thus a superposition of waves resulting in standard friedlander pressure-time histories at greater scaled distances. This finding provides clear explanation as to why experimentally the peak pressure values are lower than KB predictions for top detonated charges presented in Figures 4.3a. This does however reveal a systematic error in the majority of the presented data within this thesis, in that for near-field scenarios the complex interaction of the shock wave and detonation products results in increased uncertainty of the data.

Taylor [167,168,169] discussed in great detail the theory behind how blast waves form and hypothesised an instantaneous release of energy from an infinitely small point in space resulting in radial expansion of the products and shock. Whilst the data presented for the far-field scaled distances agree with equivalency scaling of spherical shock wave parameters, the smaller scale distances highlight a greater sensitivity of resulting blast parameters. This has been related directly to the variable detonation mechanics in shaped charges alongside detonation position and orientation.

The presence of the gauge plate clearing effect discussed in Section 3.2.2.3, shows that with near-field conditions, the reduction in the peak specific impulse value is significant when comparing numerical simulations directly to KB predictions. Whittaker et al. [179] ran numerical simulations to quantify the effects clearing has in this scaled distance region and showed that when $Z < 1.6\text{m/kg}^{1/3}$ clearing can be effectively omitted. The 1.25m simulation outlined in Figure 3.16 falls very close to this region and therefore it important to only consider the trends where clearing has been effectively ignored.

When removing the clearing effect from the 1.25m numerical model, the peak pressure for a bottom detonated trial over predicts that of a top detonated shot whilst the impulse values resort to comparing with the KB predictions remarkably well. The danger in comparing purely numerical analysis to the KB predictions is that the numerical models, and their corresponding EOS's were developed using far-field data, $Z > 3\text{m/kg}^{1/3}$. In this region the expanding fireball is no longer effecting the detached shock front. The model replicates an energy released instantaneously which results in a friedlander-like shock wave rather than one affected by the ongoing chemistry of the fireball. It would therefore be incorrect to suggest at this scale, the real-world physical mechanisms from the detonation mechanics and fireball is accurately captured.

The results presented in Figures 4.3b are processed using the curve-fitting method presented in Section 3.2.1.1, which does its best attempt at omitting the clearing effects from purely experimental data. This raises the question as to why an increase in the specific impulse is seen in comparison to KB predictions. This can be used to further explain the narrative of why the semi-empirical method becomes inaccurate for the near-field scenarios tests. Considering Figure 4.3b, the under-prediction of impulse suggests that the energy released from these high explosives is higher than TNT within the fireball region. This difference suggest one single TNT equivlency factor cannot be definitively assigned across all scaled distances.

The experimentally established positive phase duration, shown in Figure 4.3d, presents lower values to those evaluated by KB predictions by up to 15%. The large spread in the experimental recordings is directly related to the difficulty in determining this parameter, as discussed previously. This generally becomes more difficult with increased scaled distance as: (a) signal:noise is typically lower, and (b) the gradient of the latter stages of the positive phase is shallower, as can be seen in Figure 3.5.

4.2.1.3 Time of Arrival Variability

Despite the visibly low levels of variability shown in both Figure 3.10a and 4.3c, shock front time of arrival, t_a, is a somewhat overlooked parameter when compared to peak pressure and peak specific impulse despite its qualitative comparison to KB predictions. The arrival time of a blast wave can be used to evaluate the resulting pressures and impulses using Rankine-Hugoniot principles which presents a utility of arrival time as a parameter for blast design purposes. The main aim of this section is to investigate and quantify the variability of shock wave arrival times, and investigate how it varies with scaled distance.

Due to the consistency of the results presented across all three high explosives tested, it was decided that arrival time of PE4 would be assessed due to having a much larger data set, with multiple repeat shots at each scaled distance. To evaluate the precision and repeatability of the data set, the relative standard deviation (RSTD) was calculated from the pressure-gauge arrival time data (from the historic and current tests presented in this thesis: 157 in total). The results of which can be used to assess variations in the measurements from this particular experimental method with respect to scaled distance, presented in Figure 4.4.

To provide a more generalised relationship of arrival time variability with respect to scaled distances it was important to assess results which had enough repeat trials to represent real physical behaviours. Of all the scaled distances tested, there was a variety in which at least 5 nominally identical tests were conducted and so should provide a reasonable approximation to the general variability behaviour. These groups are shown in Figure 4.4 as solid markers, whilst the hollow markers presented show the remaining scaled distances tested which had less than 5 nominally identical results. Overlaid on the plot is an exponential trend connecting the groupings with 5 or more trial, which when considering the same qualitative behaviour is seen in the hollow markers, decreasing variability with increasing scaled distance, is believed to be a physical representation of how variability in arrival time changes with scaled distances specifically for top detonated charges. It has been assumed however that the same behaviour would be experienced by bottom detonated charges as a result of fluid dynamic instability formation, however to magnitude of the RSTD would be lower for equivalence scaled distances.

It is important to note the curve has been extrapolated for larger scaled distance values, $Z > 12\text{m/kg}^{1/3}$, but not for near-field conditions, $Z < 3\text{m /kg}^{1/3}$. The assumption made here is that for far-field scenarios, the propagating shock wave is unaffected by anything other than the medium it travels through, and therefore a similar relationship of variability is expected. For the near-field recordings it is however assumed the data would be affected by the sensitive detonation mechanics and to the idea of instabilities in the shock front forming and diminishing, in the intermediate range of scaled distances. The exponential relationship has been defined for the region of scaled distances tested and extrapolated as a guideline prediction outside these ranges. Future works will undertake more testing in near-field conditions, $Z < 3\text{m/kg}^{1/3}$, in the hope to show a reduction in arrival time variability associated with a smooth shock front before instabilities start to form at extreme near-field in the support of the hypothesis of shock wave instability regions[173]. It could however be that the magnitude of arrival time variability presented in Figure 4.4 would reduce if systematic detonation errors are omitted within the methodology.

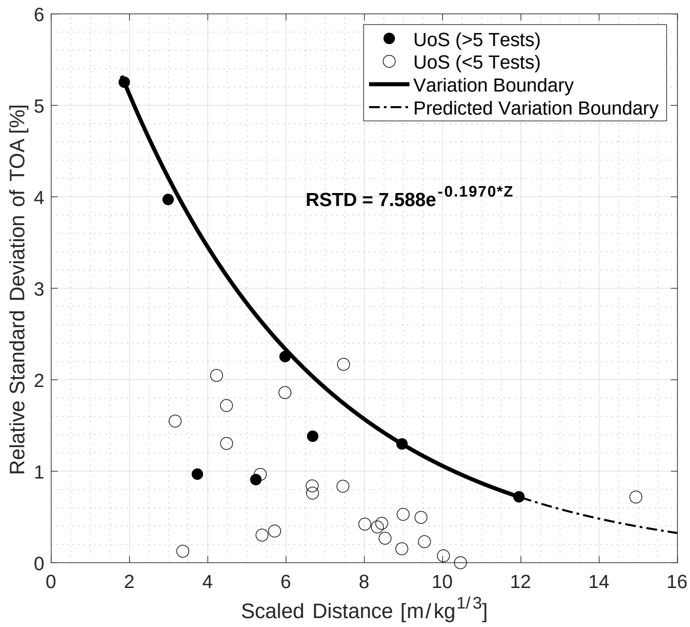

Figure 4.4: RSTD in shock wave arrival time with respect to scaled distance, from historic and current pressure gauge data

The main point to address from this analysis is that quantifying arrival time, t_a, variability with respect to scaled distance, which the parameter itself can be chosen with little ambiguity, provides a further insight into the development of a shock front and the formation of any un-spherical nature, especially in top detonated scenarios. Current predictive methods provide discrete blast parameters for a given scaled distance an explosive is away from a target. Through understanding the spread of experimentally measured t_a, improvements can be made to fast running predictive methods to provide probabilistic blast parameters within the uncertainty range for a given distance.

4.2.2 Numerical Simulation

The pressure gauge results presented within this Chapter, begin to build a coherent fundamental understanding of the nature of experimentally recorded far-field loading from a given charge composition, shape and mass. The importance of these findings provides a starting point to establish characteristics of more challenging blast loading conditions both in the near-field and those in complex environments, knowledge of which can be supplemented with high-fidelity numerical modelling.

Whilst experimental data is beneficial for understanding the real world yield and subsequent effects of a particular explosive detonation, both the costs and safety concerns related to blast trials create a need for high fidelity numerical simulations which are able to capture the behaviours within any scenario.

Understanding the mechanisms and magnitudes of blast loading on targets from both near-field detonations of high explosive, and those in complex environments, is of key importance for the analysis and design of the response of protective structures. However, there is little definitive experimental data on the measurement of these loads and consequently the predictions of numerical models of near-field blast loading are largely unvalidated.

The experimental results presented with Chapter 4 have been used to validate far-field numerical models for PE4, PE8 and PE10, using the methodology outlined in Whittaker et al.[179]. The intention was to implement the developed equations of state (EOS) for each explosive, into much more complex numerical simulations to produce validated and accurate predictions.

It is important to note that the numerical modelling discussed within this thesis is collaborative work between the University of Sheffield, Blastech LTD and DSTL, which together are attempting characterise explosives with high levels of accuracy in order to map out the effects a given charge composition, mass and shape may have in a prescribed environment to better plan and protect civilian infrastructure. Whilst DSTL have conducted the numerical simulation, the author has undertaken all experimental data capture and comparative studies.

4.2.2.1 Model Description

The baseline numerical model consisted of 250g hemispherical charges placed on the floor which were centrally detonated (of an equivalent sphere) to match the experimental procedures adopted with the testing regime. A reflective boundary was set at the edge of the model used to represent the reflective wall (be that the bunker or the blockwork wall) with a size of 2.2m in height and 4.4m in width to prevent any clearing effects within the positive phase of the reflected shock. An additional reflective boundary was set up along the ground surface to represent the concrete pad used during the explosive trials.

Afterburn is included in these free-air models to show that thermochemical analysis can suitably parametrise numerical models rather than relying on experimental methods which are very expensive and time consuming processes. The EOS was generated in a few hours using a thermochemical code. Afterburn should be included in free-field models to achieve an accurate EOS. This is to show that the model behaves in a representative way when it is included for all scenarios, whether that is relatively small amounts in free-field or large amounts in confined scenarios.

The numerical model was solved using APOLLO blastsimulator, which makes use of Adaptive Mesh Refinement (AMR), and zoom levels (distance-dependant AMR) to allow finer mesh resolution to be used within the complex regions of numerical analysis [36,109]. AMR is based on a mesh which exhibits an inconsistent resolution globally. In regions of the domain which requires a more refined resolution (i.e the detonation point, the shock front etc), the mesh refines to make more precise predictions. Other area of the mesh will reduce in resolution to allow for simulations to be undertaken faster. As the simulation progresses, as do the refined areas, and therefore providing high resolutions in the area which require them. This has the benefit of saving the computational power for the areas that require it through reducing the computational demand from areas where it is not needed. The AMR process requires a user-defined zone length, corresponding to the coarsest cell size, and a maximum resolution level size which corresponds to the smallest allowable cell size. The software then refines and un-refines different zones within the model (based on differentials of pressure, material etc) to accurately simulate the event while maximising efficiency. The model also uses “zoom levels” which allows a higher resolution level to be used for a fixed radius from the charge centre (e.g. a zoom level of 1 for 200mm would increase the maximum resolution level by 1 until a disturbance is registered at 200mm, the model would then only allow the initial maximum resolution level to be achieved for the remainder of the model). As an example, the 2m models reviewed within the remainder of this document had the following zone lengths and resolution levels:

- Zone length = 200mm, maximum resolution level = 5.
- Zoom level 3 for 200mm from charge centre.
- Zoom level 2 for 600mm from charge centre.
- Zoom level 1 for 1400m from charge centre.
- Then maximum resolution level of 5 (6.25mm) for the remainder of the model (6ms).

The Explosive EOS parameters used in this study were generated using the thermochemical code Cheetah v7, which, due to export control reasons, are not available for publication. Therefore, an alternative thermochemical code, EXPLO5, was also used to determine the EOS for the explosives. These parameters have only been used for a complementary comparison to the Cheetah study and have not been fully assessed or validated, but are provided as representative values in Table 3.2. It is important to note the developed parameters were produced purely based on the explosive composition, correct density and a best guess of plasticiser material (finding the exact composition may improve the results), all done using the same default methodology. No calibrating to experimental data or tweaking of technique or parameters to improve results was performed. The numerical model construction is also discussed in more detail within Section 3.2.2.1 which provides additional narrative to the discussion for reference.

4.2.2.2 Numerical Model Validation

Figure 4.5 presents a comparison between numerical and experimental pressure histories across a range of standoff distances for each ideal explosive tested. A high degree of similarity in the qualitative form of the pressure-time histories, for all three explosives, across the entire range of far-field stand off distances, provides confidence in the modelling approach and parameters. This finding alone gives rise to the hypothesis presented by Tyas[173] that for at least far-field scenarios, $Z > 3$ m/kg$^{1/3}$, explosive characterisation is deterministic with low levels of variability. The comparable results, when adopting a more realistic representation of the test conditions, highlights the synergistic nature of these two techniques. Numerical models have become powerful enough to not rely solely on experimental data for validation and can now be used to fault-find systemic flaws within experimental procedures.

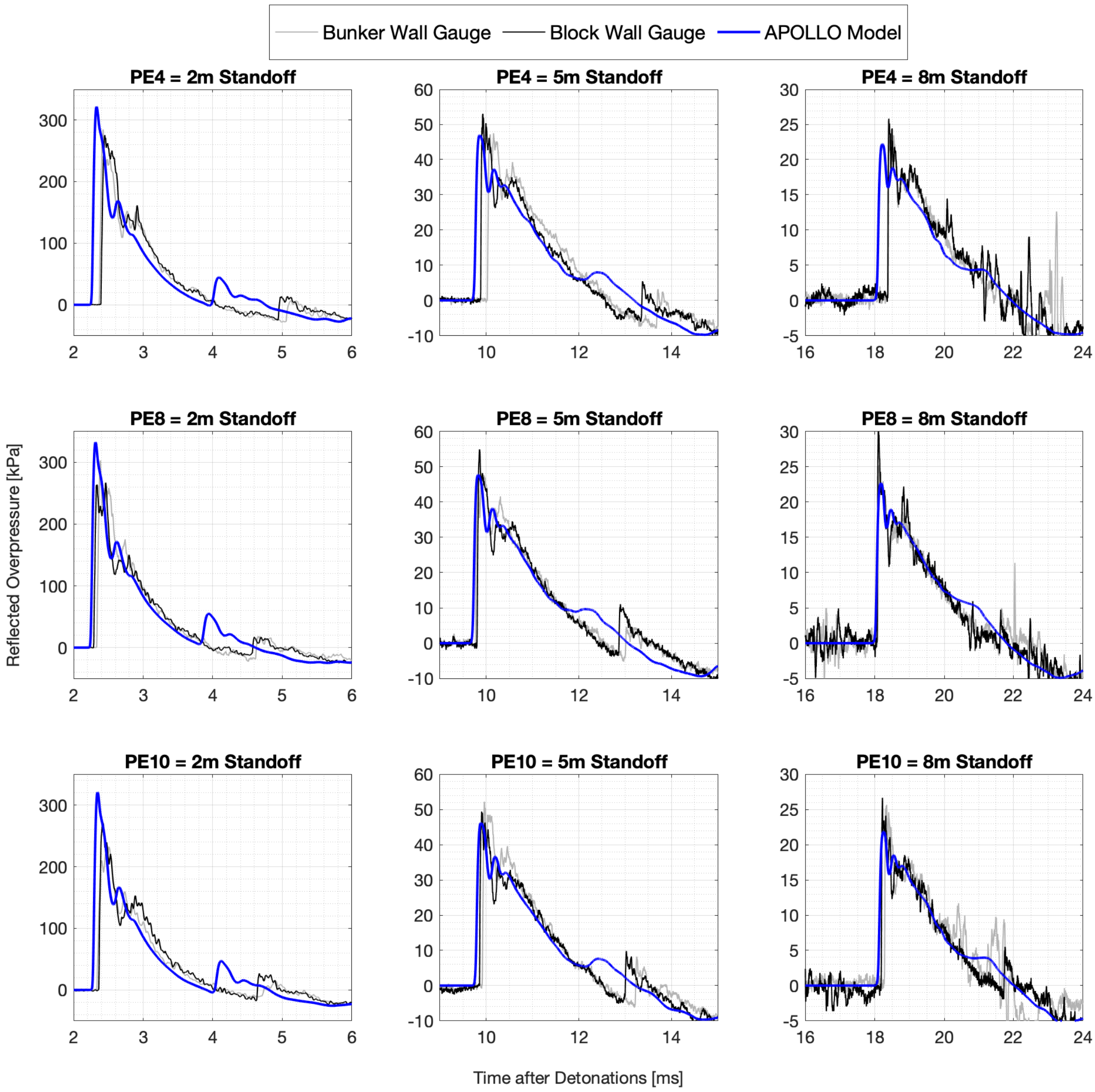

Figure 4.5: A compilation of reflected overpressure-time history plots for the three explosives tested across three different stand-off distances compared to the corresponding validated and APOLLO model predictions

Interestingly what is exhibited across each numerical simulation displayed in Figure 4.5 is a much faster arrival of the secondary shock wave when compared to experimental trials. This feature can lead to artificially high specific impulse predictions with the secondary shock arrival coinciding with the positive phase of the primary shock event. As mentioned in Section 3.2.2.1, the secondary shock arrival time varies depending on how afterburn is modelled. The current understanding of the secondary shock is that it is intimately linked to the post-detonation pressure–volume–energy relations of the fireball, which currently is not captured accurately without manual tweaks to modelling parameters[141].

4.2.3 The Negative Phase

To evaluate the findings in Rigby et al. [133], which displayed comparable predictions of negative phase parameters to well-controlled experimental testing of PE4, the same methodology and analytical techniques were adopted again for the remaining ideal explosives of PE8 and PE10. The result of which have been scaled accordingly and are presented in Figures 4.6a-c.

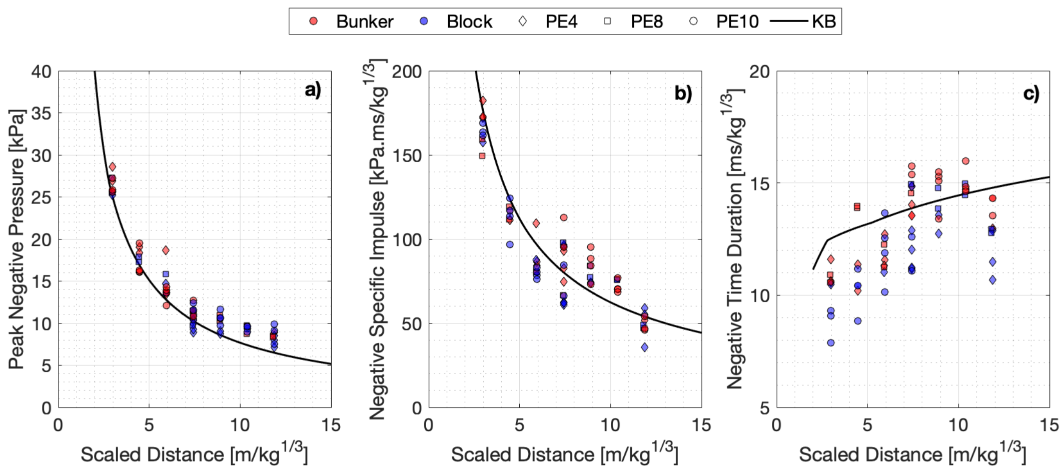

Figure 4.6: Compilation of scaled negative phase parameters results of 250g PE4, PE8 and PE10 hemispherical charges using the representative TNTe: a) Negative Pressure, b) Scaled Negative Specific Impulse and c) Negative Phase Time Duration.

The variability in each negative phase parameter is visibly greater than the positive phase parameters presented in Figures 4.2a-d for the same explosive trials. This has been linked to the increased difficulty in prescribing parameters with lower magnitudes being sensitive to electrical noise and systematic experimental features. Despite this, the main conclusions to be drawn from the data presented in the aforementioned plots is that the plastic explosives tested behave almost exactly in line with KB predictions for far-field scenarios when conducted under strict conditions. The same cannot yet be deduced across all scaled distances as the behaviour of near field loading conditions are yet to be investigated and will be part of future planned works.

4.2.3.1 Secondary Shock Data

Section 3.2.3.2 began the investigation into the secondary shock and its associated blast parameters for PE4 detonations. The study presented a consistent general behaviour with KB predictions across the far-field range of scaled distance. There was however significant discrepancies in terms of the magnitudes due to being compared directly to a primary shock. Whilst the KB predictive tools in there current form do not capture secondary shock waves accurately, the presented behaviours of the associated parameters could provide insights into the mechanisms involved in their development. This behaviour is believed to be essential for fundamentally predicting them. With this idea in mind, the secondary shock data from both PE8 and PE10 was analysed in the same way, using the corresponding TNTe values evaluated in Section 4.2.1.2 are presented in Figures 4.7a-d.

Across all three plastic explosives tested in the far-field range, the scaled secondary shock positive phase parameters compare remarkably well when compared to one another at each increment of scaled distance. The general increase in variability associated with each of the parameters, seen in Figure 4.2, has been associated with the chaotic detonation cloud medium the secondary shock has to propagate through. This, similarly to primary wave data, tends to reduce with an increase in scaled distance seen in Figures 4.7a and 4.7c. This suggests that variations related to this changing medium are insignificant once measurements are far enough away from charge centre.

A feature which is exhibited within the pressure data recorded for the secondary shock (Figure 4.7a), is an apparent plateau at $Z \simeq 10m/kg^{1/3}$ and an increase in pressure values experienced some distance afterwards. The plateauing behaviour is justified through the curtailment of pressure as distance increases until the wave effectively is obsolete, but the apparent rise in pressure holds no physical explanation. This visible increase is a systematic error within the data capture at these large scaled distances. Pressure magnitudes are so low for the secondary shocks that the assignment of parameters is extremely sensitive. Using gauges that are rated to 70 times greater than these magnitudes is flawed. The inherent electrical noise in the system accounts for ±1kPa and so contributes to the spreads seen. It is difficult to improve this using this methodology as gauges are required to be higher rated to survive the pressure from the primary wave.

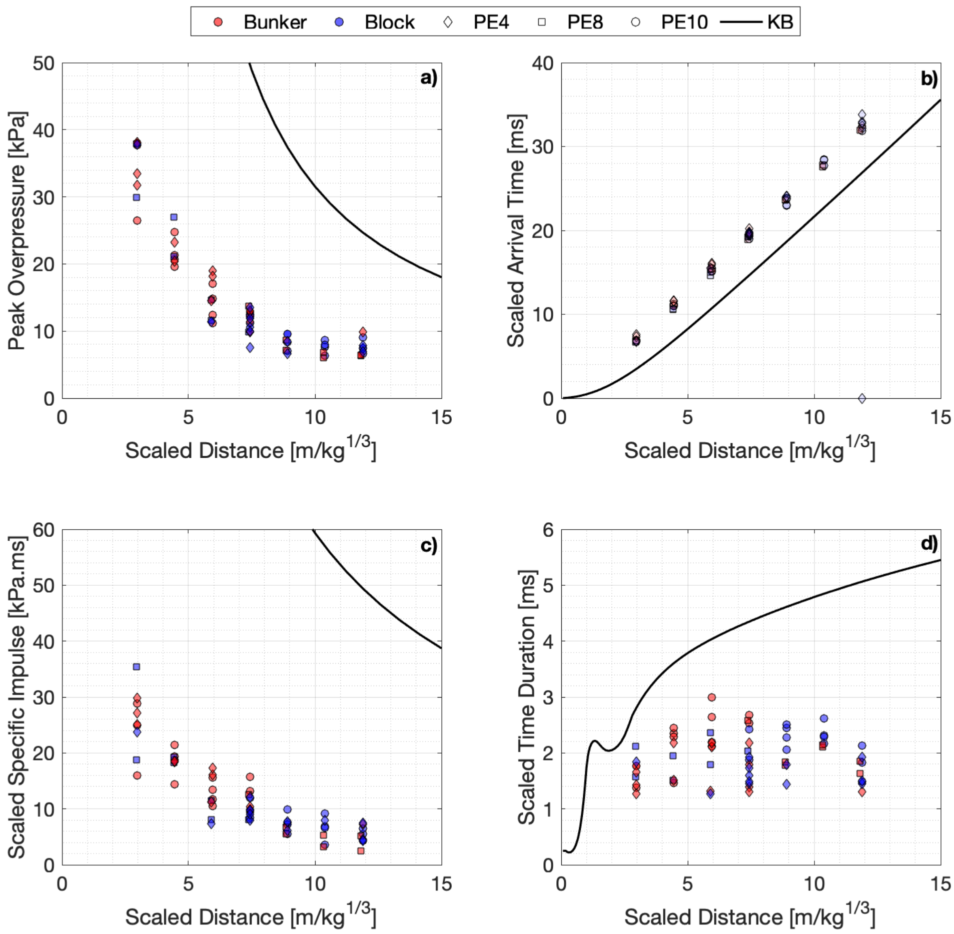

Figure 4.7: Compilation of scaled secondary shock parameters resulting from visual analysis of 250g hemispherical charges of PE4, PE8 and PE10 using the representative TNTe values: a) Negative Pressure, b) Scaled Negative Specific Impulse and c) Negative Phase Time Duration.

Clearly the ideal explosives investigated within this thesis exhibit similar behaviours to a primary wave but are not captured by KB predictions when scaling the results based on the original charge mass and established TNT equivalency values.

4.2.3.2 Secondary Shock Delay Predictor

The delay in time between the arrival of both the primary and secondary shocks is a feature which has been previously investigated success to quantify equivalent TNT yields [129]. Figure 4.8 presents the scaled secondary shock delay data across the three ideal explosives considered in this thesis. Although exhibiting a consistent behaviour with scaled distance, this could be related to the fact PE4, PE8 and PE10 have been almost identical across each parameter investigated. Rather than assuming this behaviour is consistent for all ideal explosives, it was therefore important to compare these results to historical data, providing confidence in the presented data within this thesis alongside the predictive tool developed by Rigby and Gitterman[129].

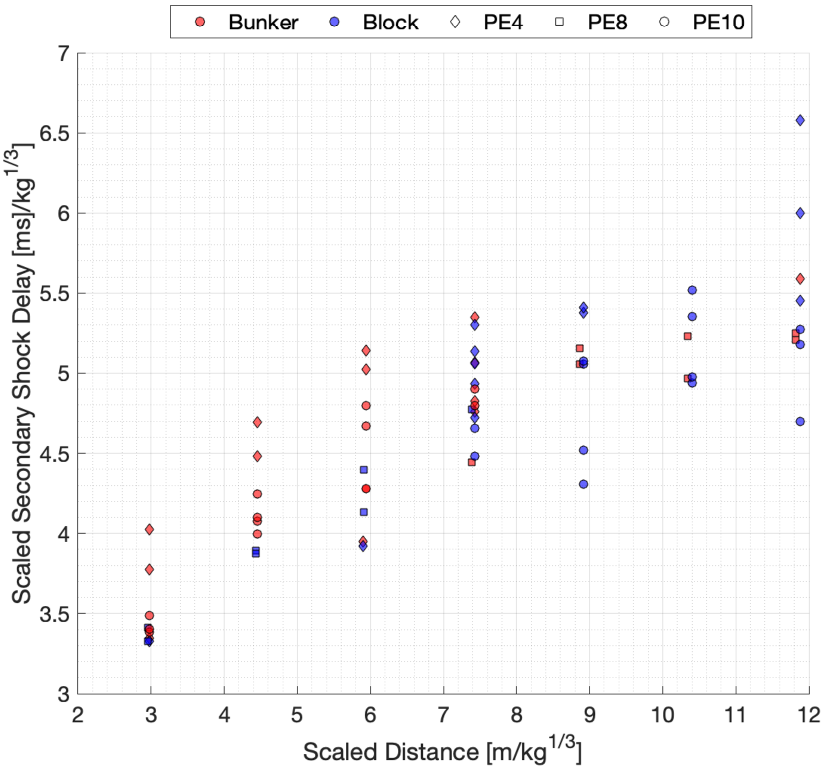

Figure 4.8: Scaled secondary shock delay with respect to scaled distance for all three ideal explosives using representative TNTe values

Through manipulation of the data, presented in Figure 2.8, by dividing the secondary shock parameter, τ_{ss} (derived by Equation 4.1), by scaled distance squared, the parameter becomes dimensionless and therefore required no physical justification. The result of this data manipulation is displayed in Figure 4.9 with a log-polynomial fit represented by Equation 4.2.

$$\tau_{ss} = \delta t_{ss} V_{od} / Z^2 (\rho W)^{1/3} \tag{4.1}$$

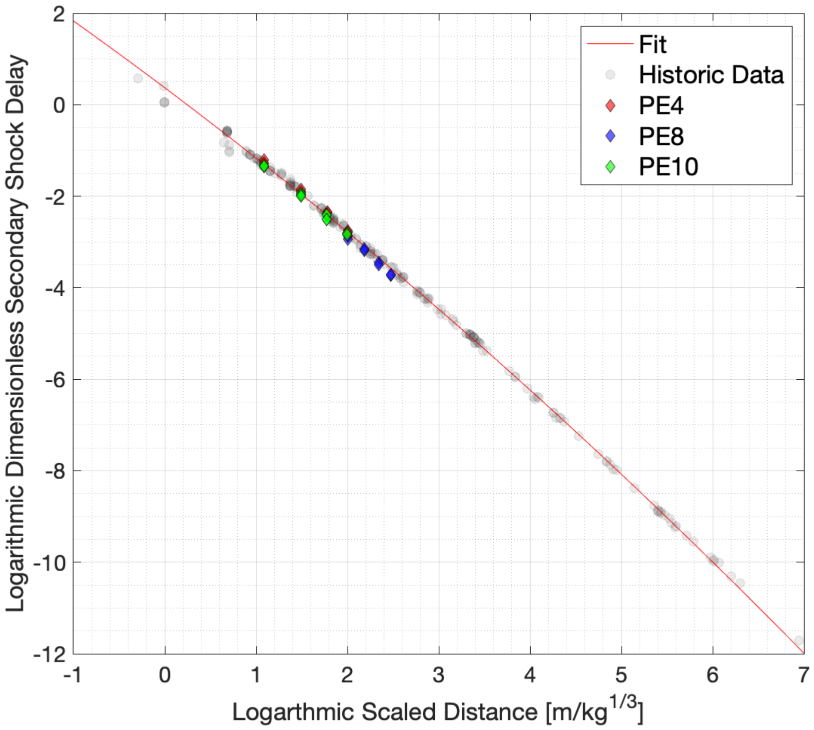

Figure 4.9: Dimensionless secondary shock delay parameter evaluated for all ideal explosives scaled accordingly compared with polynomial fit to historical data

Plotted alongside the historic data are the three ideal explosives investigated in this thesis, showing high levels of consistency when compared to all the experimental data and the newly presented fit. It is important to note that whilst the scaling of these secondary shock parameters is based on some physical mechanism, the fundamental processes underpinning the secondary shock behaviour is not yet fully understood. The fact there is such a close relationship between all the explosives considered, despite differences in velocities of detonation, packing densities and TNT equivalences, suggests that there is a real physical process relating the secondary shock to these parameters.

$$log(\tau_{ss}) = 0.3682 - 0.0351log_{10}(Z)^2 - 1.498log_{10}(Z) \tag{4.2}$$

4.2.4 Pressure Gauge Summary

This section clearly validates the analytical and experimental techniques discussed in Chapter 3 for pressure gauge type recordings across the far-field range for three plastic explosives with ideal behaviours. Alongside this, there is definitive evidence that with well-controlled experimental trials, data only exhibit high levels of consistency but both positive and negative phase blast parameters are captured remarkably well by KB predictions. With this finding, it is hoped that the industry will recognise that for far-field regimes, the yield of explosives is not inherently variable and steps can be made to improve the fundamental understanding of blast wave mechanics.

Detailed analysis into the secondary shock phenomena was undertaken in the attempt to understand the physical mechanisms behind the subsequent wave propagation and attempt to both quantify and characterise its behaviour. The work developed in this chapter provides a reasonable and logical assessment of explosive blast wave features and presents a validated prediction tool which could potentially be integrated into numerical simulations to better capture its behaviour. Whilst the fundamental mechanisms are yet to be captured accurately for the secondary shock features, these developments can hopefully drive improvements to the knowledge.

Future experimental data is required from explosives which exhibit widely different TNT equivalency values to distinguish whether the trends seen through Figures 4.7a-d are consistent across explosive composition, mass and distance. If the resulting data was consistent, considerations into a more appropriate way of scaling the results extracted from secondary shock data would be required to either agree with KB predictions of a primary wave or to develop a set of new empirical curve to supplement the established well validated predictive tool.

4.3 High Speed Video Data

This section will begin to consider the data captured using high speed cameras during far-field testing, tracking specifically the propagating shock wave in real time away from the explosive centre. With this technique of analysis being relatively new for the blast industry, it has not been fully explored. The tools developed in Sections 3.3.1.1 and 3.3.1.3 have been tested against the three ideal explosives discussed in this chapter. Comparisons have been made directly to corresponding pressure gauge data to both further validate the methods developed and to provide greater insights into the shock wave phenomena.

4.3.1 Time of Arrival Variability

With arrival time being the main feature captured during HSV recordings, it was important to assess how the parameter varied both spatially and temporally during the spherical expansion of the shock wave. Implementing the shock wave edge detection and arrival time interpolation tools for far-field high speed video recordings, as described in Sections 3.3.1.1 and 3.3.1.3 respectfully, arrival time, t_a, values were established at every 0.1 m/kg$^{1/3}$ scaled distance along each virtual *'spokes'* which start at the charge centre and plot radially outwards, in increments of 1°. The data captured through this analysis allows for a direct comparison to pressure gauge recordings which records pressure-time histories at discrete locations. The 3,163 data points as a result of implementing these methods on 10 HSV recordings of PE4 far-field detonations, 4,313 data points for PE8 from 6 recordings, and 3,639 PE10 data points from 4 recordings, were collated with respect to each increment of scaled distance. The RSTD was calculated similarly to that done for the gauge recordings seen in Figure 4.11.

The standardised range of interpolated HSV arrival time results are compared directly to pressure gauge variation of PE4 trials, with respect to scaled distance, presented in Figure 4.10. As lens distortion was not accounted for during these trials, the videos were not used as a group of collated data, and only those with the same test set up and explosive composition were compared. Regardless of this, the relative variability of arrival time recordings at specific scaled distances held fairly consistent between groupings of tests when compared to the relationship pressure gauge data had with scaled distance.

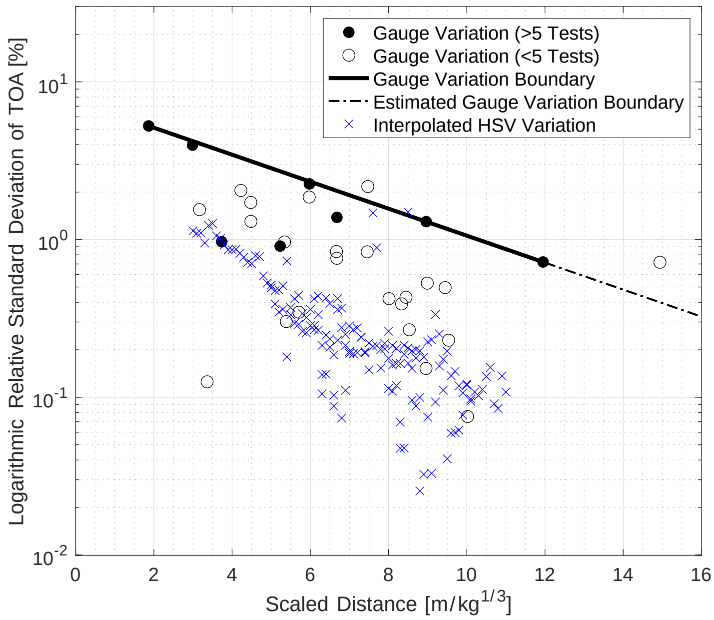

Figure 4.10: RSTD in shock wave arrival time with respect to scaled distance, when comparing pressure gauge and HSV data

A significant reduction in the variability of processed arrival times across the entire range of tested distances is experienced when using high speed video for PE4 detonations. In part, this reduction in variability is associated with the volume of data points created through the interpolation at each scaled distance. However, some of the scaled distances in question had a similar benchmark number of data points as the pressure gauge results. That being said, for the entire range tests, the two extremes had a low number of recordings established and yet there is still a noticeable reduction in processed t_a variability as scaled distance increases. This alone provides clear justification for the use of video recordings during explosive trials to enhance the precision and repeatability of blast parameters between tests.

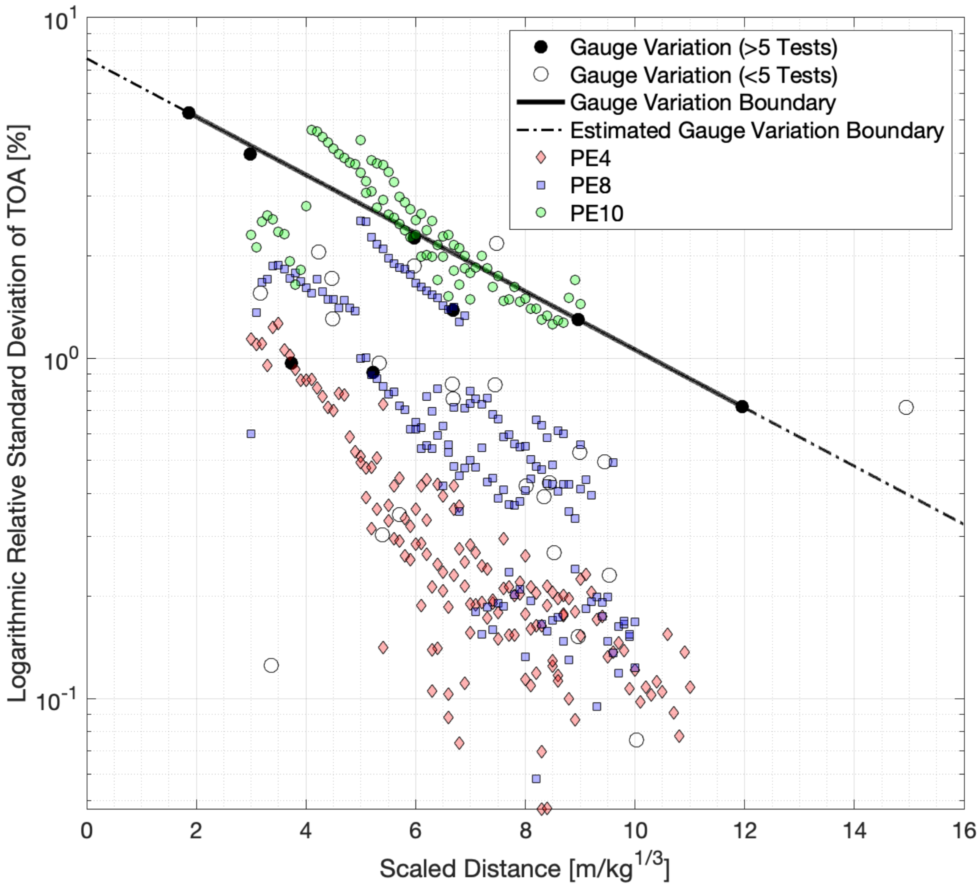

Figure 4.11: Logarithmic RSTD in shock wave arrival time as a function of scaled distance for both pressure gauge and high speed video recordings of 250g hemispheres of PE4

One thing to note is the substantial volume of interpolated data from just 10 processed PE4 videos when compared to 157 different pressure gauge recordings. The larger data set (3,163 recordings), alongside the clear improvement in repeatability and accuracy from just 10 explosive trials, presents a more cost-effective solution to experimental testing of high explosives.

The interpolated values from HSV recordings of PE8 and PE10 detonations also experience the same behaviour of reduced variability as scaled distance increases. The reason gauge data boundaries have not been presented in Figure 4.11 is due a lack of data to extract a reasonable estimate of arrival time variation with distance. Comparisons to that for PE4 are made instead to facilitate the discussion. The videos for PE10 were by far the hardest to analyse, with the lighting conditions when conducting these trials making extracting shock wave data difficult. That being said the 4 videos which data could be used provided similar levels of variation from 157 PE4 pressure gauge trials, highlighting the efficiency of this testing method. With an increase in the number of videos available, a reduction in the variability is experienced when looking at the results from the 6 PE8, and then finally the 10 PE4 videos.

The significance of Figure 4.11 is the comparable relationship between t_a variation with respect to scaled distance for both HSV and pressure gauge recordings. This is shown on a logarithmic scale to enable a clear comparison between the processed results from both methods of recording. A clear exponential reduction in t_a variability is seen with an increase in scaled distance across both methods of experimental analysis. The typical variations in the HSV data are approximately an order of magnitude lower than those in the pressure gauge data. The speculation that blast parameters exhibit high levels of inconsistency across the far-field range is disproved with these findings, explicitly suggesting far-field regimes and the corresponding blast parameters are deterministic.

4.3.2 Derivation of Explosive Yield from Arrival Time Data

To consider arrival time data as a metric for forensic explosive analysis, it is important to validate it against empirical data alongside quantifying the variability in the parameter. Rigby et al.[131], Stennett et al.[158] and Dewey[39] all present methods of quantifying the explosive yield of a real-world accidental explosion through arrival time data analysis with respect to best estimations of stand-off from the explosive centre. Their findings presented clear agreement of explosive yield and thus the TNT equivalence factor of the explosive detonated.

To verify the shock wave tracking and interpolation algorithm as an accurate means of gaining an understanding of how arrival time varies spatially across a full range of scale distances, the method was tested to estimate the apparent yield of the explosive used during the tests, which is known to be 250g PE4.

Figure 4.12 shows how the HSV-measured values of arrival time compare to a variety of different sized TNT charges and their corresponding KB predictions. It is important to note that the axes have been scaled down to visualise a clear distinction between the predictive TNT curves due to modest changes in charge mass. The HSV data shows excellent agreement with the curves for TNT between 290-320g, equating to a TNT equivalence of 1.16-1.28. The minimum mean absolute error is associated with a TNT mass of 305g, i.e. an equivalence of 1.22, which is very close to the value of 1.20 found in related studies[132]. This suggests that the optical technique presented is a reliable method for determining the TNT equivalence of explosives.

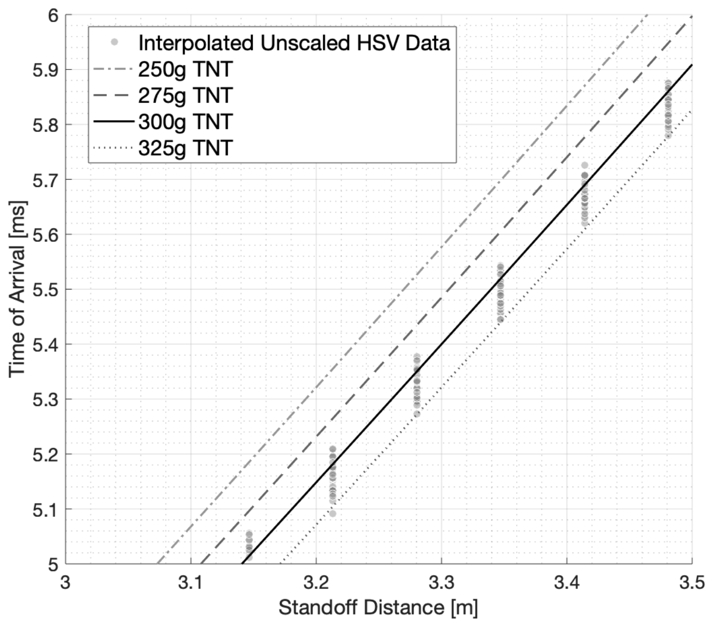

Figure 4.12: Interpolated and unscaled HSV shock wave arrival time from a 250 g PE4 hemispherical charge at 5 m stand-off compared with KB predictions for TNT hemispherical charges with different charge mass

Whilst the spread in TNT equivalence extracted from the HSV data is not significant, this could be vastly improved when considering what position on the shock wave you take to be the definitive front. The algorithm discussed in Section 3.3.1.1 makes use of image subtraction which results in clusters of pixels exhibiting change. Despite best efforts of the edge detection method, variations are therefore recorded in the shock wave position.

The Abel transformation relates a spherically-symmetric 3D field to a two-dimensional projection[34,91] which has been adapted for use in blast wave tracking through inversion of the process for tiny charges in well-controlled lab conditions[172]. The inversion however requires refraction angles obtained through effective lens calibration which was not conducted during this testing regime. Future tests should consider the use of the Abel transformation inversion to improve the accuracy of shock wave position extrapolated from a 2D video of a 3D spherical expansion.

4.3.3 Capturing Secondary Shock Data

The secondary shock parameter has been shown to be as deterministic as the primary shock in Section 3.2.3.2, provided the right assumptions are made when attempting to characterise it. However, what has yet to be established is whether secondary shock data can be captured using HSV techniques which could help provide a more fundamental understanding of the phenomena.

Adopting the same methods discussed in Sections 3.3.1.1 and 3.3.1.3 proved successful for capturing the propagating subsequent shock provided that lighting conditions were favourable and the explosive was not located too far out of the camera field of view. As the secondary shock is much weaker, the shock discontinuity is a lot more challenging to extract and therefore a lot of the videos provided unextractable data.

Despite the difficulty in extracting secondary shock data across each explosive, Figure 4.13 presents the overall secondary shock delay parameter, as discussed in Section 3.2.3.2, against the unscaled compiled pressure gauge data presented in Figure 4.8. The first thing to notice is the comparison in behaviours of the HSV extracted data to the pressure gauge data. This relationship provides enough evidence to support the validity of the ext extraction methodology for secondary shock data. The HSV data however seems to exhibit a smaller delay parameter across the explosives analysed. This is believed to be directly related to the HSV data tracking incident wave data throughout its duration for both primary and secondary shocks, where as the pressure gauges record at a discrete instance of distance. This means the secondary shock would be forced to expand against a reflected wave, decelerating its propagation and thus increasing its time of arrival when compared to the HSV data.

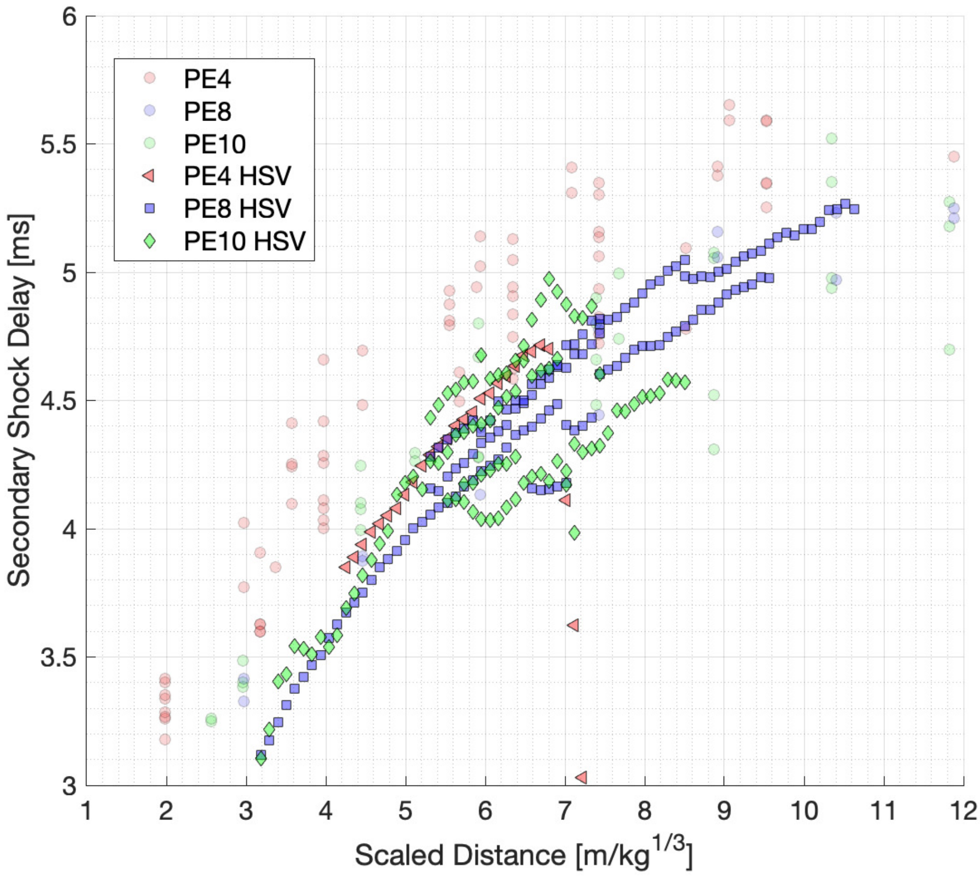

Figure 4.13: Interpolated and unscaled HSV secondary shock delay time from 250 g hemispherical ideal charges compared with pressure gauge recordings of PE4, PE8 and PE10

A learning point from early testing analysis of PE4 and PE10 was highlighted when the extracted secondary shock propagation data was either unusable or varied considerably, as seen in Figure 4.13. This knowledge was considered for the PE8 trials which were only conducted within favourable conditions resulting in all 8 shots providing credible data as opposed to only 5 of 20 trials in total for PE4 and PE10 combined.

4.3.4 High Speed Video Summary

This section makes efforts at implementing the tools developed in Chapter 3 to explore the other data which can be extracted on the three ideal explosives tested. Highlighted is the requirement for recording conditions to be considered prior to a test if only recording data using cameras. If lighting conditions are unfavourable most of the videos become difficult to extract data from without artificially editing image brightness which induces a margin of doubt in what data is being considered.

Importantly, the HSV methods have shown to produce highly accurate results for explosive yield and secondary shock delay when compared with known experimental features and the corresponding pressure gauge recordings respectively. With the secondary shock is not fully understood, work of this kind which shows clear differences between incident and reflected delay data provides further insights which can be developed to fully characterise the physical process.

4.4 Future Research of Explosive Characterisation

4.4.1 Near-Field Loading

Whilst already conducted is an in-depth and rigorous analysis of ideal explosives within far-field regimes, there is limited published work considering near-field loading conditions. Even fewer of these contain experimental-based evidence for the definitive mechanisms resulting in variability of near field blast parameters. The fireball of detonation products in this region is still expanding and driving the shock wave and so interacts with a structure in unison. KB predictions in this region are poorly defined, with limited experimental data of which exhibits significant scatter and divergence to physics-based numerical models[150].

To establish the root cause of the discrepancies between numerical simulation and the KB predictions, it is essential to record experimental data of both spatial and temporal blast parameter distribution in near-field regions. In doing so, insights into how energy is released during the initial stages of detonation can be made helping to characterise the near field effects on a composition basis.

With developments in near-field loading measurements discussed in Barr et al.[10], a rigorous test plan should be undertaken in the future to characterise the temporal and spatial behaviour of detonation within close-proximity of a reflective surface to measure localised loading conditions. The experimental trials will require high levels of precision with blast parameters showing considerable sensitivity inaccuracies in detonator placement within close proximity of the charge. This data will be used to expand the bank of data used to establish the KB predictions and hopefully provided insights into the discrepancies between that and numerical models. Future work should also build on that presented by Rigby et al.[130], which looks at implementing similar HSV techniques but for near-field fireball expansion tracking.

4.4.2 TNT Equivalence

Despite the vast quantities of published literature on TNT equivalence across a range of explosive compositions, there still holds discrepancies between researchers as to what realistic values are. This can only be a result of a general lack of consistency in experimental processes and analytics. What has never been fully justified in literature is the idea that TNT equivalence varies with scaled distance. Within near-field regimes where the propagating shock wave is sensitive to fireball thermodynamics, the statement that TNT equivalence varying may be valid. Compositions will decompose and combust at different rates which should result in variations to energy release when compared to that of TNT. However, in far-field regimes, the explosive detonation can be considered as a point source energy release[167] and therefore once the shock wave detaches from the fireball, the localised differences in detonation thermodynamics can be ignored. Effectively at these greater scaled distances, shock waves are comparable based on the speed in which they propagate through free-air and thus is believed to exhibit a constant TNT equivalence.

The techniques developed in Chapter 3 when used on a variety of ideal explosives demonstrates highly consistent blast parameter data in the far-field range which compare well to KB predictions for TNT. This provides justification and validation of developing technical procedures for data capture and analysis which considers the fundamental physical principles of shock wave propagation, relating to Objectives 2 and 3. With this in mind, the benefit of understanding how to improve our recorded data can be adopted to re-characterising other ideal explosives, attempting to quantify their effects and compare with KB predictions to establish realistic and consistent TNT equivalence values across the far-field range.[164] undertook well-controlled blast trials using PE4 across a range of mass scales, and showed general consistency of shock wave parameters regardless the mass tested. Although these masses tested are beyond what is possible for the University of Sheffield testing site, the fact that ideal explosives behave consistently both in mass and distance in the far-field range provides justification for this work. In doing so, more optimised numerical simulations can be developed to better quantify the effects these explosive compositions could have in more complex environments.

4.5 Summary

With experimental blast parameters providing the primary source of evidence to supplement the fundamental understanding of shock loading conditions on a structure, it is of paramount importance to characterise and quantify these effects resulting from a variety of compositions across a range of distances.

Stress-testing the tools developed in Chapter 3 using a large data set of small-scale hemispherical PE4 detonations against other explosives of similar idealistic behaviour was the main aim of this Chapter. Presented is a rigorous investigation into the effects various ideal explosives have on structures across the far-field range. The data was collected using both pressure gauges and high speed video recordings to further validate the methods and results through comparison of nominally identical shots.

The findings within Chapter 4 highlight the strength of KB predictions for both positive and negative phases of free-air shock wave parameters, specifically for far field scenarios, alongside the high consistency in output data from consistent well-controlled experimental trials. Despite only testing 250g hemispheres, the findings from [164] provide enough evidence that the results of consistency will transfer across mass and distance with the far-field range when considering ideal explosives of spherical shape. The methods of data capture and analysis have the potentially to be tested further when considering other non-ideal explosives, charge shape effects and near-field loading conditions.

Chapter 5

Non-Ideal Explosive Blast Characterisation

5.1 Introduction

Chapters 3 and 4 present validated experimental methodologies and analytical tools for accessing the far-field blast parameters from small scale ideal explosives in free-air, which have shown to improve the repeatability of recorded data and provide confidence in deterministic predictions of far-field detonation yields. Although having a fundamental understanding of ideal explosives is required, in reality, common explosive threats are home-made due to the relative ease and low costs associated with acquiring their constituents. This has led to a critical need to understand the effects of detonating non-ideal explosives to improve civilian safety against potential terror attacks in more realistic situations.

This Chapter will exercise the validated methods of conducting experimental work, and the corresponding data analysis, discussed in Chapter 3, to explore the yields of small scale ANFO (Ammonium Nitrate 94% and Fuel Oil 6% mixtures). The overall aim is to characterise the composition across a range of scaled distances at a smaller mass range to quantify any differences in the behaviour between that and large scale charges. The processed data will be compared to numerical simulations to access the validity of the underlying physics assumed within standard JWL equations of state. An assumption that non-ideal explosives vary on mass as well as scaled distance has been made, meaning a single value for TNTe can not be assumed. If proven correct within the findings of this chapter, it would result in discrepancies between simulated non-ideal detonations and the results from experimental trials, motioning a requirement for characterisation revisions of non-ideal explosives to capture realistic physical mechanisms ongoing in small scaled charges.

5.2 Experimental Setup

In the attempt to quantify the effects of small scale ANFO detonations a variety of experimental techniques were conducted to investigate the non-ideal behaviour which may be exhibited. This section outlines the basis of these trials making using previously validated methodologies in Chapter 3 for far-field studies but introducing a new technique of analysis for rate-stick trials.

5.2.1 Far-Field Trials

A total of 37 far-field experiments were performed at the University of Sheffield (UoS) Blast and Impact Laboratory in Buxton, UK. These trials were conducted using surface detonated hemispherical charges with mass varying between 250-1000g comprising of two different chemical compositions (Ammonium Nitrate Fuel Oil (ANFO): 35 tests and Ammonium Nitrate (AN): 2 tests). Both explosives were commercially purchased from EPC-UK to provide comparable studies both of which presented material properties as seen in Table 5.1 quoted by the supplier.

Parameter	Ammonium Nitrate + Fuel Oil (ANFO)	Ammonium Nitrate (AN)
Composition	92.5 - 95% AN, 5.0 - 7.5% FO	99% AN, ~1% Moisture
Density	0.8 g/cm^3	0.73 - 0.89 g/cm^3

Table 5.1: EPC-UK material properties of ANFO and AN which have proven useful for this body of research and article

The charges were boosted with a 3g sphere of PE10 to ensure reliable shot-to-shot detonation[112], and were done so at standoff distances of 1–9m from gauge instrumentation. It is important to note that a secondary objective from these trials considered the position of the booster/detonator and their effects on non-ideal explosive yield. With this in mind, 16 of the trials were top detonated and 21 bottom detonated. Figure 5.1 is a schematic displaying the different booster and detonator positions adopted for this testing regime. For each of the far-field trials, clear plastic sheets were heated and vacuum-formed around a 3D printed hemispherical mould, to provide a lightweight casing to facilitate negligible confinement of the ANFO prill whilst keeping a consistent shape. This was implemented to compare the results with the large bank of ideal explosive data available within the literature[49]. A small circular cut was made in the top of the vacuum formed plastic casing to enable a consistent method of filling the charge with pril.

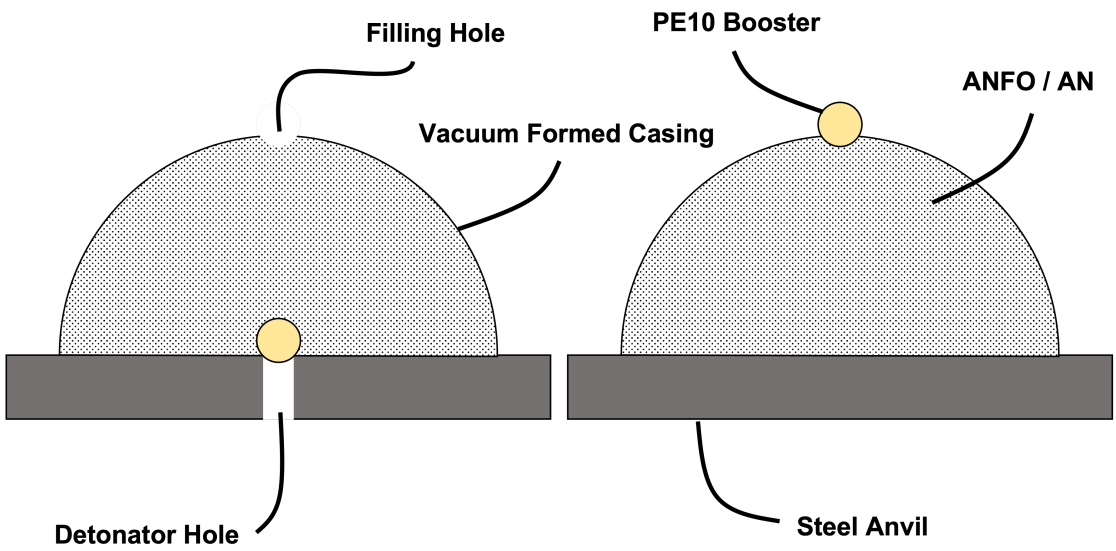

Figure 5.1: Schematic of the charge and booster locations used throughout this testing regime

The far-field experimental methodology for the non-ideal tests mirrors that discussed in Chapter 3. The explosive charges were detonated at varying stand-off distances, R_a and R_b in Figure 3.3, perpendicular to two rigid reflective surfaces in the form of a reinforced concrete bunker and a blockwork wall, separated exactly 10.0 m apart. Data was recorded using the same collection of Kulite HKM-375 piezo-resistive pressure gauges as were used for the recording of the ideal explosive detonations. The gauges were threaded through, and made flush to the surface of a small steel plate (approximately $110 \times 150 \times 10$ mm) which was fixed to these walls. The charges were placed on a small steel plate ($150 \times 150 \times 25$ mm) prior to detonation, in order to avoid repeated damage to the concrete testing pad.

For bottom detonated trials, the steel anvil had a machined hole through the centre to allow for the detonator to be in contact with the PE10 booster. The pressure was recorded using a 16-bit digital oscilloscope and TiePie software, with a average sampling rate of 195 kHz at 16-bit resolution. The recording was triggered automatically using TiePie's 'out window' signal trigger on a bespoke break-wire signal, formed by a wire wrapped around the detonator. The 'out window' trigger initiated with a voltage drop outside the normal electrical noise experienced in the break-wire. This coincides with the detonation of the charge breaking the circuit.

Data was recorded using the same collection of piezo-resistive pressure gauges as were used for the recording of the ideal explosive detonations. It is important to note that 30 of the ANFO trials were undertaken as part of a separate research project funded by CPNI (Centre for the Protection of National Infrastructure) and DSTL (Defence Science and Technology Laboratory) that has been granted permission of use in this thesis and hence denoted throughout.

Figure 5.2: Top detonated arrangement for hemispherical ANFO charges boosted with 3g PE10 sphere; the yellow tubes are installed as guides for the detonator to be positioned vertically into the booster

The Photron FASTCAM SA-Z high speed video camera, fitted with a Tamron SP AF70 70-200mm zoom (F2.8) lens, and a zebra board which ran perpendicular to the blockwork and bunker walls, was again utilised to capture far-field shock propagation. In conjunction to this, a Shimadzu ultra high speed video camera was used to record detonation wave propagation and fireball breakout of the explosive to provide insights in the early stages of the event.

5.2.2 Rate Stick Trials

As an attempt to characterise ANFO small scale shots across a whole range of parameter metrics, there was a need to establish the velocity of detonation (VOD) of ANFO and how it develops within a charge. To evaluate this, 6 rate stick trials were undertaken making use of two Shimadzu ultra high speed cameras. ANFO prill was contained within 300mm long, 3mm walled clear acrylic/PMMA (Polymethyl-Methacrylate) pipes which had varying diameters in the attempt to establish the critical diameter of ANFO and the explosives corresponding VOD. The three internal diameters of pipe tested were 50mm, 75mm and 102mm which correspond to ranges quoted within published literature for the critical diameter of ANFO[20,23,24,47,97].

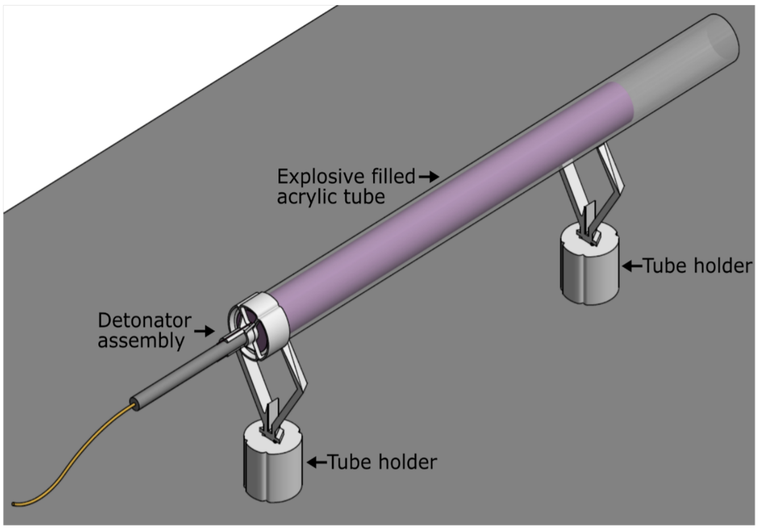

Figure 5.3: General arrangement of the rate stick trials using a 3mm wall thickness PVC clear tube, a 3D printed end cap which allows for detonator and booster placement and a reference measurement guide to enable distance tracking in the high speed videos

The pipes were sealed using a 3D printed detonator holder at one end and a lightweight fibreglass material at the other to provide minimal confinement at the pipes extents as seen in Figure 5.3. To trigger the camera, a breakwire system was wrapped around the detonator so that upon detonation a voltage drop is experienced, triggering the camera to record. The general arrangement of the detonator assembly can be seen in Figure 5.4. Five out of the six trials utilised a 3g PE10 booster to initiate the detonation process to be comparable with the data collected within the far-field studies. The final test looked at a non-boosted 50mm diameter rate stick trial.

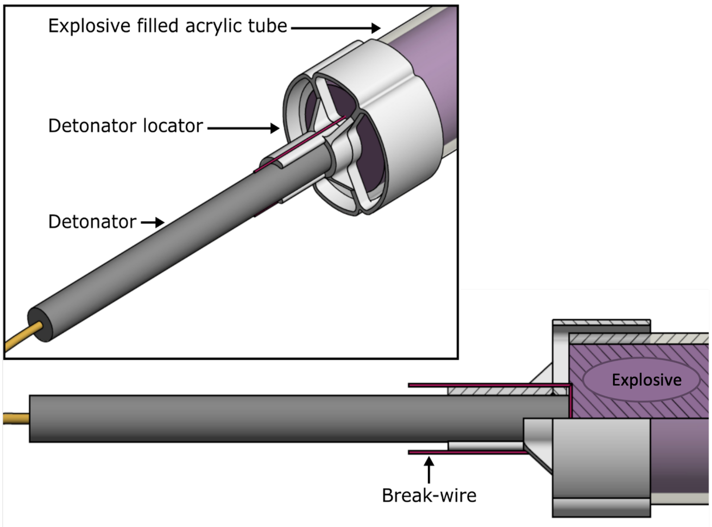

Figure 5.4: General arrangement of the rate stick trials using a 3mm wall thickness PVC clear tube, a 3D printed end cap which allows for detonator and booster placement and a reference measurement guide to enable distance tracking in the high speed videos

5.3 Pressure Gauge Results

5.3.1 Positive Phase

Having little knowledge on the yield and characteristics of small scale ANFO charges, it was essential to establish an understanding on the general qualitative behaviour recorded during testing. The aim of this is to assess if non-ideal explosives behave as consistently as ideal explosives, as seen in Figure 3.5.

Presented in Figure 5.5 are 18 individual pressure gauge recordings as a result from 250g hemispherical ANFO detonations. These were conducted across a variety of standoff ranges tested alongside varying detonator position between top and bottom detonated. For data recorded between 2–9m, it is evident that although a discrepancy in the arrival times is consistently recorded (discussed further in Section 5.3.2), the overall trends in the positive phase of the pressure-time histories show considerable agreement. This ultimately suggests that within far-field regions, the detonator position is irrelevant. A similar level of consistency is also to be experienced between non-ideal and ideal explosives. The traces at 1m standoff do present variability in the overall peak overpressure recorded. This has been directly linked to the spherical uniformity and irregularity of the detonation cloud breakout related to bottom and top detonated tests respectively.

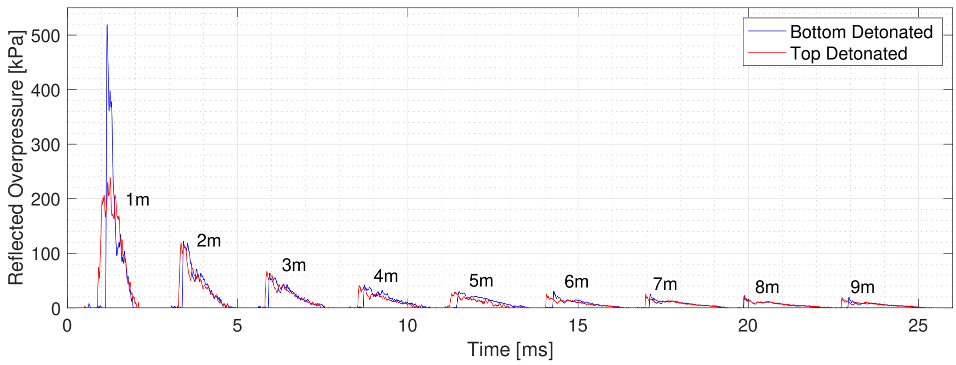

Figure 5.5: Compilation of raw data set of 250g ANFO hemispherical ground bursts, comprising of both top and bottom detonated charges, across the entire range of standoff distances tested in this regime. Positive phase is presented only.

To establish the behaviour small scale ANFO explosives exhibit when compared to TNT, it was important to adopt the same experimental analysis tools, validated for ideal explosives. This is undertaken to assess how the tools perform for non-ideal explosive detonations. Since Friedlander-like behaviours are presented in Figure 5.5, the curve fitted method was used to process the small scale ANFO data. The caveat is that this accounted for the gauge plate ringing (the phenomena discussed in Section 3.2.2) as the blast arena amendments had not been made prior to these trials being conducted. The output blast parameters resulting from the curve fitting method were collated. A TNT equivalency assessment made using an MAE analysis, comparing the ANFO data set to semi-empirical predictions based on varying masses of TNT. As per the findings of Section 3.2.1.1, the positive phase duration exhibited higher levels of variability when assigning a specific value to the parameter. This was directly linked to noise in the signal, making the true point at which conditions return briefly back to atmospheric difficult to precisely determine. In common practice, an inaccurate time duration can be remedied by tailoring the decay coefficient in the Friedlander equation such that the specific impulse is preserved. With this noted, positive phase duration was omitted from the MAE analysis in line with the previous assessment on ideal explosives.

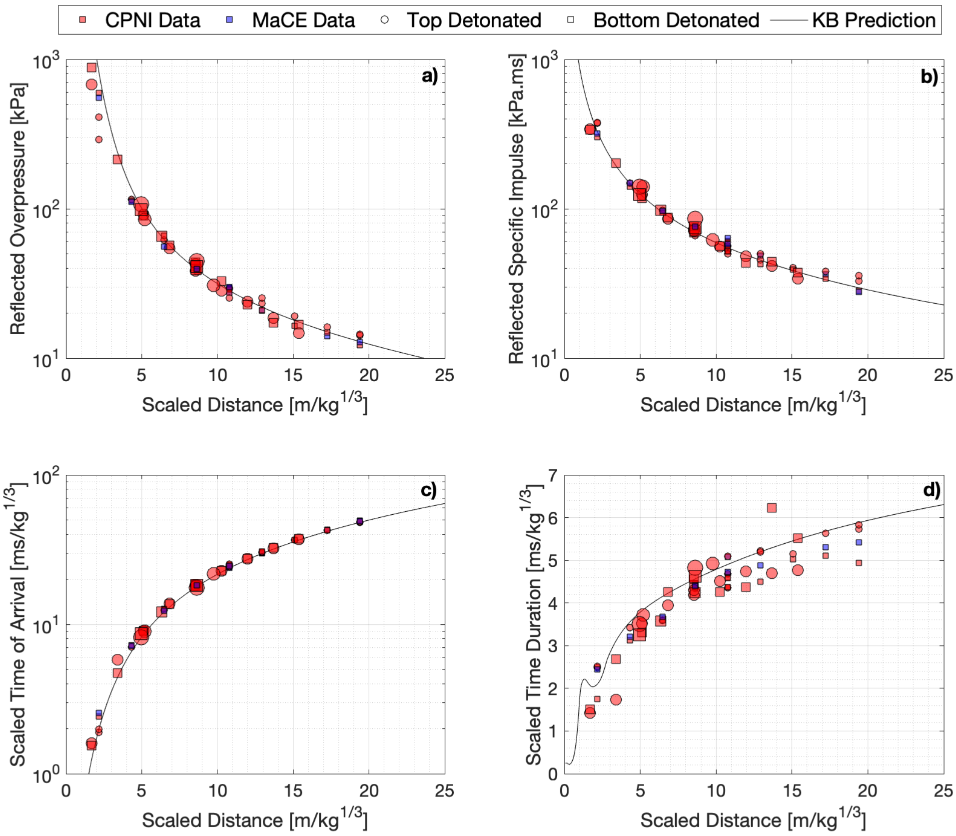

Figure 5.6: Compiled scaled blast parameters from ANFO explosive trials as a function scaled distance, compared with KB predictions, using a TNTe=0.395, with increasing marker sizes to indicate the mass of charge: a) Peak reflected overpressure, b) Scaled reflected peak specific impulse, c) Scaled arrival time, d) Scaled positive phase duration

To be in line with variability regions hypothesised Tyas[173], the MAE analysis was performed on all AN-based tests within the definitive far-field range. The aim was to attribute a TNTe factor at which the shock wave is no longer affected by ongoing fireball chemistry, instabilities and detonation cloud propagation. To establish the effects of detonator position and charge mass, the MAE analysis was undertaken for the data when separated into both nominally identical tests alongside the full data set. The results from the MAE analysis of peak reflected pressure and specific impulse converged on a TNTe = 0.395 across the entire range of scaled distances, for both charge mass and detonator position groupings. Arrival time however, presented a TNTe = 0.28 and 0.295, for bottom and top detonated trials respectively. This suggests that the shock waves resulting from small scale ANFO detonations propagate slower than an equivalent TNT mass with approximately

40% of the mass of the detonated ANFO charge. This offset in arrival time, is visually represented in Figure 5.5, and will be discussed in detail in Section 5.3.2. The arrival time of the shock waves will however be treated with caution for discussions relating directly to explosive yield.

To assess the explosive yield alone, the TNTe = 0.395 was applied to each of the recorded blast parameters and presented in Figures 5.6a-d which show a striking agreement between each experimentally recorded blast parameter (expressed as a TNT equivalent mass), and the KB predictions. It is important to note that there were 2 preliminary trials which resulted in much lower explosives yields related to not using a PE10 booster, which have been removed from the presented data to avoid speculative comparison of different testing regimes. This finding does however provide enough evidence to suggest that small scale ANFO charges cannot be reliably detonated without the presence of a booster charge.

Interestingly to note is the behaviour of the peak pressure and specific impulse values in near field scenarios, $Z < 3m/kg^{1/3}$, when comparing top and bottom detonate shots in Figures 5.6a and 5.6b. The top detonated peak pressure values recorded in the experimental trials seem When comparing peak pressure and specific impulse values, the top detonated trials exhibit different evaluated TNTe factors when compared directly to KB predictions. The bottom detonated trials present agreement in TNTe for both parameters with KB predictions. This suggests that ANFO small scale charges are sensitive to detonator position in the near-field due to differences in the detonation product mechanics occurring on breakout in line with the findings presented in Figure 5.5. It can be concluded that the energy release of an explosive, and therefore the specific impulse, is independent of detonator position. The peak pressure however is directly related to the fireball breakout and propagating shock wave shape.

What can be deduced from this finding however is that specific impulse provides a more representative TNTe across all explosives and scaled distances regardless of whether a ‘Friedlander’ shock wave has fully formed. Specific impulse loading is directly related to the total energy released from detonation rather than pressure which is time-dependant based on shock wave forming. For the near-field it is important which parameter is considered but far-field can make use of both to establish equivalency in line with findings presented by Bogosian et al.[16].

The results presented in Figures 5.6a-d contradict quoted values of TNTe for ANFO being around 0.82 across all scaled distances and masses, therefore posing implications for numerical modelling which have incorporated these assumptions within simulations. To assess the variability of the data set, it was scaled by mass alone and compared to varying KB prediction curves using a TNTe = 0.3-0.5, presented in Figure 5.7. A TNTe = 0.395±0.1 does agree with the results presented in Figure 2.14 by Figuli et al.[52], suggesting that a ±10% spread about the MAE evaluated TNTe could be related to inherent variability in ANFO trials as result of a combination of the factors mentioned in Section **??**.

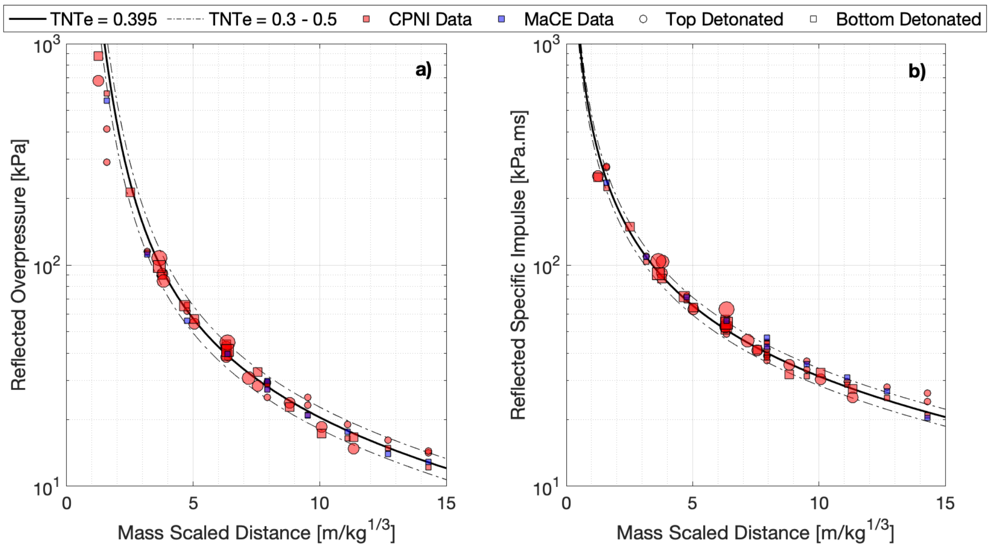

Figure 5.7: Compiled mass scaled blast parameters from ANFO explosive trials as a function mass scaled distance, compared with KB predictions, using a TNTe=0.395±0.1 to present variability bounds, with increasing marker sizes to indicate the mass of charge: a) Peak reflected overpressure, b) Scaled reflected peak specific impulse

Across a variety of experimental trials, it would become evident if the gauge data was invalid, especially where gauges were swapped out depending on their pressure rating and where the charge was situated, providing confidence in the recorded and processed blast parameters. The confidence in the data provides us with enough evidence to suggest that non-ideal explosives are not scalable across all masses and standoff distances and therefore KB predictions may not hold as much credibility when assessing these types of explosives.

For ANFO in particular, larger charges masses (i.e a greater self-confinement and longer distance for detonation wave to travel without energy loses) foster the full detonation and combustion of both AN and FO components of the composition, but in smaller charges a percentage of the energy is not fully released prior to the propagation of the air shock. The question which begins to be highlighted is why ANFO is described to exhibit a TNTe of around 0.82 across all scale distances and little further experimental work undertaken to assess the robustness of this factor across a range of masses and scaled distances other than that presented in Figure 2.14. The implication this has on the fundamental understanding of non-ideal explosives is significant and will result in any numerically modelled simulation of ANFO of low charge mass will result in over predictions in the behaviour. The contents of this chapter will make efforts at assessing the robustness of KB predictions against small mass-scale ANFO charges whilst making comparisons to the historical data captured from large scale charges.

5.3.2 Arrival Time Offset

Using the findings from the MAE analysis on peak reflected pressure and specific impulse, KB predictions of the positive phase, using a TNTe = 0.395, were overlaid on the raw data to evaluate whether the equivalency factor provided qualitatively similar trends in Figure 5.8. Whilst both the pressure and impulse trends are captured reasonably well, the arrival of the recorded shock waves is much later than an equivalent TNT blast.

With further inspection, the MAE analysis for arrival time highlighted TNTe being 0.28 and 0.295 as providing more comparable scaled arrival time values to TNT predictions for both bottom and top detonated trials respectively which equates to on average $\sim$0.3ms delay in the arrival time in comparison to the TNTe establish for pressure and impulse. This suggests that despite exhibiting TNT equivalences of around 0.395 for energy related parameters, time-based shock wave parameters from small scale ANFO charges are equivalent to even weaker detonations and therefore arrival later. It is has been hypothesised that the delay in arrival time to be a result of a combination of different factors, of which will be discussed further.

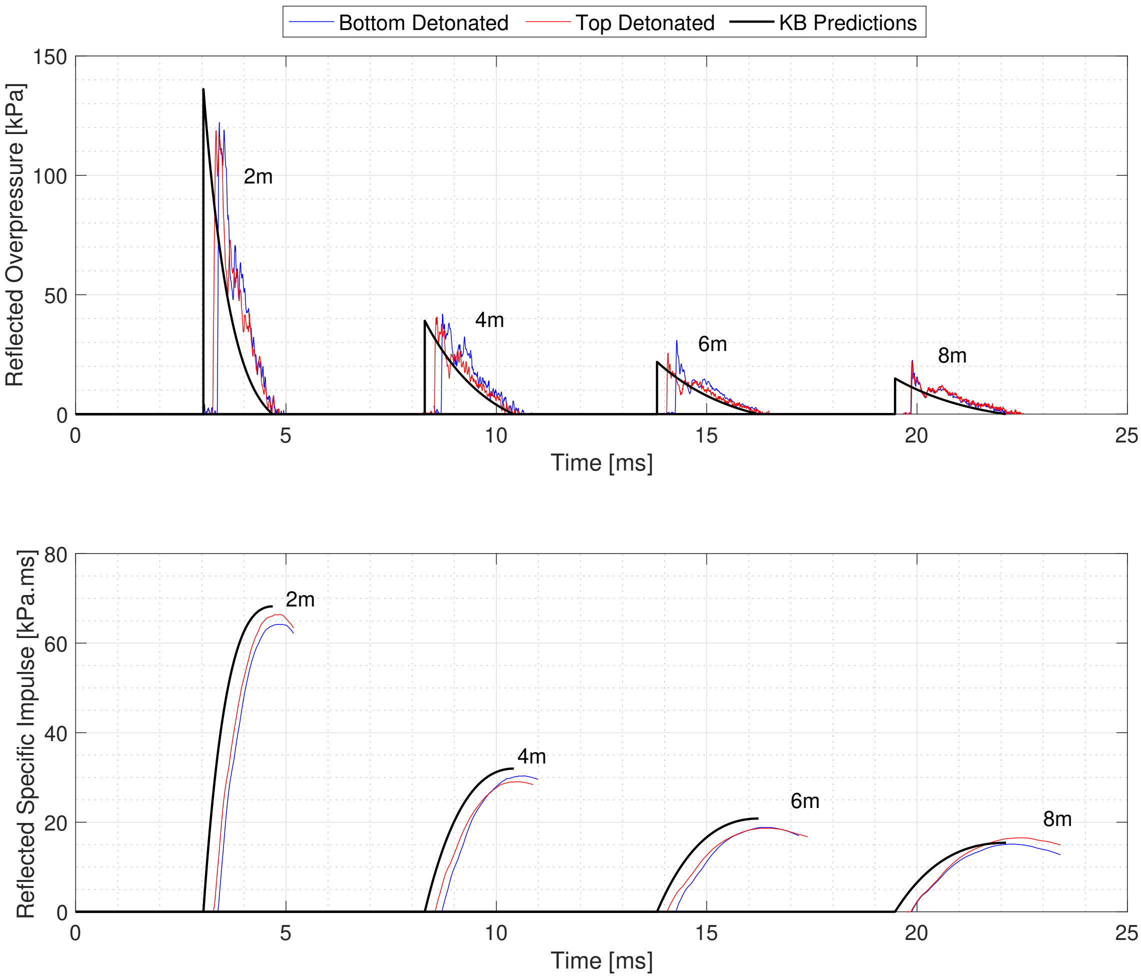

Figure 5.8: Compiled raw data from both top and bottom detonated trials at 2m, 4m, 6m and 8m standoff distance compared to KB predictions assuming a TNTe=0.395: Pressure-time history (Top) and Impulse-time history (Bottom), showing only positive phase

5.3.2.1 Mesostructure of ANFO prill

The heterogeneity of small scale ANFO charges, when compared to homogenous cast TNT explosives used to develop the KB prediction tools, is a factor which could affect the velocity of the detonation wave and therefore resulting blast parameters. Zygmunt and Buczkowski[183] investigated the influence of ANFO prill characteristics on detonation velocities and energy release and found that the prill structure and the size in these types of charges are massive influencers. Salyer et al.[140] compared the detonation velocities of two commercial ANFO types which have vastly different prill sizes and mesostructures when prepared. The results suggested that the small prill resulted in much more ideal detonation behaviours relating directly to reduction in air voids allowing for a more stable expansion of the detonation wave.

Petes et al.[112] discusses this inhomogeneity characteristic as being the potential reasoning for non-spherical propagation anomalies in the shock wave and fireball. This results in quoted blast parameter variability spreads of $\sim 7\%$ when comparing nominal trials detonating cast TNT, which is endorsed by[9] who discusses instability formation relating to imperfections in the charge surface and homogeneity.

Considering large scale ANFO charges, it is highly likely the bulk density increases due to more centrally located prill layers exhibiting void collapse through self-weight compression. Petes et al.[112] detailed that an increased bulk density will result in faster detonation velocities and thus the resulting blast parameters exhibiting larger yields for large scale charges. McKay et al.[99] and Dobrilovic et al.[41] both experimented with reducing the density of ANFO by removing prill and exchanging it with polystyrene balls to assess the changes to the velocity of detonation in rate stick trials. Zygmunt and Buczkowski[183] showed that increasing the density of ANFO charges using ground prill much higher detonation velocities were experienced, which with alongside the aforementioned articles show agreement with the theory stated by Petes et al.[112].

Conversely, the works presented by Fabin and Jarosz[47] undertook analytical studies in trying to improve the explosive yield of ANFO charges and discovered the morphology and prill size distribution did not necessarily follow the same theory. A dependence on FO absorption features of AN has shown to result in lower detonation velocities for higher density ANFO, therefore inducing variability in detonation mechanics. Sadwin and Swisdak[139] reinforced these ideas when it was reported that layer-to-layer density differences were measured throughout their large scale ANFO charge through varying detonation velocities and pressures. Consequentially to these density regions, hydrodynamic instabilities would develop leading to a considerable amount of internal turbulence and thus a degree of detonation wave propagation impedance when compared to cast TNT, all of which would result in spreads in explosive yield.

For these small scale charges, where the mass itself is not enough to provide reasonable compaction to induce full/ideal detonation of the ANFO, the air voids between each prill are believe to have a impedance influence on velocity of detonation. It is assumed that cellular disturbances of the detonation wave are generated when propagating through the prill structure, fostering multiple interactions within the complex mesostructure and disrupting the smooth isentropic expansion of the detonation wave and products.

Mi et al.[102] numerically modelled the shock-to-detonation transition in nitromethane, a non-ideal heterogeneous explosive, when incorporating different arrangements of air voids and applying varying energy shocks to the medium to induce initiation. This model presented delays during the initiation process when cavities were present in comparison to a homogeneous mixture. This provides further understanding to the complexity of the detonation process and some validation to the delays seen in Figure 5.8a-b.

Numerical simulations undertaken by Baer et al.[6] demonstrated that heterogeneous materials, like ANFO, which undergo shock loading, do not exhibit one jump state as depicted in ideal explosives but consist of a distribution of states. In the early stages of being shocked, ANFO behaves elastically, with temperature and stress corresponding to those defined by the shock hugoniot of ammonium nitrate. As the the shock wave travels through the complex mesostructure, the distribution of states show elastic and plastic deformation effects, corresponding to induced ANFO prill pore and air void collapse behind the shock front. Thereafter, when all available void space is filled, compression waves traverse through the materials that eventually equilibrate to a spatially-uniform stress state which was also hypothesised by McKay et al.[99]. When directly comparing this to a ideal homogeneous explosive, which jumps states effectively instantaneously, the time difference between those reactions could also have an effect on the offset seen in the small scale charges.

The ANFO used in these trials had a bulk density of 0.824g/cm^3 measured using a known volume and mass container, which is significantly lower than an individual prills density, quoted as between $1.2-1.4g\text{g/cm}^3$[138]. Density, or air voids percentage, is documented as having a direct relationship with the detonation velocity and thus the resulting shock wave parameters[154]. Adopting rudimentary calculations, the ratio between the bulk density of a given amount of ANFO and an individual prill results in around $60\% - 70\%$, suggesting $30 - 40\%$ is attributed to the air voids which is in line with quoted amounts by Cetner and Maranda[24]. If the ratio of measured charged density to potential density is applied to the TNTe factor established for the best fit of reflected pressure and specific impulse, a new $TNTe \simeq 0.246 - 0.328$ is established, which is in line with the MAE analysis for arrival time when compared to KB predictions.

The arrival time delay could be attributed to the complex mesostructural interaction between detonation wave, ANFO prill and the air voids. This phenomena will be much more prominent in small scale charges, with a lack of self-compaction, when compared to homogeneous TNT charges.

5.3.2.2 Detonator Position

Comparisons between top and bottom detonated charges were undertaken to establish the delay in the shock wave arrival time related to detonator position. Using the TNTe value of 0.395, the scaled distances and arrival times for the small scale ANFO trials were calculated, and through the use of interpolation, the corresponding KB prediction of arrival time could be established. The difference between the recorded scaled arrival times and the KB predictions was the offset recorded and presented in Figure 5.9.

Interestingly the findings, when comparing top and bottom detonated arrival time offset, show a consistently larger offset value attributed to bottom rather than top detonated charges, whilst also exhibiting a smaller degree of variability. This finding suggests that top detonated charges result in shock waves which travel faster than a bottom detonated charge. The velocity of detonation in ANFO has been shown to increase with charge radius[12,43,80,98] up to a maximum value and thus in top detonated charges, the detonation wave has more explosive to pass through prior to breakout. The correct orientation of the detonator when used in the top detonated scenario was subjected to human error due to being free-standing in the testing methodology. Conversely, the bottom detonated charges passed through a hole in a steel anvil, only large enough for the detonator to fit, therefore improving the directionality and thus showing a higher degree of consistency in the offset parameters at each given scaled distance seen in Figure 5.9.

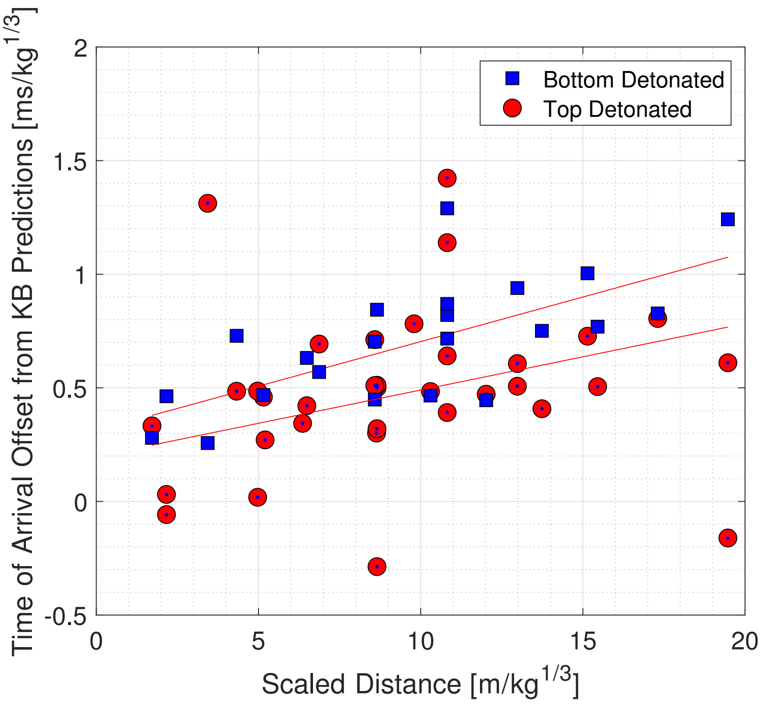

Figure 5.9: Scaled time of arrival from experimental work offset from KB predictions based on a TNTe=0.395, against scaled distance for top and bottom detonated tests with reference best fit lines .

Figure 5.9 does highlight that the offset in arrival time compared to KB increased with scaled distance for both top and bottom detonated charges. It is hypothesised that this is a feature of the ANFO shock wave de-accelerating faster than an equivalent TNT explosive based on the 39.5% equivalency. Despite detonator position making slight differences to the arrival time offset, this is second order mechanism and a more fundamental process causes the discrepancy in arrival time data.

5.3.2.3 Proportionality in the Velocity of Detonation with Charge Radius

The offsets in arrival time tends to increase with scaled distance in both scenarios of detonator position. This suggests for small scale ANFO charges the shock wave velocity is decaying faster than what a TNT charge scaled accordingly would. This finding is indicative of the relationship presented in Figure 5.6c which suggests that the decay of shock wave velocity is on a different gradient to what is experienced in TNT.

The factors mentioned above all contribute to the main overarching reason for the arrival time offset but these are believed to be second order to the real mechanism resulting in the magnitudes of offset exhibitted. TNT has a detonation velocity of around 6940m/s when compared to the published figure of approximately between 4250-4800m/s for ANFO, again related to large scale trials. However, TNT reaches this quoted maximum speed effectively instantaneously due to its ideal-like detonation characteristics. ANFO detonations on the other hand requires a specific amount of time in which the charge is sustaining, and not losing energy through propagation of products (i.e., similarly to being confined), allowing for a steady-state detonation to occur exhibiting the quoted velocity. It is therefore a reasonable assumption that comparing the internal conditions of small scale ANFO charges to TNT will result in slower detonation velocities at the instant of initiation, with the gap closing as charge diameter increases.

Figure 5.10 displays a schematic of what is hypothesised to be occurring in the detonation procedure of ANFO when compared to TNT. Upon the detonation of TNT, the velocity of the shock wave travelling through the explosive is fairly constant until breakout. At this point the propagation of the detonation products and air shock results in progressive energy loss and reductions in speed. Conversely for ANFO, the maximum velocity is not achieved instantaneously with detonation, but instead ramps up based on the secondary, non-ideal combustion of the FO component of the charge which occurs over a longer time scale. Depending on charge size, the breakout of detonation products could happen anywhere along the curve ramping up to the maximum velocity of detonation of ANFO and then will behave similarly to TNT as a free air shock, just at a lower velocity.

In the experimental trials presented within this thesis, the ANFO charges would fall into smaller scale behaviours meaning that the when comparing the trend to TNT, it is clear that the velocity of the shock reduces faster in the ANFO detonation. This would therefore create an artificial offset to arrival time data as the TNT shock wave travels faster for longer. Eventually the offset would level off when the changes in velocity with respect to time are almost the same (i.e when then curves begin to plateau and converge). The larger the ANFO charge, the closer to the maximum detonation velocity and therefore less of an offset would be induced. The initial acceleration of velocity in ANFO would result in some error arrival time within a close proximity to the charge which begins to even out at greater scaled distances. This exact feature is seen in Figure 5.6b, from the large scale ANFO trials that exhibits recordings in arrival time which are greater than KB predictions in near-field scaled distances.

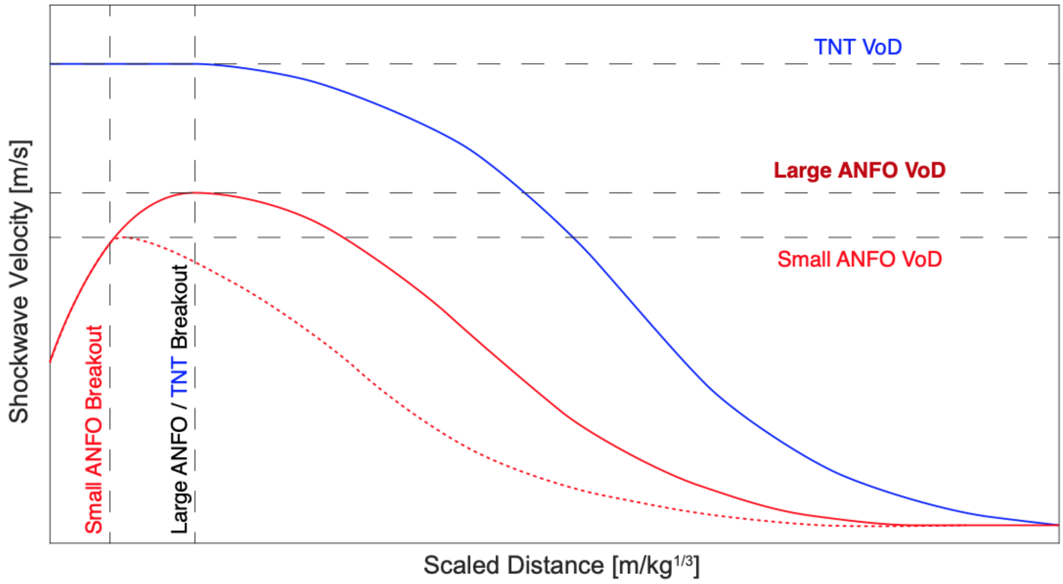

Figure 5.10: Theoretical schematic of different detonation and shock wave velocities with respect to scaled distance for TNT (Blue) and ANFO charges of various sizes (Red), with reference to the times at which detonation breakout occurs respectively to one another.

The initial offset is something which can be quantified using evaluated shock wave data for a TNT charge from KB prediction. If a velocity at detonation breakout can be recovered from these small scale ANFO charges then so can a time in which TNT would take to reach that same velocity. This would provide an initial offset at small scale distances and will be revisited in Section 5.4.1. Quantification of the increasing offset seen in Figure 5.9 is only possibly through understanding the behaviours of the shock wave from the moment it detonates up to far-field ranges.

5.3.2.4 Summary of Arrival Time Offset

Whilst all of the above offer a reasonable hypothesis as to why the captured arrival time data holds discrepancies to KB predictions, it is important to test these through other methods of analysis to provide further validation. Whilst varying detonator positions in a robust testing plan would be of interest to assess the variability of explosive yields within the near field, the results would not produce a significant progression in the characterisation of small scale ANFO charges.

Ensuring the exact formation and prill-to-prill interactions between tests is difficult for ANFO charge and therefore variations related to this are accepted as inherent to the heterogeneity of composition. With strict control measures the differences in prill size, charge density and oil absorption could be considered but it is believed to be a second order mechanism when establishing why the offset in arrival time for ANFO charges is so large.

The proportionality in the velocities of detonation between TNT and ANFO, and their general trend prior to detonation product breakout are essential for understanding the arrival time offset. HSV techniques can be used to track the velocity of both the fireball expansion and the resulting shock wave propagation from the ANFO charges which is discussed further in Section 5.4.1.

5.3.3 Disagreement to Published TNT Equivalence

The fact this small scale testing regime resulted in a generally low TNT equivalence (TNTe $\simeq 0.4$) for ANFO is a contradiction to the widely accepted figure of approximately 0.80 within the available published literature. Giglio-Tos and Reisler [61] undertook a experimental research consisting of the detonation of three large scale, 20-100 Ton, hemispherical ANFO charges which recorded blast parameters using pressure transducers and magnetic tape recording systems, resulting in a TNTe = 0.83. Petes et al. [112] expressed the desirability to use ANFO for explosive testing and provided a detailed compilation of historic testing results. These concluded on the idea that ANFO had approximately 80% of the energetic output of TNT. This thesis begins the discussion around why small scaled ANFO charges present a much lower energetic output than historically reported and what the real world implications of this are. The list below were the preliminary hypotheses based on the experimental results:

5.3.4 Was the composition of the explosive actually ANFO?

Findings from published literature details that purely ammonium nitrate detonation results in around $TNTe = 0.32 - 0.4$[3,28,110,131,158]. This has led to considering the possibility the composition of ANFO being incorrect and fuel oil not being present as requested on purchase. With this in mind, the composition was tested using a gravimetric analysis, separating the substance using petane, resulting in a yield of 5.55±0.09% and 94.45±0.09% of the tested mass found to be fuel oil and ammonium nitrate respectively.

During the detonation of ANFO consisting of 6% FO, theoretically an ideal and stoichiometrically balanced reaction occurs, meaning the oxygen molecules released as a result of the AN decomposition are enough to cause the full deflagration of FO. In our trials, with a lower percentage of FO at 5.5%, the detonation would result in a reduction in energy released ≃5%[92] through the development of nitrous oxides rather than full combustion occurring. This however does not account for the 50% effective energy loss exhibited in the recorded data. This finding led to the hypothesis being removed from consideration.

5.3.4.1 Does the scale of the charge affect the chemical reactions occurring during detonation?

Due to the fact the FO constituent of the composition not being chemically bonded to the AN, there is a lag in the reaction time, related to reaction zone size. If the detonation wave is to reach the extent of the charge prior to this chemical reaction fully occurring, the potential energy release is considered to not be fully achieved.

In small scale charges, it was discussed whether the aforementioned reaction actually occurs at all, and therefore the yield of these tests is the result of only AN detonating. To test this hypothesis, Ammonium Nitrate prill was purchased from the same provider and tested under an identical methodology to the ANFO shots (250g hemisphere and boosted with a 1g sphere of PE10). In these trials no detonation occurred in any of the pure AN shots despite being boosted. This result was evidence to suggest the fuel oil oxygen reaction had to be occurring to sustain the detonation during the ANFO trials.

It was proposed that a percentage of the potential energy from the fuel oil was released from the ANFO prill directly surrounding the booster with the PE10 providing enough energy to near-instantaneously combust the FO in its immediate vicinity. However it was speculated, within the small sized charges, that the reaction of FO combustion could not sustain effectively when the reaction zone reached the edge of the charge where a lack of confinement results in pressure and temperature losses. This behaviour would result in the detonation of ammonium nitrate, with a tiny percentage of fuel oil, similar to the first hypothesis.

Numerical modelling of small scale AN charges was undertaken, using similar methods discussed in Section 4.2.2, to establish whether or not the reduced energy release from small scale ANFO charges was captured by simulating the detonation of AN. Both Figures 5.11a-d and 5.12a-b represented experimental results for small scale ANFO trials when top and bottom detonated were compared with numerical simulations of 211.5g of AN detonation, established through removing the 5.5% FO composition and then an additional 10% mass for energy loses to the ground, in line with findings in Section 3.2.2.3.

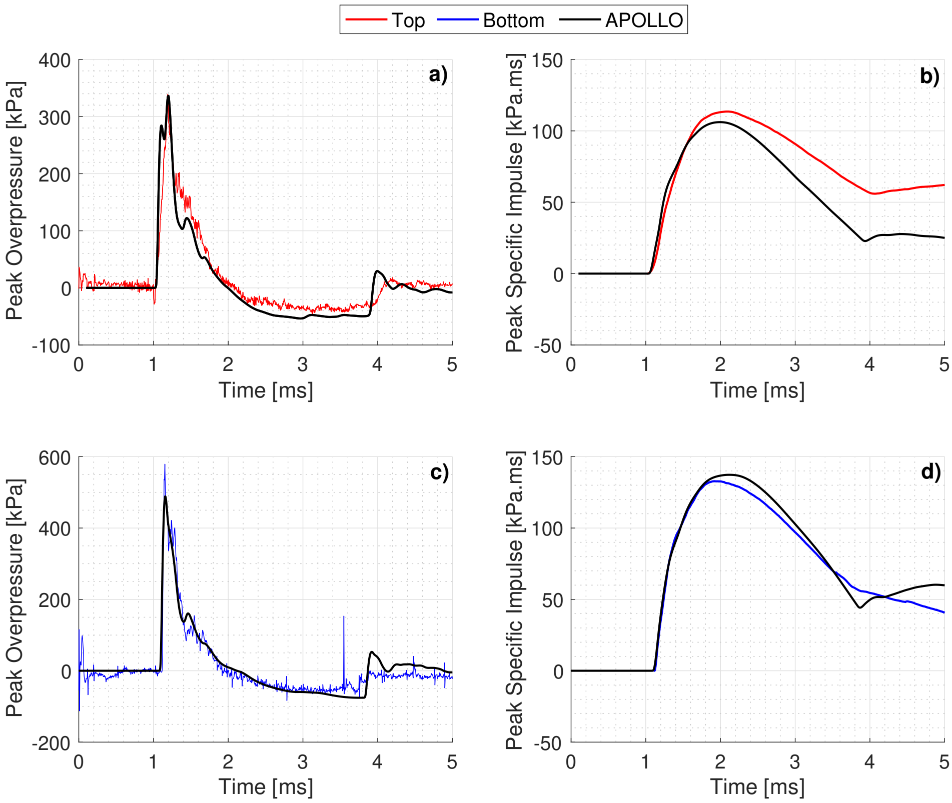

Figure 5.11: Compilation of pressure-time and impulse-time histories from 1m standoff distances which related to top (red) and bottom (blue) detonated trials compared to APOLLO simulations of AN: a) Top P-T, b) Top I-T, c) Bottom P-T, and d) Bottom I-T.

The numerical simulations provide remarkable agreement with the experimental data despite the fact a completely different explosive composition and corresponding JWL parameters have used to what is known to have been tested. The fact that the detonator position effects are captured effectively by the models provides confidence that assuming the ANFO composition behaves like pure AN at these mass scales is valid. The question posed here however is at what point does modelling the explosive as AN become invalid. Future research would consider testing a wide range of ANFO masses in free-field blast environments to quantify at what mass specifically results in a doubling of the yield through the fuel oil reaction occurring effectively.

Johansson[82] presented the numerical modelling schemes of small scale ANFO charges which were validated using experimental work extracted from the literatures which detailed a lack of accuracy when using standard JWL parameters for capturing the behaviour on ANFO. The reason for this is because in a JWL EoS, there is an assumption of instantaneous energy release which for non-ideal explosives it is known not to be the case.

Presented is an Ignition and Growth (I&G) EoS which when adopted for the same simulations, captures the behaviour of experimental ANFO detonation rather accurately. Future numerical simulation will consider the I&G EoS for non-ideal explosives in the attempt to capture their behaviours across a whole range of mass scales, alongside identifying at which regions are JWL parameters valid.

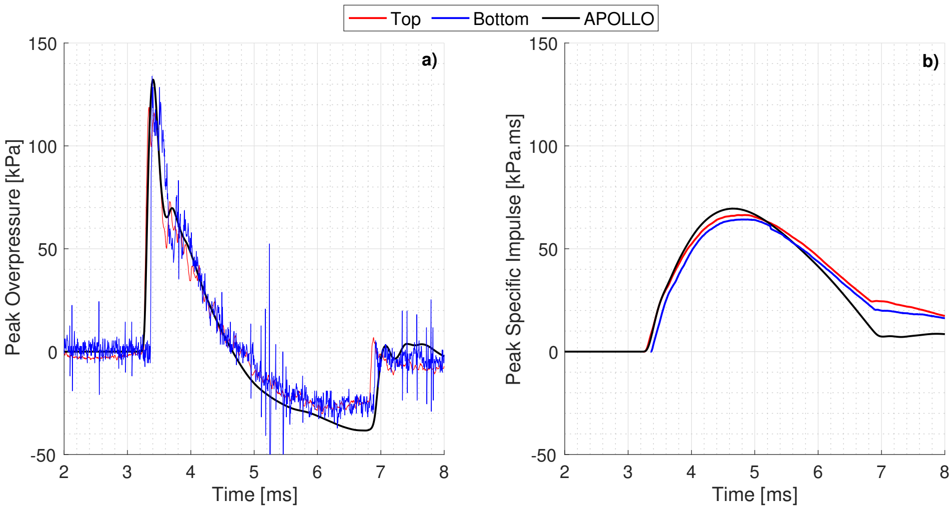

Figure 5.12: Compilation of pressure-time and impulse-time histories from 1m standoff distances which related to top (red) and bottom (blue) detonated trials: a) Top P-T, b) Top I-T, c) Bottom P-T, and d) Bottom I-T.

5.3.4.2 Is the energy equivalence reduction related to unreacted ANFO prill projectiles?

The findings from the previous two hypothesis tests lead to a further theory that the overall explosive yield reduction, compared to quoted values in literature, could be directly linked to the quoted reaction zones of non-ideal explosives being anywhere from in 10-100mm[29]. A rudimental analysis assessed the effect this radius of ANFO being un-reacted would have on the TNT equivalence for a variety of hemispherical charge sizes tested as seen in Figure 5.13.

The analysis assumed a constant reaction zone size of 13mm and a $TNTe = 0.82$ to compute a mass ratio of ANFO for the reduced mass based on the reaction zone being un-reacted compared to the actual mass tested. The ratio was multiplied by the TNTe factor to assume an actually reacted TNTe factor in these small scale trials which is displayed by the plotted curve in Figure 5.13. This plot outlines both the charge masses tested in this series, which would result in a range of $TNTe = 0.3 - 0.5$, closely matching the spread seen for the experimental data conducted within this series (denoted by the red and blue markers), and charge masses up to those tested by Petes et al.[112]. Based on these assumptions, to achieve the $TNTe = 0.82$ based on this mechanism alone, a charge mass of 10,000kg would be required.

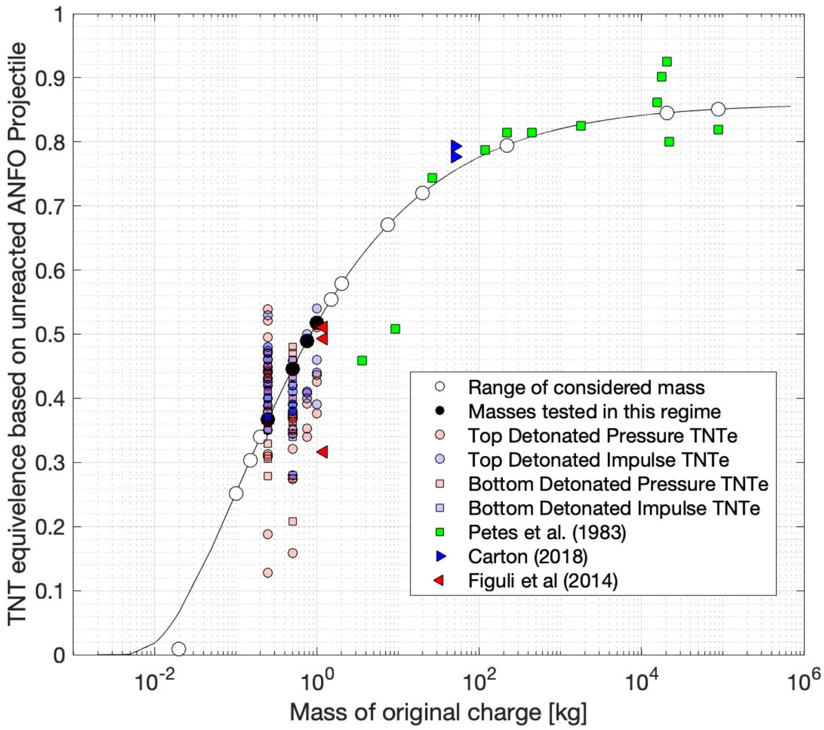

Figure 5.13: Equivalent TNTe values resulting from applying a nominal 13mm reaction zone to a given ANFO charge and assuming that the region has not fully reacted and instead is fired off as a projectile compared with extract TNTe from experimental pressure and impulse data

It is important to note that the value of TNTe and size of reaction zone have been chosen based on published values and appropriate fits the available experimental data. The experimental recordings which are much lower than the quoted range of $TNTe = 0.3 - 0.5$ are the result of being within a scaled distance of $Z < 1m\ /kg^{1/3}$, to which the top detonated position effects (see Figure 5.5) and fluid dynamic instabilities have a much greater influence on the recorded parameters and thus the inferred TNTe values, as discussed in Section 5.3.1.

5.3.4.3 Additional Testing

Whilst a mechanism which captures the behaviour of the small scale charges, it is not necessarily the definitive physical process. The irony with the potential mechanisms considered in Section 5.3.4 is that both result in an effective yield reduction of around 50% for charges of this size, which agrees with the ratio between the recorded data and published values of ANFO yield, however, neither can be definitively confirmed.

It is actually hypothesised to be a combination of the above contributors which makes quantifying and characterising the fundamental process difficult. Further test were conducted using small scale charges but with a variety of ANFO/AN composition mixes. The idea behind these tests were to investigate and quantify the influence of FO has on the primary shock wave parameters and to establish which of the aforementioned mechanisms contributed to the over energetic output.

The first lot of testing which was of interest was to vary the general composition of the AN/FO percentages to assess the effects this has for small scale ANFO charges. Petes et al.[112] presented findings in large scales charge which suggested a drop in energy release when the FO percentage varied from being stoichiometric mix at 6%. To test this feature in small scale charges to establish whether the FO was making a difference in small scale charges was to change the composition by adding in a proportion of pure AN to reduce the global percentage of FO in each charge. A total of 10 tests (5 different FO% with a repeat test) were conducted recording the pressure-time history at two standoff distances resulting in 20 individual recordings. The data was analysed using standard methods discussed throughout this thesis, and an average TNTe factor was established for the tests at each FO percentage investigated, as seen in Figure 5.14.

What this investigation did prove was that even in these small scale charges, the percentage of FO does still play an effect on the overall explosive yield output from the detonation. This was enough evidence to suggest that during the detonation of ANFO in small quantities the mechanisms as to why a lower TNTe value is evaluated is not related to just AN detonating, and is a slightly more complicated phenomena. When no FO was present, the AN composition was unable to detonate, concluding that some FO is required and is part of the energy release process for small scale charges.

It was therefore important to consider what would happen if the FO percentage was lower within the composition, but rather than a well mixed composition of ANFO with AN, having two distinct regions of AN and ANFO. This would investigate whether the reduced TNTe value seen for small scale ANFO is related to an unreacted shell of prill projecting away from the charge proportional to reaction zone sizes.

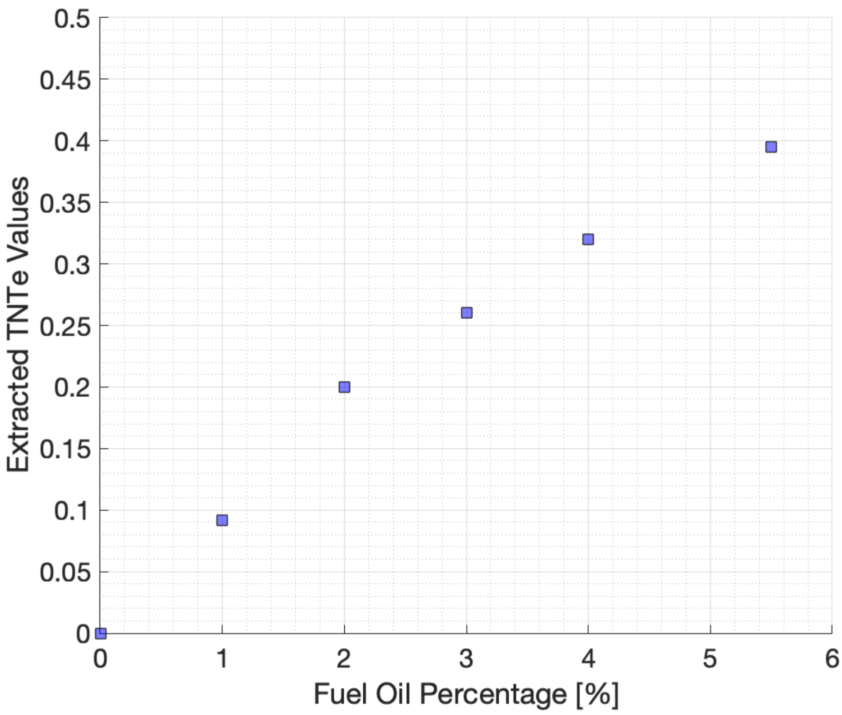

Figure 5.14: Extracted TNTe values from 250g hemispherical charge trials of ANFO varying the FO percentage by addition of pure AN

To test theories proposed in which only the FO in the direct vicinity of the booster charge is fully combusting and the remaining energy release is from the detonation of AN. To test this a double shelled hemisphere was used with the the inner shell containing ANFO and the outer shell consisting of pure AN both with 125g of the material in theory lowering the overall FO percentage down to 2.75%. With low levels of FO, it has been reported a incomplete reaction occurs and therefore lower energy releases and subsequentially slower detonation velocities[183]. Obviously with a inner vacuum formed shell to keep the two compositions separate, an extra level of confinement, albeit minimal, is provided which could have resulted in additional combustion of the FO[12].

Figure 5.15a-d shows the results of a shelled hemisphere test of AN/ANFO mix when compared to a full 250g ANFO hemisphere measured at two different standoff distances. Considering the pressure-time history plots in Figures 5.15a and 5.15b, there is very little difference between the positive phases of the shelled trials and the full ANFO tests which alone suggests that the hypothesis that the outer layer of the charge provides very little to the initial primary shocks blast parameters. However, taking into account the specific impulse plots seen in Figures 5.15c and 5.15d, there is a clear reduction between the bench mark 250g ANFO and the hypothesis testing AN/ANFO shell. Whilst the 250g ANFO trial results in a TNTe$\simeq$0.36, the shell trial exhibited a TNTe$\simeq$0.3 assuming a full 250g mass for both, suggesting there is a reduction in energy release but not what would be expected when removing 2.75% of the fuel oil which when looking at the trend seen in Figure 5.14, this composition would be expected to result in a TNTe$\simeq$0.23.The question posed here is what the reason for an explosive with half the mass of ANFO and an outer shell of AN to provide a different behaviour to the same quantities of the material but evenly mixed.

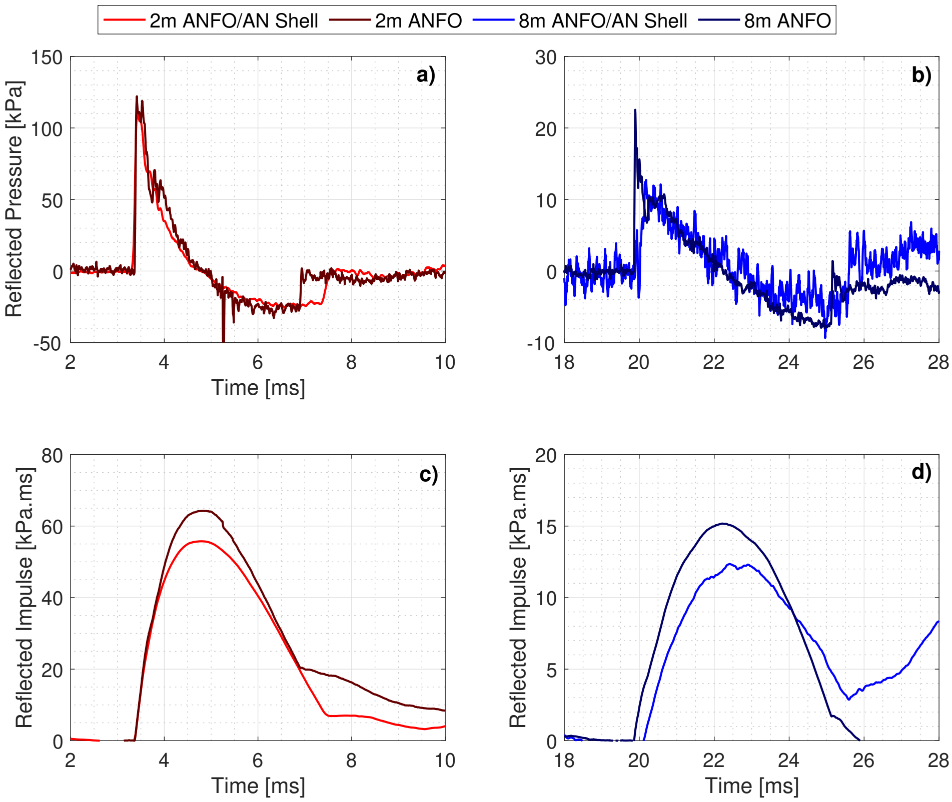

Figure 5.15: Compilation of pressure-time and impulse-time histories at 2m (red) and 8m (blue) standoff of 50/50 shells of ANFO/AN compared to 250g ANFO trials (black): a) 2m P-T, b) 8m P-T, c) 2m I-T, and d) 8m I-T.

It was considered whether the outer shell of the explosive exhibits detonation and/or combustion in any of the tests conducted. The proof of some energy release in this region is exhibited through the differences in specific impulses when comparing the shelled tested to full ANFO in Figure 5.15, therefore it can be induced that the reactions are ongoing in the outer shell and cannot be fully assumed to be unreacted material projectiles. This leads on to the idea that close to the charge centre there is enough pressure, confinement and time for the ANFO to fully react prior to any energy loses, but the outer shell does not and therefore exhibits state changes but never fully reacted by the time breakout occurs.

A realistic conclusion to make from the results of the small scale ANFO tests, and the corresponding positive phase data, is that friedlander pressure-time histories are achieved similar to those resulting from ideal explosive detonation but for non-ideal explosives the reaction zone is the main mechanism which causes the reduction in TNTe and thus is not scalable with charge mass. The shelled tests exhibit specific impulse reductions when comparing to 250g ANFO shots which are directly related to the lack of FO in the final section of the charge, and therefore no combustion could occur. It is assumed however that the outer shell of the charges only partially reacts, which is why only a small differences in the TNTe values extracted from the data is experience between the two trial types. With large charges, the reaction zone size becomes irrelevant when looking at its percentage of the whole charge mass and therefore the detonation fosters confinement, higher pressures, temperatures and more time for the reactions to occur, resulting in TNTe values close to the theoretical thermochemically derived value of TNTe=0.82. HSV work, discussed in Section 5.4, will look at quantifying a more realistic reaction zone size to improve the validity of the empirical curve derived in Figure 5.13.

5.3.5 Negative Phase

The negative phase of the small scale ANFO trials was of particular interest as again there is no previous literature which outlines its behaviour, and with the findings of discussed in Section 5.3.1 showing discrepancies between assumed knowledge and experimental data, further developments to understanding non-ideal detonation could be made. Figures 5.16a-c represent the extracted and scaled negative phase parameters for the small scale ANFO trials which do not compare to KB predictions as well as the ideal explosives discussed in Figures 4.6a-c, which was somewhat expected.

Whilst Figure 4.6c presents a general consistency in the negative phase duration parameters extracted, the spreads observed are a consequence of the difficulty in prescribing the parameter generally, and within this low pressure region even more so. It is important to note that going forward the time duration of the negative phase will be omitted from further analysis in line with the notion presented within this thesis of it not providing truly valid data despite KB predictions capturing the parameter reasonably well.

Considered the negative pressure in Figure 5.16a, when comparing to KB predictions there seems to be a much greater negative phase as a result of small scale ANFO detonations, resulting in a TNTe$\simeq$0.82 providing a more appropriate fit. Needham[107] discussed the phenomena of the negative phase and detailed the mechanism of the rising fireball creating lower pressure regions near the ground surface, which pulls the surround air towards the detonation point. This process further lowers the air density of the medium which has over-expanded during the shock waves propagation and therefore results in large negative phases within an energetic fireball. What this suggests for the small-scale ANFO trials is that the energy contained within the fireball, and subsequent shocks, is much greater than what is to be expected for standard ideal explosives, which has been related directly to the combustion of FO that was unable to occur during the initial detonation process.

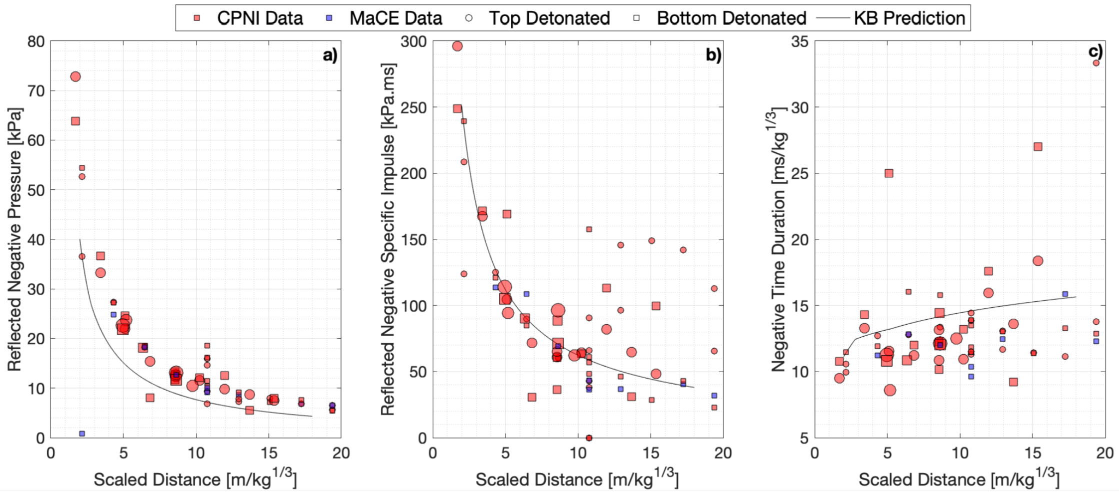

Figure 5.16: Compiled scaled negative phase blast parameters from ANFO explosive trials as a function scaled distance, compared with KB predictions, using a TNTe=0.395, with increasing marker sizes to indicate the mass of charge: a) Reflected negative pressure, b) Reflected negative specific impulse, c) Scaled negative phase duration

Scaling all the negative phase data by a larger TNTe value based on the pressure data alone would result in a shift away from the KB predictions for the negative impulse in Figure 5.16b, which based on a TNTe=0.395 seems to be captured reasonably well. This led to question whether KB predictions were reasonable representations of ANFO, and other non-ideal explosives, for the negative phase as different TNTe values could be deduced for each parameter, which is unconducive when compared to how well ideal explosives behave against prediction tool across every considered parameter in far-field regimes. With ANFO still exhibiting ideal-like behaviours, but with a lack of scalability with mass, for each increment of mass scale there should be a valid TNTe value which works across the far-field range and therefore a systematic error in the method of analysis has been highlighted.

The method of establishing the specific impulse values in Figures 5.16b and 4.6b, disregards the effect of the secondary shock during the calculation due it being so small in ideal explosives it could be omitted making minimal differences to the output results[133]. Interestingly, small scale ANFO presents as if the secondary shock is more influential on the negative phase impulse as there is disagreement between the TNTe values required for KB predictions to capture the data. An investigation into the inclusion of capturing the secondary shock parameters when calculating the overall negative phase specific impulse. In doing so, a more appropriate value of a TNTe could be established which fits across each of the blast parameters in line with findings for ideal explosions in far-field scenarios seen in Chapter 4.

With a more through examination of the data to account for the negative phase a stand alone feature of the primary blast wave by effectively omitting the effects of secondary shock was undertaken. As mentioned previously in Figure 5.16a, the negative pressure associated with small-scale ANFO seems to be better captured with a TNTe≃0.82 which had been related to the FO combustion occurring within the confines of the fireball detonation cloud. It has been therefore assumed that all parameters which are extracted after the positive phase can be scaled accordingly with the idea that there is enough temperature, pressure and time for the full energy release from the partially reacted prill projectiles due to the confinement of the detonation cloud itself. Figures 5.17a-b present the negative phase parameters, scaled using a TNTe=0.82 when considering the behaviour as a perfect blast wave and removing effects of secondary shocks.

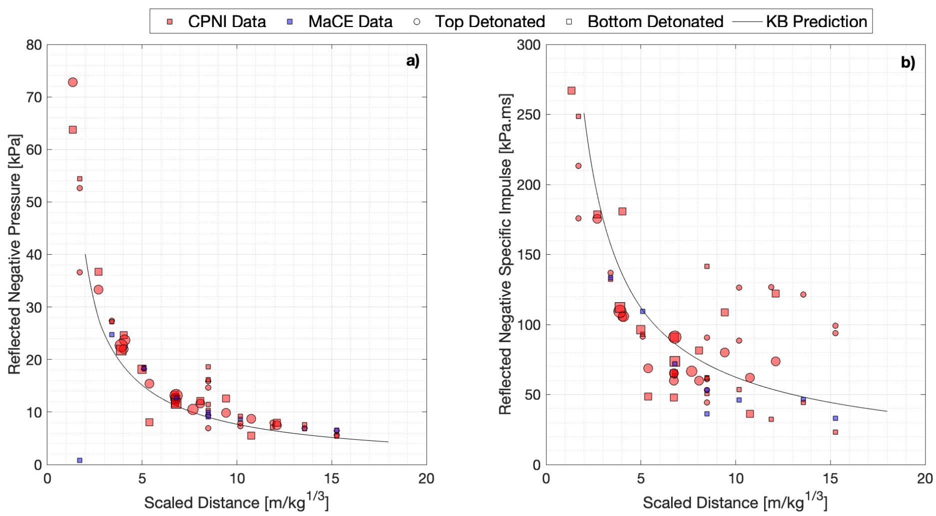

Figure 5.17: Compiled negative phase blast parameters re-worked to include secondary shock capture from ANFO explosive trials as a function scaled distance, compared with KB predictions, using a TNTe=0.82, with increasing marker sizes to indicate the mass of charge: a) Peak reflected overpressure, b) Scaled reflected peak specific impulse

Clearly seen in both Figures 5.17a and 5.17b is a general improvement on how well KB predictions capture the negative phase experimental data. This finding provides justification the KB predictions capture blast parameters extremely well in the far-field regime when considering a perfectly ideal shock wave and thus the basis of future work which could look at the superposition of ideal primary and subsequent waves to establish accurate predictions for a real-world explosive event.

5.3.5.1 Secondary Shock Data

The scaled secondary shock data, when presented against KB predictions in Figures 5.18a-d, again shows similar behaviour to the ideal explosives, with a large difference between predicted values of a primary wave but exhibiting considerable consistency across the entire data set with respect to scale distance. The general behaviours of the data and the predictive curves are comparable which does give rise to the idea that secondary shock data is as deterministic as the positive phase and future work should consider the development of similar empirical curves from a large quantity of secondary shock data resented within this thesis and published literature.

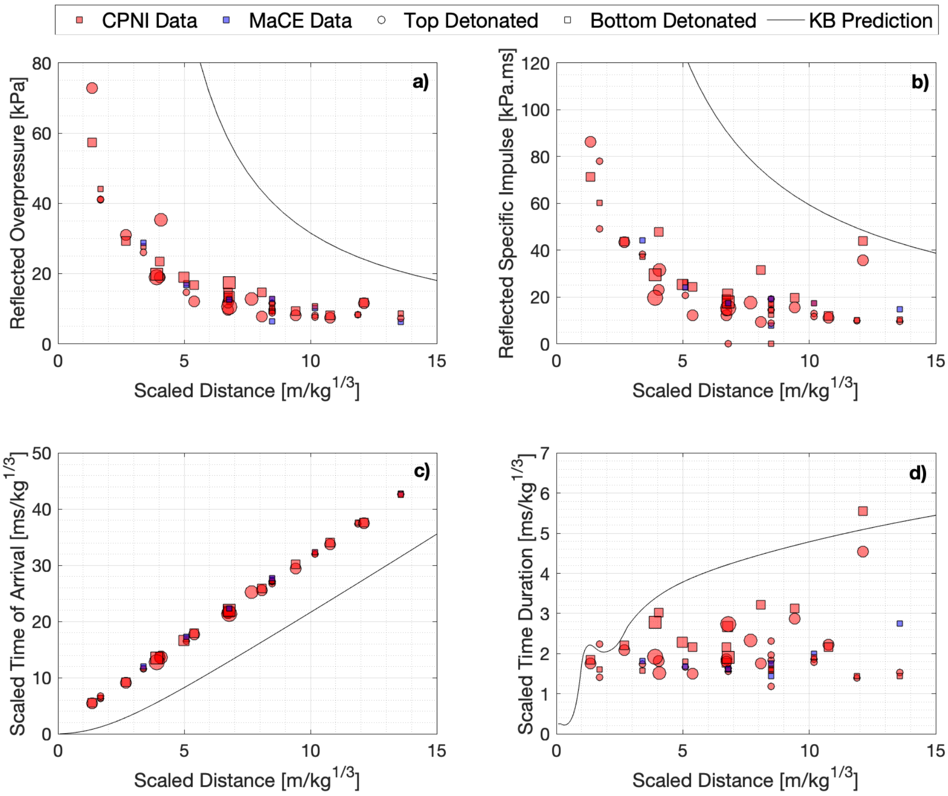

Figure 5.18: Compiled scaled secondary shock blast parameters from ANFO explosive trials as a function scaled distance, compared with KB predictions, using a TNTe=0.82, with increasing marker sizes to indicate the mass of charge: a) Peak reflected overpressure, b) Scaled reflected peak specific impulse, c) Scaled arrival time, d) Scaled positive phase duration

The issue currently faced is the idea that the secondary shock is highly dependent on the spatial and temporal characteristics of the fireball and therefore variations in the internal chemistry and energy release will increase the variation in extracted experimental data. Figures 5.19a-d present a compilation of all the secondary shock data collected within this thesis, scaled accordingly with the corresponding TNTe values.

Although the scaled data generally holds a level of comparison between the ideal and non-ideal explosives there are some clear differences exhibited which could be key to further the understanding of small scale ANFO detonations and thus other non-ideal explosives. With reference to Figures 5.19b and 5.19c, the ideal explosives seem to exhibit less energy released in the form of specific impulse but have a time of arrival which seems to be smaller than that of the ANFO trials, suggesting that the secondary shock travels faster but is a much smaller quantity of energy associated with it. In reality this finding goes back to the idea of the arrival time offset discussed in Section 5.3.2, which discussed the biggest influencer of arrival time offset to be the proportionality between the velocity of a ANFO shock wave, in comparison to one from an equivalent TNT mass. Interestingly, when approaching the near-field, $Z < 3m/kg^{1/3}$, the data for secondary shock arrival time tends towards the same point suggesting the offset between primary and secondary shock is consistent across all explosive types, related directly to the time in which it takes the secondary shock to begin to propagate. The data quickly trends away as the secondary shock in ANFO is travelling at a much lower velocity than that of the ideal explosives. The velocity proportionality theory could be explored in future research to acquire a relationship between primary and secondary shock velocities for both ideal and non-ideal explosives to then quantify the offsets presented in Figure 5.19c in a robust manner.

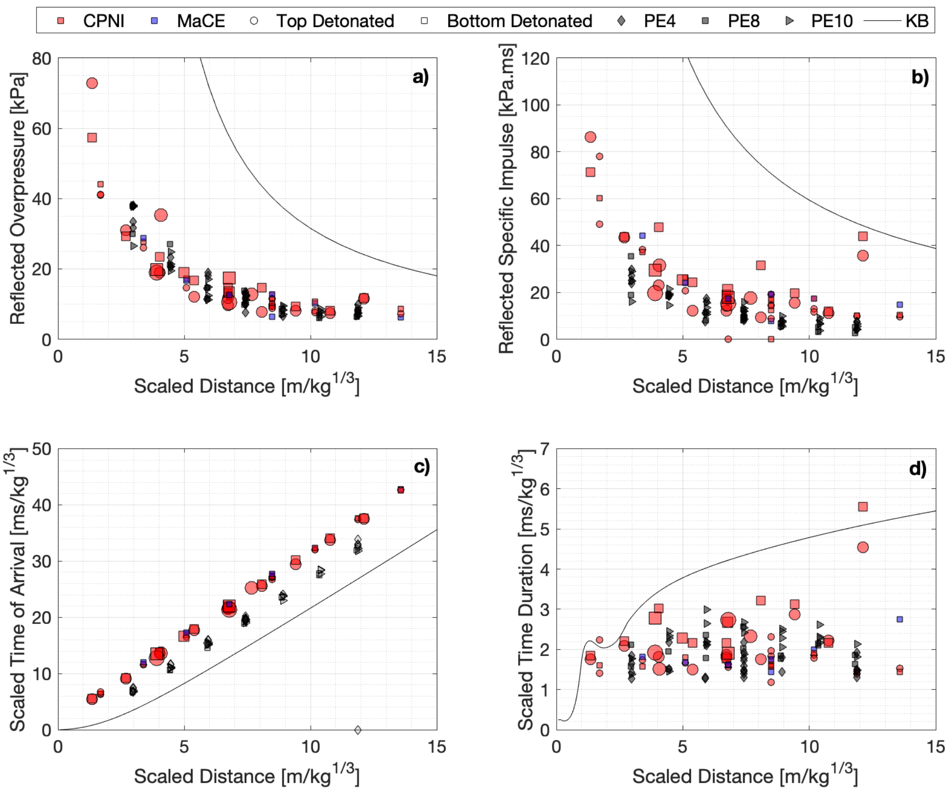

Figure 5.19: Compiled scaled secondary shock blast parameters from all considered explosive trials as a function scaled distance, compared with KB predictions, using each corresponding TNTe value, with increasing marker sizes to indicate the mass of charge: a) Peak reflected overpressure, b) Scaled reflected peak specific impulse, c) Scaled arrival time, d) Scaled positive phase duration

It was important to test the dimensionless secondary shock delay prediction tool against small scale ANFO secondary shock data provided the knowledge that all parameters after the primary wave is to be scaled with a TNTe=0.82. In order to express the secondary shock delay extracted from the data as dimensionless, there is a requirement to prescribe a velocity of detonation and packing density for the small scale ANFO. Whilst the packing density was measured pre-test to be approximately $820kg/m^3$, the velocity of detonation was uncertain from pressure gauge analysis alone. It was questioned whether the velocity of detonation used in this analysis associated to the primary shock, the secondary shock or the maximum velocity the detonation wave can achieve in the given composition. On closer inspection of the data presented within Rigby and Gitterman[129] assumed the velocity of detonation to be that associated with the maximum velocity of detonation the composition could achieve, meaning that regardless of mass scaling and the composition, the explosive secondary shock delay is normalised based on an ideal detonation. With that being said, the small scale ANFO data collected within this thesis was normalised using a velocity of detonation of 4,200m/s in line with values quoted in Petes et al.[112], to which is presented in Figure 5.20.

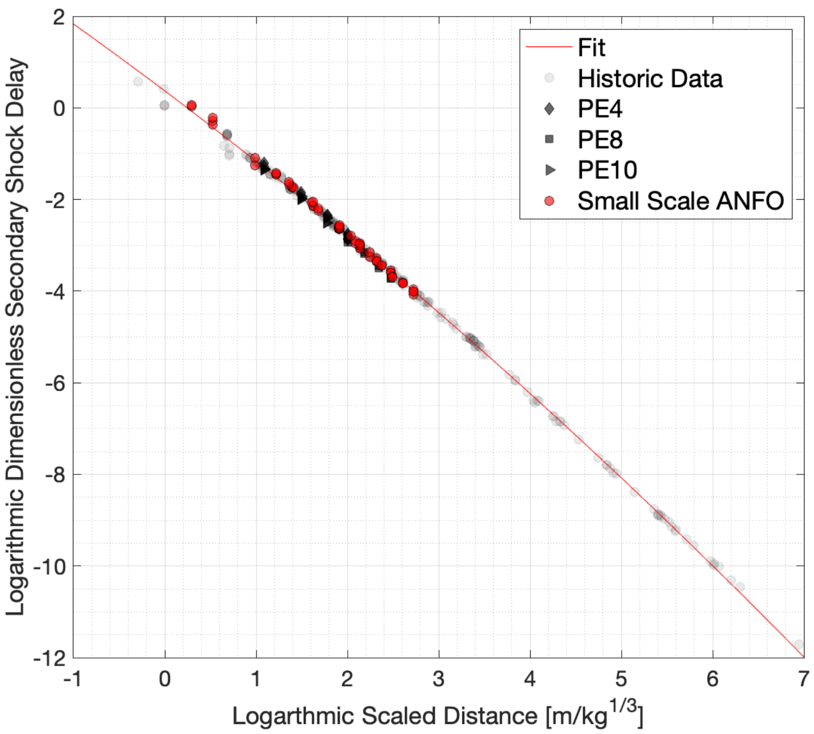

Figure 5.20: Dimensionless secondary shock delay parameter evaluated for all explosive tested in this thesis, scaled accordingly, and compared with polynomial fit to historic data

The clear comparable relationship between the normalised data and the fitted prediction provides confidence in the tool across explosive composition mass and scaled distance. The concern however in considering small scale ANFO with a velocity of detonation of 4,200m/s, similarly to large scale detonations, seems fragmented because the total energy released during detonation are different and thus the secondary shock behaviour should be too. It proposed that the energy which is not released during the development of the primary shock is gained during the propagation of the secondary shock, resulting in a halving of the blast parameters associated with the primary shock and doubling of the secondary shock parameters. This would explain why the delay time between primary and secondary shock arrival time is unaffected by this process as one the primary wave propagates slower and the secondary faster than they should when compared to large scale charges. This knowledge justifies the reason for assuming the maximum detonation velocity regardless of composition and mass scaling because even during non-ideal detonation the same quantity of energy is released just over much lower time scales, and with understanding the two aforementioned parameters proportionality even if the energy is not captured by the primary wave, subsequent waves will.

5.3.6 Pressure Gauge Summary

The section has considered the pressure gauge data recorded from the detonation of small scale ANFO charges with a thorough investigation into the mechanisms resulting in a TNTe=0.395 for primary shock wave positive phase parameters, and a TNTe=0.82 for all parameters subsequent to the breakout of the primary shock (i.e negative phase of the primary wave and the secondary shock parameters). Discrepancies were exhibited in the TNTe of arrival time for both primary and secondary shocks which was related directly to the proportionality of velocity between small scale ANFO and TNT, which was not visible for ideal explosives discussed in Chapter 4, but in reality is probably a feature to consider during future analysis.

The pressure gauge analysis of small scale ANFO has provided insights into the behaviours of non-ideal explosives provided the reaction zone size is order of magnitudes larger than the explosive charges diameter. At each increment of mass, ANFO detonations result in friedlander shock wave behaviours which could be considered to be ideal, with a constant TNTe, across an entire range of standoff when compared to KB predictions. However, there is proportionality between mass and the associated TNTe, until a limit is reached where no amount of additional charge mass will effect the overall explosive yield. It is therefore paramount for a more robust mechanism of predicting non-ideal explosive behaviour.

Interestingly, the findings for the secondary shock analysis suggest that of the total potential energy of a given charge, there is a ratio of energy split between the primary and subsequent shocks. The amount of energy released during the primary shock development in small scale ANFO is approximately half than what was expected, however the development of subsequent shocks encompassed around double the amount of energy. This idea has been speculated when considering the fact all the measured parameters which are confined within, and affected by, the detonation cloud for longer durations seem to exhibit far more energy in small scale ANFO than what is experienced in ideal explosives.

5.4 High Speed Video Analysis

The methods discussed in Chapter 4 have been adopted for the far-field trials using hemispherical ANFO charges to test their applicability to non-ideal explosives. The results from an individual trial at 5m standoff from a reflective wall was processed using the aforementioned methods and is presented in Figure 5.21. The data required a $TNTe = 0.3$ in order for the scaled arrival time data to replicate KB predictions. This is parallel to the findings from the MAE analysis undertaken on the pressure gauge data evaluating a lower TNTe factor (TNTe=0.28) for arrival time when compared to other blast parameters (TNTe=0.395). This finding establishes confidence in the pressure gauge recordings triggering at the correct time and the time of arrival offset being a real physical feature of small scale ANFO charges. The reason for the offset in arrival time has yet to be fully established and therefore it is hoped that with the use of high speed video in conjunction with the theory of shock wave velocities presented in Figure 5.10, and their relationship to TNTe, an approximation for the offset could be deduced.

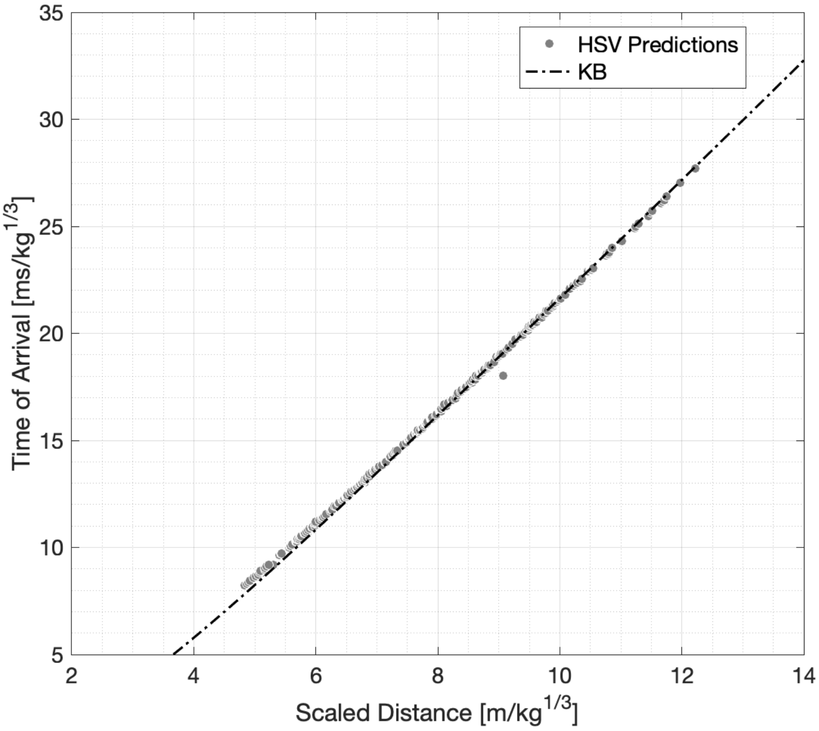

Figure 5.21: Shock front arrival time from a bottom detonated 250g ANFO hemispherical charge placed at a 5 m stand-off, recorded using HSV and scaled using TNT equivalence factor of 0.3 to compare to KB predictions

5.4.1 Fireball Breakout

Figure 5.22 displays two snapshot images taken from a bottom detonated hemispherical 250g charge recorded at 1,000,000fps. The average velocity of the detonation wave can be approximated using the known distance the wave has travelled in these tests, 53mm, divided through by the time taken to reach this position which was 28,000ns, resulting in a average velocity of ∼1900m/s. Considering Figure 5.10, it is a safe assumption that the velocity at breakout would be higher than this value due to the acceleration in ANFO detonation velocity from point source to charge extents and therefore is probably closer to a velocity of ≃2700m/s, calculated from using the TNTe=0.395 established from pressure gauges data analysis and multiplying it by the detonation velocity of TNT which is 6950m/s. This finding is a reasonable approximation for supporting the notions regarding the lower TNTe value established from the far-field trials.

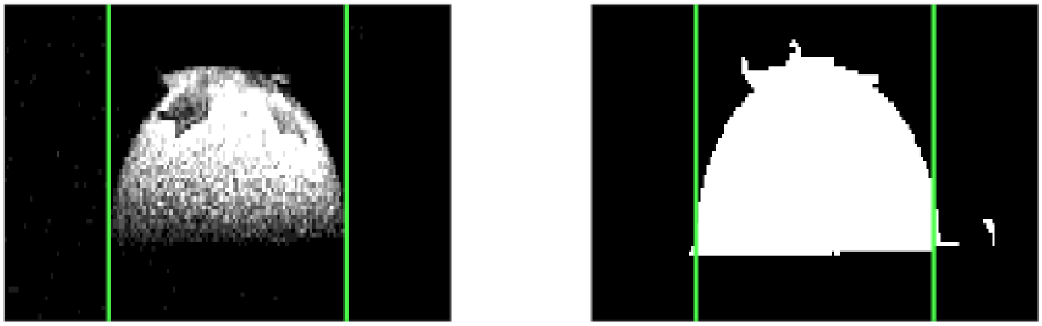

Figure 5.22: Ultra high speed video footage of a bottom detonated 250g hemispherical trial displaying the comparison between charge diameter at the time of detonation and at the point in which the detonation wave reached the charge's extents and products began to expand; this is denoted by the charge size extending passed the green lines spaced 80pixels apart in both plots.

However, as discussed in Section 5.3.2, the lower TNTe value established from shock wave arrival time is when the data is compared to free-air shock propagation for TNT which during the early stage detonation process behaves very differently to ideal ANFO. It can be assumed that TNT from the moment it detonates, it does so with a velocity of around 6950m/s across the entirety of its charge radius and then begin to decay when breakout occurs. As ANFO behaves differently, with an increasing velocity with charge radius, the best approximation which can be made for ANFO a average velocity of the detonation wave across the radius to make it comparable to an almost perfect average velocity of 6950m/s in TNT. By making this assumption of average velocities, the difference in time it takes for a 250g TNT hemisphere to reduce down from 6950m/s to the average ∼1900m/s would provide a reasonable theoretical approach to why an offset is recorded.

Figure 5.23 outlines the aforementioned theoretical approach and highlights an offset in arrival time of around 0.32ms between the detonation a 250g hemisphere of TNT and the time in which it begins to behave like a 250g hemisphere of ANFO based on HSV analysis of the fireball breakout. This offset value is similar to that presented in Section 5.3.2 when looking at the arrival time offset attributed to the pressure gauge data when comparing between the pressure and impulse evaluated TNTe=0.395 and the KB predictive curve, which gives justification towards this theory. Whilst ideal explosives exhibit similar velocity profiles to TNT, non-ideal explosive like ANFO need to be characterised differently, with shock wave arrival time being investigated based on the propagation dynamics of the detonation wave and subsequent shock wave.

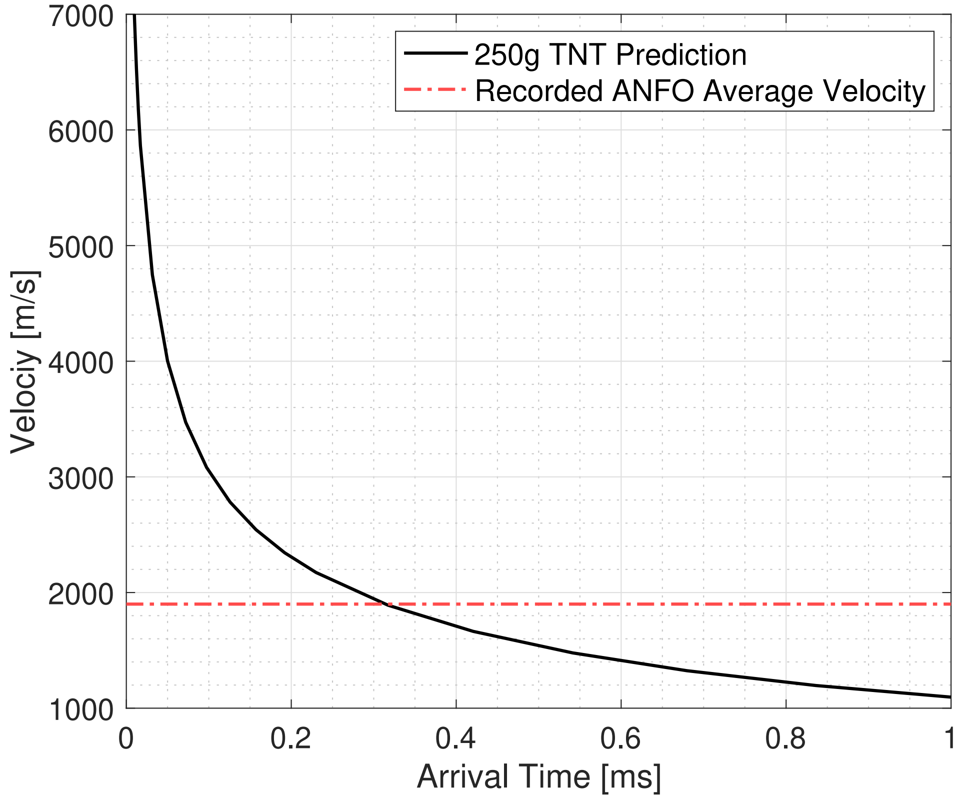

Figure 5.23: Shock wave velocity with respect to arrival time for a 250g TNT explosives evaluated through KB predictions with reference to the average vlocity extracted from the HSV of hemispherical ANFO detonation

5.4.2 Variability Analysis

The same variability analysis undertaken in Section 4.3.1 to establish whether ANFO also behaves in a deterministic manner when relating the consistency of arrival time data to the scaled distance at which the recording was taken. Figure 5.24 shows arrival time variability across the top and bottom detonated (denoted by TD and BD respectively) ANFO hemispherical detonations with respect to scaled distance. The estimated gauge variation boundary (GVB) presented in Figure 4.11 for PE4 trials was used to test the confidence in the fit as a deterministic predictor for far-field free-air shock waves developed from different explosives.

The estimated GVB can be seen to generally hold credibility for the ANFO hemispheres tested and this provides confidence as this an upper bound for arrival time variability across the far-field range for all explosives. It is important to note that at the two extremities of the recording scaled distances, the variability in the data is higher based on the shear lack of data points recorded. These positions correspond to the furtherest parts of the cameras field of view and therefore are subject to lens distortion and can be omitted.

One finding that can be deduced which is in line with that of the pressure gauge data is that the variability of both bottom and top detonated shots are similar which gives rise to the consistency of each individual trial and the increase in variability as scaled distance enter the instability regions between $0.1 < Z < 3m/kg^{1/3}$ regardless of the differences in arrival time associated with detonator position discussed in Figure 5.9.

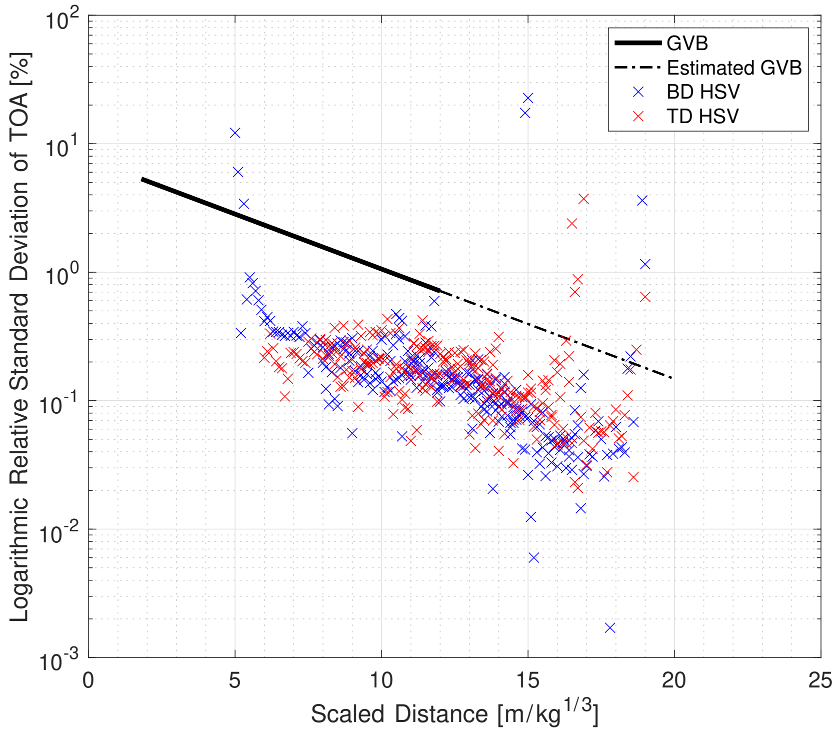

Figure 5.24: Logarithmic RSTD in shock wave arrival time of 250g hemispherical ANFO trials as a function of scaled distance for high speed video recordings, compared to empirical model detailed within Farrimond et al.[49]

.

5.4.3 Rate Stick Trials

The rate stick tests documented within this thesis were recorded using ultra high speed video cameras recording at between 250,000-500,000fps in order to capture the detonation wave propagation throughout each trial. The main reason for the variability of the frame rate is due to the filming capability of the camera used limited to a set number of frames, therefore in order to capture the fireball/shock wave propagation from the end of the cylinders a slower frame rate was required.

The video recordings displayed in Figure 5.25 shows the general behaviour of the ANFO rate stick trials, which was consistent across all pipe sizes tested and therefore is not a diameter dependent feature within the bounds of this experimental regime. The first snapshot shows the 3g PE10 booster detonating and causing a preliminary flash to be seen percolate through the voids in the prill. As the snapshots progress through time intervals 0.05ms, a clearly defined detonation wave can be seen to form, with a seemingly expanding bright region to which has been attribute to the ongoing chemical reactions attempting to find an equilibrium. The final snapshot shows the front of the reaction zone reaching the end of the pipe, at which point the bright zone succeeding it begins to compress until it reaches the end of the pipe too. The fireball/shock wave only begins to propagate away from the end of the tube when the bright zone is fully compressed which provides the understanding that the propagating pressure wave would be related to the position at which the cylinder begins to expand (the back of the bright zone) and the front face of the bright zone is a reaction wave which has effectively little-to-no pressure associated with it but induces decomposition of the explosive. The brighter region size of particular interest as it is speculated that this could be the reaction zone of ANFO which if quantified could be included in Figure 5.13 to both verify the projectile theory and the assumption of a 13mm reaction zone for this sized charge.

Using similar methods discussed by Rigby et al.[130] to track near-field blast loading, the displacement of the front and back faces of this bright region were tracked using the 'Canny' edge detection in-built MATLAB function, as it was found to perform optimally for high contrast tracking. The back face of the bright region was defined by the position at which the cylinders began to laterally expand which provided to be more challenging to capture due to chaotic nature of the expanding detonation products. This was overcome by utilizing a threshold procedure to capture the brightest pixels, between a value of 0-255 within each frame, and then assigning a range between the max value and a percentage (determined through trial and error) of the assigned pixel intensity, to which the edge detection function would consider. Anything outside of this threshold was omitted from the analysis, and assumed to be too dark to be the reacting region of the charge. To verify the assigned positions of the reaction zone, the tracked positions were plotted at regular intervals over the whole frame itself as seen in Figure 5.26.

Using a pre-test photo taken from the high speed camera, displaying known dimensions of the rate stick, the video was calibrated through assigning define boundaries of the pipe external walls to achieve a real-world pixel size. The tracked positions from the source of detonation were calibrated to be a real-world distance travelled along the rate stick which was also differentiated, with respect to time, resulting in the velocity of the propagation of each front.

Rather than viewing the whole pipe in its entirety with one analysis and the attempt to nullify any irregularities in the fronts bright regions behaviours, three randomly assigned box strips across the width of the rate stick were considered for the regions of analysis in the attempt minimise any curvature effects and irregularities across the entire front. These three independent processed data sets are to be used as self-validation of the results extracted from recordings.

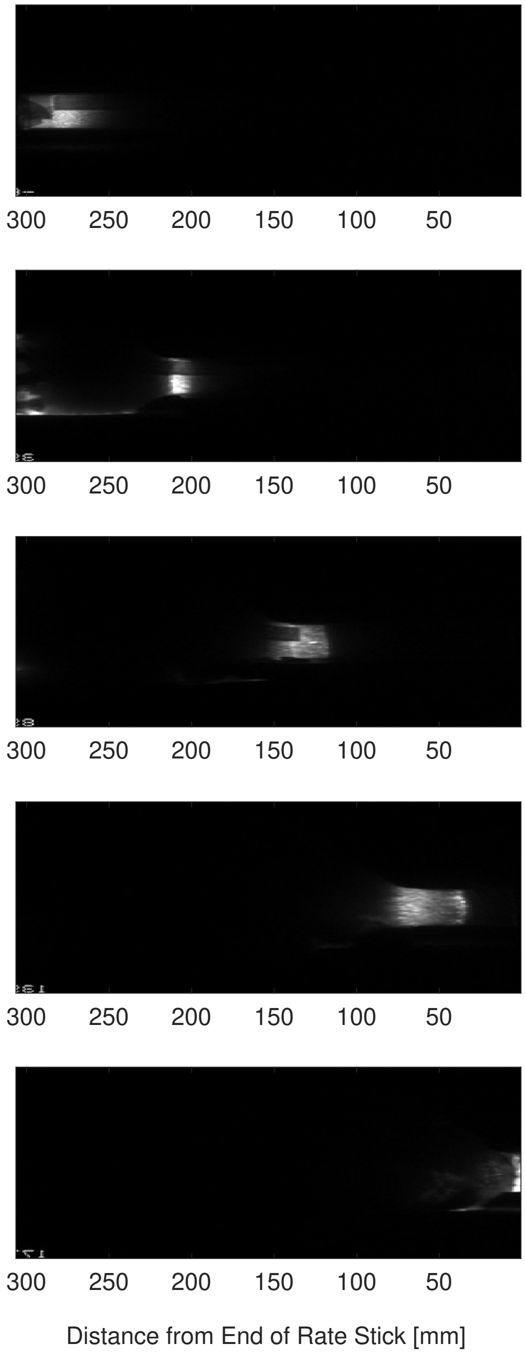

Figure 5.25: High speed video snapshots with 0.05ms intervals between each plot displaying the propagation of the detonation wave along a 300mm length 50mm diameter PMMA pipe

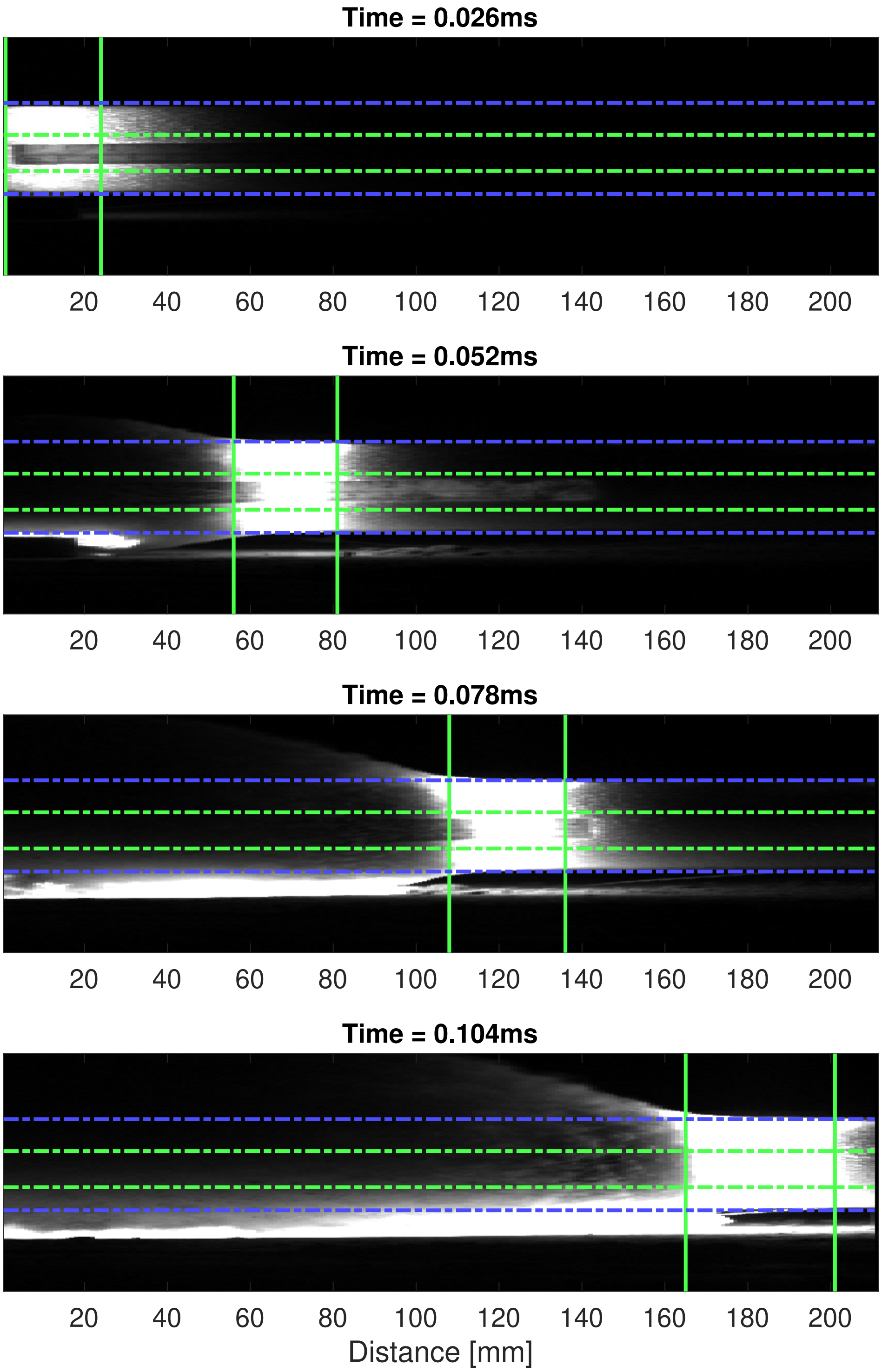

Figure 5.26: High speed video snapshots of 104mm internal diameter ANFO filled PMMA tube at $t = 0.026, 0.052, 0.078$ *and* $0.104ms$ *after detonation, highlighting the reaction zone positions assigned (green lines) for the given region considered (green dashed lines) alongside the widths of the pipe (blue dashed lines).*

4211 Figure 5.27 displays the same video recording as Figure 5.26 but only considering the

4212 region defined by the green dashed lines. The reduced region of analysis results in a con-
4213 sistent reaction zone and therefore a definitive position can be established for each trial.
4214 The three regions of analysis were chosen at random between the confines of the rate sticks
4215 width, to establish a probabilistic catheterisation of reaction front position and velocity.
4216 These parameters were evaluated from both horizontal and vertical calibration pixel sizes
4217 across all three analysis regions and were compared to assess the accuracy and validity of
4218 the analytical data processing tool which can be seen in Figure 5.28.

4219

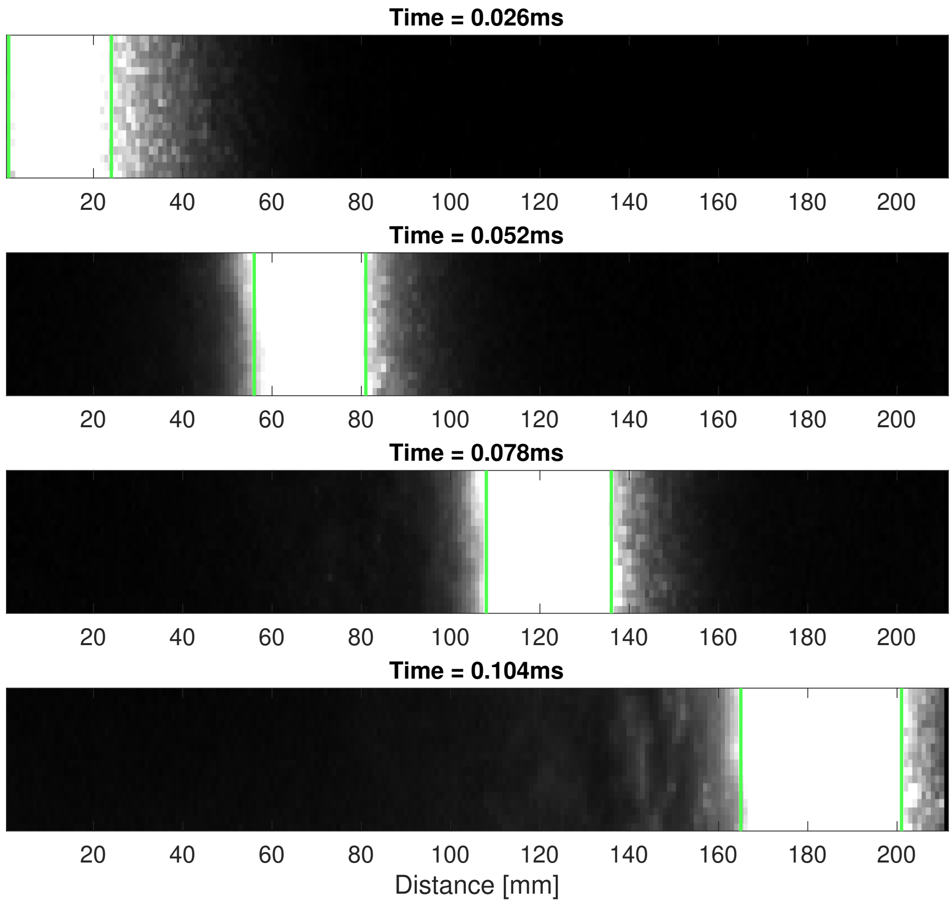

Figure 5.27: High speed video snapshots of 104mm internal diameter ANFO filled PMMA tube at $t = 0.026, 0.052, 0.078$ and $0.104ms$ after detonation, zoomed into the area box region considered.

4220 Figures 5.28a and 5.28b display the validation of the methodology process which consid-
4221 ered the three different regions of analysis, all of which that are calibrated using both
4222 vertical and horizontal pixels sizes. The results from these different processes suggest
4223 not only is the calibration correct, resulting in accurate data, but the regional choices
4224 on the pipe result in a general consistency of both velocity and reaction zone size. It

is believed the initial flash duration discussed in Figure 5.25, corresponds to the time it takes before the measured reaction zone of the ANFO charges to visually appear without doubt through the illuminated prill. The initial flash from the detonator/booster reduces the precision of the visual interpretation of the ANFO detonation wave alone hence why, during the opening ~80mm along the rate stick across both figures, spikes in the data is experienced which was a finding verified by Bohanek et al.[17]. After this, the data begins to behave consistently and therefore can be considered to be credible and represenative of the decomposition of ANFO, similar to the discussion made by Araos and Onederra[4], until ~200-250mm at which point, the data become corrupted by either detonation product breakout or systematic experimental oversights of securing tape blocking the view of the reaction zone. With this in mind, all subsequent plots discussing the rate stick trials will be confined to these limits of distance along the pipe to avoid discussing the inefficacy of unverified data.

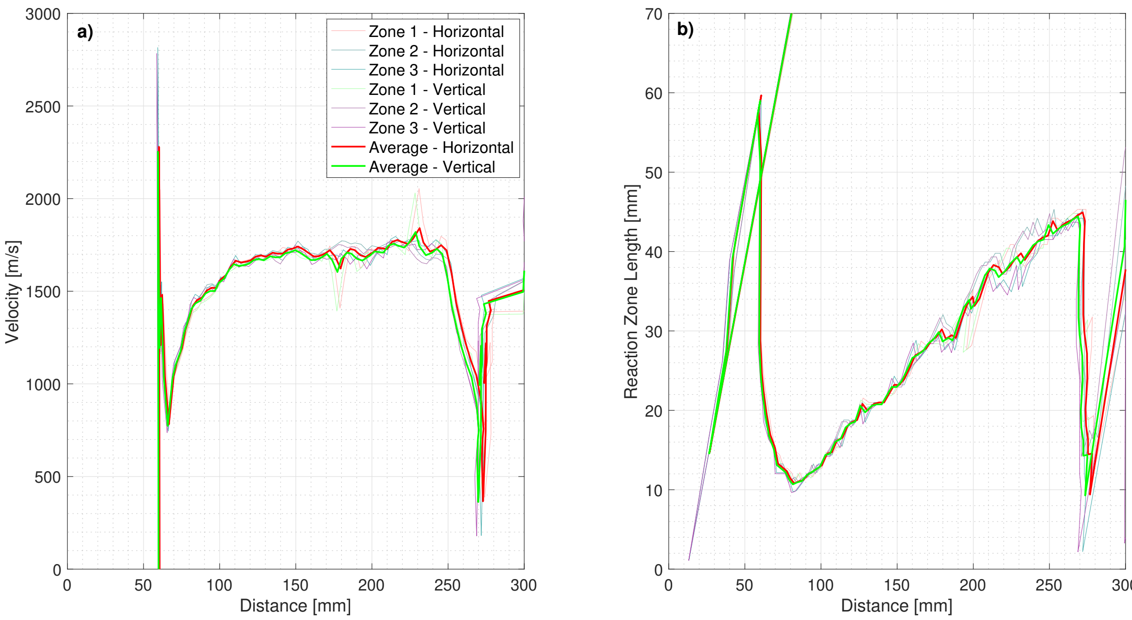

Figure 5.28: HSV tracking results from a 50mm internal diameter rate stick trial, calibrated both vertically and horizontally, smoothed using a 15 point moving average to present: a) Detonation front velocity and b) Reaction zone length with respect to distance travelled along the pipe.

5.4.3.1 Compiled Results

The results from the six different conducted rate stick trials subjected to the aforementioned analytical procedure are presented in Figures 5.29a and 5.29b for the lengths along the rate sticks which provide valid data which is representative of the decomposition an detonation of ANFO. When considering the smallest diameter pipes (50mm internal) which made use of a PE10 booster charge, denoted by the grey coloured lines, all exhibit consistency in velocity and reaction zone size across three nominally identical shots, providing confidence in the level of repeatability in the analytical methods developed between test, therefore verifying its application for the remaining tests to be qualitatively compared.

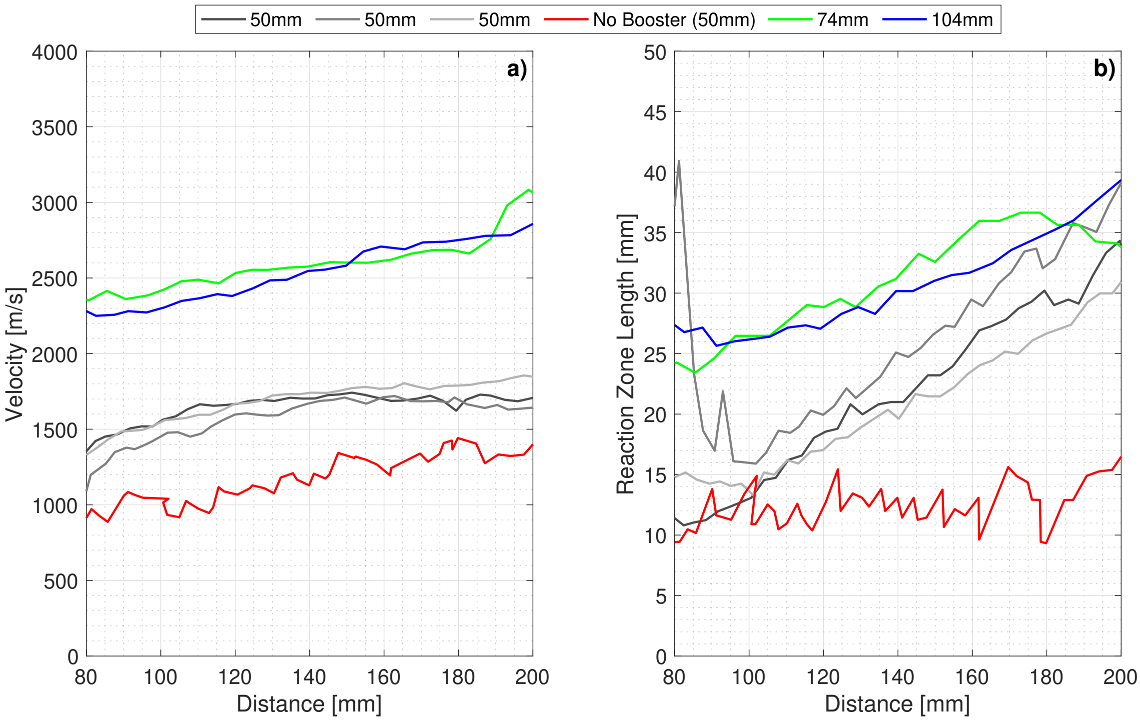

Figure 5.29: HSV tracking results from all ANFO rate stick trials conducted within this thesis, smoothed using a 15 point moving average to present: a) Detonation front velocity and b) Reaction zone length with respect to distance travelled along the pipe.

The non boosted 50mm diameter pipe shot presented much lower overall velocities and reaction zone than the boosted trials, with only a slight general increase in both with respect to distance along the rate stick. This finding is thought to infer the critical diameter of ANFO to be around that of this pipe used in these trials due to the fact the energy loses due to the expansion of detonation products almost equals the energy released through detonation. What this does begin suggest is that the minimum bright zone size required to detonate ANFO successfully is represented by around 12mm which begins to point towards the theory proposed within Figure 5.13.

The interesting finding when considering the 50mm internal diameter pipes is that upon exhibiting behavior represenative of ANFO detonation, a velocity of detonation measurement of 1000m/s and 1200-1400m/s has been extracted for the non-boosted and boosted trials respectively. The latter of which reaches steady state detonation recording a velocity of ∼1700-1800m/s which is much lower than the quoted value for ANFO (∼4200m/s). The non-boosted 50mm rate stick test results in a consistent velocity of ∼1000m/s, due to the lack of additional initial energy provided by the booster to induce the chemical reaction process within the confinement of the charge prior to any detonation product expansion. The 50mm diameter rate sticks clearly are large enough to sustain the detonation reaction but the energy losses through the lateral fireball and product expansion is enough to freeze out any further energy gained from the decomposition of the ANFO. With these values in mind, a direct comparison can be made to the quoted value which results in a ratio of between ≃25-43% depending on the values chosen which is believed to be further evidence to the reduced yield from small scale ANFO charges when to large charge trials conducted.

The larger diameter rate stick trials (74mm and 104mm internal diameters) exhibited a much higher initial velocity which has been initially tracked ∼2300m/s, both increasing at similar rates to peak values of around 2800m/s after a 200mm run along the rate stick but no levelling off like what is exhibited in the 50mm diameter pipes. This is related to the fact the large diameter pipes induce a longer duration of confinement and therefore the energy loss through lateral expansion of these rate stick was no longer enough to restrain a minimum steady-state velocity but instead result in an increase in energy released and front velocity with respect to distance along the rate stick.

Considering the trajectory of these velocities, it is approximated that a rate stick of around 500mm long is requred to exhibit the quote velocities of large scale ANFO, assuming no plateauing occurs at these charge diameters. The 74mm and 104mm internal diameter pipes show similar patterns of behaviour for both reaction zone length and velocity development which highlights the fact that the energy loss through lateral expansion of these rate sticks was no longer enough to restrain steady-velocities of the recorded fronts but instead resulted in an increase in energy release and velocity. This begins the debate as to whether the definition of the critical diameter of an explosive is the minimum size at which a cylindrical charge has to be to sustain a steady-state detonation is correct for non-ideal explosives and whether this could be the reason for a variety of different critical diameters quoted within published literature.

Qualitatively, the 104mm pipe seems to result in an increasing velocity at a greater rate than those recorded in the 74mm pipe. This is logical if less energy is being lost laterally whilst simultaneously gaining energy from the decomposition of ANFO but there is a larger surface area associated with the 104mm diameter pipe which will result in larger energy losses. This finding could be an artefact of the 15 point moving average applied to the raw data and should be treated with caution, assuming that the general physical mechanisms are similar. It is expected that with an increased minimum radius until detonation product breakout, the quicker the rise time in velocity to maximum theoretical value for ANFO. Using the data presented, this finding is not something which can be concluded on and would require a much more extensive rate-stick test plan across a range of pipe sizes and lengths with multiple repeats to establish its validity.

The measured reaction zone sized across all trials conducted with a booster exhibits an increase with distance travelled along the rate stick. As discussed previously, it is posited that as the ANFO detonates, under optimal conditions of confinement, the reaction zone length will increase in size. With the detonation cloud expansion only starting to occur when the back face of the zone reaches the charge extents, it is a reasonable suggestion that the larger the measured reaction zone, the more decomposition of ANFO occurs. This would result in a greater efficiency in the energy release of the composition as there would be more time and confinement for the deflagration of FO to occur. With this in mind, there key measurement of the reaction zone is at the beginning of the rate stick prior to any increase in length as this will identify the the amount of ANFO which could in theory will not react in any detonation.

It was hypothesised that the reaction zone measured in the rate stick trials could infer the range in size the zone could be depending on the test-to-test variability in the charges, directly relating to prill form and their macrostructural arrangement. Taking the non-boosted 50mm trials presented in Figures 5.29a and 5.29b, a near steady-state detonation is displayed and therefore the trial was close to the critical diameter of non-boosted ANFO. With this in mind, it would suggest the constant behaviour in the measured reaction zone length of between 9-17mm, taking the range recorded, is the minimum size required to detonate ANFO and therefore the size in which quantifies the amount of ANFO which may be unreacted on breakout of the detonation products and the primary shock wave.

Undertaking a similar analysis presented in Figure 5.13, the TNTe values were calculated for effective masses of ANFO resulting from the reaction zone sizes of 9mm and 17mm in line with the aforementioned findings and is presented in Figure 5.30. What can instantly be deduced from this plot is the fact that almost all the collected data, both from this research and historical is captured by the theoretical mechanism proposed and therefore provides justification to the theory of unreacted prill projectiles. Whilst there is agreement, the definitive mechanism is still to be established and future experimental testing should consider both the attempt of capturing this mechanism using high speed video and investigate the mass range which minimal data is presented for between 1-50kg, to verify if a general increase in TNTe is recorded in line with theoretical prediction.

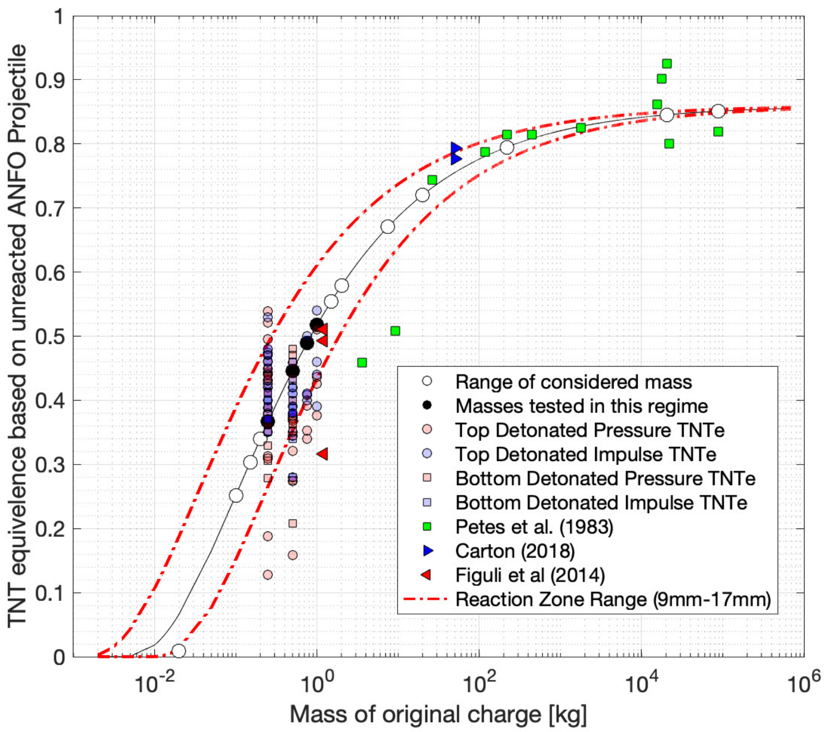

Figure 5.30: Equivalent TNTe values resulting from applying a nominal 13mm reaction zone to a given ANFO charge and assuming that the region has not fully reacted and instead is fired off as a projectile compared with extracted TNTe values from experimental pressure and impulse data, making reference to the reaction zone range recorded Figure 5.29b.

5.4.4 High Speed Video Summary

The validated HSV data processing tools developed within this thesis have been compared to the non-ideal explosive ANFO, in the attempt to characterise the mechanisms underlying the lower explosive yields associated with small scale charges and provide both theoretical and empirical quantifications to support the hypotheses made.

The results from using the originally developed tools provided confidence than small scale ANFO charges at each increment of mass behave with ideal-like characteristics, exhibiting the ability to be scaled by a single given TNTe value in far-field ranges.

The use of KB velocity relationships provided further insights into why the arrival time of small scale ANFO charges do not have a directly comparable relationship to TNT when comparing to other blast parameters extracted. The development of detonation velocity within the ANFO composition was not measured as part of these tests, but an average velocity from detonation to breakout was inferred which allowed comparison to the behaviour of an ideal explosive and therefore TNT. Implementing this theoretical approach resulted in arrival time offset which closely matched the pressure gauge data when compared to KB predictions.

Rate stick trials were undertaken in the attempt to further understand the internal detonation mechanisms and processed within smaller scale ANFO charges. An automated tracking algorithm was developed and self-validated in terms of its accuracy of tracking and the consistency in the test data through comparing three nominally identical shots which resulted in highly consistent data. The remaining trials were the conducted using a variety of pipe diameters and non-boosted charges. Through the analysis there is a clear relationship presented between confinement and/or charge diameter with the development of velocity.

One rate stick trial which was at quoted values of the critical diameter of ANFO (50mm internal diameter) and was not boosted, resulted in near steady state conditions, which not only verified the critical diameter but also presented the minimum conditions to achieve detonation. The reaction zone measurement for this trial was utilised to improve the mechanism of unreacted ANFO projectile prediction presented in Figure 5.30, which justified the behaviour of both small and large scale ANFO trials and presents ranges of potentially TNTe fluctuations based on the uncontrollable variables associated with heterogeneous prilled ANFO detonation. Whilst reasonable justification for these mechanisms have been presented, a much larger and rigorous testing regime for ANFO, across mass scales is required to help further validate the hypothesis presented.

5.5 Future Research into Non-Ideal Detonations

The investigation into small scale ANFO has provided a significant gap in the current understanding of non-ideal explosive characterisation and the mechanisms which result in there effective and overall potential explosive yields. Whilst there are studies which attempt to quantify a range of explosives which exhibit non-ideal behaviours, a distinct lack of thorough investigation is presented within published literature to quantify yields based on both mass and distance. The implication of assuming non-ideal explosives exhibit the same chemical processes during detonation as ideal explosives across an entire mass range is a general over prediction of the explosive output. If numerical models are not able to capture the yield of particular composition accurately across a full range of masses, a uncertainty within design regimes occur with the knock on effect of over-engineering each element of protection. Conducting well-controlled experiential trials for a number of commonly used home made explosives, varying both mass and standoff distance, will enable a global understanding of explosive loading conditions which can be integrated within probabilistic load characterisation for optimised protective schemes of element design.

In addition, this compilations of experimental data can be used to develop more robust numerical modelling schemes through the validation of thermochemical code values developed for EoS of each explosive. The method presented within this thesis makes use of the JWL EoS for small scale but adjusted to model AN alone which is known to be incorrect despite the accuracy of the simulation across the far-field range. Further investigation into the use of Ignition and Growth (I&G) EoS should be undertaken to accurately capture the detonation mechanics of non-ideal explosives across a whole range of masses.

Future work should look at undertaking a quantitative analysis of shock wave velocity across a full range of distances as a result from small scale ANFO charges using timer pins within the composition itself, alongside tracking the wave using incident gauges and/or HSV from detonation through to free-air propagation. In doing so, empirical comparisons can be made between the recorded data and the KB derived shock wave velocities for TNT, to further access the hypothesis suggested in Figure 5.10 and to attempt to quantify the offset associated with the disproportional shock wave velocity of TNT and ANFO.

Chapter 6

Summary, Conclusions and Future Work

6.1 Summary

This thesis has aimed to characterise and quantify the effects of a shock wave in far-field regimes resulting from the detonation of both ideal, and non-ideal, explosives using validated analytical data processing methods.

Explosive detonation and the subsequent parameters which follow have been investigated for many decades but despite best attempts to understand their effects, a clear divide has been presented for the fundamental nature of shock wave dynamics and the variability exhibits. Whilst designing infrastructure to withstand extreme dynamic loading poses difficulty when considering where a charge may be in relation to the structure, alongside its composition and mass, making it harder is the uncertainty on how deterministic the yields of an explosive are. If explosives exhibit high levels of variability within simple scenarios, the engineer can have no confidence of ensuring designs are robust enough to withstand extreme loading.

If variability levels can be established with respect to the distance a given charge is away from a target, a more probabilistic approach can be undertaken by a designer which exhibits a higher level of safety confidence. It is therefore of high importance to assess current practices of experimental work to highlight reasons as to why explosive yields are viewed as chaotic by some in the industry and provided a robust approach to undertaken well-controlled trials to reduce the inconsistency in data. Chapter 2 provides a review of the current literature as well as background theory to blast wave phenomenology alongside state-of-the-art predictive methods for explosive yields in free-air scenarios. Chapter 3 proposed the development of numerous data processing tools which are exposed to PE4 experimental data and undergo synergetic validation with numerical simulations to highlight systematic features within methodologies, their effects and how they can be mitigated. Chapter 4 exercises the tools on a large data set of three ideal explosives in the attempt to both validate the tools across a wide range of ideal explosives and to identify whether ideal explosives exhibit deterministic behaviours across the far-field range of scaled distances. The methods which were validated in the aforementioned chapters were the used in Chapter 5 to study their applicability to small-scale non-ideal explosives, such as ANFO. The results of which provided fundamental insights into the characterisation of non-ideal explosives.

Findings from the PhD thesis provide a robust and validated far-field data set across a number of small-scale explosive compositions which should be used as a benchmark, not only for the level of repeatability achievable from well-controlled far-field trials, but as a final highlight to the blast community that far-field parameters are deterministic and are captured remarkably well by semi-empirical KB predictions. The industry's more modern construct of explosive detonation exhibiting significant and inherent variability across the entire range of scaled distances is the result of probabilistic based regimes which collated trial data which had systematic errors in their approach of conducting and analysing.

The investigation into the detonation of small scale non-ideal explosive, ANFO, has provided fundamental developments to the understanding of how detonation mechanics effect the overall charge yield. Despite non-ideal behaviour, when a composition exhibits detonation, provided the minimum reaction zone size is smaller than the charge diameter, it will result in a Friedlander ideal-like pressure-time history but the equivalency to TNT will vary based on the minimum charge radius and therefore mass. Through a theoretical approach, validated with experimental data, a fast look up tool for ANFO detonations is provided to estimate the explosive parameters depending on mass scaling.

6.2 Conclusions

The resulting work documented within this thesis can be summarised in the following conclusions which are listed in chronological order of appearance within the thesis:

- When considering the far-field range alone, well-controlled experimental trials result in highly deterministic blast parameters across both the positive and negative due to exhibiting low levels of variability from nominal identical testing regimes. This finding has been shown across both ideal and non-ideal explosives in Figures 3.10 and 5.6.
- The prediction curves developed by Kingery and Bulmash[87] not only capture the results of ideal explosive detonation in far-field regimes remarkably well, but are a sign of incredible prowess in both theoretical and empirical understanding of blast wave phenomenology during the times the trials were conducted.
- Systematic features, such as detonator position (Figure 3.16), gauge mounting apparatus (Figure 3.15) and so on, albeit seemingly negligible in the grand scheme of explosive detonation, present issues in acquiring deterministic behaviours as scaled distances reduce into near-field regimes due to detonation mechanisms and shock wave interactions being highly sensitive to small changes respectively.
- The secondary shock phenomena presents similar levels of consistency with scaled distance in the far-field regime as the primary shock and therefore prediction curves, similar to those presented by Kingery and Bulmash[87], has been presented in Figure 4.7.
- The use of high speed video recordings and subsequent validated data processing methods has shown to result in comparable data to that recorded with pressure gauges (Figure 4.11), but providing parameters across a much broader range of scaled distances from a small number of recordings.
- Non-ideal explosives, although exhibit friedlander-like pressure-time histories, are not scalable with mass like ideal explosives. The small-scale ANFO detonation results in a much lower explosive yield than quoted TNTe values within published literature suggest, established from large scale trials, depicted in Figure 5.7.
- Small scale ANFO detonations exhibit a seemingly delayed arrival time when compared to equivalent TNT detonations in Figure 5.7. This has been related to the

detonation and shock wave velocity profile inconsistencies between an ideal explosive behaviour and that of ANFO. Upon detonation of an ideal explosive, the detonation wave is assumed to propagate as its maximum velocity until reaching the edge of the charge at which point a decay in the velocity occurs. ANFO however sees an increase in detonation wave speed with the distance it has to travel through the explosive charge. This results in a clear discrepancy between arrival time predictions across the smaller charge diameters tested, but becomes increasingly negligible in line with charge diameter, in line with Figure 5.10.

- The negative phase of small scale ANFO detonations present reasonably higher magnitudes of parameters, comparing better with quoted figures of ANFO TNTe=0.82 in Figure 5.17. This has been deduced to be the effect of any ANFO which did not have enough time to full detonated during the first pass of the primary detonation wave, releases its energy sometime after, creating a more vigorous and energetic fireball which in turns results in an increased suction effect at ground level and thus large negative phases pressures and more powerful secondary shock features.

- The mechanism underlying the reason as to why small scale ANFO resulting in much lower yield in for positive phase parameters has been directly linked to the behaviour of the characteristic reaction zone size for ANFO, projecting away from the charge effectively unreactive. The mechansim has been comprehensively compared against test data from a range of scales and is found to encapsulate the data remarkably well in Figure 5.30.

- Non-ideal explosives can be predicted by both empirical prediction tools and numerical simulations, therefore exhibiting ideal-like behaviours at each increment of mass. It is therefore important to make use of a third dimension to prediction tools for non-ideal explosions which consider the characteristic reaction zone projectile mechanism for a given composition which can be established using rate stick trials.

6.3 Evaluation and Future Work

Chapter 3 made a distinct effort to develop data processing methodologies for standard free-air explosive trials in the attempt to assess the validity of deterministic regions of explosive yield presented by Tyas[173]. An extensive data set, comprising of 144 recordings of small-scale hemispherical PE4 detonations over the far-field range, was utilised to verify the processing tools ability to capture blast wave parameters and evaluate them through comparisons to Kingery and Bulmash[87] semi-empirical predictions. The background to characterising explosive yield, particularly in the far-field regime, is lack of agreement in the consistency of recorded parameters. Borenstein[18] state the reasons believed for a wide range of variability assumption have been made for explosive yields is down to the way each individual decided to assess the results. Extrinsic and intrinsic sources of variability were not completely outlined in each published article, with conclusions drawn from the data which may not have been scientifically accurate. This has led parts of the industry to believe explosive detonation is inherently variable, which fosters anomalous, or widely varying, data to be accepted as given without a through critique being undertaken. Whilst a generalised understanding of explosive yield regardless of explosive size, shape, composition and separation distance from a target (extrinsic) is important for probabilistic-based analyses, as to is a more robust and scientific understanding of a definitive situation is required for high confidence in prescribed loading for specific scenarios. Through establish well-controlled experimental methodologies, validated and improved through numerical simulation, clear improvements in the understanding of explosive variability has been established, with both positive and negative phase parameters not only exhibiting deterministic behaviours but are also captured remarkably well by the KB prediction tools, agreeing with the works of Esparza[45] and Rickman and Murrell[125] and verifying the hypothesis posed by Tyas[173].

In near-field regimes, where the blast wave parameters are driven by the expanding detonation products and fireball, higher levels of variability has been recorded. This ties in with the uncertainty in of KB predictions in this regime where physics-based numerical simulations are shown diverge rapidly as scaled distances are reduced Cormie et al.[32]. Whilst preliminary work at the University of Sheffield has made attempts at capturing spatial and temporal variations of near-field loading[51,134,174], there is still a lot of work required to provide a robust understanding of these extreme conditions. Barr et al.[10] has developed a new capability which vastly improves the resolution of the data capture presented in the aforementioned articles. Through a rigorous testing regime using this capability of near-field scaled distances and explosive charge compositions, the results would be used to provide better guidance for explosive quantification and characterisation through the full detonation process.

Non-ideal explosives are discussed within literatures as exhibiting varying rates of energy release, depending on homogeneity, with discussion into how detonation mechanics internally within the charge, measuring velocity of detonation, changes with charge diameter and/or confinement [5,80]. There is little investigation into the characterisation of shock wave development from non-ideal explosives and with what is available consisting of predominantly large scale trials which has been taken as a given across all mass scales [68]. This is contradictory to the aforementioned articles which finds significant variations when considering the release of energy from non-ideal explosives being across longer timescales. To exhibit full potential release, non-ideal explosives need confinement from either a surrounding material or additional charge mass which results in enough time before breakout to exhibit the full chemical decomposition. Smaller scale charges by nature therefore result in partial energy releases and cannot be defined by a single value of TNTe in line with the theories presented for ideal explosives. Chapter 5 has proven this finding by adopting the same well-controlled methodologies and validated data processing tools whilst detonating small scale ANFO charges which resulted in much lower TNTe values than what has historically been published. Whilst a mechanism for the reduction in yield has been presented, it is important to test this theory with future larger scale trials, in the attempt to categorise at which mass scales do normal TNT equivalency rules apply, in which a non-ideal explosive exhibits ideal-like behaviours, and where the explosive yield becomes highly dependent on the mass.

Although ANFO was the only non-ideal explosive tested in this thesis, it is not the only one of interest or threat. Future works will consider the effects of other non-ideal explosive compositions to see if they too exhibit behaviours similar to ANFO with another dimension of scaling with mass. A more comprehensive dataset of non-ideal detonations across both mass and distance scales is required to provide confidence in the ability to not only understand explosive events but to capture them accurately with numerical simulation.

The conclusions made throughout the entirety of this thesis should provide evidence to the idea of deterministic blast wave features across a number of explosives in particular for far-field scenarios, and therefore any other suggestion should be put down to either systematic errors in data acquisition or results reporting extrinsic variability. The findings should ultimately be taken forward into the analysis of near-field, where the fundamental quantification is lacking, to see if similar characterisation methods can be adopted.

Bibliography

[1] Akhavan, J. [2011], *The Chemistry of Explosives: Edition 3*, The Royal Society of Chemistry, Cambridge.

[2] Ammann, O. and Whitney, C. [1963], 'Industrial engineering study to establish safety design criteria for use in engineering of explosive facilities and operations'. Report for Picatinny Arsenal. New York: Ammann and Whitney.

[3] Aouad, C. J., Chemissany, ., Mazzali, P., Temsah, Y. and Jahami, A. [2021], 'Beirut explosion: TNT equivalence from the fireball evolution in the first 170 milliseconds', *Shock Waves* **31**, 813–827.

[4] Araos, M. and Onederra, I. [2017], Rectangular and Circular Explosive Charges - Detonation Study using High-Speed Video, *in* '9th World Conference on Blasting and Explosives', Stockholm, Sweden.

[5] Araos, M. and Onederra, I. [2019], 'Preliminary detonation study of dry, wet and aluminised ANFO using high-speed video', *Central European Journal of Energetic Materials* **16**(2), 228–244.

[6] Baer, M. R., Gartling, D. K. and DesJardin, P. E. [2012], 'Probabilistic models for reactive behavior in heterogeneous condensed phase media', *Combustion Theory and ¡odelling* **16**, 75–106.

[7] Baker, W. E. [1973], *Explosions in air*, University of Texas Press: Austin.

[8] Baker, W. E., Cox, P. A., Westine, P. S., Kulesz, J. J. and Strehlow, R. A. [1983], *Fundamental Studies in Engineering 5: Explosion hazards and evaluation.*
URL: *http://deepblue.lib.umich.edu/handle/2027.42/25541*

[9] Balakrishnan, K., Genin, F., Nance, D. V. and Menon, S. [2010], 'Numerical study of blast characteristics from detonation of homogeneous explosives', *Shock Waves* **20**, 147–162.

[10] Barr, A. D., Rigby, S. E. ., Clarke, S. D., Farrimond, D. G. and Tyas, A. [2023], 'Temporally and Spatially Resolved Reflected Overpressure Measurements in the Extreme Near Field', *Sensors* **23**(964).

[11] Bdzil, J. B., Aslam, T. D., Henninger, R. and Quirk, J. J. [2003], 'High-Explosives Performance', *Los Alimos Science* **28**, 96–110.

[12] Boganek, V., Suceskka, M., Dubrilovic, M. and Hartlieb, P. [2022], 'Effect of confinement on detonation velocity and plate dent test results for anfo explosive', *Energies* **15**(4404), 1–9.

[13] Bogosian, D., Ferritto, J. and Shi, Y. [2002], Measuring uncertainty and conservatism in simplified blast models, *in* '30th Explosives Safety Seminar', Atlanta, GA, USA, 13-15 August.

[14] Bogosian, D., Powell, D. and Ohrt, A. [2019], Consequences of Applying Objective Methods for Selecting Peak Pressure from Experimental Data, *in* 'International Symposium of the Interaction of Effects of Munitions with Structures (ISIEMS)', Panama City, Florida, 21-25 October, p. 11.

[15] Bogosian, D., Yokota, M. and Rigby, S. E. [2016], TNT equivalence of C-4 and PE4: a review of traditional sources and recent data, *in* '24rd international symposium on military aspects of blast and shock (MABS)', Halifax, Nova Scotia, Canada, 19-23 September.

[16] Bogosian, D., Yu, A., Dailey, T. and Ohrt, A. [2014], Statistical Variation in Reflected Airblast Parameters from Bare Charges, *in* '23rd international symposium on military aspects of blast and shock (MABS)', Oxford, England, 7-12 September.

[17] Bohanek, V., Tumara, B. S., Serene, C. H. Y. and Suceska, M. [2023], 'Shock initiation and propagation of detonation in anfo', *Central European Journal of Energetic Materials* **16**, 1–13.

[18] Borenstein, E. [2009], Sensitivity analysis of blast loading parameters and their trends as uncertainty increases, PhD thesis, The State University of New Jersey, USA.

[19] Brode, H. L. [1955], 'Numerical simulations of spherical blast waves', *Journal of Applied Physics* **26**(6), 766–775.

[20] Buczkowski, D. [2014], 'Explosive Properties of Mixtures of Ammonium Nitrate(V) and Materials of Plant Origin – Danger of Unintended Explosion', *Central European Journal of Energetic Materials* **11**, 115–127.

[21] Canny, J. [1986], 'A Computational Approach to Edge Detection', *IEEE Transactions on Pattern Analysis and Machine Intelligence* **8**(6), 679–698.

[22] Carton, E. [2018], Air Blast Mitigation Using Water Foam Coverage, *in* '25nd Military Aspects of Blast and Shock Symposium (MABS)', The Hague, Netherlands, 24-27 September.

[23] Catanach, R. A. and Hill, L. G. [2002], 'Diameter effect curve and detonation front curvature measurements for anfo', *AIP Conference Proceedings* **620**, 906–909.

[24] Cetner, Z. and Maranda, A. [2014], 'Selected parameters of heavy-ANFO explosive materials', *High Energy Materials* **T.6**, 31–37.

[25] Chabia, A. J., Bass, R. C. and Hawk, H. L. [1965], Measurements of wave fronts in earth, air and explosive produced by a 500-ton hemisphere of tnt detonated on the surface of the earth, Technical Report SC-RR-64-442, Sandia National Laboratories, Albuquerque, New Mexico, USA.

[26] Chapman, D. L. [1899], 'On the rate of explosions in gases', *Philosophical Magazine* **47**(284), 90–104.

[27] Chiquito, M., Castedo, R., Lopez, L. M., Santos, A. P., Mancilla, J. M. and Yenes, J. I. [2019], 'Blast Wave Characteristics and TNT Equivalent of Improvised Explosive Device at Small-scaled Distances', *Defence Science* **69**, 328–335.

[28] Cochrane, K. [2006], Moranbah Ammonium Nitrate Project, Technical report, Dyno Nobel Asia Pacific Limited, Salt Lake City, Utah.

[29] Cook, M. A. [1968], 'Explosives—a survey of technical advances', *Industrial and Engineering Chemistry* **60**, 44–55.

[30] Cooper, P. W. [1990], Comments on TNT Equivalence, *in* '20th Internation Pyrotechnics Seminar', Colorado Springs, Colorado, July 24th-29th.

[31] Cooper, P. W. [1996], *Explosives Engineering*, VCH Publications, New York.

[32] Cormie, D., Mays, G. and Smith, P. [2019], *Blast effects on buildings 3rd Edition*, Vol. 3, ICE Publishing.

[33] Cranz, C. [1926], *Lehrbuch der Basllistik*, Springer Germany, Berlin.

[34] Dasch, C. J. [1992], 'One-dimensional tomography: a comparison of Abel, onion-peeling, and filtered backprojection methods', *Applied Optics* **31**(8), 1146–1152.

[35] Davis, V. W., Goodale, T., Kaplan, K., Kriebel, A. R., H.B, M., Melichar, J. F., Morris, P. J. and Zaccor, J. N. [1973], Nuclear weapons blast phenomena, volume 4: Simulation of nuclear airblast phenomena with high explosives, Technical Report 1200-4, DASA, Washington DC, USA.

[36] Dennis, A. A., Pannell, J. J., Smyl, D. J. and Rigby, S. E. [2021], 'Prediction of blast loading in an internal environment using artificial neural networks', *International Journal of Protective Structures* pp. 1–28.

[37] Dewey, J. M. [1964], 'The air velocity in blast waves from t.n.t. explosions', *Proceedings of the Royal Society of London. Series A. Mathematical and Physical Sciences* **279**(1378), 366–385.

[38] Dewey, J. M. [2005], 'The tnt equivalence of an optimum propane–oxygen mixture', *Journal of Physics D: Applied Physics* **38**, 4245–4251.

[39] Dewey, J. M. [2021], 'The TNT and ANFO equivalences of the Beirut explosion', *Shock Waves* **31**, 95–99.

[40] Dobbs, N., Cohen, E. and Weissman, S. [1968], 'Blast pressures and impulse loads for use in the design and analysis of explosive storage and manufacturing facilities', *Annals of the New York Academy of Sciences* **152.1**, 317–338.

[41] Dobrilovic, M., Bohanek, V. and Skrlec, V. [2013], 'Influence of the initiation energy on the velocity of detonation of anfo explosive', *Central European Journal of Energetic Materials* **10**, 555–568.

[42] Edwards, T. Y. [1977], Proceedings of the dice throw symposium, Technical Report - DNA 4377P-1, Defence Nuclear Agency, Santa Barbara, California, USA.

[43] Esen, S., Souers, P. C. and Vitello, P. [2005], 'Prediction of the non-ideal detonation performance of commercial explosives using the dene and jwl++ codes', *International Journal for Numerical Methods in Engineering* **64**, 1889–1914.

[44] Esparza, E. D. [1986*a*], Airblast measurements and equivalency for spherical charges at small scaled distances, *in* '22nd Department of Defence Explosive Safety Seminar', Anaheim, California, USA, 26-28 August, pp. 2029–2057.

[45] Esparza, E. D. [1986*b*], 'Blast measurements and equivalency for spherical charges at small scaled distances', *International Journal of Impact Engineering* **4**(1), 23–40.

[46] Esparza, E. D. and Moroney, J. J. [1979], Reflected blast measurements at small scaled distances for m26e1 propellant, Technical Report - Contractor Report ARLCD-CR-79010, Southwest Research Institute, San Antonio, Texas.

[47] Fabin, M. and Jarosz, T. [2021], 'Improving ANFO: Effect of Additives and Ammonium NitrateMorphology on Detonation Parameters', *Mqterials* **14**(5745), 1–12.

[48] Fan, Z. [2009], *Shock Waves Science and Technology Reference Library*, Vol. 4, Springer.

[49] Farrimond, D. G., Rigby, S. E., Clarke, S. D. and Tyas, A. [2022], 'Time of arrival as a diagnostic for far-field high explosive blast waves', *International Journal of Protective Structures* pp. 1–24.

[50] Farrimond, D. G., Woolford, S., Tyas, A., Rigby, S. E., Clarke, S. D., Barr, A., Whittaker, M. and Pope, D. J. [2023], 'Far-field positive phase blast parameter characterisation of RDX and PETN based explosives', *International Journal of Protective Structures* pp. 1–38.

[51] Fay, S., S. Clarke, J. A. W., Tyas, A., Bennett, T., Reay, J., Elgy, I. and Gant, M. [2013], Capturing the spatial and temporal variations in impulse from shallow buried charges, *in* '15th International Symposium on the Interaction of the Effects of Munitions with Structures (ISIEMS)', Potsdam, Germany, 17-20 September, pp. 1–9.

[52] Figuli, L., Kaviky, V., Jangl, S. and Ligasova, Z. [2014], Analysis of field test results of ammonium nitrate fuel oil explosives as improvised explosive device charges, *in* '13th International conference of Structures under shock and impact (SUSI XIII)', New Forest, UK, 3-5 June.

[53] Fisher, E. M. [1950], Spherical Cast TNT Charges Air Blast Measurements, Technical Report NOLM-10780, Naval Ordnance Laboratory, White Oak, Maryland , USA.

[54] Fisher, E. and Pittman, J. F. [1953], Air blast resulting from the detonation of small TNT charges, Technical Report NAVORD Report 2890, Naval Ordnance Laboratory, White Oak, Maryland, USA.

[55] Forbes, J. W. [2013], *Shock Wave Compression of Condensed Matter: A Primer (Shock Wave and High Pressure Phenomena)*, Springer.

[56] Formby, S. A. and Wharton, R. K. [1996], 'Blast characteristics and TNT equivalence values for some commercial explosives detonated at ground level', *Journal of Hazardous Materials* **50**, 183–198.

[57] Freidlander, F. G. [1946], 'The diffraction of sound pulses. I. Diffraction by a semi-infinite plate', *Proceedings of the Royal Society of London. Series A. Mathematical and Physical Sciences* **186**, 322–344.

[58] Fried, L. E. [1994], Cheetah 1.0 users manual, Technical Report - LLNL Report: UCRL-MA-117541, Lawrence Livermore National Laboratory, Livermore, CA, USA.

[59] Gerasimov, S. I., Mikhailov, A. L. and A.Trepalov, N. [2017], 'Shock wave distribution in an explosion of an explosive material with plastic filler', *Combustion, Explosion and Shock Waves* **53**, 689–695.

[60] Gerasimov, S. I. and Trepalov, N. A. [2019], 'Video Recording of an Air Blast Wave Resulting from Initiation of a Light-Sensitive Explosive Composition', *Combustion, Explosion and Shock Waves* **55**(5), 606–612.

[61] Giglio-Tos, L. and Reisler, R. E. [1970], Air blast studies of large ammonium nitrate/fuel oil explosions, Technical Report - Memorandum No. 2057, Ballistic Research Laboratories, Aberdeen Proving Ground, Maryland, USA.

[62] Gitterman, Y. and Hofstetter, R. [2012], 'Gt0 explosion sources for ims infrasound calibration: Charge design and yield estimation from near-source observations', *Pure and Applied Geophysics* **171**(3-5), 599–619.

[63] Glass, I. I. [1974], *Shock Waves and Man*, University of Toronto Institute of Aerospace Studies.

[64] Goodman, H. J. [1960], Compiled free-air blast data on bare spherical pentolite, Technical Report No. 1092, Ballistic Research Laboratories, Aberdeen Proving Ground, Maryland, USA.

[65] Goodman, H. J. and Giglio-Tos, L. [1978], Equivalent weight factors for four plastic bonded explosives: PBX-108, PBX-109, AFX-103, and AFX-702, Technical Report ARBRL-TR-0205, Ballistic Research Laboratories, Aberdeen Proving Ground, Maryland, USA.

[66] Granstrom, S. A. [1956], Loading characteristics of air blast from detonating charges, Technical Report No. 100, Transactions of the Royal Institute of Technology, Stockholm, Sweden.

[67] Grisaro, H. Y. and Edri, I. E. [2017], 'Numerical investigation of explosive bare charge equivalent weight', *International Journal of Protective structures* **8**(2), 199–220.

[68] Grisaro, H. Y., Edri, I. E. and Rigby, S. E. [2020], 'TNT equivalency analysis of specific impulse distribution from close-in detonation', *International Journal of Protective structures* **12**(3), 315–330.

[69] Groves, T. K. [1962], Surface burst 100-ton tnt hemispherical - free field air blast overpressure, Technical Report No. 269, Defence Research Establishment Suffield, Ralston, Alberta.

[70] Hargather, M. J. and Settles, G. S. [2007], 'Optical measurement and scaling of blasts from gram-range explosive charges', *Shock Waves* **17**(4), 215–223.

[71] Hargather, M. J. and Settles, G. S. [2010], 'Natural-background-oriented schlieren imaging', *Experiments in Fluids* **48**(1), 59–68.

[72] Hobbs, M. J., Barr, A. D., Woolford, S., Farrimond, D. G., Clarke, S. D., Tyas, A. and Willmott, J. R. [2022], 'High-Speed Infrared Radiation Thermometer for the Investigation of Early Stage Explosive Development and Fireball Expansion', *Sensors* **22**(6143).

[73] Hoffman, A. J. and Mills, S. N. [1956], Air blast measurements about explosive charges at side-on and normal incidence, Technical Report 988, Ballistic Research Laboratories, Aberdeen Proving Ground, Maryland, USA.

[74] Hopkinson, B. [1915], *British ordnance board minutes*, 13565 edn, The National Archives, Kew, UK.

[75] Horie, Y. [2009], *Shock Waves Science and Technology Reference Library*, Vol. 3, Springer.

[76] Hyde, D. W. [1988], 'Users' Guide for Microcomputer Programs CONWEP and FUNPRO - Applications of TM5-885-1'. US Army Waterways Experimental Station, Vicksburg, MS, USA.

[77] Hyde, D. W. [1991], 'Conventional weapons program (ConWep)'. US Army Waterways Experimental Station, Vicksburg, MS, USA.

[78] Igra, O. and Seiler, F. [2016], *Experimental methods of shock wave research*, Springer International Publishing, Switzerland.

[79] Institute for Economics and Peace [2022], 'The 2022 global terroism index'.

[80] Jackson, S. I. and Short, M. [2015], 'Scaling of detonation velocity in cylinder and slab geometries for ideal, insensitive and non-ideal explosives', *Journal of Fluid Mechanics* **773**, 224–266.

[81] Jeremc, R. and Bajic, Z. [2006], 'An approach to determining the TNT equivalent of high explosives', *Scientific Technical Review* **LVI**(1), 58–61.

[82] Johansson, L. [2011], Numerical Study of Non-Ideal Explosive Detonations, PhD thesis, Lulea University of Technologu.

[83] Johnson, O. T., Patterson, J. D. and Olson, W. C. [1957], A simple mechanical method for measuring the reflected impulse of air blast waves, Technical Report - Memorandum no.1088, Ballistic Research Laboratories, Aberdeen Proving Ground, Maryland, USA.

[84] Jouguet, E. [1905], 'On the propagation of chemical reactions in gases', *Journal de Mathématiques Pures et Appliquées* **6**(2), 5–85.

[85] Kennedy, W. D. [1946], Explosions and explosives in air, *in* 'Effects of Impact and Explosions. Summary Technical Report of Div. 2, NDRC, Vol.1, Washington, DC, AD 221 586'.

[86] Kingery, C. N. [1966], Air blast parameters versus distance for hemispherical tnt surface bursts, Technical Report 1344, Ballistic Research Laboratories, Aberdeen Proving Ground, Maryland, USA.

[87] Kingery, C. N. and Bulmash, G. [1984], Airblast parameters from TNT spherical air burst and hemispherical surface burst, Technical Report ARBRL-TR-02555, Ballistic Research Laboratory, Aberdeen Proving Ground, Maryland, USA.

[88] Kingery, C. N. and Coulter, G. [1982], Tnt equivalency of pentolite hemispheres, Technical Report ARBRL-TR-02456, Ballistic Research Laboratories, Aberdeen Proving Ground, Maryland, USA.

[89] Kingery, C. N. and Pannill, B. F. [1964], Peak overpressure vs scaled distance for tnt surface bursts (hemispherical charges), Technical Report - Memorandum No. 1518, Ballistic Research Laboratories, Aberdeen Proving Ground, Maryland, USA.

[90] Kinney, G. F. and Graham, K. J. [1985], *Explosive Shocks in Air*, Springer-Verlag Berlin Heidelberg.

[91] Kolhe, P. S. and Agrawal, A. K. [2009], 'Abel inversion of deflectometric data: comparison of accuracy and noise propagation of existing techniques', *Applied Optics* **48**(20), 3894–3902.

[92] Konya, A. and Konya, C. J. [2019], 'Blasting mechanics revisited: Characteristics of explosives', https://www.pitandquarry.com/blasting-mechanics-revisited-characteristics-of-explosives.

[93] Kucera, J., Anastacio, A. C., Selesovsky, J. and Pachman, J. [2017], Testing optical tracking of blast wave position for determination of its overpressure, *in* '6th International Conference on Military Technologies (ICMT)', Brno, Czech Republic, 31st May - 2nd June, pp. 70–73.

[94] Lozano, E. [2020], Reactive Burn Modelling of Non-Ideal Explosives, PhD thesis, Colorado School of Mines.

[95] Lutzky, M. [1965], Theoretical Versus Experimental Results for Air Blast From One-Pound Spherical TNT and Pentolite Charges at Sea Level Conditions, Technical Report NOTLR 65-57, Naval Ordnance Laboratory, White Oak, Maryland , USA.

[96] Lyons, S. [2012], Characterisation of Blast Wave Variability, PhD thesis, The University of Newcastle, Australia.

[97] Maranda, A., Paplinksi, A. and Galezwski, D. [2010], 'Investigation on detonation and thermochemical parameters of aluminized ANFO', *Journal of Energetic Materials* **21**, 1–13.

[98] Matyas, R., Zeman, S., Trzcinski, W. and Cuziloi, S. [2008], 'Detonation performance of tatp/an-based explosives', *Propellants, Explosives and Pyrotechnics* **33**(4), 296–300.

[99] McKay, M. W., Hancock, S. L. and Randall, D. [1974], 'Development of a low-density ammonium nitrate/fuel oil explosive and modelling of its detonation properties', *Technical Report DNA 3351 F* . Physics Internation Company, San Leandro, California.

[100] Meshkov, E. E. [1969], 'Instability of the interface of two gases accelerated by a shock wave', *Fluid Dynamics* **4**(5), 101–104.

[101] Meyer, R., Kohler, J. and Homburg, A. [2011], *Explosives - Sixth, Completely Revised Editions*, Wiley VCH Verlahshesellschaft, Weinheim, Germany.

[102] Mi, X., Michael, L., Loannou, E., Nikiforakis, N., Higgins, A. J. and Ng, H. D. [2019], ‘Meso-resolved simulations of shock-to-detonation transition in nitromethane with air-filled cavities’, *Journal of Applied Physics* **125**, 1–22. 245901.

[103] Mizukaki, T., Wakabayashi, K., Matsumura, T. and Nakayama, K. [2014], ‘Background-oriented schlieren with natural background for quantitative visualization of open-air explosions’, *Shock Waves* **24**(1), 69–78.

[104] Murphy, M. J. and Adrian, R. J. [2010], ‘PIV space-time resolution of flow behind blast waves’, *Experiments in Fluids* **49**, 193–202.

[105] National Academies of Sciences, E. and Medicine [2018], *Reducing the Threat of Improvised Explosive Device Attacks by Restricting Access to Explosive Precursor Chemicals*, Washington, DC: The National Academies Press.

[106] Needham, C., Brisby, J. and Ortley, D. [2020], ‘Blast wave modification by detonator placement’, *Shock Waves* **30**, 615–627.

[107] Needham, C. E. [2010], *Blast Waves*, Springer Germany, Berlin.

[108] Ohashi, K., H.Kleine and Takayama, K. [2001], Characteristics of blast waves generated by milligram charges, *in* ‘23rd International Symposium on Shock Waves’, Fort Worth, USA, 22-27 July, pp. 187–193.

[109] Pannell, J. J., Panoutsos, G., Cooke, S. B., Pope, D. J. and Rigby, S. E. [2021], ‘Predicting specific impulse distributions for spherical explosives in the extreme near-field using a Gaussian function’, *International Journal of Protective Structures* **12(4)**, 437–459.

[110] Pasman, H. J., Fouchier, C., Park, S., Quddus, N. and Laboureur, D. [2020], ‘Beirut ammonium nitrate explosion: Are not we really learning anything?’, *Process Safety Progress* **e12203**, 1–18.

[111] Paterson, S. [1995], ‘The structure of the reaction zone in a detonating explosive’, *Symposium on Combustion* **5**(1), 672–684.

[112] Petes, J., Miller, R. and McMullan, F. [1983], ‘User’s guide and history of anfo as a nuclear weapons effect simulation explosive’, *Technical Report DNA-TR-82-156* . Kaman Tempo, Alexandria, Virginia.

[113] Popper, K. R. [1963], *Science as Falsification - Conjectures and Refutations*, Routledge and Keagan Paul.

[114] Price, D. [1967], 'Contrasting patterns in the behavior of high explosives', *Symposium (International) on Combustion* **11**, 693–702.

[115] Rae, P. J. and McAfee, J. M. [2018], 'The Blast Parameters Spanning the Fireball from Large Hemispherical Detonations of C-4', *Propellants, Explosives, Pyrotechnics* **43**(7), 694–702.

[116] Randers-Pehrsons, G. and Bannister, K. A. [1997], 'Airblast loading model for DYNA 2D and DYNA 2D', *Technical Report ARL-TR-1310* . Aberdeen Proving Ground, MD, USA.

[117] Rayleigh [1882], 'Investigation of the character of the equilibrium of an incompressible heavy fluid of variable density', *Proceedings of the London Mathematical Society* **s1-14**(1), 170–177.

[118] Reisler, R. E., Keefer, J. H. and Ethridge, N. H. [1995*a*], Measurement techniques and instrumentation: Volume 1 - nuclear era (1945-1963), Technical report, Applied Research Associates Inc., Albuquerque, New Mexico.

[119] Reisler, R. E., Keefer, J. H. and Ethridge, N. H. [1995*b*], Measurement techniques and instrumentation: Volume 2 - the high explosives era (1959-1993), Technical report, Applied Research Associates Inc., Albuquerque, New Mexico.

[120] Reisler, R. E., Keefer, J. H. and Giglio-Tos, L. [1966], Basic air blast measurements froma 500-ton tnt detonation: Project 1.1 - operation snowball, Technical Report - Memorandum No. 1818, Ballistic Research Laboratories, Aberdeen Proving Ground, Maryland, USA.

[121] Reisler, R., Pettit, B. and Kennedy, L. [1976], Air blast data from height-of-burst studies in canada, vol 1: Hob 5.4 to 71.9 feet, Technical Report 1950, Ballistic Research Laboratories, Aberdeen Proving Ground, Maryland, USA.

[122] Reisler, R., Pettit, B. and Kennedy, L. [1977], Air blast data from height-of-burst studies in canada, vol 1: Hob 45.4 to 144.5 feet, Technical Report 1990, Ballistic Research Laboratories Report 1990, Aberdeen Proving Ground, Maryland, USA.

[123] Remennikov, A. M. [2003], 'A REVIEW OF METHODS FOR PREDICTING BOMB BLAST EFFECTS ON BUILDINGS', *Journal of Battlefield Technology* **6**(3), 1–6.

[124] Richtmyer, R. D. [1960], 'Taylor instability in shock acceleration of compressible fluids', *Communications on Pure and Applied Mathematics* **13**(2), 297–319.

[125] Rickman, D. D. and Murrell, D. W. [2007], 'Development of an improved methodology for predicting Airblast pressure relief on a directly loaded wall', *Journal of Pressure Vessel Technology, Transactions of the ASME* **129**(1), 195–204.

[126] Rigby, S. [2014], Blast Wave Clearing Effects on Finite-Sized Targets Subjected to Explosive Loads, PhD thesis, University of Sheffield, UK.

[127] Rigby, S. E. [2021], Blast wave time of arrival : A reliable metric to determine pressure and yield of high explosive detonations, Technical Report 079, Fire and Blast Information Group.

[128] Rigby, S. E., Fay, S. D., Tyas, A., Warren, J. and Clarke, S. D. [2015a], 'Angle of incidence effects on far-field positive and negative phase blast parameters', *International Journal of Protective Structures* **6**(1), 23–42.

[129] Rigby, S. E. and Gitterman, Y. [2016a], Secondary shock delay measurements from explosive trials, *in* '24th International Symposium on Military Aspects of Blast and Shock (MABS)', Halifax, Nova Scotia, Canada, 18-23 September.

[130] Rigby, S. E., Knighton, R., Clarke, S. D. and Tyas, A. [2020a], 'Reflected Near-field Blast Pressure Measurements Using High Speed Video', *Experimental Mechanics* **60**(7), 875–888.

[131] Rigby, S. E., Lodge, T. J., Alotaibi, S., Barr, A. D., Clarke, S. D., Langdon, G. S. and Tyas, A. [2020b], 'Preliminary yield estimation of the 2020 Beirut explosion using video footage from social media', *Shock Waves* **30**(6), 671–675.

[132] Rigby, S. E. and Sielicki, P. W. [2014], 'An investigation of TNT equivalence of hemispherical PE4 charges', *Engineering Transactions* **62**(4), 423–435.

[133] Rigby, S. E., Tyas, A., Bennett, T., Clarke, S. D. and Fay, S. D. [2014b], 'The Negative Phase of the Blast Load', *International Journal of Protective Structures* **5**(1), 1–20.

[134] Rigby, S. E., Tyas, A., Clarke, S. D., Fay, S. D., Reay, J. J., Warren, J. A., Gant, M. and Elgy, I. [2015b], 'Observations from Preliminary Experiments on Spatial and Temporal Pressure Measurements from Near-Field Free Air Explosions', *International Journal of Protective structures* **6**(2), 175–190.

[135] Rigby, S. E., Tyas, A., Fay, S. D., Clarke, S. D. and Warren, J. A. [2014a], Validation of Semi-Empirical Blast Pressure Predictions for Far Field Explosions - Is There Inherent Variability in Blast Wave Parameters?, *in* '6th International Conference on Protection of Structures Against Hazards', Tianjin, China, 16-17 October, pp. 1–9.

[136] Robbe, C., Nsiampa, N., Oukara, A. and Papy, A. [2014], 'Quantification of the uncertainties of high-speed camera measurements', *International Journal of Metrology and Quality Engineering* **5**, 201–209.

[137] Rudlin, L. [1963], On the origin of shockwaves from spherical condensed explosions in air - part 1: Results of photographic observations of pentolite hemispheres at ambient conditions, Technical Report NOTLR 62-182, Naval Ordnance Laboratory, White Oak, Maryland , USA.

[138] Sadwin, L. D. and Swisdak, M. M. [1970*a*], 'An/fo charge preparation for large scale tests', *Technical Report NOLTR 70-205* . United States Naval Ordnance Laboratory, White Oak, Maryland.

[139] Sadwin, L. D. and Swisdak, M. M. [1970*b*], 'Blast characteristics of 20 and 100 ton hemispherical an/fo charges, nol data report', *Technical Report NOLTR 70-32* . United States Naval Ordnance Laboratory, White Oak, Maryland.

[140] Salyer, T. R., Short, M., Kiyanda, C. B., Morris, J. and Zimmerly, T. [2010], Effects of Prill Structure on Detonation Performance of ANFO, *in* '14th International Detonation Symposium', Coeru D'Alene, Idaho, 11-16 April.

[141] Schwer, L. and Rigby, S. E. [2017], Reflected Secondary Shocks: Some Observations using Afterburning, *in* '11th European LS-Dyna Conference 2017', Salzburg, Austria.

[142] Scott, D. G. [2019], Small-Scale Characterization of Shock Sensitivity for Various Non-ideal Explosives Based on Detonation Failure and Behaviour, PhD thesis, Purdue University, Indiana.

[143] Shear, R. E. and Day, B. D. [1959], Tables of thermodynamic and shock front parameters for air., Technical Report - Memorandum Report 1206, Ballistic Research Laboratories, Aberdeen Proving Ground, Maryland, USA.

[144] Shear, R. E. and Wright, E. Q. [1962], 'Calculated peak pressure-distance curves for pentolite and tnt', *Ballistic Research Laboratories Memorandum Report 1423* . Aberdeen Proving Ground, Maryland, USA.

[145] Shelton, F. H. [1988], *Reflections of a Nuclear Weaponeer*, Shelton Enterprises.

[146] Sherkar, P., Shin, J., Whittaker, A. and Aref, A. [2016], 'Influence of Charge Shape and Point of Detonation on Blast-Resistant Design', *Journal of Structural Engineering* **142**, 1–11.

[147] Shi, Y., Wang, N., Cui, J., Li, C. and Zhang, X. [2022], 'Experimental and numerical investigation of charge shape effect on blast load induced by near-field explosions', *Process Safety and Environmental Protection* **165**, 266–277.

[148] Shin, J., Whittaker, A. and Aref, A. [2019], 'Influence of Charge Shape and Point of Detonation on Blast-Resistant Design', *Journal of Structural Engineering* **145**, 1–15.

[149] Shin, J., Whittaker, A. S. and Comie, D. [2015], 'TNT Equivalency for Overpressure and Impulse for Detonations of Spherical Charges of High Explosives', *International Journal of Protective Structures* **6**, 567–579.

[150] Shin, J., Whittaker, A. S. and Comie, D. [2015b], 'Incident and Normally Reflected Overpressure and Impulse for Detonations of Spherical High Explosives in Free Air', *International Journal of Protective Structures* **141**(12), 567–579.

[151] Shirbhate, P. A. and Goel, M. D. [2021], 'A Critical Review of TNT Equivalence Factors for Various Explosives', *Recent Advances in Computational Mechanics and Simulations* **103**, 471–478.

[152] Simoens, B. and Lefebvre, M. [2011], 'Influence of different parameters on the tnt-equivalent of an explosion', *Central European Journal of Energetic Materials* **8**(1), 53–67.

[153] Simoens, B. and Lefebvre, M. [2015], 'Influence of the shape of an explosive charge: Quantification of the modification of the pressure field', *Central European Journal of Energetic Materials* **12**(2), 195–213.

[154] Sitkiewicz-Wolodko, R., Maranda, A. and Paszula, J. M. [2019], 'Modification of anfo detonation parameters by addition of ground of ammonium nitrate (v) and aluminium powder', *Central European Journal of Energetic Materials* **16**(1), 122–134.

[155] Smale, W. R. and Sigs, R. C. [1961], Surface burst of 100 ton tnt hemispherical charge, Technical Report No. 205, Defence Research Establishment Suffield, Ralston, Alberta.

[156] Smith, P. D., Rose, T. A. and Saotonglang, E. [1999], 'Clearing of blast waves from building facades', *Proceedings of the Institution of Civil Engineers: Structures and Buildings* **134**(2), 193–199.

[157] Sochet, I., Gardebas, D., Calderara, S., Marchal, Y. and Longuet, B. [2011], 'Blast Wave Parameters for Spherical Explosives Detonation in Free Air', *Open Journal of Safety Science and Technology* **1**, 31–42.

[158] Stennett, C., Gaulter, S. and Akhavan, J. [2020], 'An Estimate of the TNT-Equivalent Net Explosive Quantity (NEQ) of the Beirut Port Explosion Using Publicly-Available Tools and Data', *Propelants, Explosives, Pyrotechnics* **45**, 1675–1679.

[159] Stimac, B., Skrelec, V., Dobrilovic, M. and Suceska, M. [2021], 'Numerical modelling of non-ideal detonation in anfo explosives applying wood-kirkwood theory coupled with explo5 thermochemical code', *Defence Technology* **17**, 1740–1752.

[160] Stoner, R. G. and Bleakney, W. [1948], 'The attenuation of spherical shock waves in air', *Journal of Applied Physics* **19**, 670.

[161] Suceska, M. [2018], Explo5 user's guide, Technical report, OZM Research S.R.O,, Hrochův Týnec , Czechia.

[162] Sultanoff, M. and McVey, G. [1954], Shock pressure at and close to the surface of spherical pentolite charges inferred from optical measurement., Technical Report 917, Ballistic Research Laboratories, Aberdeen Proving Ground, Maryland, USA.

[163] Swisdak, M. [1975], Explosion effects and properties. Part 1: Explosion effects in Air, Technical Report NSWC/WOL/TR-65-116, Naval Ordnance Laboratory, White Oak, Maryland , USA.

[164] Tang, L., Bird, D., Rigby, S. E., Tyas, A. and Warren, J. [2017], Reflections on Variability of Blast Pressure Measurement at Different Scales, *in* '17th international symposium on the interaction of the effects of munitions with structures', Bad Neuenahr-Ahrweiler, Germany, 16-20 October.

[165] Tang, L., Rigby, S. E. and Tyas, A. [2018], Validation of Air3D for scaled experimental pressure and impulse data, *in* '25th International Symposium on Military Aspects of Blast and Shock (MABS)', The Hague, Netherlands, 24-27 September.

[166] Tarver, C. M. and Urtiew, P. A. [1997], Theoretical and computer models of detonation in solid explosives, Technical Report - LLNL Report: UCRL-JC-128755, Lawrence Livermore National Laboratory, Livermore, CA, USA.

[167] Taylor, G. I. [1950a], 'The formation of a blast wave by a very intense explosion I. Theoretical discussion.', *Proceedings of the Royal Society of London. Series A. Mathematical and Physical Science* **201**, 159–174.

[168] Taylor, G. I. [1950b], 'The formation of a blast wave by a very intense explosion II. The atomic explosion of 1945', *Proceedings of the Royal Society of London. Series A. Mathematical and Physical Science* **201**, 175–186.

[169] Taylor, G. I. [1950c], 'The dynamics of the combustion products behind plane and spherical detonation fronts in explosives', *Proceedings of the Royal Society of London. Series A. Mathematical and Physical Science* **200**, 235–247.

[170] Taylor, G. I. [1950d], 'The instability of liquid surfaces when accelerated in a direction perpendicular to their planes. I', *Proceedings of the Royal Society of London. Series A. Mathematical and Physical Sciences* **202**(1068), 81–96.

[171] Thiboutot, S., Brousseau, P. and Ampleman, G. [2015], 'Deposition of petn following the detonation of seismoplast plastic explosive', *Propellants, Explosives and Pyrotechnics* **40**, 329–332.

[172] Tobin, J. D. and Hargather, M. J. [2016], 'Quantitative Schlieren Measurement of Explosively-Driven Shock Wave Density, Temperature, and Pressure Profiles', *Propelants, Explosives, Pyrotechnics* **41**, 1050–1059.

[173] Tyas, A. [2019], Blast loading from high explosive detonation: What we know and don't know, *in* '13th International Conference on Shock and Impact Loads on Structures (SILOS)', Guangzhou, China, 14-15 December, pp. 65–76.

[174] Tyas, A., Reay, J. J., Fay, S. D., Clarke, S. D., Rigby, S. E., Warren, J. A. and Pope, D. J. [2016], 'Experimental studies of the effect of rapid afterburn on shock development of near-field explosions', *International Journal of Protective Structures* **7**(3), 452–465.

[175] Tyas, A., Warren, J. A., Bennett, T. and Fay, S. [2011], 'Prediction of clearing effects in far-field blast loading of finite targets', *Shock Waves* **21**(2), 111–119.

[176] US Department of Defence [2008], 'Structures To Resist the Effects of Accidental Explosions'. UFC 3-340-02. US DoD, Washington, DC.

[177] von Neumann, J. [1942], Theory of detonation waves, Technical report, Institute for Advanced Study. Nation Defence Research Committee of the office of Scientific Research and Development.

[178] Weibull, W. [1950], Explosion of spherical charges in air: Travel time, velocity of front, and duration of shock waves, Technical Report X-127, Ballistic Research Laboratories Report, Aberdeen Proving Ground, Maryland, USA.

[179] Whittaker, M. J., Klomfass, A., Softley, I. D., Pope, D. J. and Tyas, A. [2018], Comparison of Numerical Analysis with Output from Precision Diagnostics during Near-Field Blast Evaluation, *in* '25th International Symposium on Military Aspects of Blast and Shock (MABS)', The Hague, Netherlands, 24-27 September.

[180] Wu, C., Fattori, G., Whittaker, A. and Oehlers, D. J. [2010], 'Investigation of Air-Blast Effects from Spherical-and Cylindrical-Shaped Charges ', *International Journal of Protective Structures* **1**(3), 345–362.

[181] Xiao, W., Andrae, M. and Gebbeken, N. [2020], 'Effect of Charge Shape and Initiation Configuration of Explosive Cylinders Detonating in Free Air on Blast-Resistant Design', *Journal of Structural Engineering* **146**, 1–13.

[182] Zukas, J. A. and Walters, W. [1998], *Explosive Effects and Applications - Shock Wave and High Pressure Phenomena*, Springer-Verlag, New York.

[183] Zygmunt, B. and Buczkowski, D. [2007], 'Influence of ammonium nitrate prills properties on detonation velocity of anfo', *Propellants, Explosives and Pyrotechnics* **32**(5), 411–414.